

SEMIANNUAL REPORT BIOLOGY AND MEDICINE

REPOSITORY

Lawrence Berkeley Laboratory

COLLECTION

*Main Library - UCRL Reports*BOX No. *NA*FOLDER *NA*

*Donner Laboratory
and
Donner Pavilion*

BEST COPY AVAILABLE

TWO-WEEK LOAN COPY

This is a Library Circulating Copy
which may be borrowed for two weeks.
For a personal retention copy, call
Tech. Info. Division, Ext. 5545

Spring 1967

RECEIVED
LAWRENCE
RADIATION LABORATORY
DEC 8 1967
LIBRARY AND
DOCUMENTS SECTION

LAWRENCE RADIATION LABORATORY - UNIVERSITY OF CALIFORNIA - BERKELEY

11 15 110

UCRL - 17481
cy. 2

SPRING 1967

**SEMIANNUAL REPORT
BIOLOGY AND MEDICINE**

John H. Lawrence, M.D., Editor

**DONNER LABORATORY AND DONNER PAVILION
LAWRENCE RADIATION LABORATORY UNIVERSITY OF CALIFORNIA
BERKELEY, CALIFORNIA**

AEC Contract No. W-7405-eng-48

1175171

FOREWORD

This issue of our semiannual report again reflects, but does not completely cover, the research activity of the program in Biology and Medicine. The remarkable visualization in depth of organisms is beautifully demonstrated in the scanning electron microscope studies of Hayes, Pease, Camp, and McDonald. Further contributions of laminar flow electrophoresis are reported in the lipoprotein studies of Tippetts, Mel, and Nichols. An elegant new method for monitoring red cell life span distribution, which has usefulness in space medicine, is reported by Landaw. There are several new contributions in the field of hematology in the papers by Winchell, Van Dyke, Price, Anger, Fawwaz, Schooley, Garcia and their associates. New radiobiological studies with high intensity pulsed X rays and high LET radiations are reported by Todd and associates and by Dewey and Haynes. Finally, Feola et al. report further studies with negative pions, and the role of capillaries in radionecrosis is discussed by McDonald and Hayes.

TABLE OF CONTENTS

Stereoscopic Scanning Electron Microscopy of Living <i>Tribolium confusum</i> THOMAS L. HAYES, R. F. W. PEASE AND ANN'S. CAMP	1
Scanning Electron Microscopy of Sectioned Tissue LARRY W. McDONALD, R. F. W. PEASE AND THOMAS L. HAYES	8
Stable-Flow Free Boundary (Staflow) Electrophoresis: Three Dimensional Fluid Flow Properties and Applications to Lipoprotein Studies ROGER D. TIPPETTS, HOWARD C. MEL AND ALEXANDER V. NICHOLS	16
Studies of RBC Lifespan Distribution Using Endogenous ^{14}CO Production STEPHEN A. LANDAW	43
Erythrokinetics in the Dietary Hypercholesteremia of Guinea Pigs WILLIAM K. YAMANAKA, H. SAUL WINCHELL AND ROSEMARY OSTWALD	58
Similarity in Distribution of Skeletal Blood Flow and Erythropoietic Marrow DONALD C. VAN DYKE	70
Differences in Distribution of Erythropoietic and Reticuloendothelial Marrow in Hematologic Disease DONALD C. VAN DYKE, CAROL J. SHKURKIN, DAVID C. PRICE, YUKIO YANO, AND HAL O. ANGER	86
First-Pass Hepatic Deposition of Intestinally Absorbed Iron in Patients with Low Plasma Latent Iron-Binding Capacity RASHID A. FAWWAZ, H. SAUL WINCHELL, MYRON POLLYCOVE AND THORNTON W. SARGENT	97
Decreased Thymidine Synthesis and Increased ^3H -Thymidine Incorporation into DNA by Human Bone Marrow Cultured with Aminopterin SERENE L. VIMOKESANT, H. SAUL WINCHELL, MYRON POLLYCOVE AND MATTHEW B. FISH	106
A Summary of Some Studies on Erythropoiesis Using Anti-Erythropoietin Immune Serum JOHN C. SCHOOLEY, JOSEPH F. GARCIA, LINDA N. CANTOR AND VIRGINIA W. HAVENS	110
Erythropoietin Therapy in the Renoprival Patient DONALD C. VAN DYKE, MYRON POLLYCOVE AND JOHN H. LAWRENCE	127
Pulsed High Intensity X Rays: Inactivation of Human Cells Cultured <u>in vitro</u> and Limitations on Usefulness in Radiotherapy PAUL W. TODD, H. SAUL WINCHELL, JOSE M. FEOLA AND GARY E. JONES	133
Sensitivity of <i>Micrococcus radiodurans</i> to Densely Ionizing Radiations DAVID L. DEWEY AND ROBERT H. HAYNES	138
Effect of Negative Pions on the Proliferative Capacity of Ascites Tumor Cells (Lymphoma) Grown in vivo JOSE M. FEOLA, CHAIM RICHMAN, MUDUNDI R. RAJU, STANLEY B. CURTIS AND JOHN H. LAWRENCE	145
The Role of Capillaries in the Pathogenesis of Delayed Radionecrosis of Brain LARRY W. McDONALD AND THOMAS L. HAYES	154
Staff Publications	171
Author Index	175

Stereoscopic Scanning Electron Microscopy of Living *Tribolium confusum*

Thomas L. Hayes, R.F.W. Pease and Ann S. Camp

The scanning electron microscope has been used to produce stereoscopic pictures of living *Tribolium confusum* at magnifications up to 1300. The physiological implications of survival in the environment of electron beam scanning are discussed.

INTRODUCTION

The scanning electron microscope utilizes a fine, moving beam of electrons (diameter as small as 50 Å) to probe the specimen for a variety of kinds of physical, chemical, and electrical information. As the scanning beam is swept across the specimen, the electron beam of a standard cathode ray tube is driven in synchrony with it and the brightness of the cathode ray beam is modulated by the signal from one of several detectors. The secondary radiation produced by the interaction of the scanning electron beam is not imaged but is only used to convey information about the particular point being bombarded. The image is a result of the synchrony between the scanning beam on the microscope column and the beam of the cathode ray tube. The resulting 1:1 correspondence of points on the specimen with points on the face of the cathode ray tube serves to identify the location of the information seen by the detectors. The separation of information and localization allows many different kinds of information to be gained while utilizing the localization possible with an electron beam. Different kinds of secondary radiation are produced by the interaction of the electron beam with the specimen and each carries a particular kind of information. For example, visible light may be produced and give information about the molecular structure of the biological material itself or the location of light-producing stains within the specimen. Operated in this mode, the scanning electron microscope could be described as a high resolution fluorescence microscope (1). Secondary electrons are another form of radiation produced by the interaction of the scanning beam with the specimen. Since production of these secondary electrons is a function of the angle between the scanning beam and the surface of the specimen, stereoscopic information can be obtained. The scanning electron microscope operated in this mode can be described as a high resolution stereoscopic microscope (2). In addition, ultraviolet radiation, characteristic X rays, backscattered electrons, energy loss electrons, and specimen current are all produced in the specimen and might be used to build up the scanning electron microscope image. The principles of the instrument and several of its modes of operation have been recently reviewed (3).

The present paper deals with an attempt to visualize living Tribolium confusum by using the scanning electron microscope in the secondary electron mode of operation. There are several advantages both physiologically and morphologically if the specimen can be viewed while it is living. Morphologically, the reduction in the possibility of artifacts and the simplicity of sample preparation are important. Physiologically, the possibility of observing "on-going" processes would be most valuable. Also, the tiny electron beam may be utilized as a microradiation source in radiobiological studies (4).

METHODS

The scanning electron microscope used in this study was constructed at the University of California, Berkeley. The electron optical column consists of two magnetic lenses which focus a demagnified image of the electron gun crossover on the specimen surface; the focused spot so formed has a diameter of about 500 Å. The spot is scanned in a rectangular raster in synchrony with the spot of the display cathode ray tube by means of magnetic deflection yokes which are driven by custom-built scan generators. The magnification is varied by changing the size of the scan; on this microscope, magnifications from 30X to 125,000X are possible.

The specimens of Tribolium confusum were obtained from the colony maintained at our laboratory for several years for radiobiological studies (5, 6). The living insects in the egg, larval, pupal, or adult stage were placed in a small aluminum foil boat approximately 5×3×3 mm and the boat attached to the stage of the scanning electron microscope. The microscope column was then evacuated and the specimen viewed using 25-keV electrons and a beam current of about 10^{-11} amp. Secondary electron collection provided the signal for image production and the resulting micrographs were therefore stereoscopic in nature. Viewing time ranged from 10 min to 1 hr.

When electron microscopy had been completed, the insect was returned to normal environmental conditions and checked for survival. The criteria for survival were hatching for the eggs, metamorphosis to pupae for the larvae, metamorphosis to the adult for the pupae, and return of normal activity for the adult. All specimens were followed for at least 1 month after electron microscopy to determine long term survival.

Micrographs were produced by Polaroid photography of the display cathode ray tube, using Type 42 or Type 55 P-N film.

RESULTS

Larval, pupal, and adult forms of Tribolium confusum, as reported previously, are capable of surviving the vacuum and electron beam bombardment used for scanning electron microscopy (4). Observation times on the order of 1/2 hr were tolerated.

Figures 1 through 6 are illustrations of scanning electron micrographs of a living larva (Figs. 1, 2), pupa (Figs. 3, 4), and adult (Figs. 5, 6). The stereoscopic information and large depth of focus are apparent particularly in micrographs of the larval foot (Fig. 2) and



Fig. 1. Leg of living larva. $\times 200$.
JHL-6476



Fig. 2. Foot of living larva. $\times 1000$.
JHL-6474

1175176



Fig. 3. Head area of living pupa. $\times 130$.
JHL-6475



Fig. 4. Surface of pupal head over eye. $\times 520$.
JHL-6472

1175177



Fig. 5. Antenna tip of living adult. $\times 1000$.
JHL-6468



Fig. 6. Eye of living adult. Note hexagonal primitive lattice array of spines in the eye. $\times 1300$.
JHL-6469

the pupal head (Fig. 4). The increase in resolution over the light stereomicroscope is demonstrated in the adult antenna tip (Fig. 5) and the adult eye (Fig. 6).

DISCUSSION

The ability of eggs, larvae, pupae, and adults of Tribolium confusum to survive the extreme environmental conditions necessary for electron beam scanning illustrates again the great physiological adaptability of the insects. The conditions of high vacuum, temperature elevation, and radiation dose must be withstood by the organism.

In order to survive high vacuum the insect must be able to conserve water and forego oxygen. Other insects have been shown to survive extremely dry environments. The starved mealworm is able to conserve its water for a month against an environment of absolutely dry air (7). It has been estimated that 60-70% of water loss is through the spiracles and that loss through the cuticle takes place mainly at the intersegmental membranes. Under vacuum conditions, the spiracles may close very tightly or the diffusion rate of water across the tracheal walls may be drastically reduced because of rapid drying of these walls (8).

By weight loss and freezing experiments, we have tested the ability of the adult Tribolium to conserve water against a vacuum of 10^{-3} mm Hg for short periods of time. Adult Tribolium do not suffer any appreciable weight loss during the first few minutes of evacuation. Death due to freezing, which is probably mediated by water present in the tissue, still occurs in adults subjected to a vacuum environment. Since activity increases water loss, the fact that the insect does not move while in the vacuum would tend to help conserve water.

The survival of several insect species after exposure to anaerobic conditions for 1/2 hr or more has been described (9). Such metabolism often results in an oxygen debt which requires some hours to pay off.

Local elevation of temperature due to the electron bombardment has been estimated to be only 0.005°C (4), which should not be troublesome, but the dose rate of ionizing radiation may reach 10^7 rads/sec. Since the radiation is in the form of low energy electrons (25 keV) it would seem reasonable to assume that the cuticle can absorb this dose and protect the underlying tissues. Although viewing in the scanning electron microscope does not inhibit metamorphosis into the next stage of development, there is a definite shortening of life span once the insect has reached adulthood. This could well be an effect of radiation, and further studies using the scanning electron microscope as a micro radiation source are planned. The effect of exposure on reproductive capacity is not yet known.

The great depth of field and stereoscopic information available from the secondary electron mode allow us to use the scanning electron microscope to produce high magnification pictures that compare quite well with experienced vision. The advantage in learning and synthesizing information in this form may be considerable.

ACKNOWLEDGMENTS

This work has been supported by the U. S. Atomic Energy Commission and the Joint Services Electronics Program. The construction of the Scanning Electron Microscope was largely supported by the U. S. A. F. Avionics Laboratory.

REFERENCES

1. Pease, R. F. W., and Hayes, T. L.; Nature 210: 1049, 1966.
2. Hayes, T. L.; Pease, R. F. W., and McDonald, L. W.; Lab. Invest. 15: 1320-1326, 1966.
3. Oatley, C. W.; Nixon, W. C., and Pease, R. F. W.; Advan. Electron. Electron Phys. 21: 181-247, 1965.
4. Pease, R. F. W.; Hayes, T. L.; Camp, A. S., and Amer, N. M.; Science 154: 1185, 1966.
5. Beck, J. S.; Rad. Res. 19: 569, 1963.
6. Amer, N. M.; Slater, J. V., and Tobias, C. A.; Rad. Res. 16: 574, 1962.
7. Buxton, P. A.; Proc. Roy. Soc. (London) 106 (B): 560-577, 1930.
8. Mellanby, K; Biol. Rev. 10: 317-333, 1935.
9. Wigglesworth, V. B.: The Principles of Insect Physiology, London, Methuen and Company, 1953, pp. 416-417.

Scanning Electron Microscopy of Sectioned Tissue

Larry W. McDonald, R.F.W. Pease and Thomas L. Hayes

Previous reports from this laboratory have presented applications of the scanning electron microscope in several areas of biology and medicine. These applications have included the stereoscopic representation of human cells and tissue at magnifications up to $\times 10,000$ (3), for the use of the scanning electron microscope in the cathodoluminescent mode (7), and the scanning electron microscopy of living insects (8). This present report deals with the observation of standard-size light microscopy sections of tissue, the same section being viewed with the scanning electron microscope and the light microscope. The increased information gained by the use of the scanning electron microscope over the light microscope includes 3-dimensional representation and increased resolution. In addition, the size of the section that can be examined with the techniques described here is more than 1000 times larger in area than the ultrathin sections necessary for conventional electron microscopy. An application of this method has been mentioned briefly in the paper by McDonald and Hayes (5) describing delayed radionecrosis of brain. It is felt that this technique may add a valuable approach to the study of many tissues and organs and that it may develop into a useful tool for the pathologist.

METHODS

Glutaraldehyde was used for vascular perfusion fixation of the rabbit brain and kidney. It was used as a 5% solution in 0.1 M phosphate buffer at pH 7.4. This fixative was described by Sabatini, Bensch, and Barrnett (10) for fixation by immersion. Its use for fixation of the central nervous system by vascular perfusion has been described by Schultz and Karlsson (11). Perfusion of the brain was done with the animal under Nembutal anesthesia and was continued for 1 hr using approximately 800 ml of fixative. This procedure is described in detail in another paper (5). The kidney was perfused in the same general manner as the brain. The perfused tissue was removed from the animal, dehydrated through graded alcohols, and embedded in paraffin with the use of the schedule under method 1 in the Manual of Histologic and Special Staining Techniques (4).

Formalin was used as a 4% solution of formaldehyde in a 0.24 M sodium acetate solution at pH 6.9 to 7.0. This fixative was used on a human renal biopsy specimen and a segment of coronary artery from autopsy. The tissue was left in fixative for 18 hr and then dehydrated through graded alcohols and embedded in paraffin by using the same schedule as for the glutaraldehyde-fixed tissues described above.

Sections $4\ \mu$ thick were cut from the paraffin blocks of both the glutaraldehyde- and formalin-fixed tissues. These sections were mounted on glass cover slips, the paraffin removed with xylene, and hematoxylin and eosin staining used in anticipation of subsequent light microscopic histology. The sections were then coated with a thin conducting layer of platinum-palladium alloy deposited by evaporation in a vacuum evaporator at a 90° angle to the section. This conducting layer of metal prevents charging of areas of the section in the electron beam. The cover slips were placed on the stage of the scanning electron microscope with the section toward the scanning electron beam and making a 45° angle with this beam. After having been viewed with the scanning electron microscope, the cover slips were dipped in dry ethanol, then xylene twice, and mounted with Permount on glass slides for light microscopy, the tissue section being between the slide and the cover slip in the usual manner.

The scanning electron microscope used in this study was constructed at the University of California Electronics Research Laboratory. The operation of the instrument has been discussed in detail elsewhere (3, 6). In brief, the electron beam spot is scanned in a rectangular raster in synchrony with the spot of a display cathode ray tube by means of magnetic deflection yokes which are driven by custom-built scan generators. The magnification is varied by changing the scan current in the yokes of the microscope column. The current Berkeley instrument has a spot diameter of about $500\ \text{\AA}$ and is used for biologic materials at magnifications up to about $\times 10,000$. All electron micrographs shown in this study were formed by the secondary electron mode of operation. All scanning electron micrographs were Polaroid type 42 or PN photographs of the cathode ray display tube.

RESULTS

In the sections of irradiated rabbit brain the basement membrane of a small blood vessel stands out prominently due to its increased thickness (2, 5) and probably also due to its increased rigidity which holds it above the depressed adjacent section's surface. These features are shown in Fig. 1. The height of the blood vessel wall is equal to the thickness of the $4\ \mu$ section. The observation of vertical surfaces in a 3-dimensional aspect is brought out in the figure. Red blood cells, both within the vessels and in sites of perivascular hemorrhage, show in their 3-dimensional aspect. The greater resolution of the scanning electron micrographs and their 3-dimensional information, as compared with light micrographs, are brought out in Fig. 2.

In Fig. 3 a section of a vasa vasorum of a human coronary artery as seen by scanning electron microscopy is shown. The detail in this $\times 1000$ scanning electron micrograph is greater than that which can be obtained with the light microscope, and the 3-dimensional aspect of the partially crenated and compressed erythrocytes can be seen.

A normal rabbit kidney is shown in Fig. 4. The scanning electron micrograph (Fig. 4C) shows the depth of the $4\ \mu$ section and the apparent rigidity of the basement membrane of the glomerular capillaries. Also the 3-dimensional relationship of the capillaries to the mesangium is more apparent in the scanning electron micrograph.



Fig. 1. A, Light micrograph. Area of delayed radiation lesion of rabbit sensory cortex. The tissue was fixed by supravital glutaraldehyde perfusion, embedded in paraffin, sectioned at $4\ \mu$, mounted on cover slips, stained with hematoxylin and eosin, and then platinum-palladium coated as described in the text. B, Scanning electron micrograph. Same section as in Fig. 1A viewed in the scanning electron microscope showing the section thickness and the apparent rigidity of the basement membrane of the vessel wall. The sections were examined in the scanning electron microscope, and then the cover slips were mounted on slides with Permount for the light microscopy. An area of perivascular hemorrhage is shown. A, $\times 860$; B, $\times 960$.

JHL-6392 + JHL-6398



Fig. 2. Erythrocytes (top) by scanning electron microscopy to show the 3-dimensional features and greater detail of the wall of a vascular channel. $\times 4900$.

JHL-6401

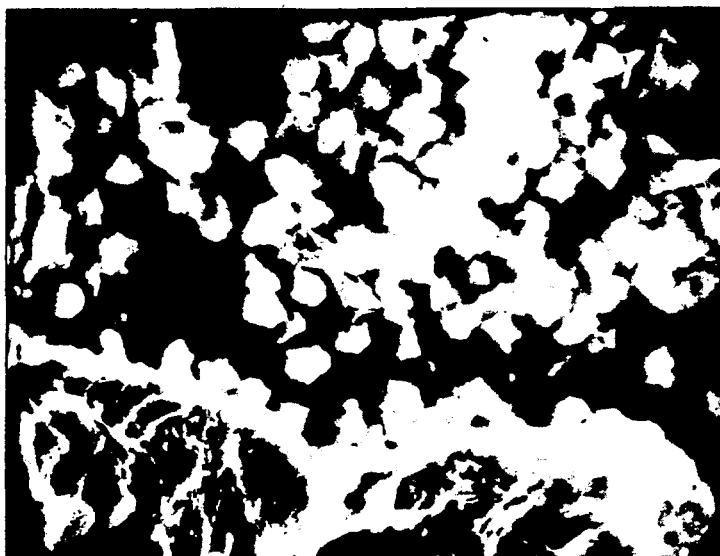


Fig. 3. Vasa vasorum of a human coronary artery near a developing atherosclerotic plaque (not shown) by scanning electron microscopy. Partially crenated and compressed erythrocytes are seen in the lumen (upper two-thirds of field). $\times 1000$.

XBB677-3910

A sclerosed glomerulus of a diabetic kidney (Fig. 5) shows "adhesions" between capillary loops in the scanning electron micrographs. The material of the mesangial deposits forming the nodular lesions in the glomerulus is prominent in the scanning pictures; the surfaces of the nodules appear rough, indicating a variability in rigidity within the deposit. This is consistent with the findings of irregularly shaped deposits seen in ultrathin sections by conventional electron microscopy (1).

DISCUSSION

The scanning electron microscope has been applied to the examination of sectioned tissue. The morphology which has been shown by this technique has been known from light microscopy and conventional electron microscopy by the examination of many sections and serial sections, but the integrated, 3-dimensional picture can now be seen in a single photograph. With the scanning electron microscope, we have examined sections of the standard size for light microscopy with magnifications ranging from $\times 50$ to $\times 5000$. Since the beam does not pass through the sections, no troublesome grid bars obscure the view as in transmission electron microscopy. When methods are developed to etch out differentially cellular structures so that they may be seen as differences in elevation on the section surface, magnifications of $\times 10,000$ or more will be useful with sectioned tissue with the use of the present instrument. With the technique as presently developed, little additional information is gained with magnifications above $\times 5000$. At these magnifications, however, the resolution is much greater than can be obtained with the light microscope.

The scanning electron microscope may also be used to examine ultrathin sections in the electron transmission mode. In the secondary electron mode which we have used here, there is a limit of approximately 100 \AA to the resolution (9). This, however, is not the case in the transmission mode where the scanning spot size is the main factor limiting resolution.

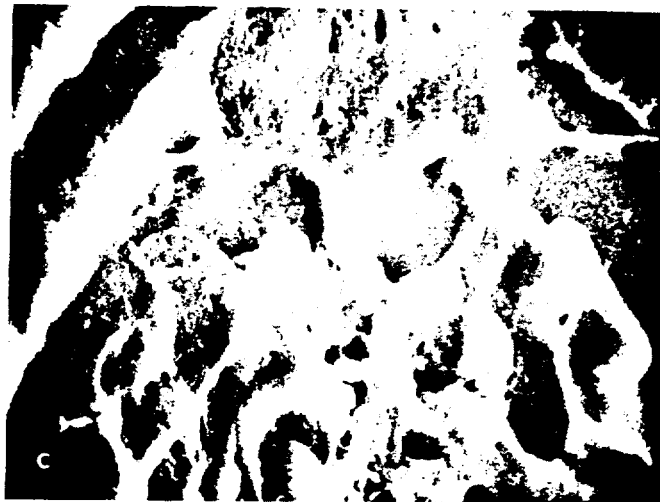
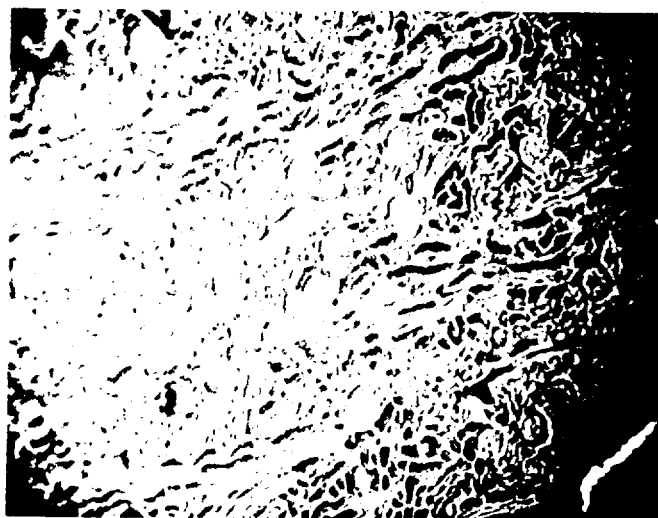


Fig. 4. A, Scanning electron micrograph of $4\ \mu$ section of rabbit kidney. B, Light micrograph. C, Scanning electron micrograph of same glomerulus as in B and slightly above and to left of center of A. A, $\times 50$; B and C, $\times 1000$.

XBB677-3911

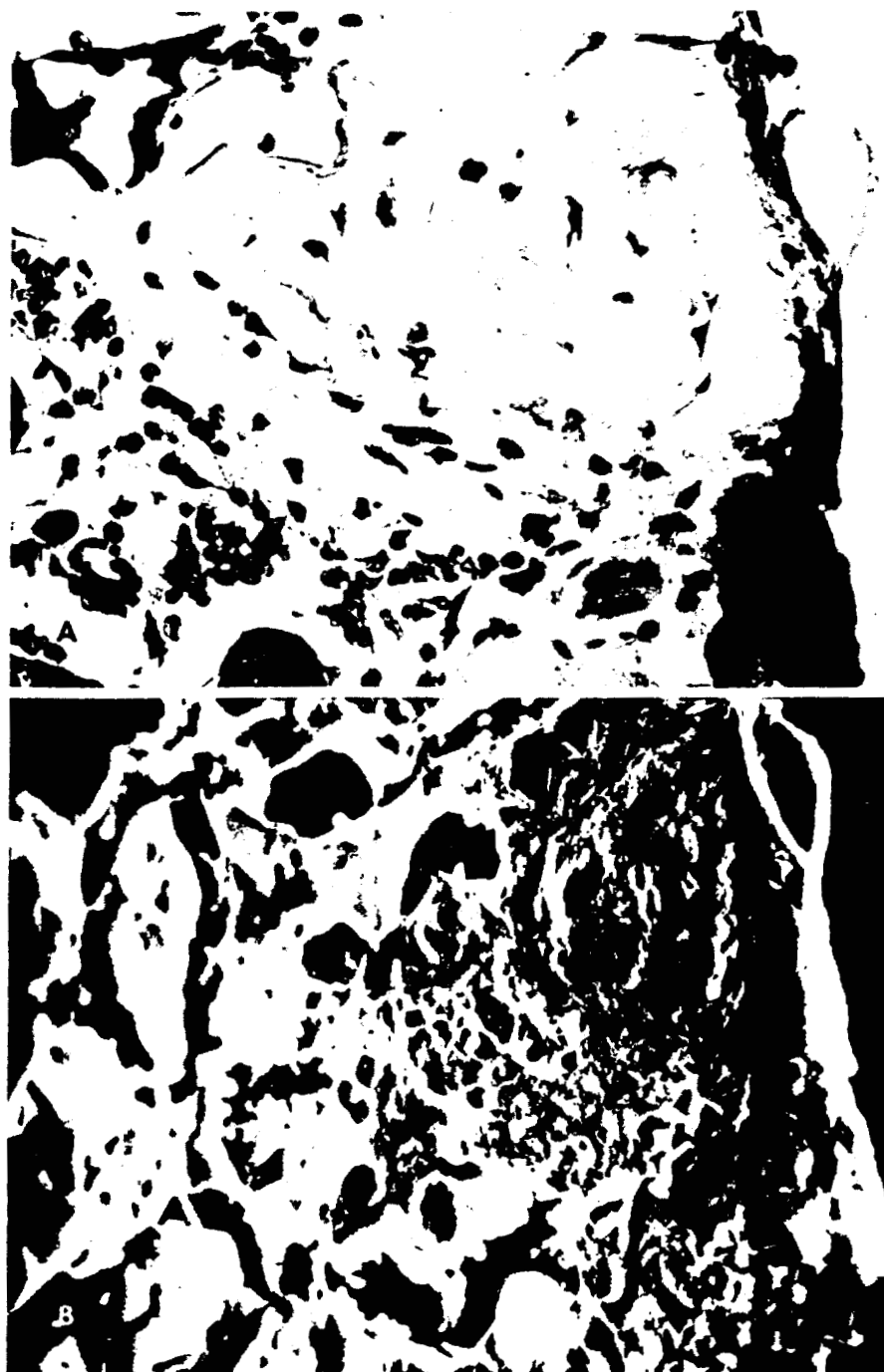


Fig. 5. A, Light micrograph and B, Scanning electron micrograph. Sclerosed glomerulus from renal biopsy of diabetic kidney. The sclerosed glomerulus is in the upper right area. The fold of the edge of the section stands out prominently on the right of the scanning electron micrograph. A and B, $\times 500$.

XBB677-3912

For example, the brush border of the proximal convoluted tubule of the kidney has been resolved with the use of the Berkeley scanning electron microscope in the transmission mode.

Some of the energy loss of the electron beam can be converted to light when the tissue section is penetrated (cathodoluminescence), and this light may also be collected through the cover slip to form an image with electron microscopic resolution (7). We are presently exploring the application of the instrument to sectioned tissue in this manner.

Still another approach, which is being used by A. V. Crewe and associates at Argonne National Laboratory, Lemont, Illinois, is the formation of different images depending upon what energy of transmitted electrons is used to form the image. From the energy spectrum of the electrons passing through an area of the specimen, one can obtain information about the chemical composition of the area.

SUMMARY

Tissue sections of the standard size used for light microscopy have been successfully viewed with the scanning electron microscope at magnifications up to $\times 5000$. In addition to examining large tissue sections with a resolution exceeding that of the light microscope, the micrographs show 3-dimensional aspects of tissue structure. Other approaches to utilizing the full resolution of the scanning electron microscope for the examination of large tissue sections are discussed.

ACKNOWLEDGMENTS

This work has been supported in part by the Joint Services Electronic Research Program and by the United States Atomic Energy Commission. The construction of the scanning electron microscope was largely supported by the United States Air Force Avionics Laboratory and by the University of California.

REFERENCES

1. Bergstrand, A., and Bucht, H.; Electron Microscopic Investigations on the Glomerular Lesions in Diabetes Mellitus (Diabetic Glomerulosclerosis); in Lab. Invest. 6: 293, 1957.
2. Cervos-Navarro, J.; Elektronenmikroskopische Befunde an den Capillaren des Kaninchengehirns nach der Einwirkung ionisierender Strahlen; in Arch. Psychiat. Z. Path. 205: 204, 1964.
3. Hayes, T. L.; Pease, R. F. W., and McDonald, L. W.; Applications of the Scanning Electron Microscope to Biologic Investigations; in Lab. Invest. 15: 1320, 1966.
4. Manual of Histologic and Special Staining Techniques, p. 10. Armed Forces Institute of Pathology, 1957, Washington, D. C.
5. McDonald, L. W., and Hayes, T. L.; The Role of Capillaries in the Pathogenesis of Delayed Radionecrosis of Brain; in Amer. J. Pathol., in press.
6. Oatley, C. W.; Nixon, W. C., and Pease, R. F. W.; Scanning Electron Microscopy. In Advances in Electronics (and Electron Physics), edited by Marton, L., Vol. 21, pp. 181-247, New York, Academic Press, Inc., 1965.

7. Pease, R. F. W., and Hayes, T. L.; Scanning Electron Microscopy of Biological Material; *Nature* 210: 1049, 1966.
8. Pease, R. F. W.; Hayes, T. L.; Camp, A. S., and Amer, N. M.; Electron Microscopy of Living Insects; *Science* 154: 1185, 1966.
9. Pease, R. F. W., and Nixon, W. C.; High Resolution Scanning Electron Microscopy; *J. Sci. Instr.* 42: 81, 1965.
10. Sabatini, D. D.; Bensch, K., and Barrnett, R. J.; Cytochemistry and Electron Microscopy. The Preservation of Cellular Ultrastructure and Enzymatic Activity by Aldehyde Fixation; *J. Cell Biol.* 17: 19, 1963.
11. Schultz, R. L., and Karlsson, V.; Fixation of Central Nervous System for Electron Microscopy by Aldehyde Perfusion. II. Effect of Osmolarity, pH of Perfusate, and Fixative Concentration; *J. Ultrastruct. Res.* 12: 181, 1965.

Stable-Flow Free Boundary (StaFlo) Electrophoresis: Three Dimensional Fluid Flow Properties and Applications to Lipoprotein Studies

Roger D. Tippetts, Howard C. Mel and Alexander V. Nichols

I. INTRODUCTION

Previous papers have described the theory and practice of the stable-flow free-boundary (StaFlo) method (12, 13, 14) and the application of StaFlo electrophoresis or sedimentation to the study of small molecules (10, 11, 14), proteins (11), an enzyme substrate reaction (15), living cells (12, 13, 14, 16), isolated chloroplasts (19, 21), and lipoproteins (27). These studies used analytical and/or separation processes applied to particles dissolved or suspended in a continuously flowing free solution system, in that part of the apparatus called the "StaFlo chamber." The previous analysis was based on the approximation of vertical plug flow within the StaFlo chamber, experimentally demonstrated by flow pattern photographs and observations on collection fractions. The possible implications of non-uniform or parabolic flow in the horizontal (thickness) dimension for StaFlo migration properties were discussed, but no experimental measurements were available on the true nature of this flow.

In the present paper we report: (1) detailed measurements on the local fluid flow velocities throughout a 3-dimensional StaFlo chamber, revealing (a) the limits of the vertical plug flow approximation, particularly near the top and bottom walls (membranes), and (b) the parabolic nature of the third-dimensional (horizontal) flow profile away from the inlets and outlets; (2) the "3-dimensional" StaFlo apparatus, and its implications for 3-dimensional volume flow, its system for establishing a "programmed electric field" in free solution, and a slit-lamp technique for viewing the cross section of a sample migration pattern in the flow system; (3) the consequences of these flow properties for rate type migration processes, illustrated by the electrophoretic migration and separation of serum lipoproteins. This work was begun as part of a broader study on lipoproteins. The portion presented here, though including some new results for lipoproteins, is primarily intended to make the StaFlo method a more quantitative analytical, as well as a higher resolution preparative tool for biological studies. It may also reveal some useful information on a specialized type of laminar fluid flow.

II. EXPERIMENTAL

A. THE STAFLO APPARATUS The StaFlo apparatus [as designed by Mel (10, 11, 12) and modified by Tippetts (27)] consists of a variable-speed multiple channel pump, a multiple

collection system, necessary connecting tubing, electrode wash reservoirs and sumps, an electrophoretic power supply, associated optical equipment, and a stable-flow free-boundary (Staflow) cell consisting of the Staflow migration chamber and the upper and lower electrode chambers (see Figs. 1 and 2).

The present variable-speed multiple-syringe drive pump was designed to drive up to 12 syringes. These syringes can be of any normal size up to 50 ml. We used polyethylene plastic syringes (Plastipak-sterile, disposable plastic syringe, Becton-Dickinson & Co., Rutherford, N. J.) because of their non-fragile nature, noncritical requirements of alignment of syringe barrel with syringe piston, and the very great uniformity from syringe to syringe within a given lot number.

The pump is powered by a 1/70-horsepower, 0 to 1725-rpm, shunt-wound electric motor (Bodine Electric Co., Chicago, Ill.), having a variable-speed power supply (Minarik Electric Co., Los Angeles, Calif., model Sh-14). The motor has a shaft projecting from each end. The high-speed shaft drives the pump for fast flush of the Staflow chamber and for filling the syringes. The low-speed shaft reduces the speed and is used to pump the fluids at a slow constant rate during Staflow runs. The pump can also be driven in reverse.

When 50 ml Plastipak syringes are used, the liquid is pumped at a flow rate of 0.65 ml/sec on high-speed maximum, and 0.018 ml/sec on low-speed maximum.

Electrode wash reservoirs are 2000 ml separatory funnels which supply streams of the same composition as or different compositions from those of the Staflow chamber streams.

The flow rate through the electrode chambers is normally larger than that of any stream within the Staflow chamber by a factor of about 10. The electrode wash solutions' flow rates are measured by floating-ball flowmeters (Fischer & Porter Co., Holbord, Pennsylvania, Tube No. 02-F 1/8-16/5/36).

The electrophoretic migration power supply (Model 5051 A, transistorized, Power Designs Inc., Westbury, N. Y.) supplies 0 to 50 Vdc, 0-1.5 A, with a voltage drift of less than 100 millivolts per day at constant ambient temperature.

The Staflow cell RT II (Fig. 3) is made of a central migration chamber (Staflow chamber) which consists of inlet and outlet flow divider pieces sandwiched between transparent plates of Lucite, glass, or quartz. The inlet and outlet pieces are made of Lucite, each having 36 channels arranged in a rectangular array of 3 wide by 12 high. All three inlet channels at each level are fed by a single syringe. However, each outlet channel flows into its own individual container within the multiple collection system. Plastic syringe barrels of all the same size have proved to be excellent for this purpose. The internal dimensions of the Staflow chamber are 30 cm long \times 3.0 cm high \times 0.8 cm wide. The upper and lower electrode compartments, made of Lucite, match the central migration chamber in length and width. Each electrode chamber is 0.25 cm high, and contains five platinum electrode segments 0.8 cm

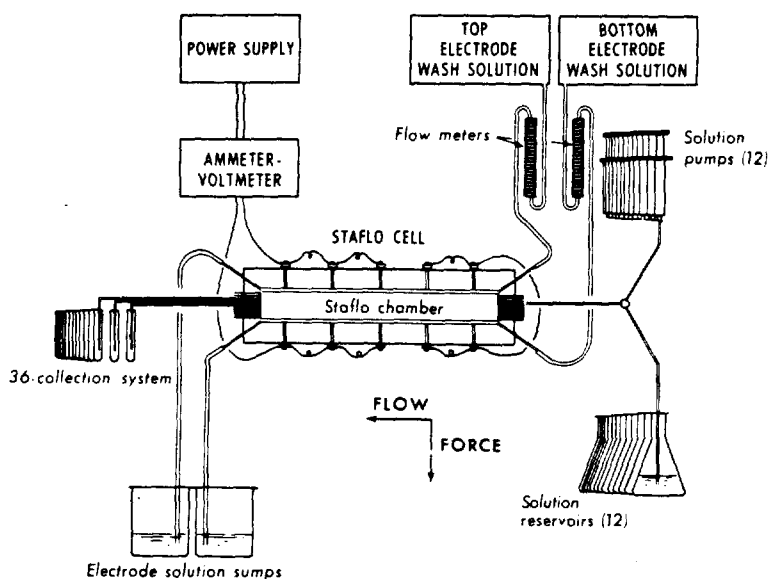


Fig. 1. Schematic drawing of Staflo apparatus.

MU-36571

wide \times about 5.95 cm long, separated from each other by a gap of about 0.05 cm. These three cell parts are clamped together with cellophane membranes (dialysis tubing) between them, forming three physically separated chambers: the upper and lower electrode chambers, and the central Staflo chamber in which the electrophoretic (or sedimentation) migrations occur.

B. MATERIALS All experiments described in this paper used a 12-solution sucrose density gradient varying (in steps of 0.4% wt/vol sucrose) from 0.0% in stream 1 to 4.8% in stream 12. All of these streams were pumped into the Staflo chamber at equal and constant rates except in the case of the "thin-sample" technique used in the lipoprotein experiments. In this technique the sample was pumped at a rate of 0.3 times that of any other stream, and under the present conditions assumed a vertical height (thickness) of about 0.3 times that of the other streams (see discussion, ref. 27). The upper and lower electrode compartments were filled with solutions of the same sucrose compositions as streams 1 and 12, respectively. Three sets of additional experimental conditions and techniques were as follows:

- 1) For the direct measurement of the fluid velocity profiles: Every stream contained human blood diluted 5000 times by volume with 0.9% (wt/vol) NaCl. The suspended RBC were viewed in dark field with a low-power microscope over an actual field width of 1.6 mm. The light from the microscope lamp used for illumination was passed through a water bath of at least 11.5 cm thickness to reduce to a negligible value its heating effect upon the solutions within the Staflo chamber. The time necessary for the suspended RBC to cross the field of view was determined by a stop watch.

- 2) For the indirect measurements of the fluid velocity profiles: Alternate streams contained 0.04% (wt/vol) blue dextran (mol wt 3×10^6) or colorless dextran (mol wt 6×10^5), with the odd-numbered streams being blue.

- 3) For the electrophoresis of human serum lipoproteins: Each stream, including the electrode wash streams, contained as buffer LKB 3276-GB High Resolution Buffer Salt;

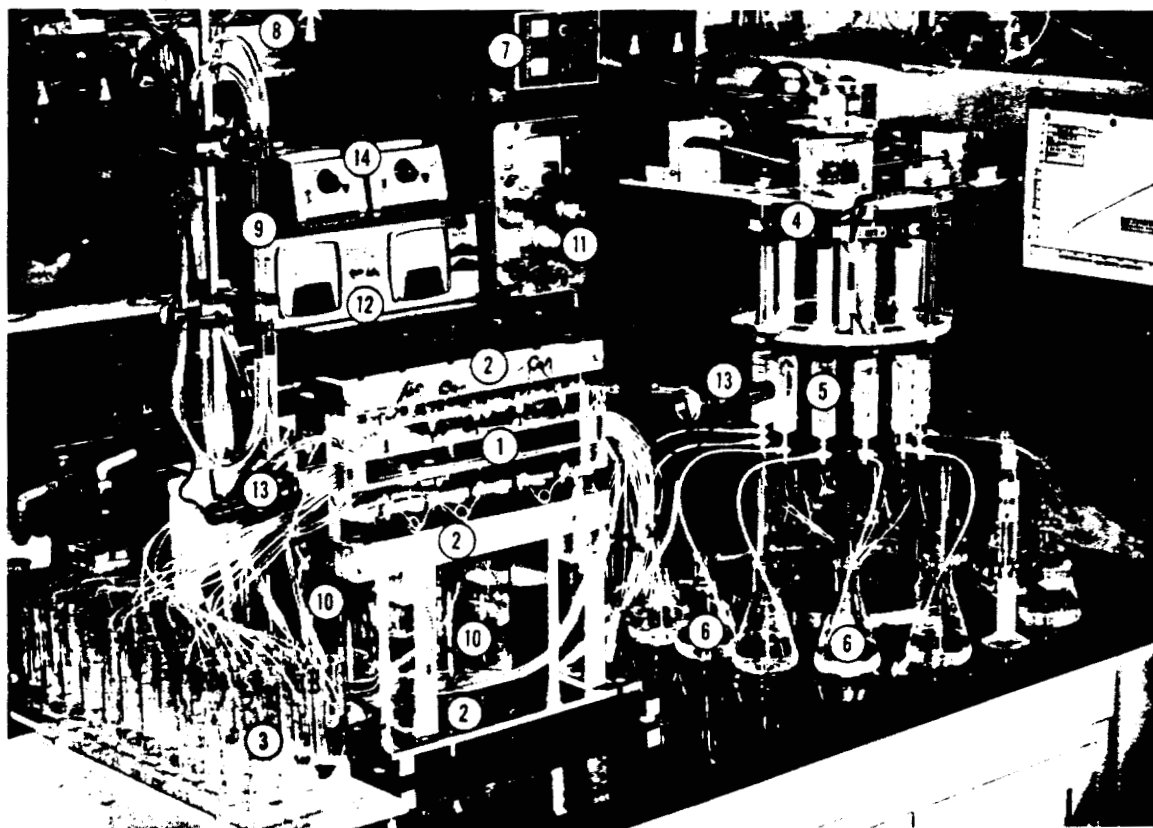


Fig. 2. Stable-flow free-boundary (Staflow) apparatus.

1. Staflow cell.
2. Staflow-cell clamp and supporting leveling stand.
3. Collection system on leveling table.
4. Syringe drive.
5. Solution pump syringes.
6. Solution reservoirs.
7. Syringe drive power supply.
8. Electrode wash solution reservoirs (located above pictures).
9. Electrode wash flowmeters.
10. Electrode solution sumps.
11. Electrophoresis power supply.
12. Ammeter-voltmeter.
13. Side lights.
14. Side-lighting power supplies.

JHL-5217

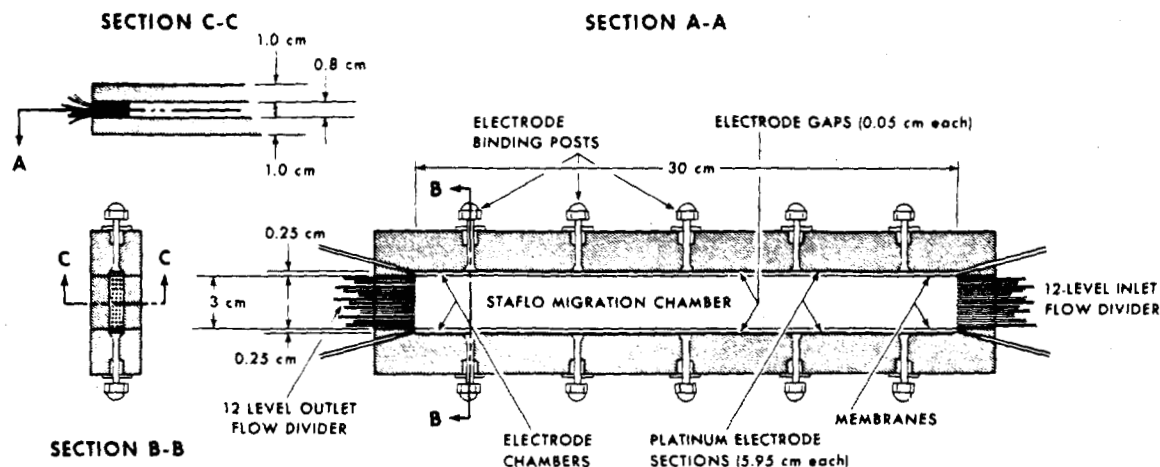


Fig. 3. Schematic drawing of the Staflo cell.
MU-36561

$1.2 \times 10^{-2} \text{ M}$ tris, $5 \times 10^{-4} \text{ M}$ EDTA, $1.83 \times 10^{-3} \text{ M}$ H_3BO_4 . The lipoprotein samples were dialyzed for at least 18 hr against this same buffer but at $2/3$ the above concentration. In all lipoprotein experiments only distilled-deionized water was used. Human serum lipoprotein samples (ultracentrifugal fractions $S_f 0-10^5$) were secured by the method of Lindgren, Nichols and Wills (3). Chicken egg yolk lipoproteins were prepared in a similar manner. Before introduction into the Staflo chamber the sample's density was adjusted with solid sucrose to a value intermediate between those of the streams immediately above and below it.

C. MANIPULATION At the beginning of a Staflo experiment it is necessary to remove any air bubbles from the inlet and outlet tubing and from the Staflo chamber. This is done by tilting the Staflo cell and flushing with degassed water. The appropriate density gradient solutions are then introduced into the Staflo chamber by one of the following methods. (Either method requires the equivalent of about five to six Staflo chamber volumes of liquid.) 1) The solutions are pumped into the Staflo chamber under turbulent flow conditions for about two or three chamber volumes, followed by two or three chamber volumes of liquid under laminar flow conditions; or 2) about five to six chamber volumes of liquid are pumped in under laminar flow conditions. This latter method requires a longer time than the former. However, both do achieve the same steady state conditions for experimentation.

Initially the fluid within each of the individual containers of the outlet collection apparatus should be at the same, or nearly the same, level (12, 13, 27). When the steady state condition has been achieved, the flow pattern (Fig. 6) is symmetrical from top to bottom. The steady state condition is conveniently described in terms of the parameter average residence time, τ_{av} , which is the time required to pump a volume of fluid equal to the volume of the Staflo chamber.

III. MEASUREMENTS OF LINEAR VELOCITY PROFILES

Point-to-point linear fluid velocities measured in the central x - y * plane of the Staflo chamber at various downstream (y) positions are given in Table 1. For experimental techniques see Section II B, conditions 2. The smoothed velocity curves for three different downstream positions are given in Fig. 4A. Point-to-point linear velocity measurements at a single downstream position (18 cm) but at several cross-stream (z -direction) locations are given in Table 2 with the corresponding smoothed curves shown in Fig. 5.

A. VERTICAL VELOCITY PROFILES Figure 4A demonstrates: 1) a point-to-point vertical plug flow region in the central portion of the 3-cm-high Staflo chamber, and 2) a variable velocity region occurring as the membranes are approached, characterized by higher velocity protuberances or "horns." At the 18 cm downstream position, for example, the deviation from plug flow occurs over roughly the top and bottom quarters of the Staflo chamber where the peak linear velocities are approximately 17% greater than the central plug velocity. As the outlet is approached, the width of the "horns" decreases and the positions of maximum velocity approach the membranes; i.e., the region of vertical plug flow widens. Thus the average linear flow rate does not decrease continuously from the center of the Staflo chamber to the upper and lower membranes as in classical laminar flow systems.

An alternative method of studying Staflo flow properties is the "dye stripe" method, previously described (12). Alternating colored liquid streams are pumped at the same constant volume flow rate into the Staflo chamber and the "flow pattern" (configuration of the "dye stripes") noted or photographed. (See Section II B, conditions 2.) Given the fixed-volume nature of the Staflo chamber, under steady state conditions the inlet-outlet volume flow rates for each individual stream must be equal. With the simultaneous siphon feature of the collection apparatus each stream exits at its respective outlet (12).

Gradient and flow conditions are chosen such that even with the small density differences commonly used between adjacent horizontal streams, under the action of gravity, the streams remain separate and intact each with an approximately rectangular cross section.[†] Hence the vertical height ("stripe width") of any stream at any downstream position (y) should be approximately inversely proportional to the linear velocity for the stream at that point, averaged over the stream's x - z cross section. Differences in linear velocity between streams should therefore manifest themselves by differences in "stripe width." Figure 6 is a close-up photograph of the inlet portion of the Staflo chamber. Streams 1 and 12 are seen to be wider, while streams 2 and 3, 10 and 11, are somewhat thinner than the central streams 4 through 9. Parallax tends to exaggerate the relative thickness of the upper and lower streams, but

* x -axis: Vertical axis, normal to the length and width of the Staflo chamber, coincides with the direction of gravity; positive downward.

y -axis: Horizontal axis; coincides with the length direction of the Staflo chamber; positive in the direction of bulk fluid flow.

z -axis: Horizontal axis, normal to the face (length direction) of the Staflo chamber, measured from the center, positive direction from front to back. (See Figs. 1, 7, 11.)

[†]Deviations from this behavior will be discussed in a subsequent paper. (See also ref. 27.)

Table 1. Linear fluid velocities in the center x-y plane, calculated from times of flight of human RBC within the Staflo chamber, at distances from the inlet as indicated. Duplicate readings are given for each position. Average residence time $\tau_{av} = 16.6$ min. Velocities in units of 10^{-2} cm/sec.

Distance from upper membrane (cm)	Distance from the Inlet (cm)										Inlet-outlet stream position
	29.0		24.0		18.0		12.0		1.0		Top membrane
0.1	3.33	3.33	2.46	2.35	2.25	2.13	3.13	3.01	3.33	3.33	
0.2	4.44	4.44	4.00	3.90	4.21	4.00	4.00	3.90	5.00	4.84	1
0.3	5.33	5.33	5.00	5.00	4.84	4.84	4.84	4.57	5.16	4.71	
0.4	5.16	5.16	5.16	5.33	5.16	5.33	5.00	5.00	5.00	5.16	2
0.5	4.44	4.70	5.00	5.00	5.16	5.51	5.00	5.00	5.16	5.16	
0.6	4.57	4.57	4.70	4.70	5.16	5.16	4.57	4.70	5.33	5.16	3
0.7	4.57	4.44	4.21	4.21	4.70	4.44	4.44	4.44	5.33	5.33	
0.8	4.57	4.44	4.21	4.21	4.44	4.32	4.10	4.10	4.84	5.00	
0.9	4.57	4.57	4.21	4.10	4.32	4.21	4.10	4.10	4.71	4.57	4
1.0	4.57	4.57	4.21	4.10	4.21	4.21	4.00	4.00	4.71	4.71	
1.1	4.57	4.57	4.21	4.21	4.57	4.57	3.80	3.90	4.44	4.44	5
1.2	5.00	4.57	4.32	4.21	4.57	4.32	4.10	4.10	4.44	4.71	
1.3	4.57	4.57	4.10	4.10	4.44	4.44	4.21	4.00	5.00	4.71	
1.4	4.84	4.84	4.00	4.00	4.57	4.21	4.10	4.10	4.21	4.44	6
1.5	4.57	4.84	4.21	4.21	4.57	4.44	4.00	4.00	4.21	4.21	
1.6	4.44	4.57	4.21	4.21	4.57	4.57	4.21	4.21	4.21	4.32	7
1.7	4.44	4.44	4.21	4.21	4.44	4.57	4.00	4.10	4.32	4.32	
1.8	4.44	4.44	4.10	4.10	4.57	4.57	4.21	4.10	4.44	4.44	
1.9	4.44	4.44	4.10	4.10	4.57	4.44	4.21	4.21	4.71	4.71	8
2.0	4.44	4.44	4.10	4.10	4.44	4.32	4.44	4.21	4.71	4.71	
2.1	4.44	4.21	4.21	4.21	4.44	4.21	5.00	4.57	4.32	4.44	9
2.2	5.00	4.70	4.21	4.21	4.57	4.44	5.16	5.33	4.57	4.57	
2.3	4.70	4.44	4.10	4.21	4.57	4.57	5.16	5.33	5.00	5.00	
2.4	4.44	4.44	4.57	4.57	4.70	4.84	5.00	5.33	4.57	4.71	10
2.5	5.00	5.00	4.57	4.57	5.16	5.16	5.00	5.00	5.00	4.71	
2.6	5.00	5.00	4.70	5.00	5.33	5.16	4.10	4.00	4.57	4.57	
2.7	5.00	5.00	4.84	5.00	5.16	5.33	4.10	4.21	4.44	4.21	11
2.8	5.16	5.33	4.57	4.44	4.34	4.44	3.13	3.07	3.33	3.47	
2.9	4.44	4.44	3.55	3.47	3.33	3.33	--	--	1.77	2.00	12
3.0	0.20	0.16	--	--	0.76	0.76	--	--	--	--	
											Bottom membrane

1175195

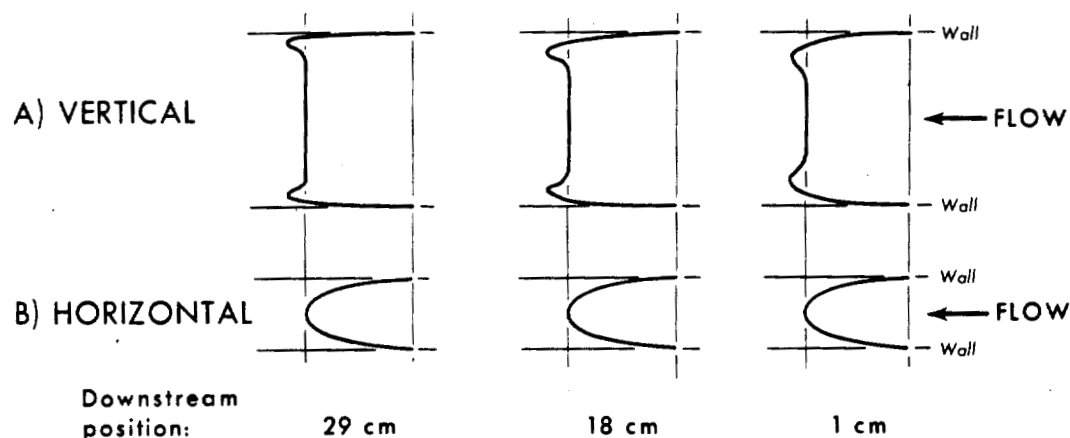


Fig. 4. Smoothed linear velocity profiles for various downstream (y) positions.

- A. Vertical profiles measured in the central (x-y) plane of the Staflo chamber for $\tau_{av} = 16.6$ min (plotted from data of Table 1).
- B. Horizontal profiles, valid for any horizontal (y-z) plane. Based on a large number of measurements, many unpublished. (Data for the 18 cm position at all levels, for $\tau_{av} = 16.6$ min, are given in Table 2; data for the 29 cm position at level 7, for $\tau_{av} = 17.9$ min, given in Fig. 7.)

MUB-13148

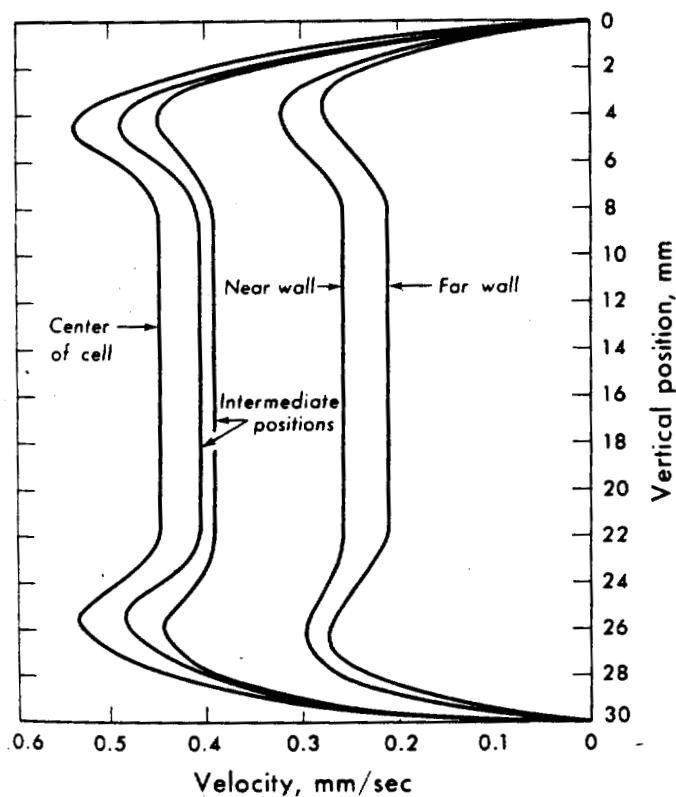


Fig. 5. Smoothed vertical linear velocity profiles, 18 cm downstream from the inlet of the Staflo chamber for $\tau_{av} = 16.6$ min. The slight difference between the curves for near wall, far wall, and intermediate positions is due to unsymmetrical positioning of the microscope and not to a departure of fluid flow from horizontal parabolic profile (plotted from data in Table 2).

MU-36569

1175196

Table 2. Linear fluid velocity as calculated from times of flight of human RBC measured 18 cm from the inlet of the Staflo chamber. Average residence time $\tau_{av} = 16.6$ min. Duplicate readings are given for each position. Velocities in units of 10^{-2} cm/sec.

Distance from upper membrane (cm)	Distance from near wall (mm)										Inlet-outlet stream position
											Top membrane
0.0	0.80	--	--	--	--	--	0.76	0.76	0.70	0.80	
0.1	1.61	0.16	2.00	1.88	2.25	2.13	2.19	2.19	1.28	1.39	1
0.2	2.66	2.66	3.90	3.80	4.21	4.00	3.80	3.80	2.46	2.58	
0.3	3.13	3.07	4.44	4.57	4.84	4.84	4.32	4.57	--	--	
0.4	3.26	3.13	5.00	5.00	5.16	5.33	4.84	5.00	2.71	2.75	2
0.5	3.13	3.20	4.57	4.57	5.16	5.51	4.57	4.32	2.66	2.66	
0.6	2.85	2.85	4.70	4.70	5.16	5.16	4.10	4.32	2.62	2.62	3
0.7	2.80	2.80	4.21	4.21	4.70	4.44	4.10	4.21	2.35	2.35	
0.8	2.50	2.58	4.21	4.21	4.44	4.32	3.90	4.00	2.22	2.22	
0.9	2.50	2.58	4.10	4.00	4.32	4.21	3.72	3.72	2.07	2.07	4
1.0	2.58	2.62	4.00	4.00	4.21	4.21	4.00	4.00	2.02	2.10	
1.1	2.58	2.58	4.10	4.10	4.57	4.57	3.90	4.00	2.05	2.02	
1.2	2.58	2.58	4.10	4.10	4.57	4.32	3.90	3.90	2.05	2.02	5
1.3	2.66	2.66	4.00	4.10	4.44	4.44	3.90	3.90	2.00	2.00	
1.4	2.58	2.58	4.10	4.00	4.57	4.21	3.80	4.00	2.05	2.00	6
1.5	2.62	2.58	4.10	4.00	4.57	4.44	4.00	3.90	2.00	--	
1.6	2.58	2.58	4.00	4.00	4.57	4.57	3.90	3.90	2.05	--	7
1.7	2.62	2.58	4.00	3.90	4.44	4.57	4.00	4.00	2.13	2.13	
1.8	2.62	2.66	4.10	4.00	4.57	4.57	3.90	4.00	2.10	--	
1.9	2.46	2.42	3.90	4.00	4.57	4.44	3.90	3.90	2.02	1.95	8
2.0	2.50	2.50	4.00	4.00	4.44	4.32	4.10	3.90	2.10	2.07	
2.1	2.46	2.46	3.90	4.00	4.44	4.21	3.90	3.90	2.10	2.07	
2.2	2.58	2.58	4.00	4.10	4.57	4.44	4.00	4.00	2.10	2.10	9
2.3	2.71	2.66	4.21	4.00	4.57	4.57	4.00	3.90	2.72	2.28	
2.4	2.75	2.66	4.32	4.70	4.70	4.84	4.10	4.00	2.38	2.42	10
2.5	2.75	2.75	4.70	4.70	5.16	5.16	4.21	4.21	2.46	2.58	
2.6	2.96	2.96	4.70	4.70	5.33	5.16	4.32	4.57	2.66	2.62	11
2.7	2.75	2.75	4.44	4.44	5.16	5.33	4.21	4.21	2.66	2.62	
2.8	2.66	2.66	4.00	4.10	4.32	4.44	3.90	3.90	2.28	2.22	
2.9	1.96	1.86	3.20	3.07	3.33	3.33	3.13	3.13	1.60	1.63	12
3.0	0.77	0.62	0.89	0.80	0.76	0.76	0.57	0.50	0.62	0.57	
											Bottom membrane



Fig. 6. Close-up view of inlet portion of Staflo chamber showing steady state "dye stripe" flow pattern; $\tau_{av} = 16.6$ min.

JHL-5238

nevertheless the qualitative conclusions from the point-to-point velocity measurements about relative flow rates (Fig. 4A) are corroborated by the relative stripe thickness.

Examination of such dye stripe flow patterns for downstream regions indicates that as the outlet region is approached, these width differences become smaller, and the widths of all streams tend toward that of the central streams. Each entering stripe exits then almost entirely through its corresponding outlet after the residence time passage through the Staflo chamber, as was previously reported for a different apparatus and different experimental conditions (12). This behavior is also consistent with the point-to-point velocity measurements and is simply a manifestation of the Staflo flow stability principles of: 1) stable density gradients, 2) operation under laminar flow conditions, and 3) the negative hydrostatic-hydrodynamic feedback which insures regulated (and approximately equal) outflow rates from each outlet (12, 13).

In the previous analysis of Staflo vertical flow properties, limited to the approximation of overall vertical plug flow, no systematic distortion of the vertical flow profile was reported (13). The present measurements, by focusing attention on the near top and bottom regions, and by use of a Staflo chamber allowing better visibility of these regions, permit determining the quantitative limits to this approximation. The zero and near-zero top and bottom velocity regions (which necessarily must exist in any conduit at the walls) are compensated by somewhat higher velocity "horns." The quantitative consequences of these deviations from

plug flow for vertical migration processes are considered in Section V C. But because they are relatively small, and because in an average sense they tend to be self-correcting, the average uniform vertical plug flow approximation will generally continue to be satisfactory. An analogous horizontal (z) direction plug flow model is far from satisfactory, however, as will now be seen.

B. HORIZONTAL VELOCITY PROFILE Plots of the flow velocities in the horizontal (z) direction of the Staflo chamber give parabolas as indicated schematically in Fig. 4B. This is true for all vertical heights, with the possible exception of the regions at the membranes, as can be inferred from the data in Table 2, or from the envelopes of the curves in Fig. 5. It was not possible to investigate the immediate vicinity of the membranes sufficiently thoroughly to establish an accurate flow profile there because of the difficulty of viewing this region with the microscope. According to Murphy (17) and Nikuradse (18), flow is not parabolic in such a region, measured in a similarly shaped chamber but without Staflo principles operative.

In another experiment, horizontal profile measurements were made 18 mm down from the upper membrane, at positions close to the outlet. Average steady state residence time was $\tau_{av} = 17.9$ min; all other parameters remained unchanged. At distances greater than approximately 1 cm from the outlets, good parabolic flow profiles were obtained. Closer than 1 cm, the outlets began to affect the velocity profiles somewhat, causing them to depart from parabolic form (Fig. 7).

IV. THE "3-DIMENSIONAL" STAFLO APPARATUS AND ITS HORIZONTAL VOLUME FLOW RELATIONS

Consider the fraction of the total volume flow passing through a given fractional width of the Staflo chamber. If perfect plug flow existed in the horizontal (z) direction, then for each layer $1/3$ of the volume flow would be confined to exactly $1/3$ of the chamber width. However, since it was shown that the horizontal flow profile is actually parabolic, a different volume flow to width relationship must obtain.

The work reported here was performed with a "3-dimensional" apparatus having 36 individual outlet channels arranged in a 3 wide by 12 high rectangular array. This permitted sampling each of the 12 flowing layers at three horizontal positions. With all 36 (uniform) collection containers hydrostatically and hydrodynamically unified through the Staflo chamber, the same outlet-level feedback control was observed for this outlet array as was observed in the original Staflo apparatus having 12 collection containers with a single vertical 12-channel outlet array. In this way, a precise boundary condition was imposed, of equal outflow rates for each of the three horizontal channels in a given layer, so that each collected exactly $1/3$ of the total volume flow for that layer. In this enlarged system it was of importance to determine exactly which geometrical portion of the layer was being sampled by each of these three adjacent channels.

It was experimentally observed that the fluid in the central portion of the Staflo chamber did not mix with that near the walls [except for some special types of microconvection phenomena which are discussed elsewhere (27)]. This means that in general the center outlet for any layer sampled only the central portion of that layer.

In Fig. 8 is plotted (half of) the z -direction parabolic linear velocity profile. The area under the curve is proportional to the total volume flow rate for a layer of infinitesimal thickness dx . The area above any portion of the z -axis is then proportional to the volume flow rate through the corresponding portion of the layer. The coordinate z_1 is to be computed such that $2 \times \text{Area I} = 2 \times 1/3 (\text{Area I} + \text{Area II})$, or

$$\int_0^{z_{\max}} v dz = 3 \int_0^{z_1} v dz \quad (1)$$

Solving, we find that

$$\frac{z_1}{z_{\max}} = 0.226. \quad (2)$$

This result is interpreted to mean that $1/3$ of the volume flow passes through the center 22.6% of the chamber width.

It may be well to underscore here the qualitative differences between the horizontal and vertical effects of the outlet-level-control feedback. With the 2-dimensional array and collection system, this control does indeed establish this additional constant horizontal out-flow condition as originally proposed (12); but it does not impose a corresponding horizontal plug flow throughout most of the Staflo chamber, as does the analogous control in the vertical sense. The existence of (non-plug) horizontal laminar flow (except very near the outlet and inlet) is believed to result primarily from the lack of stabilizing density gradients, plus the smaller dimension in the horizontal sense.

V. RATE TYPE MIGRATION PROCESSES: LIPOPROTEIN STUDIES

Having investigated in some detail the 3-dimensional fluid flow properties within the Staflo chamber, we are in a position to consider the effects of these flow properties upon vertical migration of sample. We will restrict consideration to rate type migrations (14, 27) and to electrophoresis, although the discussion is also pertinent to other migration processes such as gravity sedimentation. Before taking up this discussion it is pertinent to consider a technical innovation called "programmed electric field" which has been used in our experiments and which has permitted a finer control of electrophoresis than previously.

A. THE PROGRAMMED ELECTRIC FIELD A number of authors have discussed the problem of interfacial or gradient density stability in non-flow and flow gradient systems subject to superimposed electrophoretic solute migration (2, 13, 15, 22, 24, 25, 26, 28). Such instabilities were not found to be troublesome in earlier Staflo work, in part because of the nature and concentrations of migrating solutes, but also in part because of the geometry of the electrode systems employed: either the platinum electrode did not extend all the way to

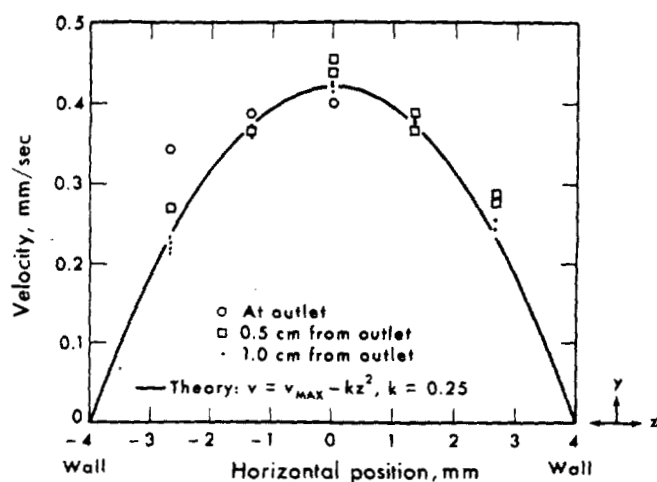


Fig. 7. Horizontal linear velocities measured near the outlets in the y-z plane at level 7. $\tau_{av} = 17.9$ min. The curve is the parabola having the equation shown,

MU-36572

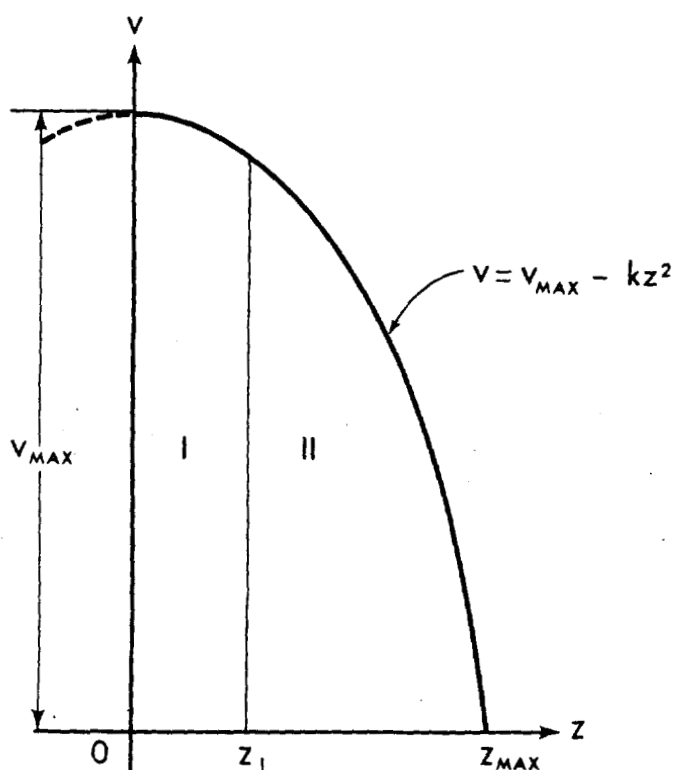


Fig. 8. Linear and volume flow relations for a fluid slab of thickness dx at any given vertical position (x) within the Staflo chamber (of half width z_{max}). Only one-half of the symmetrical y-z linear velocity profile is pictured. The coordinate z_1 is calculated to satisfy the relation: $2 \times \text{Area I} = 1/3 \times 2 \times (\text{Areas I} + \text{II})$. The areas are proportional to the volume flow rates through the corresponding fractional portions of the Staflo chamber.

MUB-13149

1175201

the inlet or a certain fraction of the electrode (up to 40%) was deliberately covered with an insulating material (11, 19). This permitted time for diffusion to stabilize the gradient regions and allowed a gradual transition into the region of full electric field for a migrating solute.

When protein experiments were started using an apparatus having only a single continuous strip electrode, instabilities sometimes developed if electrophoresis commenced just beyond the inlet of the Staflo chamber. These took the form of a visible convectional disturbance with resulting poor migration and reduced resolution of components. If the electric field were initially reduced or absent while diffusion occurred, stable electrophoretic migration could take place under exactly the same initial concentration, density, and fluid flow rate conditions, though at a downstream position (later time). Thus, this instability appeared to be of the above interfacial type wherein the initial density stability was upset by the effect (on local solution density) of the rapidly electrophoresing solute (24, 26). For better control over this phenomenon and over Staflo electrophoresis in general, a convenient and flexible method for varying the electric field and for establishing different fields in different regions of the Staflo chamber (even with high conductivity fluid present throughout) appeared desirable.

The first step was the construction of a segmented electrode system with five sections of approximately 6 cm each (separated from each other by a gap of $\sim 1/2$ mm) replacing the original continuous electrode (see Figs. 1 and 3). Depending upon which type of external connections was used, it was possible to use such an arrangement to lower the electric field in a given region of the Staflo cell in two basically different ways: 1) the electrode(s) in that region could be left unconnected or floating; and 2) the electrode(s) could be left unconnected to the electrophoresis power supply but shorted [top electrode(s) to bottom electrode(s)]. Experimentally, arrangement 1) was found to behave in a fashion intermediate between the earlier "no electrode" arrangement and arrangement 2).

Arrangement 2) has proved to be particularly effective for improving electrophoretic migrations because it reduces the effective electrical field between the electrodes to a value approximating zero. Furthermore, this is accomplished without introducing undesirable side effects that might be expected to occur, such as shorting out the power supply, draining off too much current in the shunt circuit, or providing too much extraneous heat. This results from the fortunate experimental fact that extreme polarization occurs at the small gap between the electrophoresis electrodes and the shorted electrodes. The small gas bubble which is formed and maintained in the gap acts as a very high resistance and reduces the shorting current to a few percent of the total current. During steady state operation of the Staflo apparatus, the total and shorting currents are nearly constant. Taking the commonly measured shorting currents (~ 5 -10 mA) with the measured external shunt resistance (~ 1 ohm), one calculates an electric field strength between the shorted electrodes of less than 0.1% of the electrophoresis field strength.

The use of several electrode segments also permits variant forms of electrophoresis. Different voltages can be impressed across the Staflo chamber at various places along the length of the cell, and the polarity can be reversed from place to place. Thus it becomes

possible to "program" the electric field to suit the needs of any particular experiment. A simple application of a programmed electric field is illustrated in Fig. 12.

B. THE LIPOPROTEINS Human serum lipoproteins are recognized to play an important role in normal metabolism and in disease. Few free-solution analytical electrophoretic data are available for these substances (1, 7), and a preparative electrophoretic separation method is also lacking. It is almost a requirement that, because of their tendency to adhere to surfaces, electrophoretic studies on these species be carried out by free solution methods, and for preparative separations zonal methods are strongly indicated. For these reasons Staflo electrophoresis (a free solution analytical and preparative zonal method) appeared particularly promising. A brief introduction to these substances is given here, as a preliminary to the subsequent discussion of their migration behavior (Section V D).

The lipoproteins are complex macromolecules consisting primarily of lipids and proteins (6). They are found in the serum of all normal mammals. Elevated (or lowered) concentrations of specific ultracentrifugal classes of lipoproteins have been closely correlated with certain pathological conditions including coronary disease and obesity (4). Lipoproteins contain between 1% and 99% lipid by weight and have estimated hydrated densities varying between 1.32 and 0.95 g/ml. Their molecular weights range from about 7×10^4 to 10^{11} , but most of those present in the blood serum range in molecular weight from about 2×10^5 to 10^7 and contain between 40% and 95% lipid respectively. The lipid moieties are composed of varying quantities of cholesterol esters, cholesterol, glycerides, unesterified fatty acids, and phospholipids (9). The relative amount of these particular lipids change from one lipoprotein class to another, as do their amino acid compositions. From the available data the lipoproteins appear to have electrophoretic mobilities which vary with the amount of unesterified fatty acids present in any class of lipoprotein (5, 8, 20). Chicken egg yolk lipoproteins have also been used in this investigation because of their abundance and ease of study. They appear similar in many respects to human serum lipoproteins though they are clearly not identical.

As this study progressed it became clear that we had an incomplete understanding of the fluid flow properties of the Staflo apparatus and also that the existing versions of the apparatus were limited in their applicability for the particular experimental conditions found useful for the study. On the other hand these serum lipoproteins collectively possessed many properties which favored their use for a study of the migration properties of an electrophoresing sample within the Staflo chamber. Some of these are: 1) densities near that of water, 2) reasonable solubility, 3) relatively high electrophoretic mobilities at the pH and ionic strengths used in the work, and 4) sufficient size to scatter visible light efficiently. This last property has made it possible to evaluate directly and instantaneously the electrophoretic migration of the lipoprotein sample.

C. EFFECT OF VERTICAL FLOW PROFILE The experimental data of Section III A developed the picture of a systematic deviation from idealized plug flow for the vertical flow profiles. Furthermore, the actual profile was seen to vary from point to point within the Staflo chamber. Since we are primarily interested in Staflo processes involving vertical

migration of solutes (e.g., electrophoresis or sedimentation), the cogent question to ask is: what are the quantitative consequences of these deviations from vertical plug flow on the migration path of one or more solutes? This kind of question also bears on considerations of analytical and preparative resolution of the Staflow method to be discussed in detail in a later paper. We will answer this question by considering the residence time τ for the various parts of the Staflow chamber and for various hypothetical migration behavior, as compared with the residence time τ_{plug} valid for the vertical plug flow region.

1. Any kind of migration through the central plug flow region. * By definition, in this region $\tau = \tau_{\text{plug}}$.
2. Individual sample particles migrating across a whole "horn." The area integrated across a whole "horn" closely approximates the area under an equivalent width of the plug flow region, so we can expect that $\tau \approx \tau_{\text{plug}}$.
3. Entire sample stream, components of zero mobility. In this closed system, for streams remaining intact, with Staflow feedback operative, the average stream's residence time is proportional to the reciprocal of its volume flow rate or to the reciprocal of its average vertical thickness. Computations from the flow rate data as well as analysis of the dye stripe patterns, indicate that (for the average over each whole stream): for streams 4-9, $\tau = \tau_{\text{plug}}$; for streams 3 and 10, $\tau = 0.91 \tau_{\text{plug}}$; for streams 2 and 11, $\tau \approx 0.87 \tau_{\text{plug}}$. For streams 1 and 12, adjacent to the membranes, the average τ appears to be about $1.2 \tau_{\text{plug}}$, with a possible continuous variation from $0.9 \tau_{\text{plug}}$ to a value which approaches infinity at the membrane.
4. Sample stream, migration starting in position corresponding to maximum velocity of horn,† components of non-zero mobility. Since in any normal experiment we would avoid causing to migrate towards the membrane a sample entering near the membrane, we will consider only migrations across the "horn" toward the central plug flow region. Several sub-cases can be considered.
 - a) Particles of high mobility moving soon into the plug flow region: $\tau \approx \tau_{\text{plug}}$.
 - b) Particles of nearly zero mobility (similar to case #3): $\tau \approx 0.87 - 0.91 \tau_{\text{plug}}$.
 - c) Particles of intermediate mobility such that they electrophorese just to the beginning of the plug flow region by the time the outlet is reached (see data in Table 1):
 $\min \tau \approx 0.85 \tau_{\text{plug}}$.
 - d) Full thickness sample stream, particles of the same intermediate mobility as in c); average for the whole stream: $\tau \approx 1/2 (\tau_{\text{plug}} + \min \tau)$ or $\tau = 0.92 \tau_{\text{plug}}$.

We may generally summarize these consequences of the vertical flow profile experiments as follows:

- (i) For almost any useful rate migration, with samples migrating through streams 3 and 10, to a very good approximation $\tau = \tau_{\text{plug}}$. Thus the average vertical plug flow assumption

* For simplicity, consideration of the variation of τ with z position is deferred until Section V D. It should be evident that $(\tau_{\text{plug}})_{\text{av}} = \tau_{\text{av}}$.

† Note that because of the diffusion time generally allowed before starting electrophoresis (see Section V A), if the sample enters the position of maximum "horn" velocity at the inlet (e.g., ~stream 3), by the time the field commences, the position of "horn" maximum will have moved up and out of stream 3 approximately to stream 2 (see Fig. 4A and Table 1).

will continue to be adopted for most experiments.

(ii) The maximum deviation of τ from τ_{plug} for a full width migrating stream will usually be less than about 10%, for the thinnest streams maybe up to about 17%. With carefully controlled conditions it is possible to see differences in τ of this magnitude, as changes in slope of the migration pattern.*

Since this analysis and statements 1 to 4 follow from the data of Tables 1 and 2, the quantitative conclusions depend on the particular (though typical) conditions of the experiments.

D. EFFECT OF HORIZONTAL FLOW PROFILE Using the data from Section III B, let us now calculate the steady state sample distribution profile in the vertical x-z plane at the outlet for a thin sample initially distributed uniformly throughout the x-z cross section of the sample layer, undergoing only vertical electrophoresis. The following additional conditions are assumed or have been shown to hold: 1) constant electric field strength is assumed; 2) the electrophoretic mobility of each species is taken as constant; 3) the entire liquid system is considered as non-convective and non-turbulent; 4) the horizontal fluid flow velocity profile within the Staflo chamber (Section III B) is given by:

$$v = v_{\text{max}} - k z^2, \quad (3)$$

where v is the linear velocity at any horizontal z position, z is measured from the center of the Staflo chamber, z_{max} is the half-width of the Staflo chamber, and k is a constant; and 5) vertical plug flow is assumed.

Before proceeding with the derivation, some additional definitions are necessary. All primed (') symbols refer to the region where electrophoresis actually occurs. Thus L is the length of the Staflo chamber, L' the length of the (unshorted) electrophoresis electrode. For the experiments reported here,

$$L' = 0.6 L. \quad (4)$$

(See Fig. 11.) The residence time τ , the time that any infinitesimal volume element spends within the Staflo chamber, is related to the flow velocity by

$$\tau = \frac{L}{v}. \quad (5)$$

Because of the parabolic nature of the horizontal profile, the average residence time for an infinitesimal volume element is related to the minimum residence time by

$$\tau_{\text{min}} = 2/3 \tau_{\text{av}} \quad (6)$$

and similarly

$$\tau'_{\text{min}} = 2/3 \tau'_{\text{av}}. \quad (7)$$

An obvious consequence of equations 3 and 5 is the existence of a variety of residence times τ as a function of z . From equations 4 and 5 for all electrophoresis times τ' (in any given x-y

* For certain experiments (e.g., cell sedimentation separations), the deviations from vertical plug flow could be (and have been) used in such a way that they lead to slightly increased preparative resolution.

plane),

$$\tau' = 0.6 \tau. \quad (8)$$

The basic equation of electrophoresis is

$$\lambda = \mu \tilde{E} \tau', \quad (9)$$

where λ (cm) is the distance electrophoresed, μ (cm/sec)/(volt/cm) is the electrophoretic mobility, and \tilde{E} (volt/cm) the (here constant) electric field strength. Combining equations 3, 5, and 9:

$$\lambda = \frac{2 \mu \tilde{E} \tau'_{av} z_{max}^2}{3(z_{max}^2 - z^2)}. \quad (10)$$

It is also very useful to have equation 10 expressed in terms of mobility, an important physical chemical property of any species. Solving for μ gives

$$\mu = \frac{3 \lambda (z_{max}^2 - z^2)}{2 \tilde{E} \tau'_{av} z_{max}^2}. \quad (11)$$

Equation 10 is the equation for the sample migration profile in the x-z plane at the outlet and gives a curve having the general form of an arch (see Figs. 9 and 10). Since the equation holds for any τ' , it can also be considered to apply at positions other than the outlet. The minimum migration distance, λ_{min} , occurs when $z = 0$ and after a time interval of $2/3 \tau'_{av}$. The migration distance theoretically increases without bound as the wall is approached (i.e., $z \rightarrow z_{max}$). Thus the curve for the electrophoretic migration distance λ does not intersect the wall but approaches it asymptotically.

This theoretical result has been tested by comparing actual photographs of sample migration profiles (as revealed by a slit-lamp illumination technique discussed in Section V E) with the theoretical migration curves calculated from equation 10, using the measured values of λ_{min} . One such comparison is shown in Fig. 10. The calculated curves are seen to coincide very well with the actual experimental profiles. This gives us some confidence in the assumptions outlined at the beginning of this section and which underlie the derivation of equation 10.

A 3-dimensional representation of a sample migration pattern corresponding to x-z profiles of the type shown in Figs. 9, 10, and 13 is given in Fig. 11. This figure also indicates schematically the operation of "shorted" and "electrophoresis" electrodes and an illustration of a programmed electric field (Section V A). Note that a straight-on side view of such a migration pattern would show an apparent widening of the initial thin (rectangular) sample stream during the electrophoresis. We refer to this phenomenon as "laminar defocusing." The effective widening may appear to the eye and may actually be considerably smaller than might be expected from a photograph such as Fig. 10, because of the saturation properties of the film. Thus, in Fig. 10, there is probably a considerably lower concentration (hence a relatively smaller amount) of material in the downward-extending "arms" than in the principal

THEORETICAL MIGRATION PROFILE: $\frac{\lambda}{\frac{2}{3}\mu\tau_{av}\tilde{E}}$ vs. $\frac{z}{z_{max}}$

$$\lambda = \frac{2}{3}\mu\tau_{av}\tilde{E}\left(\frac{z_{max}^2}{z_{max}^2 - z^2}\right)$$

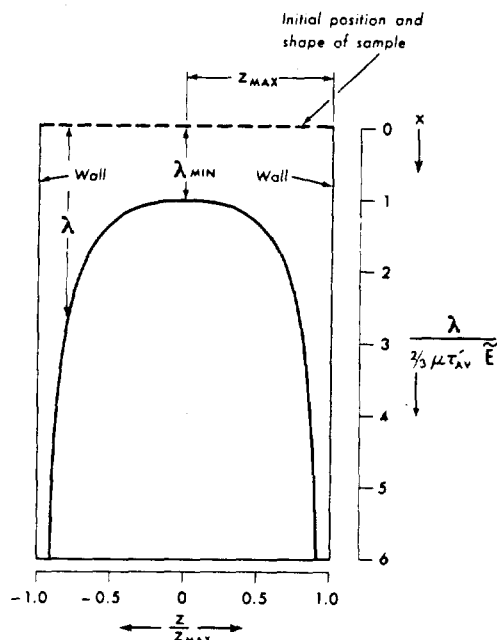


Fig. 9. Theoretical Staflo electrophoretic sample migration profile in the vertical x-z plane at the outlet, for a very thin monodisperse sample initially distributed uniformly and horizontally across the whole width of the Staflo migration chamber.

MU-36574

central portion. Evidence for this is given by the relatively narrow band of light-scattering material extending to the right (upstream) in Fig. 10.

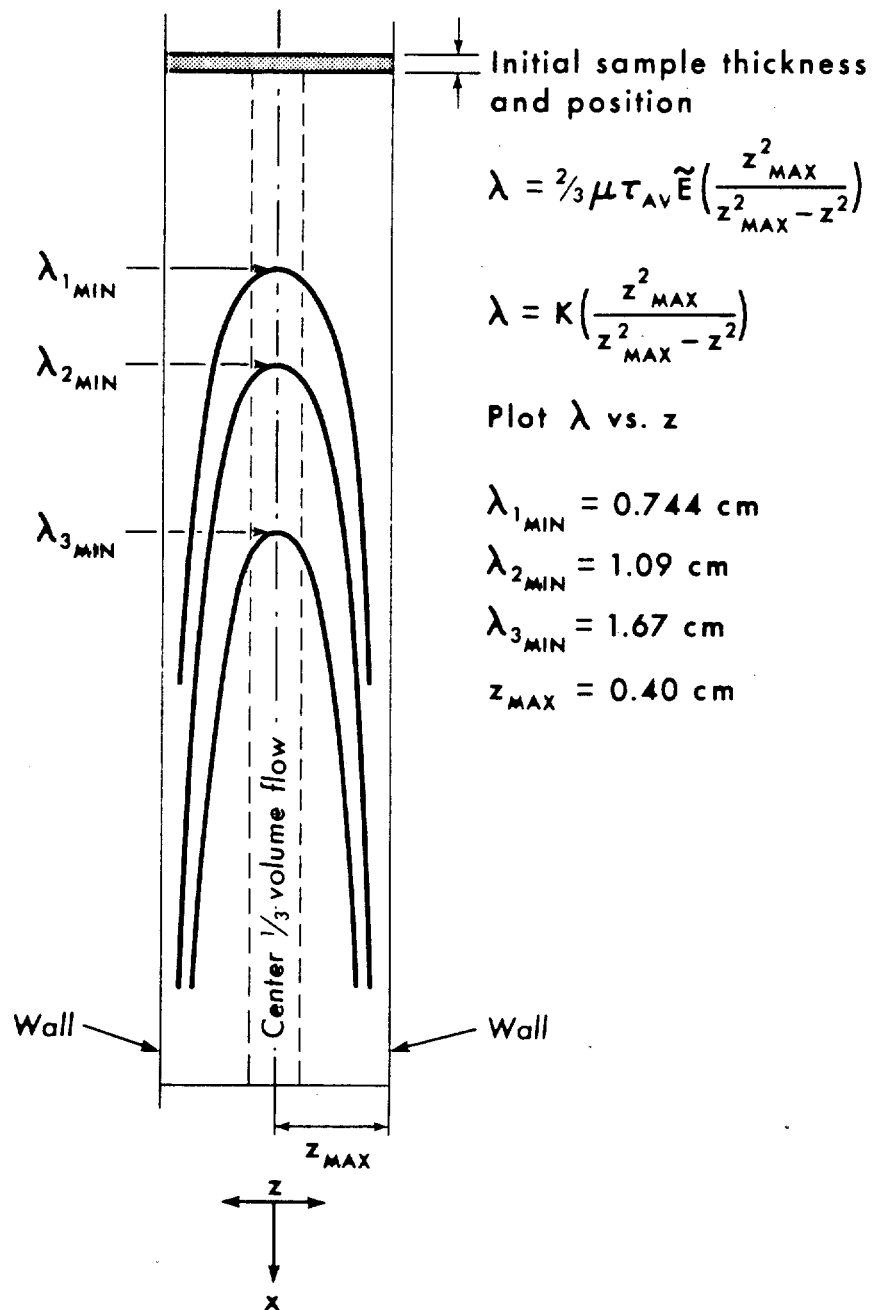
An electrophoretic migration pattern for a low-density human serum lipoprotein (S_f 0-10⁵) is shown in Fig. 12. The sample enters through inlet #3, flows through a 12 cm region of no electric field, then electrophoreses downward during the remaining 18 cm passage. In reality this sample contained a second, slower migrating electrophoretic component which is invisible in this photograph since it scatters light much less effectively. The constant migration slope, a quantity which depends upon flow rate, field strength, and mobility, as well as on pH and ionic strength of the solution, is evidence for the constancy of these parameters. From equation 11 [and using the applicable experimental conditions 3) Section II B, with pH 8.8, $\tilde{E} = 7$ volts/cm; $\tau_{av}' = 1224$ sec; $\lambda_{2min} = 1.38$ cm] we calculate the approximate minimum electrophoretic mobility for the particular S_f 20-10⁵ class of lipoproteins to be

$$\mu = 2.4 \times 10^{-4} \text{ (cm/sec)/(volts/cm)}.$$

This is an example of an analytical application of the Staflo method.

Figure 13 is an example of Staflo electrophoresis of a chicken egg yolk lipoprotein sample which contained three fractions by ultracentrifugal criteria. Migration conditions were similar to those in the experiment of Fig. 12. Section AA is an enlarged photograph of the migration profile also seen by scattered light using the slit-lamp technique (Section V E) just before the outlet, and indicates separation of at least three (and probably more) electrophoretic

OVERLAY OF THEORETICAL MIGRATION PROFILE



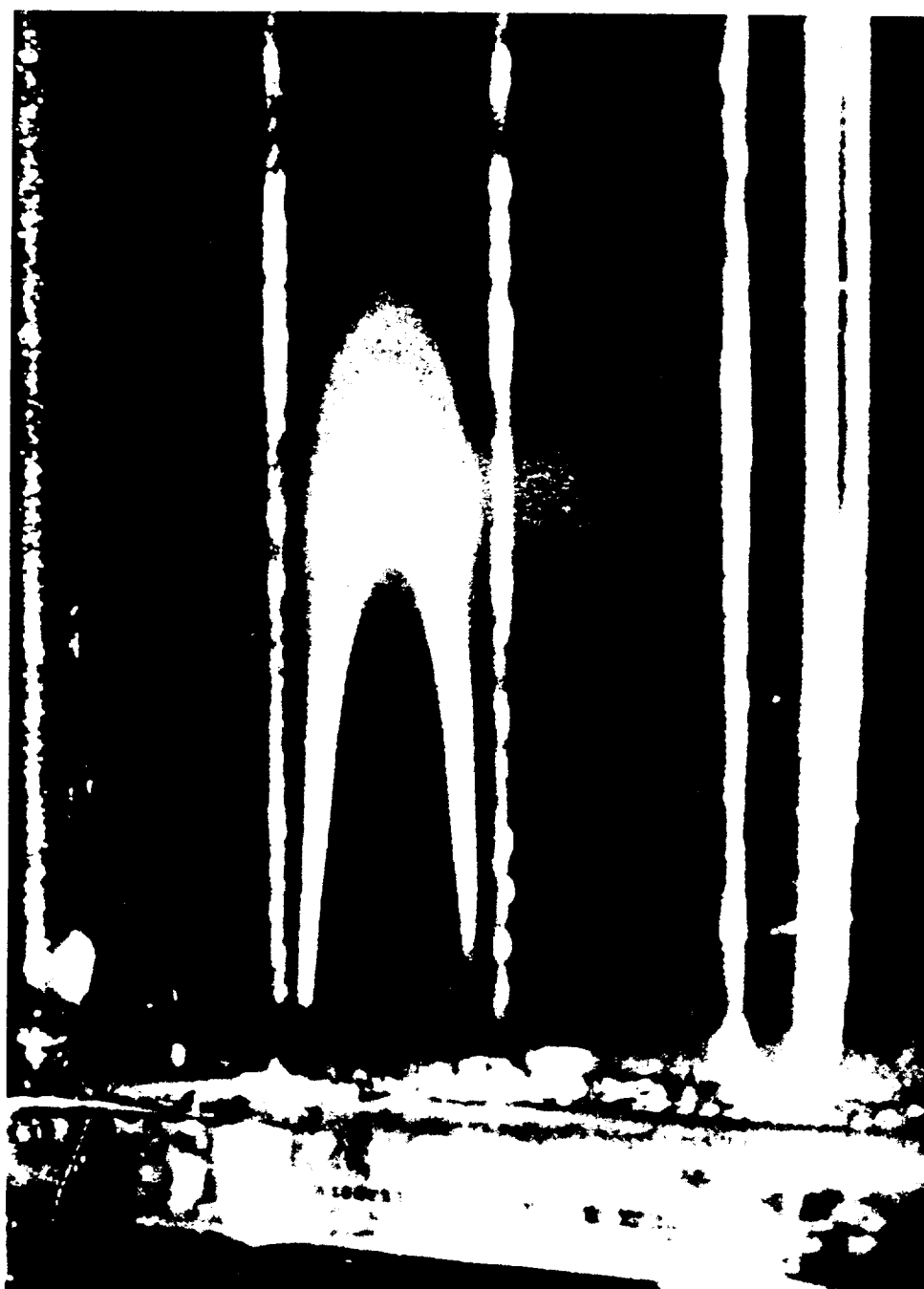


Fig. 10. Experimental Stafo electrophoretic migration pattern in the vertical x-z plane at the outlet. The sample is a 0.3% (wt/vol) human serum lipoprotein fraction, introduced as layer 6. Enlarged (foreshortened) photograph made by the slit-lamp technique. Overlay: theoretical migration profiles, calculated according to equation 10.

JHL-5257 and D5-4771

1175209

fractions. For the two faster fractions, the migration profiles are in good qualitative agreement with the theory of Section V D.

It should be pointed out that the various lipoprotein classes as defined by ultracentrifugal flotation methods are not single species but are populations having small, continuous variations in density (23). Such populations might also be expected to exhibit a range in electrophoretic mobilities. This in fact appears to be the case as can be seen from Figs. 10 and 13, where a given "separated" electrophoretic fraction (defined by its limiting arch-shaped envelopes, as e.g., $\lambda_{2\min}$ and $\lambda_{3\min}$ in Fig. 10) is considerably wider, at the $z = 0$ position, than is the initial sample.* From the magnitude of the final fraction thickness relative to the vertical spacing for the 2-dimensional outlet arrays in this Staflo cell (and in other, presently available higher resolution cells), two to four subfractions could be preparatively collected from a single fraction such as the bottom one in Fig. 10.

E. THE SLIT-LAMP TECHNIQUE The technique for viewing and photographing sample migration profiles such as those shown in Figs. 10, 12, and 13 is as follows. A thin vertical plane of light, formed by projecting the image of a thin slit with a slide projector, is directed normally to and focused approximately at the central x-y plane of the Staflo chamber. When the chamber is viewed obliquely at an angle of about 45° , the images seen are those given in the three figures. That is, those parts of the sample unilluminated remain invisible and the sample's cross section stands out in bold contrast to them. Because of the oblique angle of viewing, the photographs are not straight-on cross sections but foreshortened ones. (This foreshortening does not enter into the previous analytical calculations.) In order for a sample profile to give rise to such an image, it must either scatter light or fluorescence. Since most macromolecular and all cell samples do one of these to some extent at least, the method is of quite general utility.

After discovery of this observation method, a search of the literature of other fields revealed that a similar slit-lamp technique has long been employed for ophthalmological purposes (3).

VI. SUMMARY AND CONCLUSIONS

Staflo apparatus—previously unpublished features. Operation is described for a "3-dimensional," 36-channel Staflo cell having a 2-dimensional (3 wide by 12 high) outlet array. A new, segmented, "programmable" electrode system adds considerable flexibility to electrophoresis capabilities. An optical technique, based on the use of a focused luminous slit, permits viewing cross-sectional sample migration profiles.

Hydrodynamic properties of the "3-dimensional" Staflo system. Detailed local flow velocity measurements in the Staflo chamber show that the assumption of average vertical plug flow is good for almost all practical experiments. Horizontal (cross stream) flow profiles, however,

*The argument can be made that this widening is not an artifact, resulting from such factors as local non-uniform resistivity, if the envelopes calculated from equation 10 fit the experimental profiles.

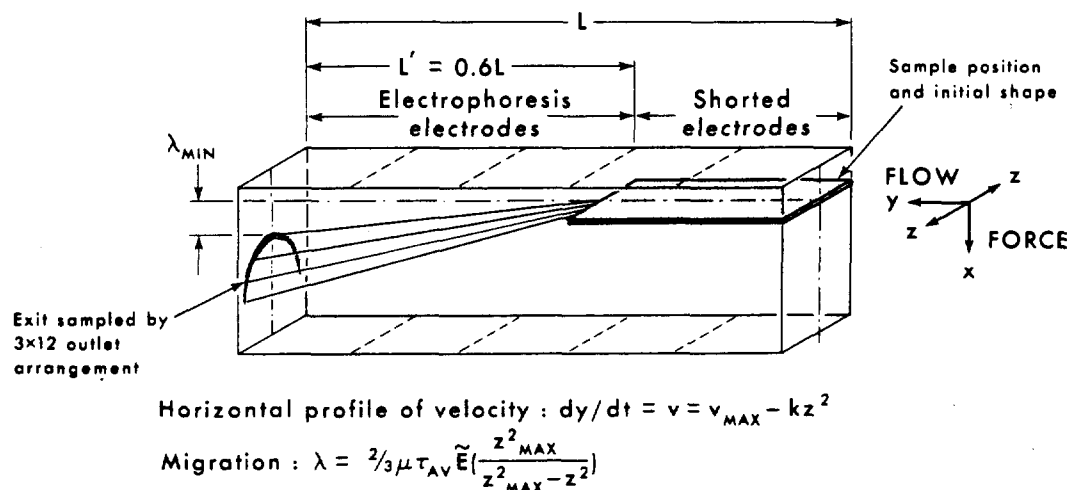


Fig. 11. Schematic perspective drawing of a Staflo electrophoretic migration pattern for a monodisperse thin sample. (The rays are shown only for the front half of the pattern).

MU-36566

are found to be parabolic almost everywhere throughout the 3-dimensional volume. The experiments reported here were performed under specific (though typical) experimental conditions of flow rate, solution densities, viscosities, etc. Similar quantitative measurements should eventually be made over a wide range of values for such variables. (Since one cannot exclude the possibility of a major functional dependence of these Staflo properties on particular apparatus parameters, it will also be eventually desirable to make additional measurements of this type using Staflo chambers of different dimensional characteristics. However, from operation of a large number of other Staflo chambers, having differences in overall dimensions, flow divider design, inlet and outlet spacing, total number of channels, etc., there is no present reason to expect major qualitative differences from the behavior reported here.)

Sample migration behavior. This has been investigated for "rate type" migrations of thin-slab samples initially distributed uniformly across the Staflo chamber cross section, and subject only to vertical migrations. As a result of the parabolic (cross stream) flow profiles, an arch-shaped cross-sectional sample migration profile is calculated theoretically and verified experimentally. The equation derived provides a more refined analytical expression for determination of (electrophoretic) mobilities in Staflo experiments than was previously available. A mobility determination is given for a sample of low density human serum lipoproteins, and a preparative electrophoretic separation described for a multicomponent egg lipoprotein sample. The value of the "3-dimensional" Staflo cell for higher resolution preparative separations following this type of migration is clearly evident.

Migrations of the above type actually constitute only a portion of the total spectrum of useful Staflo migrations. For non-rate-type migrations [e.g., where solutes are concentrated by "conductivity barriers" or at their isoelectric points in a pH gradient (14)] the sample

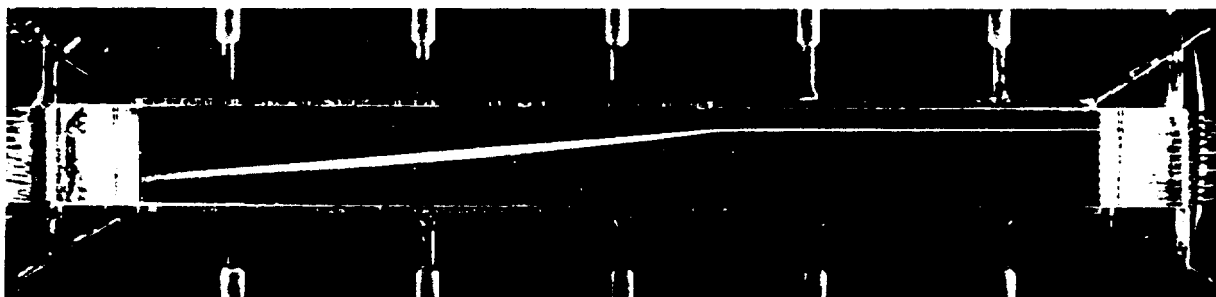


Fig. 12. Steady state Stafo electrophoretic migration pattern for a sample of low density lipoprotein ($S_0 \cdot 10^{-3}$) viewed by scattered light. Note the effect of the programmed electric field, with 40% of the electrodes shorted (right end). The electrolysis bubbles in the left 60% of the electrode chambers are flushed out sufficiently rapidly so as not to affect adversely the overall electrophoretic migration. (The numbers on the flow dividers are upside down but the migration is down as shown.)

JHL-5242

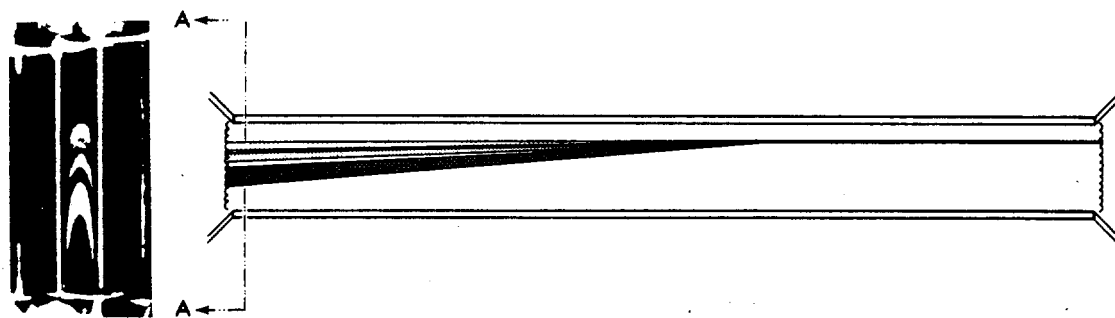


Fig. 13. Schematic drawing of an actual Stafo-electrophoretic separation of a "3 component" chicken (egg-yolk) lipoprotein sample with the first 40% of the electrodes shorted. The photograph (Section AA) made by the slit-lamp technique shows clearly the "laminar defocussing" phenomenon (Section VD) for a multicomponent sample.

JHL-6587

spreading tendency ("laminar defocusing") is effectively controlled by other opposing tendencies, so the simpler "2-dimensional" type analysis for overall average sample migration behavior can still often be used effectively. Furthermore, a variety of interesting phenomena of a different class has been observed or can be postulated in other experiments which will be reported and analyzed in a later publication. These involve some movement of sample in a horizontal (cross stream) as well as in a vertical direction, leading to a nonuniform distribution of sample across the Staflo chamber cross section. This can result in a drastic alteration of the arch-shaped sample migration profiles even for pure "rate type" migration processes, as for example in phenomena of "central sharpening" (27). For preparative separations involving these other types of migrations the original simplor (1 by 12 type vertical outlet array) Staflo apparatus may continue to be the apparatus of choice, on practical grounds of convenience.

In conclusion, it seems worthwhile to call attention to a certain aspect of the interdisciplinary nature of this study. As pointed out in the text, a principal motivation for commencing this work was the biological interest in lipoproteins themselves. It soon became apparent that these substances possessed a number of physical properties suiting them particularly well for investigating the interaction between general sample migration behavior and fluid flow properties in Staflo experiments. Thus there developed an interplay between the biological interests of the sample under study and the particular method used for the study. This interplay has given us a better knowledge of the Staflo apparatus and lays the groundwork for more definitive studies of the lipoproteins as well as of other biological (or non-biological) samples.

VII. GLOSSARY

<u>Symbol or term</u>	<u>Meaning</u>	<u>Units</u>
Flow pattern	The overall face-on appearance of the free boundary streams flowing from inlets to outlets in the Staflo chamber. (Fig. 6 is the inlet portion of a dye-stripe flow pattern.)	-
Flow profile (horizontal)	Linear fluid flow velocity profile in Staflo chamber, in any y-z plane; normally parabolic in shape (see Figs. 4B and 7).	-
Flow profile (vertical)	Linear fluid flow velocity profile in Staflo chamber in any x-y plane (see Figs. 4A and 5).	-
\tilde{E}	Electric field strength	V/cm ²
k	Apparatus parameter in laminar flow equation	(cm/sec)/cm ²
L	Length of Staflo chamber	cm
L'	Length over which electrophoresis takes place	cm
Laminar defocusing	The vertical widening of a sample stream migrating vertically according to rate type migration principles, resulting from the horizontal (z-direction) laminar flow profile.	-
S _f	Ultracentrifugal flotation coefficient	svedbergs
Sample migration pattern	The overall face-on appearance of a continuously flowing sample migrating vertically in the Staflo chamber (see Figs. 12 and 13 right).	-

1175213

<u>Symbol or term</u>	<u>Meaning</u>	<u>Units</u>
Sample migration profile	The appearance or shape of a migrating sample's cross section (see Figs. 9, 10, 11, 13 left).	-
Staflö	Short for "stable-flow free-boundary"	-
Staflö cell	Consists of upper and lower electrode chambers and Staflö chamber	-
Staflö chamber	Chamber in which electrophoretic or sedimentation migrations occur	-
v	Linear fluid flow velocity within Staflö chamber	cm/sec
v_{\max}	Maximum v ; occurs for $z = 0$	cm/sec
V	Volts	V
x	Vertical height coordinate	cm
y	Horizontal length coordinate	cm
z	Horizontal width coordinate	cm
z_{\max}	Half horizontal width of Staflö chamber	cm
λ	Electrophoretic migration distance	cm
λ_{\min}	Minimum λ ; occurs at $z = 0$	cm
μ	Electrophoretic mobility	(cm/sec)/(V/cm)
τ	Residence time; the time any given volume element resides in the Staflö chamber.	sec
τ_{av}	Average residence time; time required to pump a volume of fluid equal to the volume of the Staflö chamber	sec
τ_{\min}	Minimum residence time; occurs for $z = 0$	sec
τ'_{\min}	Minimum residence time for electrophoresis	sec
τ_{plug}	Residence time at any z position in the vertical plug flow region; $(\tau_{\text{plug}})_{\text{av}} = \tau_{\text{av}}$	sec

VIII. REFERENCES

1. Blix, G; Tiselius, A., and Svensson, H.; Lipids and Polysaccharides in Electrophoretically Separated Blood Serum Proteins; J. Biol. Chem. 137: 485, 1941.
2. Brakke, Myron K.; Zone Electrophoresis of Dyes, Proteins, and Viruses in Density-Gradient Columns of Sucrose Solutions; Arch. Biochem. Biophys. 55: 175, 1955.
3. Doggart, James Hamilton: Ocular Signs in Slit-lamp Microscopy, St. Louis, The C. V. Mosby Co., 1949.
4. Gofman, J. W.; deLalla, O.; Glazier, F.; Freeman, N. K.; Lindgren, F. T.; Nichols, A. V.; Strisower, B., and Tamplin, A. R.; The Serum Lipoprotein Transport System in Health, Metabolic Disorders, Atherosclerosis and Coronary Heart Disease; Inst. of M. Physics, Delmont, Calif., 1954, p. 413. Reprinted from Plasma, Milan, 1959, Anno II, No. 4.
5. Gordon, R. S., Jr.; Interaction Between Oleate and the Lipoproteins of Human Serum; J. Clin. Invest. 34: 477, 1955.
6. Gurd, F. R. N.: Lipid Chemistry, edited by D. J. Hanahan, New York, John Wiley & Sons, Inc., 1960, p. 277.
7. Kankel, H. G., and Trautman, R.; The α -lipoproteins of Human Serum. Correlation of

- Ultracentrifugal and Electrophoretic Properties; *J. Clin. Invest.* 35: 641, 1956.
8. Lindgren, F. T., and Nichols, A. V.; Structure and Function of Human Serum Lipoproteins; in *The Plasma Proteins*, Vol. II, edited by Frank W. Putman, New York and London, Academic Press, 1960, Chap. 11.
 9. Lindgren, F. T.; Nichols, A. V., and Wills, R. D.; Fatty Acid Distributions in Serum Lipids and Serum Lipoproteins; *Am. J. Clin. Nutr.* 9: 13, 1961.
 10. Mel, H. C.; New Method of Continuous Free Boundary Electrophoresis; *J. Chem. Phys.* 31: 559, 1959.
 11. Mel, H. C.; Biological Mixtures, Some Biophysical Problems, and the Stable-Flow Free-Boundary Method; Lawrence Radiation Laboratory Report UCRL-9108, Feb. 1960.
 12. Mel, H. C.; Stable-Flow Free-Boundary Migration and Fractionation of Cell Mixtures. I. Apparatus and Hydrodynamic Feedback Principles; *J. Theoret. Biol.* 6: 159, 1964.
 13. Mel, H. C.; Stable-Flow Free-Boundary Migration and Fractionation of Cell Mixtures. II. Laminar Flow and Density Gradient Stability; *J. Theoret. Biol.* 6: 181, 1964.
 14. Mel, H. C.; Stable-Flow Free-Boundary (Staflow) Migration and Fractionation of Cell Mixtures. III. Migration Principles--Sedimentation and Electrophoresis; *J. Theoret. Biol.* 6: 307, 1964.
 15. Mel, H. C.; On the Stability of Flow-Formed Interfaces, and a Diffusion-Gravity Controlled Enzyme-Substrate Reaction; *Chem. Eng. Sci.* 19 (11): 847, 1964.
 16. Mel, H. C.; Mitchell, L. T., and Thorell, B.; Continuous Free-Flow Fractionation of Cellular Constituents in Rat Bone Marrow; *Blood* 25: 63-72, 1965.
 17. Murphy, Glenn; *Mechanics of Fluids*, 2nd ed., Scranton, Penn., International Textbook Co., 1952, p. 148.
 18. Nikuradse, J.; Untersuchungen über turbulente in nicht kreisförmigen Rohren; *Ingenieur-Archiv* I: 306, 1930.
 19. Nobel, P. S., and Mel, H. C.; Electrophoretic Studies of Light-Induced Charge in Spinach Chloroplasts; *Arch. Biochem. Biophys.* 113: 695-702, 1966.
 20. Oncley, J. L.; Gurd, F. R. N., and Melin, M.; Preparation and Properties of Serum and Plasma Proteins. XXV. Composition and Properties of Human Serum β -lipoproteins; *J. Am. Chem. Soc.* 72: 458-464, 1950.
 21. Packer, L.; Nobel, P. S.; Gross, E. L., and Mel, H. C.; Fractionation of Spinach Chloroplasts by Flow Sedimentation-Electrophoresis; *J. Cell Biol.* 28: 443-448, 1966.
 22. Philpot, J. St. L.; The Use of Thin Layers in Electrophoretic Separation; *Trans. Faraday Soc.* 36: 36-46, 1940.
 23. Searcy, Ronald L., and Bergquist, Lois M.; *Lipoprotein Chemistry in Health and Disease*, Springfield, Ill., Charles C. Thomas, 1962, Table I, p. 9.
 24. Svensson, Harry; Hagdahl, L., and Lerner, K. D.; Zone Electrophoresis in a Density Gradient. Stability Conditions and Separation of Serum Proteins; *Sci. Tools* 4: 1, 1957.
 25. Svensson, Harry, and Valmet, Erkki; Large-Scale Density Gradient Electrophoresis. Part II. A Simple Experimental Technique Securing Perfectly Stable Zones and Full Utilization of the Separation Capacity of a Density Gradient Column; *Sci. Tools* 6: 13, 1959.
 26. Svensson, H.; Zonal Density Gradient Electrophoresis, in *Analytical Methods of Protein Chemistry*, Vol. I., edited by P. Alexander and R. J. Black, New York, Pergamon Press, 1957, pp. 193-244.

27. Tippetts, R. D.; Stable-Flow Free-Boundary Electrophoresis Theory and Practice as Applied to the Study of Human Serum Lipoproteins, Ph.D. thesis, Lawrence Radiation Laboratory Report UCRL-16290, 1965.
28. Tiselius, A., and Flodin, Per; Zone Electrophoresis, in Advances in Protein Chemistry, Vol. VIII, New York, Academic Press, 1953, p. 461.

1175216

Studies of RBC Lifespan Distribution Using Endogenous ^{14}CO Production

Stephen A. Landaw

Considerable interest has centered upon the determination of red blood cell (RBC) lifespan in normal and disease states. Although some information concerning RBC lifespan can be obtained from studies of the reticulocyte count, daily fecal stercobilin excretion, and the endogeneous production of non-labeled carbon monoxide (1), it is only with the use of tracers that detailed information can be obtained for quantitative definition of the parameters describing the distribution of RBC lifespans in the circulating blood.

The previously available tracer methods for determination of these parameters have been adequately reviewed elsewhere (2, 3, 4, 5). It has been stated (2) that most of the methods in current use suffer from one or more defects. The ideal method should have most, or all, of the following characteristics:

1. The time delay in the appearance of the material at the site of sampling, following its production, must either be minimal or readily measured.
2. The procedure should introduce minimal or no interference with normal physiology.
3. Uptake of the label into circulating RBC should approximate a "pulse" label, and continued availability of the label should be minimal.
4. Continuous collection of the material under study should be possible.

Recently a method was introduced for the in vivo detection and quantitation of endogenously produced ^{14}CO in the expired air of mammals, following injection of glycine-2- ^{14}C (6). The number two carbon atom of glycine is incorporated into the heme moiety of circulating RBC hemoglobin, and is the unique source of the 4 methene bridge carbon atoms of heme (7). When RBC are destroyed in the body, the heme ring is opened at the alpha-methene bridge carbon atom, with the oxidation of this carbon atom to carbon monoxide (8, 9). Thus, one mole of carbon monoxide is produced per mole of heme catabolized. Correspondingly, one mole of ^{14}CO is produced per mole of "labeled heme" catabolized. The ^{14}CO thus produced is excreted rapidly and quantitatively in the breath, without oxidation to $^{14}\text{CO}_2$ (10, 11). Therefore, the excretion rate of ^{14}CO in the breath reflects the destruction rate of labeled heme in the body. Since most of the ^{14}CO produced in animals after the first week arises from degradation of hemoglobin heme, RBC destruction can be studied continuously, without recourse to venesection or collection of other body fluids. In this paper, a kinetic analysis of RBC production and destruction in the mouse and rat will be presented, using analysis of ^{14}CO appearance

in expired air following administration of glycine-2- ^{14}C . The method will be discussed in terms of the characteristics outlined above.

MATERIALS AND METHODS

Animals used were 300-400 gram, male buffalo rats, and 17-26 gram, female LAF₁ mice. Rats were studied individually, following intravenous injection of 50 μCi of glycine-2- ^{14}C , under light ether anesthesia. LAF₁ mice were studied in groups of 5 animals, each mouse receiving 10 μCi of the labeled glycine intravenously, without anesthesia. Labeled CO was detected and quantitated as described elsewhere (6).

Uptake of the labeled glycine into heme of circulating RBC was studied in three normal rats. Following injection of the labeled glycine, small aliquots of peripheral blood (less than 0.15 ml each) were removed via tail vein puncture at 1, 2, 3, 6, and 10 days. The total amount of blood removed from each animal was less than 5% of the calculated total blood volume. RBC were washed three times in saline, and hemin was extracted and crystallized by the method of Labbe and Nishida (12). The hemin crystals were dissolved in pyridine, and hemin concentrations were determined spectrophotometrically. Hemin activity was determined by counting aliquots of the hemin solutions by liquid scintillation, in a toluene-PPO solution, with suitable standardization for the color quenching caused by the hemin. Duplicate determinations of hemin specific activity (dpm/mg) agreed within 2%. Uptake of the ^{14}C label into circulating RBC was analyzed in the usual fashion, using semilogarithmic paper, and a visual best fit to the data points.

The corrected data points for ^{14}CO excretion rate were fitted to appropriate mathematical formulae with a variable metric minimization ("VARMIT") least-squares fitting program (13). This is an iterative gradient method which determines local minima of differentiable functions with up to 40 dependent variables. This program, as modified by E. R. Beals, Lawrence Radiation Laboratory, Berkeley, was run on a CDC-6600 digital computer.

RESULTS AND DEVELOPMENT OF MATHEMATICAL MODELS Figure 1 compares the results obtained with this method with the labeling pattern of circulating rat RBC hemoglobin. In the period 10-40 days after injection of the labeled glycine, there is little change in hemoglobin activity, and excretion of labeled CO is minimal. In the period 40-90 days after injection, when there is a great decrease in hemoglobin activity, production of ^{14}CO is maximal. These findings suggested that the curve of excretion rate of ^{14}CO versus time after injection of labeled glycine would be approximated by the first derivative of the corresponding heme activity curve.

Mathematical treatment of heme activity curves has been adequately presented by others (2, 3, 4). The simplest formula, applied to the senescent destruction of circulating labeled cells produced following a pulse label, is derived from the Verhulst-Pearl growth curve, and has the form:

$$F(t) = \frac{C}{1 + e^{\alpha(t-T)}} \quad (1)$$

$$F'(t) = \frac{-d}{dt} [F(t)] = \frac{\alpha C e^{\alpha(t-T)}}{[1 + e^{\alpha(t-T)}]^2} \quad (2)$$

where C is the maximum specific activity of heme, T is the mean potential RBC lifespan for senescent death, t is the time after injection of the labeled precursor, and α is the coefficient of uniformity of lifespans about T . Using a set of values for the parameters T , C , and α in equation 1, and representing the ^{14}CO excretion rate curve as equation 2—the first derivative of equation 1—the results shown in Fig. 2 were obtained. The curve of ^{14}CO excretion rate versus time is seen to be symmetrically distributed about T , with a shape that is roughly gaussian. Both α of equations 1 and 2, and σ of the gaussian are measures of distributions about a mean. σ , the standard deviation, increases as the spread around a mean

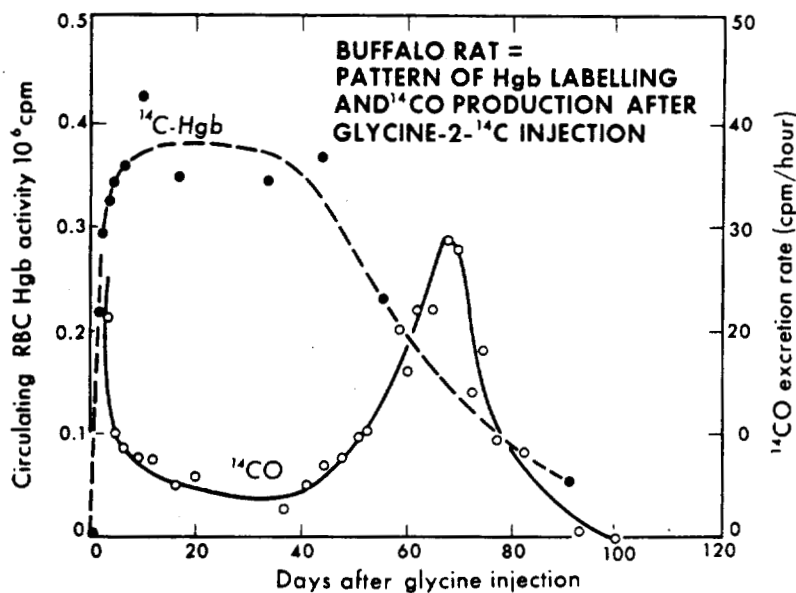


Fig. 1. Labeling pattern of RBC Hgb (closed circles, left ordinate) and breath CO (open circles, right ordinate) following injection of glycine-2- ^{14}C in normal buffalo rats. Only the downslope portion of the "early peak" for ^{14}CO production is shown.

MUB-11283

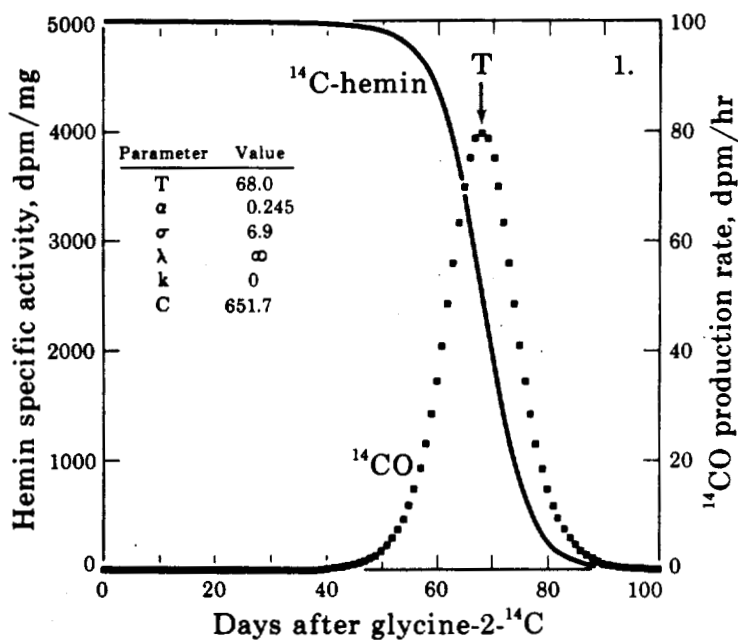


Fig. 2. Computer output showing theoretical labeling pattern for RBC hemin and breath CO from equations 1 and 2, using an arbitrary set of values for C, T, and α . Hemin specific activity has been stated in terms of dpm/mg, normalized to a maximum of 5000, for graphical purposes only. See text for discussion of parameters used.

DBL672-1546

portion of the heme specific activity curve could be approximated by equation 4, with an average value of λ of 1.19, or a mean labeling time of 0.9 day.

It can be appreciated that the non-instantaneous appearance of label in the circulating RBC causes an error in the determination of the true potential RBC lifespan on the order of the mean labeling time. The true potential RBC lifespan (T') can be approximated by:

$$T' = T - 1/\lambda . \quad (5)$$

In the rat, this correction is less than 1 day, while in man it is ten times larger. Shemin and Rittenberg introduced another mathematical form for this correction. They treated RBC destruction by examining the first derivative of the heme specific activity curves. The time at which the first derivative was maximal was taken as the mean potential RBC lifespan (T). The first derivative, corrected for delayed appearance of label in the circulating RBC, was obtained by adding the correction factor

$$-\frac{d}{dt} [\text{Heme}(t)]_{\text{corr}} = \frac{d}{dt} [\text{Heme}(t)] + \frac{1}{\lambda} \cdot \frac{d^2}{dt^2} [\text{Heme}(t)] . \quad (6)$$

The peak of this corrected first derivative was taken as the corrected mean potential RBC lifespan (T'). In the example given in their paper, this gave a value of T' of 127 days, whereas the uncorrected data gave a value of T of 133 days. It should be noted that equation 5 yields a value for T' of 124 days, only slightly different from the value obtained using the mathematically determined correction factor of equation 6.

Berlin, Hewitt, and Lotz (15) supplied a correction for the continuous availability of label in the glycine pool, by studying the specific activity of urinary hippuric acid, in man, following ingestion of non-labeled benzoic acid. Their results suggested that the continuous availability of label in the glycine pool causes a significant change in the descending portion of the heme specific activity curve. While this component was not specifically corrected for in our experiments, its effects contributed to the empirical correction inherent in equation 4.

With these corrections in mind, equation 1 can be improved by the following function:

$$\text{Heme}(t) = \frac{(1 - e^{-\lambda t}) C e^{-kt}}{1 + e^{\alpha(t-T)}} = (1 - e^{-\lambda t}) \cdot G(t) . \quad (7)$$

The appropriate form of the ^{14}CO excretion rate, the first derivative of $G(t)$ is

$$\text{CO}(t) = \frac{C e^{-kt} [2k + \alpha e^{\alpha(t-T)}]}{[1 + e^{\alpha(t-T)}]^2} = -G'(t) . \quad (8)$$

With the Shemin-Rittenberg correction, equation 8 becomes

$$\text{CO}(t)_{\text{corr}} = -[G'(t) + \frac{1}{\lambda} \cdot \frac{dG'(t)}{dt}] . \quad (9)$$

Figure 4 presents curves generated from equations 7 and 8, using a given set of values for C , k , T , α , and λ . Note that these curves approximate the shape of the curves

1175221

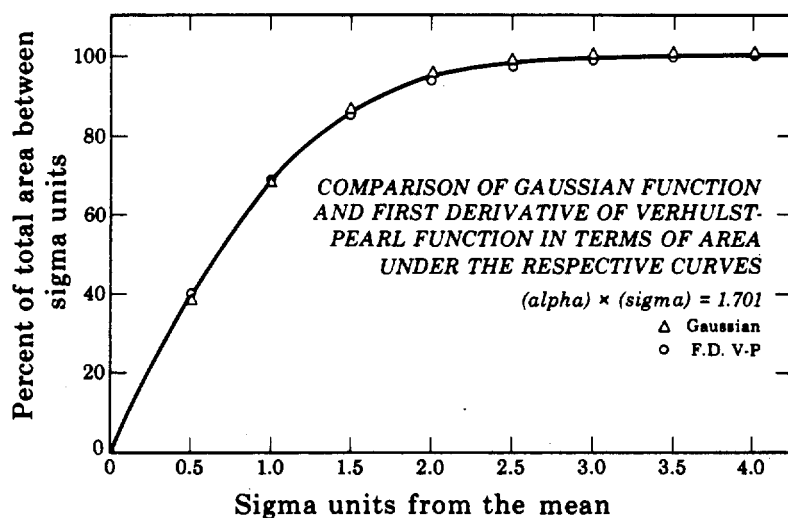


Fig. 3. Comparison of Verhulst-Pearl function (equation 2) with a Gaussian distribution in terms of area under the curves between sigma units. Comparable values of sigma and alpha were obtained from equation 3. Note the extremely close agreement.

DBL675-1633

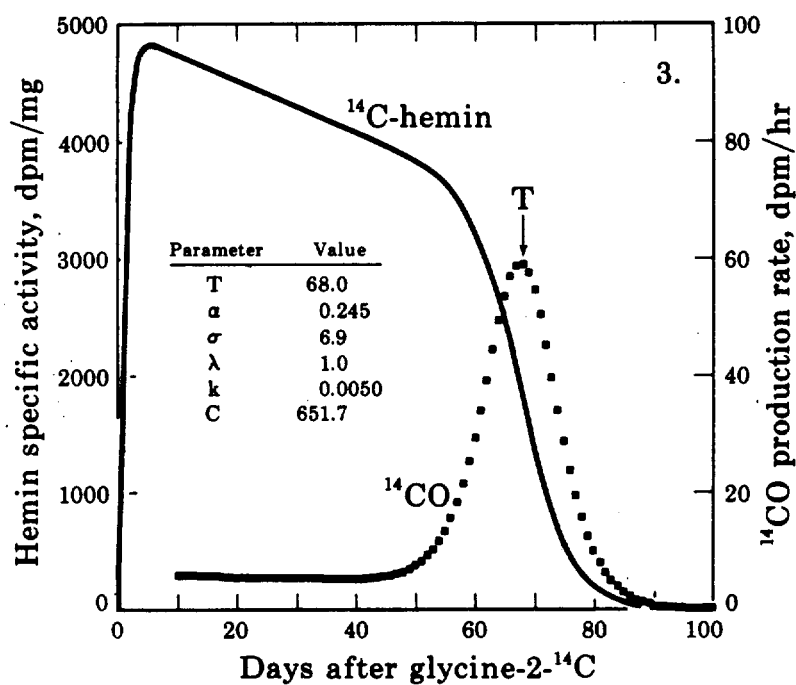


Fig. 4. Computer output showing theoretical labeling pattern for RBC hemin and breath CO from equations 7 and 8, using an arbitrary set of values for C, T, alpha, K, and lambda. Note again that hemin specific activity is normalized to a maximum of 5000 dpm/mg. The similarity between this figure and Fig. 1 should be noted.

XBL672-541

obtained from actual data in the rat, as shown in Fig. 1, in the period 20-90 days following injection of the labeled glycine. In the period before 20 days, there is another process which causes the production of labeled CO, the so-called "early peak," which has been described for labeled bilirubin (16), fecal stercobilin (17), and breath CO (6, 18). This early peak is partly associated with erythropoiesis, and partly associated with the turnover of non-hemoglobin hemes, especially the heme enzymes of the liver (19, 20). Only the downslope portion of this early peak is shown on Fig. 1, but it can be seen that its contribution to ^{14}CO production is considerable in the first few weeks after injection of labeled glycine. Labeled CO can, in actuality, be detected for more than 80 days in the hypertransfused (plethoric) mouse, in which erythropoiesis has been totally abolished. This is shown in Fig. 5, in which the ^{14}CO excretion rate following injection of labeled glycine is compared in one set of normal LAF₁ mice and one set of hypertransfused LAF₁ mice. Note that the late production of ^{14}CO , due to the destruction of labeled RBC, is entirely absent in the plethoric mice. However, the early peak is still quite prominent. In addition, ^{14}CO production can be seen to continue at a low, but significant, level from the end of the downslope of the early peak to more than 80 days after injection of the label.

In an attempt to account for this component of ^{14}CO production, it was assumed that the downslope portion of the early peak could be approximated by a single exponential function. The downslope of the ^{14}CO curves were plotted on semilogarithmic paper. For almost all of the rats and mice the data points could be connected by a single exponential regression line in the period between 3 and 14-21 days after injection of the label. This single exponential regression line was then continued up to 100 days, as the component of ^{14}CO production due to the processes responsible for the early peak. This correction probably underestimates the contribution from these processes. As discussed by Berlin, Hewitt, and Lotz (15), the continuation of these processes probably reflects the continued availability of label in the glycine pool as well as the processes responsible for the early peak.

The data points of ^{14}CO excretion rate were corrected for the above processes by subtracting the corresponding points of the single exponential extrapolation of the downslope of the early peak. Since most, or all, of the ^{14}CO production during the first 2-3 weeks was encompassed by this correction factor, it was impossible to determine the survival of labeled RBC less than about 20 days old by this method. Therefore, only the corrected data points obtained more than 20 days after injection of the labeled glycine were submitted for computer analysis. In an effort to obtain data on the survival of RBC less than 20 days old, cross-transfusion studies were performed in two rats. Two normal donors were given labeled glycine in the usual fashion. One animal was sacrificed 24 hr after injection of 100 μCi of labeled glycine, while the other was sacrificed 14 days after injection of 50 μCi of the labeled glycine. Approximately 2-3 ml of washed RBC were transfused intravenously into normal compatible hosts. In this manner, the only radioactivity in the hosts resided in the transfused RBC, and the components of ^{14}CO production due to the turnover of non-hemoglobin hemes and continuous availability of label in the glycine pool were absent. In only one host were there enough early data points to attempt a formulation of RBC survival in the period between 3 and 20 days after injection of the label. Results from these studies are presented in the subsequent section.

1175223

In summary, then, one factor for correction of ^{14}CO production related to the early peak was obtained for each animal from the downslope of the early peak obtained in that particular animal. This probably represents a minimal correction for the components of ^{14}CO production due to the turnover of non-hemoglobin hemes, ^{14}CO production associated with erythropoietic activity, plus the continuous availability of label in the glycine pool. The other factor for correction of the delayed appearance of labeled RBC in the circulation, λ , was determined separately in three normal rats, and the resulting average value was used for all the normal animals in this series. The corrected data points obtained more than 20 days after injection of the label were then submitted for the least-squares best fit to equation 8, the output of which gives the parameters α , C , k , and T . Sigma is then estimated from equation 3. The corrected mean potential RBC lifespan (T') is obtained from equation 5, or by applying the best-fit parameters from equation 8 to equation 9. A second program is now in process for fitting the corrected data points directly to equation 9. The output of this program yields the parameters α , C , k , and T' . Preliminary, unpublished results indicate that this latter program does not give a significantly better fit to the data points.

RESULTS OF THE DIGITAL COMPUTER ANALYSIS OF DATA IN RATS AND MICE

Complete data were available for 3 normal rats, 10 normal mice, and 2 cross-transfused rats. Partial data were available from 3 other rats in which early peak determinations were not performed. An example of results obtained in the normal rat is shown in Fig. 6, and in a group of 5 simultaneously-injected mice in Fig. 7. In both cases the best-fit curve for the downslope of the early peak is shown as a dashed line. The best fit to equation 8 for the uncorrected data points is shown as curves labeled "A," while the best fit for the corrected data points is shown as curves labeled "B." The parameters T , sigma, and k obtained for each of the two methods are also shown on the figures. It can be noted that the main difference is in the best-fit value for k , the parameter for random hemolysis. Uncorrected values for k averaged 1.18%/day, while the corrected values averaged 0.66%/day, in the rat. The corrected value agrees well with the value of 0.48%/day obtained by Belcher and Harriss, using ^{59}Fe in the rat (21).

Figure 8 shows results obtained in one of the cross-transfused rats. Data points are shown as solid circles, and the least-squares best fit to equation 8 is shown as a solid line. The excellent fit of the data points to the equation used can be seen for all points after 20 days. Before 20 days, the data points are all lower than the theoretical curve, suggesting that the cells are not as liable to random destruction at this period of time. These early data points fit, with some precision, a single exponential build-up of the form shown in equation 4, with a mean time of approximately 8 days. Experiments are now in progress to further delineate this "aging" function.

Mean RBC lifespans for the combined modes of death (random hemolysis and senescent death) were estimated by the use of three different models for the survival of RBC less than 20 days old. In one method, mean survival of all cells surviving more than 20 days was calculated (T_{m20}). This is clearly an overestimation, since the cross-transfused animals showed RBC death before 20 days. In the second method, mean survival was calculated by

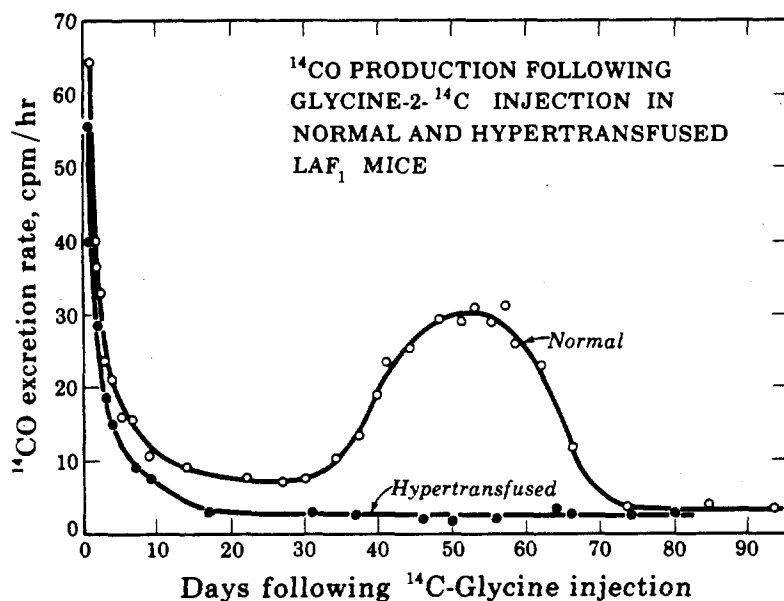


Fig. 5. ¹⁴CO excretion rate in normal and hypertransfused LAF₁ mice. Note that the "late peak" of ¹⁴CO production, due to the destruction of labeled circulating RBC, is entirely absent in the hypertransfused mice. However, the "early peak" is still present, although diminished in magnitude, followed by persisting, low level excretion of ¹⁴CO.

DBL673-1558

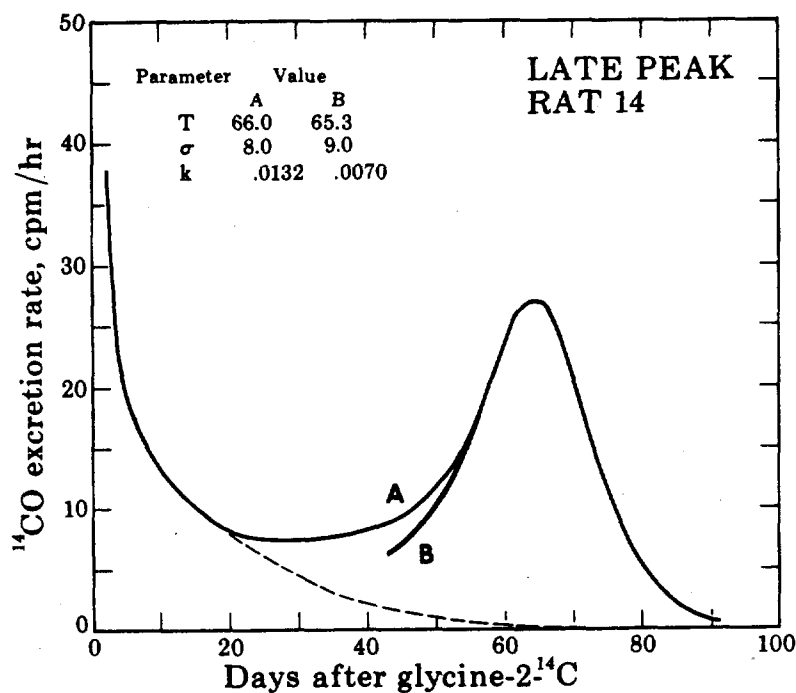


Fig. 6. ¹⁴CO excretion rate in a normal buffalo rat following injection of labeled glycine. Only the downslope portion of the "early peak" is shown, the extrapolation of which is shown as the dashed line. The least-squares best fit to the uncorrected data points is shown as curve A. The best fit to the corrected data points is shown as curve B. The best-fit parameters for each are also shown in this figure.

XBL672-544

1175225

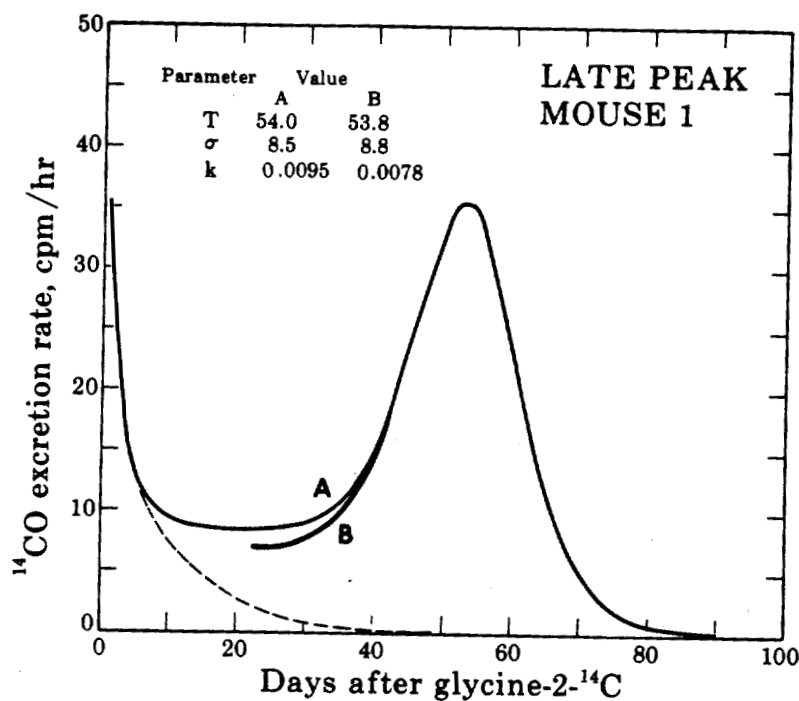


Fig. 7. ^{14}CO excretion rate in a group of five normal LAF₁ mice following injection of labeled glycine. See legend of Fig. 6 for explanation.

XBL672-539

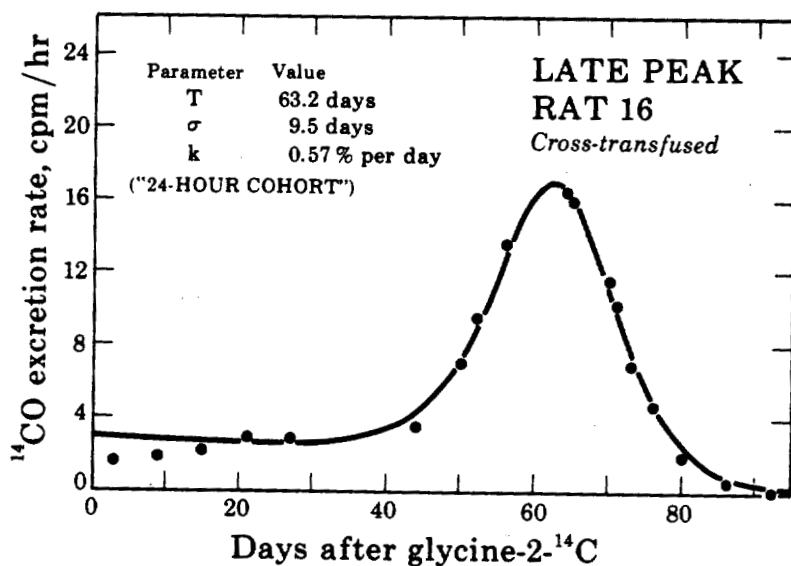


Fig. 8. ^{14}CO excretion rate in a normal buffalo rat transfused with washed, labeled rat RBC. The labeled cells were obtained by sacrificing a donor rat 24 hr after injection of labeled glycine. Data points are shown as closed circles. The least-squares best fit to equation 8 is shown as a solid line.

XBL672-542

assuming that random hemolysis was initiated at day 0 at the same rate as that found after day 20 (T_{m0}). This mean is probably an underestimation, since most of the labeled cells do not appear in the circulation until 2-6 days after injection of the label. The third mean was derived from results obtained in the cross-transfused rat shown above, with a single exponential form for the data points from equation 8 before 20 days. This mean (T_m) seems to represent the best estimate of the true mean survival, although T_{m20} is the only measure obtained without data extrapolation. In all cases mean survival was determined from the definition of the mean:

$$T = \frac{\sum_{t=0}^{120} CO(t) \cdot t}{\sum_{t=0}^{120} CO(t)} \quad (10)$$

($t = 0, 1, 2, 3, \dots, 120$).

The final results for mice and rats for the parameters T' , σ , k , and T_m are shown in Table 1. The number of animals studied for determination of each parameter is shown in parentheses, and the standard deviation about these means is shown when this calculation was possible.

DISCUSSION OF COMPUTER PROGRAM RESULTS The results shown in Table 1 for the buffalo rat agree closely with values reported by others for the mean potential RBC lifespan (T'), random hemolysis (k), and distribution of lifespans about the mean (σ) (21-25). The value obtained for the mean overall RBC lifespan (T_m) is also in the range of reported values, although the methods previously used to determine T_m are not similar to the one used here.

Belcher and Harriss (21) discussed the determination of mean overall RBC lifespan, and presented an integral equation for the determination of this mean. This formula, however, does not take into account the time taken for the labeled cells to enter the circulation, and leaves in question the survival of cells less than 2-3 weeks old, since this information may be lost in the uptake portion of the hemin curves. At this time there is not enough data to fully describe the survival of the RBC produced less than 20 days after injection of labeled glycine. The data points shown in Fig. 8 were obtained in a cross-transfused animal, in which the handling of blood may have caused artifacts in the survival of these cells. However, the values obtained for T , K , and α in the two cross-transfused rats were not significantly different from those obtained in normal rats, so that manipulation and host factors did not cause significant changes in the survival pattern of these cells.

Since the values obtained for random hemolysis (k) in the cross-transfused rats agreed with the corrected values for k in the normal animals, and not with the uncorrected values (cross-transfused = 0.51, corrected normals = 0.66, uncorrected normals = 1.18%/day), it was concluded that the form of the correction for the early peak ^{14}CO production was an

Table 1. Summary of results for parameters of RBC destruction in the buffalo rat and LAF₁ mouse. The number of animals used for each determination is shown in parentheses. The standard deviation about these average values is shown whenever this calculation was possible. The average value for C is not shown in this table.

Animal	Corrected mean potential lifespan T'	Standard deviation of potential lifespan σ	Random hemolysis k	Mean overall RBC lifespan T_m
Buffalo rat	64.8 ± 1.5 (7)	8.4 ± 1.3 (8)	0.0060 ± 0.0020 (5)	56.2 (7)
LAF ₁ mouse	52.8 (10)	10.5 (10)	0.0064 (10)	47.3 (10)

adequate approximation. These corrected values also agree with two other, independent estimates of random hemolysis obtained in this laboratory (26).

Since the glycine does not act as a true "pulse" label, it may be argued that the values of alpha and sigma obtained are in error, since labeled cells enter the circulation over a prolonged period of time. In this case, alpha values would be too small (3), and sigma values too large. This phenomenon is not corrected for in equation 8, but is specifically corrected for in equation 9. We were able to estimate the limits of the error involved in using equation 8 instead of equation 9 in the following manner: In those rats given 50 μ Ci of labeled glycine directly, the average value for sigma was 8.4 days; in the rat cross-transfused with "14-day old" cells, sigma was 8.2 days; in the rat cross-transfused with "24-hour old" cells, sigma was 9.5 days. It can be noted that there is no significant trend in the best-fit value for sigma with decreasing labeling time. Thus, either the method employed is insensitive to these changes or they are not significant in comparison with the other errors inherent in this system.

Parameters of RBC destruction obtained for the LAF₁ mouse do not agree closely with reports in the literature. Burwell, Brickley, and Finch (27) reported a mean lifespan of 20-30 days in the mouse, using ⁵⁹Fe, and noted that few cells seemed to survive after the 40th day. Their results also seem to show that RBC destruction occurred almost exclusively by random hemolysis. Using DFP³², van Putten (24) found a mean potential RBC lifespan of 40.7 days, and concluded that the labeling pattern was strongly suggestive of a true lifespan without random hemolysis. The results obtained by Edmondson and Wyburn (25) were similar to those reported by van Putten, with a mean potential RBC lifespan of 42 days, using DFP³². Although these two latter articles reported that the loss of activity with time was linear, inspection of the curves illustrated in both articles suggests that the best fit through the data points would be an exponential and not a straight line, which would imply a small component of random hemolysis, or elution of the DFP³² label. Ehrenstein (28), using glycine-2-¹⁴C as a hemin

label in mice, found a mean corrected potential RBC lifespan of 40-43 days in normal male TE mice, and 46 days in normal male C3H mice. The author found no evidence of random hemolysis in either group. Since in the present study, the shape of the ^{14}CO curves obtained in the LAF_1 mice was similar to those obtained in rats, it was concluded that the component of random hemolysis in this mouse strain is of the same order of magnitude as in the buffalo rat. Indeed, the average value for k was approximately the same in both species.

The values herein reported for T' and T_m may be in error due to the fact that the values for λ and the time-dependence of "random hemolysis" necessary for these determinations were obtained in normal rats. Although it is possible that these factors may be different in the mouse, this cannot have a great effect on the results obtained for T' , since incorporation of glycine into mouse RBC is even faster than in the rat. The calculated values for the mean overall RBC lifespan were: $T_{m20} = 50.0$, $T_m = 47.3$, $T_{m0} = 45.1$ days. It should be noted that, although the average values for mean potential RBC lifespan obtained by the DFP³² method (24, 25) and the glycine-2- ^{14}C method (28) were in the range of 40-46 days, a few normal mice were found by van Putten to have RBC lifespans of 50-59 days, in closer agreement with the values herein reported.

The value reported for σ , 10.5 days, is greater than that obtained for individual rats. It is possible that this value is excessive due to the fact that the mice were studied in groups of five. If each animal were to have a different value for T' and/or σ , this would result in a wider peak of ^{14}CO production, with a greater value of σ being obtained. However, as can be seen in Fig. 5, no individual peaks can be detected in the averaged peak obtained.

The values obtained for the parameter C , not shown in the figures or in Table 1, represent the maximum incorporation of the labeled glycine into the alpha-methene position of circulating RBC heme. Since glycine is the precursor for 8 carbon atoms of heme (8), the total amount of labeled glycine incorporated into RBC heme is 8 times greater. Knowing C , and the amount of activity originally injected, this amount can be calculated, and averaged 0.30% of the injected dose in the rat, and 0.35% in the mouse, not greatly different from the values reported by Robinson et al. (29).

SUMMARY

By studying the appearance of endogenously produced ^{14}CO in the breath following injection of glycine-2- ^{14}C , a continuous measure of the in vivo rate of destruction of labeled heme can be obtained. By suitable analysis of such data, parameters of RBC destruction can be defined in a physiologic manner, without recourse to venesection or examination of other body fluids. A mathematical model for such analysis is presented, along with application to data obtained in the buffalo rat and LAF_1 mouse. In the rat, the corrected mean potential RBC lifespan was found to be 64.8 days, with a component of random hemolysis of 0.60%/day. The standard deviation of lifespans about the mean averaged 8.4 days, and the mean overall RBC lifespan was estimated as 56.2 days. In the mouse, the mean corrected potential RBC lifespan was 52.8 days, with random hemolysis of 0.64%/day, and a standard deviation of

1175229

lifespans about the mean of 10.5 days, with an estimated mean overall lifespan of 47.3 days. Since the model presented is generally applicable, it is entirely suitable for the determination of parameters of RBC destruction in other animals, including man, in normal and disease states.

ACKNOWLEDGMENTS

The author is indebted to Dr. H. Saul Winchell for his valuable advice during the planning, execution, and presentation of these studies; to Dr. John H. Lawrence for supporting all phases of this work; to Mr. M. Horovitz for programming and executing most of the computer programs used in this study; and to Miss Kay Stoddard for her valuable technical assistance.

This work was supported, in part, by a Special Fellowship from the National Heart Institute, National Institutes of Health.

REFERENCES

1. Engstedt, L.; *Acta Med. Scand.*, supp. 332: 159, 1957.
2. Berlin, N. I.; Waldman, T. A., and Weissman, S. M.; *Physiol. Rev.* 39: 577, 1959.
3. Eadie, G. S., and Brown, I. W.; *Blood* 8: 1110, 1953.
4. Winchell, H. S.; in *Progress in Atomic Medicine*, edited by J. H. Lawrence, New York, Grune and Stratton, 1967, in press.
5. Berlin, N. I.; in *The Red Blood Cell*, edited by C. Bishop and D. M. Surgenor, New York, Academic Press, 1964.
6. Landaw, S. A., and Winchell, H. S.; *J. Nucl. Med.* 7: 696, 1966.
7. Wittenberg, J., and Shemin, D.; *J. Biol. Chem.* 185: 103, 1950.
8. Sjöstrand, T.; *Acta Physiol. Scand.* 24: 314, 1951.
9. Ludwig, G. D.; Blakemore, W. S., and Drabkin, D. L.; *Biochem. J.* 66: 38, 1957.
10. Tobias, C. A.; Lawrence, J. H.; Roughton, F. J. W.; Root, W. S., and Gregersen, M. I.; *Am. J. Physiol.* 145: 253, 1946.
11. Metz, G., and Sjöstrand, T.; *Acta Physiol. Scand.* 31: 384, 1954.
12. Labbe, R. F., and Nishida, G.; *Biochim. Biophys. Acta* 26: 437, 1957.
13. Davidon, W. C.; Argonne National Laboratory Report ANL-5990 (Rev. 1959).
14. Shemin, D., and Rittenberg, D.; *J. Biol. Chem.* 166: 627, 1946.
15. Berlin, N. I.; Hewitt, C., and Lotz, C.; *Biochem. J.* 58: 498, 1954.
16. Israels, L. G.; Skanderbeg, J.; Guyda, H.; Zingg, W., and Zipursky, A.; *Brit. J. Haematol.* 9: 50, 1963.
17. London, I. M.; West, R.; Shemin, D., and Rittenberg, D.; *J. Biol. Chem.* 184: 351, 1950.
18. White, P.; Coburn, R. F.; Williams, W. J.; Goldwein, M. I.; Rother, M. L., and Shafer, B. C.; *Blood* 24: 845, 1964.
19. Robinson, S. H.; Owen, C. A.; Flock, E. V., and Schmid, R.; *Blood* 26: 823, 1965.
20. Schwartz, S.; Ibrahim, G., and Watson, C. J.; *J. Lab. Clin. Med.* 64: 1003, 1964.
21. Belcher, E. H., and Harriss, E. B.; *J. Physiology* 146: 217, 1959.
22. Berlin, N. I.; Meyer, L. M., and Lazarus, M.; *Am. J. Physiol.* 165: 565, 1951.

1175230

23. Stohlman, F.; *Proc. Soc. Exptl. Biol. Med.* 107: 884, 1961.
24. van Putten, L. M.; *Blood* 13: 789, 1958.
25. Edmondson, P. W., and Wyburn, J. R.; *Brit. J. Exptl. Pathol.* 44: 72, 1963.
26. Landaw, S. A.; unpublished results.
27. Burwell, E. L.; Brickley, B. A., and Finch, C. A.; *Amer. J. Physiol.* 172: 718, 1953.
28. Ehrenstein, G. V.; *Acta Physiol. Scand.* 44: 80, 1958.
29. Robinson, S. H.; Tsong, M.; Brown, B. W., and Schmid, R.; *J. Clin. Invest.* 45: 1569, 1966.

Erythrokinetics in the Dietary Hypercholesteremia of Guinea Pigs

William K. Yamanaka, H. Saul Winchell and Rosemary Ostwald

Hemolytic anemia has been reported in association with dietary hypercholesteremia in rabbits (6, 14, 16, 5) and guinea pigs (10, 11, 12), hyperlipemia and alcoholism in man (22, 7), and hypocholesteremia of α -beta-lipoproteinemia in man (15).

Pinter and Bailey (14) in their study of dietary hypercholesteremia in rabbits, have presented evidence for an intracorporeal defect causing hemolysis in such animals. However, it was not clear from this work whether significant extracorporeal factors were also operative.

Definition of the erythrokinetics involved in the hemolytic anemia of guinea pigs is the subject of the present communication. The survival of circulating red cells in normal and anemic guinea pigs was determined by the use of both 2- ^{14}C -glycine and DF ^{32}P . The results for normal guinea pigs are discussed in relation to data in the literature and are compared with those in the anemic, hypercholesteremic guinea pig. Evidence is presented indicating that both intracorporeal and extracorporeal defects are operative in the hemolytic anemia of the hypercholesteremic guinea pig. The results are interpreted in terms of a possible mechanism which may also be operative in the anemia associated with the diverse abnormalities in lipid metabolism mentioned above.

MATERIALS AND METHODS

ANIMALS Young male guinea pigs, weighing about 250 g came from the same colony (Dependable Animal Supply, Martinez, California) but were not inbred. They were fed a semi-synthetic diet containing 30% casein, 10% cottonseed oil, and amounts of vitamins and minerals adequate for normal growth with or without addition of 1% cholesterol (13). Development of the anemia was monitored by periodic blood counts. When the blood count had fallen from a normal of 5-6 mill/mm³ to less than 4 mill/mm³ the animals were considered sufficiently anemic for labeling experiments.

LABELING OF RED BLOOD CELLS (RBC) Di-isopropylfluorophosphate- ^{32}P (DF ^{32}P) (New England Nuclear Corp., Boston, Mass., 1 mg/ml sterile propylene glycol), containing 250 $\mu\text{Ci}/\text{mg}$ DFP, and glycine-2- ^{14}C (same source, 1.7 mg in 10 ml sterile saline), containing 250 $\mu\text{Ci}/\text{mg}$ glycine, were used for labeling RBC in vivo. 0.2 ml of DFP solution was administered into the exposed jugular vein of the animal under ether anesthesia. This

procedure was necessary because of the inaccessibility of conveniently located veins of sufficient size in the guinea pig. The procedure was well tolerated with amounts up to 0.4 ml of solution. Glycine was administered by IP injection at a dose of 15-20 $\mu\text{Ci}/100 \text{ g body wt.}$

Blood samples were obtained from one of the larger ear veins 24 hr after administration of the label and subsequently 2-3 time/wk. Approximately 0.2 ml of blood was obtained at each sampling, and an estimated additional 0.05 ml was lost from the body at that time. Each blood sample was added to 9 ml saline. Red blood cells were separated by centrifugation, washed three times with saline, and resuspended in saline. A microhematocrit of the final suspension was obtained. 100 μl of the RBC suspension, in the case of the DFP-labeled cells, or of the hemolysate, in the case of the glycine-labeled cells, were counted on a gas-flow counter (Nuclear Chicago Gas-Flow Counter with a micromil window of surface density of less than 150 $\mu\text{g}/\text{cm}^2$). All samples from a given animal were counted at the same time. Total sample counts ranged from 250-8000 with corresponding background count during the same time interval of 100-150. Less than 15% of the samples had total sample counts below 500, with most of these occurring at the end of the RBC-survival curves.

CROSS TRANSFUSIONS To provide satisfactory controls, one donor and two recipient animals were used for each set. Thus both cholesterol-fed (C-fed) and control donors supplied blood for one C-fed and one control animal. 3 to 6 ml of blood were withdrawn from the exposed jugular vein of the donor animals under ether anesthesia, by means of a heparinized syringe. While the needle was still in the vein, the syringe was detached, and the withdrawn blood was replaced from another donor. In two of the donors (C-6 and A-3) the withdrawn blood was replaced with 3 ml of blood and 3 ml of saline. The labeled blood was then administered to a similarly prepared recipient animal (i.e., one from which an equivalent volume of blood had been withdrawn before administration of the labeled blood). Total blood volume was therefore not materially altered in either of the donor or the recipient animals, a condition necessary for the evaluation of counting data. The time between labeling and transfusion was 24 hr for DF^{32}P -labeled cells, in order to be as short as possible and still allow the donor animal to recover from the surgical trauma connected with the labeling procedure. In the case of glycine-2- ^{14}C -labeled cells, the period was 2-3 days, the time found to yield the maximum number of labeled cells (see Figs. 2 and 3).

EVALUATION OF DATA Survival of the circulating red cells randomly labeled with DF^{32}P was estimated by plotting the radioactivity as a function of time after labeling, on both linear and semilogarithmic paper. When the radioactivity decreased in a linear fashion, the data were fitted to a function of $y = mx + b$, where $y = ^{32}\text{P}$ activity in red cells, m = slope of the linear regression curve, and b = zero time intercept. This zero time intercept was taken as "100%" value in the subsequent calculations. The uncorrected mean red-cell survival time was then taken as the ratio b/m . When the radioactivity decreased in an exponential fashion, the data were fitted to a function of the form $y = ae^{-rt}$, where a = zero time intercept and r = slope of the curve. The mean life span of the red cells in this case was taken as $1/r$. In both cases a digital computer program was used to obtain the least-squares best fit of the data to the regression form used. The size of each blood sample removed for counting

1175233

(estimated total volume 0.25 ml) represents a sufficiently large fraction of the total blood volume to require a correction when calculating survival times of circulating RBC. This was accomplished for the cells labeled with $DF^{32}P$ by subtracting the fractional turnover rate of labeled RBC, due to blood sampling, from the total measured fractional turnover rate. The fractional loss of red cells from the animals due to blood sampling was taken as equal to the averaged daily loss of blood divided by the estimated blood volume calculated on the basis of body wt.

The survival time of circulating red cells, labeled as "cohorts" of similar age by means of $2-^{14}C$ -glycine, was similarly estimated. The shape of the curve relating radioactivity and time after labeling was used to judge whether or not marked random hemolysis was present. When significant random hemolysis did not appear to be present, the mean survival time (MST) of the cohorts of cells was estimated as the time interval between the points at which 50% of the plateau values was reached on the ascending and on the descending limbs of the curve (1). When marked random hemolysis was present, the MST was estimated to be $1/r$, where r = slope of the curve fitted to the function $y = ae^{-rt}$.

RESULTS

When circulating red cells of normal guinea pigs are randomly labeled with $DF^{32}P$, their survival can be approximated by a linear regression line ($y = mx + b$) (see Fig. 1). When a cohort of these red cells is labeled with $2-^{14}C$ -glycine, the function describing the number of ^{14}C -labeled cells remaining in the circulation versus time is consistent with linear survival and hemolysis due to senescence (Fig. 2). The lack of a definite hemolytic component in normal ^{14}C -labeled cells transfused into a normal recipient (Fig. 2) further suggests that the degree of random hemolysis in the guinea pig must be fairly small.

The MST of normal guinea pig red cells, as estimated from $DF^{32}P$ -labeling, varied from 54-60 days (3 animals with a mean of 59 days). When estimated by $2-^{14}C$ -glycine labeling, it was similar—57-70 days (4 animals with a mean of 63.5 days) (Table 1).

Random labeling of the red cells of anemic guinea pigs with $DF^{32}P$ revealed a pattern of survival which could best be fitted by a function of the form $y = ae^{-rt}$. The results demonstrated a markedly shortened mean red-cell survival time and a pattern consistent with random hemolysis (Fig. 1, Table 1).

When $2-^{14}C$ -glycine was administered to anemic animals, the maximum number of ^{14}C -labeled cells in the circulation was reached within 2-4 days and then diminished rapidly in an exponential fashion (Fig. 3). This result suggests that hemolysis of circulating cells in anemic hypercholesteremic guinea pigs is random in the sense that not only the older cells in the population are liable to time-independent, probabilistic hemolysis but also the young, newly formed cells.

To determine whether intracorporeal defects or extracorporeal factors or both were operating in these animals, the survival of labeled red cells in cross-transfusion

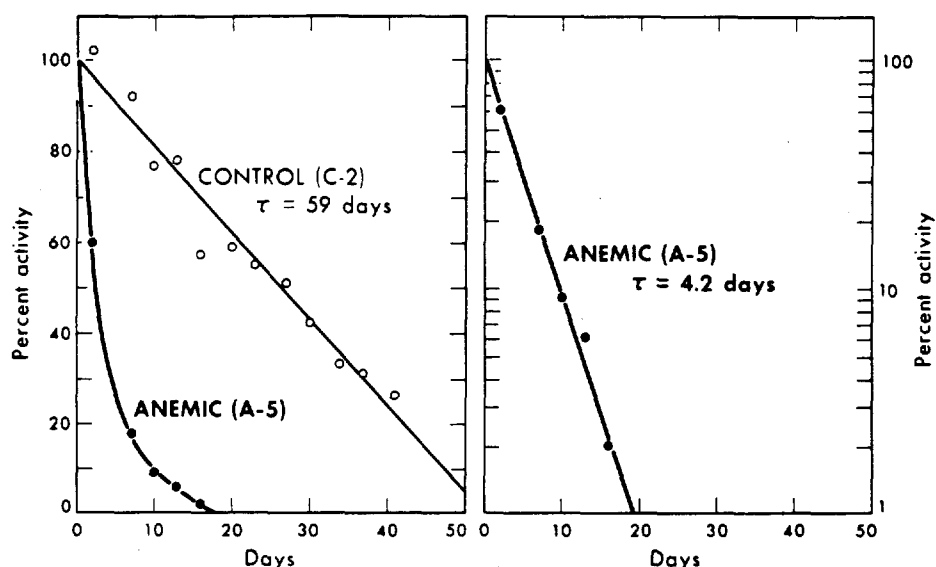


Fig. 1. Left: survival of $DF^{32}P$ -labeled red cells in a normal control and an anemic, hypercholesteremic guinea pig. The abscissa is expressed in days following intravenous injection of $DF^{32}P$, the ordinate, as percent of the zero intercept value for each set of data. In the case of the data for the control animals, the zero intercept value of b is taken from the linear regression equation, $y = mx + b$, and in the case of the anemic animal, the zero intercept value is taken as a from the exponential regression equation, $y = ae^{-\frac{t}{\tau}}$. For both the linear and exponential regression functions, the best fitting parameters were obtained by minimization of least squares of differences, by means of the digital computer. Right: a semilogarithmic plot of the data in the anemic animal. τ = survival time of labeled red cells.

DBL672-1531

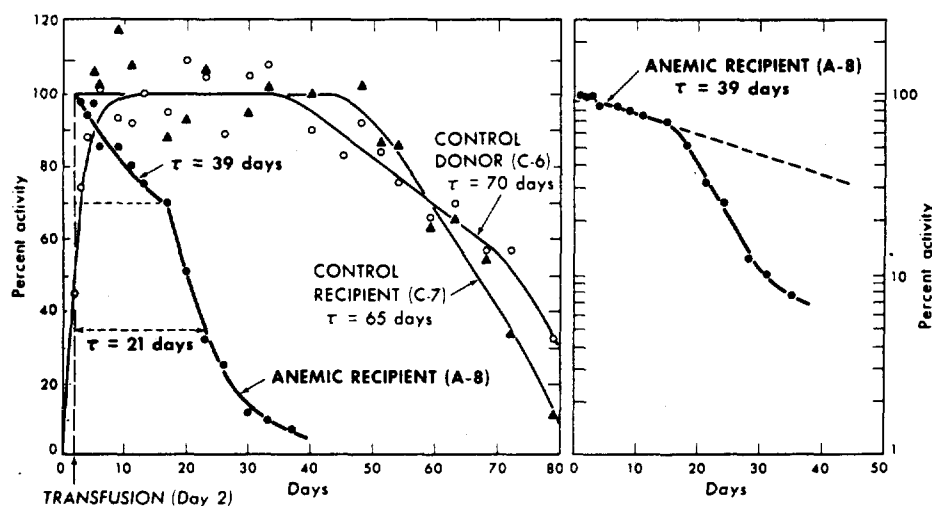


Fig. 2. Survival of glycine-2- ^{14}C -labeled red cells in a normal control donor, in a cross-transfused, normal recipient and in a cross-transfused, anemic, hypercholesteremic recipient guinea pig. For the normal, control animals the ordinate values are expressed as percent of the averaged ^{14}C -activity during the plateau phase. For the anemic animal the ordinate values are expressed as percent of the value obtained by extrapolation to the time of cross-transfusion. The method for estimation of mean survival of cells dying from senescent hemolysis is described in the text. The ^{14}C -activity of normal red cells transfused into an anemic recipient are plotted both on Cartesian (left) and semilogarithmic (right) coordinates. From 0 to 18 days, the data fit a regression function of the form $y = ae^{-\frac{t}{\tau}}$. Subsequent to 18 days, the curve takes on a sigmoidal shape. τ = as in Fig. 1.

DBL672-1533

1175235

Table 1. Mean survival time of red blood cells from cholesterol-fed anemic and normal control guinea pigs. *

Animal No.	Body wt at time of labeling, g	RBC at time of labeling, $\times 10^6/\text{mm}^3$	Label	MST, [†] days
C-1	500	N [‡]	DF ³² P	64
C-2	621	N	DF ³² P	59
C-3	648	N	DF ³² P	54
C-4	500	N	Glycine-2- ¹⁴ C	57
C-5	616	N	Glycine-2- ¹⁴ C	62
C-6	850	N	Glycine-2- ¹⁴ C	70
C-7	845	N	Glycine-2- ¹⁴ C	65
A-1	664	4.14	DF ³² P	22
A-2	620	2.60	Glycine-2- ¹⁴ C	5
A-3	457	3.07	Glycine-2- ¹⁴ C	7
A-4	624	4.20	Glycine-2- ¹⁴ C	10

*MST in cross-transfused animals are given in Table 2.

[†]Mean survival time.

[‡]Blood counts over 5 mill/mm³.

experiments was studied. The results of these experiments are summarized in Table 2, and examples are shown in Figs. 2, 3, and 4. When a cohort of newly formed red cells from a normal control animal was transfused into another normal recipient, the subsequent survival pattern obtained was consistent with senescent hemolysis with normal MST (Fig. 2). This result suggests that in the strain of guinea pig used, cross-transfused cells survive normally in a recipient animal. When labeled cells from the same normal control donor were transfused into an anemic recipient, the number of ¹⁴C-labeled cells in the anemic recipient's circulation diminished rapidly in a biphasic pattern. The initial, slow component indicated a markedly abnormal random destruction of approximately 2.6% of the cell population per day. At about the 18th day following the cross-transfusion, the rate of destruction of labeled cells in the anemic recipient markedly increased. If we consider the group of cells involved in the second, fast component of destruction as being victims of premature senescence, we can estimate their survival as described in the methods section. In the example shown in Fig. 2, this value was approximately 21 days. Other examples of biphasic patterns of red cell survival are listed in Table 2 (animals A-5, A-6, and A-7). These results indicate that normal cells are destroyed in an abnormal fashion in a hypercholesteremic anemic guinea pig. The pattern of survival appears to have two components, one related to increased random hemolysis and the other consistent with premature senescence. Iso-immunization as a cause of the biphasic pattern of destruction of transfused blood cells cannot be absolutely excluded on the basis of the experimental results. It appears to be unlikely, however, because no acceleration of cell removal was observed in other cases of transfusions (see Figs. 2 and 3, animals C-6 - C-7,

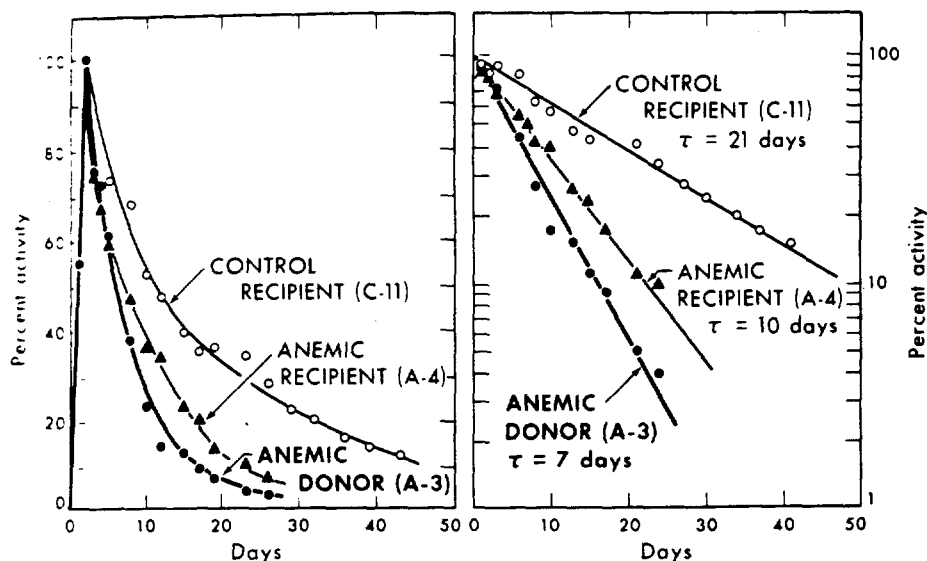


Fig. 3. Survival of glycine-2- ^{14}C -labeled red cells in an anemic, hypercholesteremic donor, a cross-transfused, anemic recipient and in a cross-transfused, normal control recipient guinea pig. The ordinate values are expressed as percent of the value obtained by extrapolation of the function $ae^{-t/\tau}$ to zero time. The data points before the time of maximum labeling of cells were not used. In all three cases, survival of ^{14}C -labeled red cells subsequent to the time of maximum labeling fit well a single exponential function consistent with the presence of random hemolysis. The slightly decreased rate of random hemolysis in the anemic recipient animal as opposed to that in the anemic donor animal reflects the less severe degree of anemia in the recipient as compared with the donor. τ = as in Fig. 1. Left: Cartesian coordinates; right: semilogarithmic coordinates.

DBL672-1534

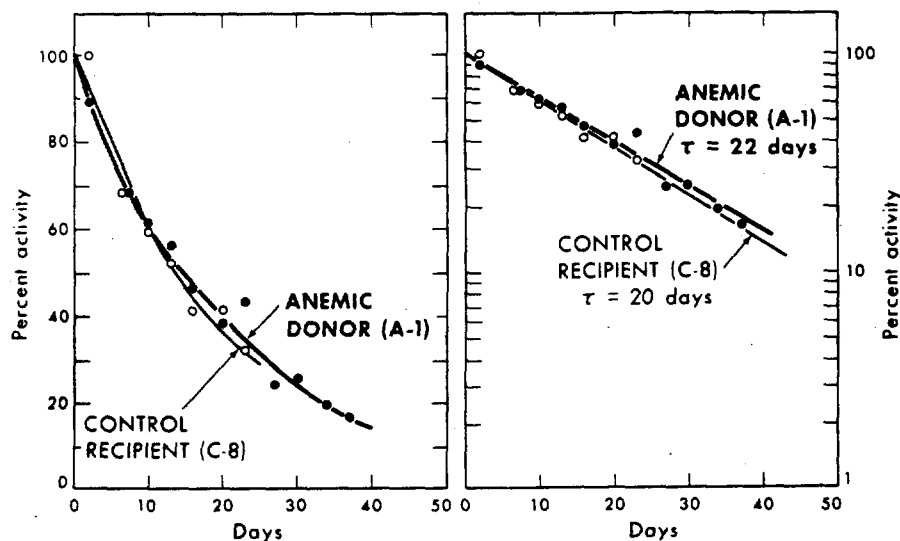


Fig. 4. Survival of DF^{32}P -labeled red cells in an anemic, hypercholesteremic donor and in a cross-transfused, normal control recipient guinea pig. Ordinate and abscissa units are the same as those used in Fig. 1. The survival of ^{32}P -labeled red cells in the anemic donor and the normal recipient are plotted both on Cartesian (left) and semilogarithmic (right) coordinates. The curves shown are those obtained with the least-squares best fit of the data to the form $y = ae^{-t/\tau}$. τ = as in Fig. 1.

DBL672-1532

1175237

Table 2. Mean survival times for red blood cells from cholesterol-fed, anemia and normal control guinea pigs after cross-transfusions.

Animal No.	Treatment	RBC, $\times 10^6/\text{mm}^3$	Label	MST, * days
C-2	Control donor	N [†]	DF ³² P	59
A-5	Anemic recipient	3.70	DF ³² P	4 [‡]
C-3	Control donor	N	DF ³² P	54
A-6	Anemic recipient	4.50	DF ³² P	22 [‡]
C-5	Control donor	N	Glycine-2- ¹⁴ C	62
A-7	Anemic recipient	4.60	Glycine-2- ¹⁴ C	19 [‡]
C-6	Control donor	N	Glycine-2- ¹⁴ C	70
C-7	Control recipient	N	Glycine-2- ¹⁴ C	65
A-8	Anemic recipient	4.70	Glycine-2- ¹⁴ C	21, §39
A-1	Anemic donor	4.14	DF ³² P	22
C-8	Control recipient	N	DF ³² P	20
A-9	Anemic donor	3.07	Glycine-2- ¹⁴ C	**
C-9	Control recipient	N	Glycine-2- ¹⁴ C	31
A-2	Anemic donor	2.60	Glycine-2- ¹⁴ C	5
C-10	Control recipient	N	Glycine-2- ¹⁴ C	9
A-3	Anemic donor	3.07	Glycine-2- ¹⁴ C	7
A-4	Anemic recipient	4.20	Glycine-2- ¹⁴ C	10
C-11	Control recipient	N	Glycine-2- ¹⁴ C	21

* Mean survival time.

[†] Blood count over 5 mill/mm³.

[‡] Overall MST.

§ Fast component 21 days, 70% of cells (days 15-35); slow component 39 days, 30% of cells (days 0-18).

** Died soon after labeling.

A-3 - A-4, and A-3 - C-11; Table 2 animals A-1 - C-8 and A-2 - C-10). Smith and McKinley (17), using inbred as well as different strains of guinea pigs, observed no differences of survival of ⁵¹Cr-labeled autologous and isologous RBC and only a slightly increased rate of disappearance of homologous cells, and they concluded that the survival curve of such homologous cells showed no evidence of "immune clearance."

Figures 3 and 4 (as well as the pair A-2 - C-10 in Table 2) show the effects of a "normal" environment on the survival of anemic cells labeled with ^{14}C and ^{32}P , respectively. In all cases the survival of these cells was well below a normal 59-64 days, indicating an intracorporeal defect of the anemic cells. In the case of DF^{32}P -labeled cells, which represent a random group of cells of all ages, the survival times in the anemic donor and in the control recipient were approximately the same. The survival of the glycine-2- ^{14}C -labeled cells in a control recipient, although not normal, was greater than in either the anemic donor or an anemic recipient. These cells represent a cohort of cells of uniform age. They had been exposed uniformly to the effects of the extracorporeal hemolytic surrounding for only 1-2 days before transfusion into the control recipient. Consequently, their survival in a "normal" environment was determined by the "intracorporeal" defect only, while the survival of those cells remaining in an anemic circulation was influenced by both the intracorporeal defect and extracorporeal factors.

DISCUSSION

CIRCULATING RED-CELL SURVIVAL TIME IN NORMAL GUINEA PIGS Previous measurements of MST of circulating RBC in normal guinea pigs yielded values of 83 days with ^{59}Fe (2), 60-70 days and 80-90 days with ^{51}Cr (4, 17). The value of 83 days for the life span of guinea pig red cells reported by Everett and Yoffey (2) was obtained under the assumption that the rate of new blood-cell production was equal to the rate of appearance of ^{59}Fe -labeled cells in the circulation following administration of the tracer. Evidence has been obtained which suggests that this is not a valid assumption because of the presence of a bone marrow-red blood cell pool the members of which are not significantly assimilating plasma radioiron. [See review, H. S. Winchell, 1967 (20).]

Smith and McKinley (17) estimated the MST by fitting an equation of the form $(1 - \underline{K}_1 t)e^{-\underline{K}_2 t}$ to the survival of ^{51}Cr -labeled cells. \underline{K}_1 was identified with "the constant daily change in the proportion of surviving cells" (e.g., loss due to senescence) and \underline{K}_2 was identified with the random loss of ^{51}Cr from elution and from random hemolysis. From their data the authors calculated an extrapolated extinction time of 112 days ($1/\underline{K}_1$) for autologous guinea pig RBC. They questioned the reliability of the extrapolation, however, because of the wide (95%) confidence interval (74-230 days) and suggested an "estimate" of 80-90 days for survival of guinea pig RBC. This value was obtained by an estimate of the "extinction" value of the asymptotic curve past the last measured point of 70 days, and is therefore open to question.

Our data indicate a MST of circulating RBC of 59 days when measured with DF^{32}P and of 64 days when measured with 2- ^{14}C -glycine. This agrees well with a maximum life span of 60-70 days reported by Grönroos (4). If it is present, random hemolysis must be small, judging from the linearity of the survival curves of DF^{32}P -labeled cells and the lack of a random hemolytic component in the survival curve of ^{14}C -labeled cells from blood of a normal animal transfused into a normal recipient.

RED-CELL KINETICS IN ANEMIC GUINEA PIGS In anemic hypercholesteremic guinea pigs the marked shortening of red-cell survival time is associated with random hemolysis. The course of the anemia appears to be related to a progressive increase in the rate of random hemolysis and incompletely increased, compensatory erythropoiesis.

The increased hemolysis of hypercholesteremic guinea pigs appears to be due both to intracorporeal defects and extracorporeal factors. The presence of intracorporeal defects is evidenced by shortened survival of labeled cells from anemic donors in normal recipients. These defects are associated with obvious morphological abnormalities (Fig. 5) similar to those seen in hypercholesteremic rabbits (16) and in man with acanthocytosis of α - β -lipoproteinemia (18). In the latter condition, hemolysis is mild, variable, or even absent, in contrast to the hypercholesteremic guinea pig and rabbit.

We have previously shown a markedly abnormal lipid composition of the red cells and bone marrow of hypercholesteremic, anemic guinea pigs (12, 13). Such abnormalities have also been shown in RBC membranes of hypercholesteremic rabbits (5) and in acanthocytes of man (15, 19). The importance of a normal lipid composition for the integrity of the red-cell membrane seems well established (8). It therefore appears that the abnormal composition of red cells is at least an important component of the intracorporeal defects that lead to morphological abnormalities and shortened cell survival of hypercholesteremic rabbits and guinea pigs and to certain diseases of man.

The presence of extracorporeal factors that cause hemolysis in hypercholesteremic guinea pigs is suggested by the diminished survival of normal red cells in such animals, apparently caused by a hemolytic milieu of the host. Although not reaching the same conclusion, Pinter and Bailey (14) obtained similar results in their cross-transfused hypercholesteremic rabbits. They showed that ^{51}Cr -labeled cells from normal rabbits had an abnormal pattern of survival in hypercholesteremic rabbits. They found that the 20% of labeled cells remaining in the circulation by the 14th day was removed at an abnormally accelerated rate. The most consistent interpretation of their data would seem to be that the accelerated destruction of that portion of transfused normal cells which had been circulating in the anemic host for an extended period of time was the result of some extracorporeal factor in the host.

It is known that the lipid constituents of the red cells exchange with lipid components of plasma. For instance, cholesterol of human red cells has been shown to have a turnover time of 8-24 hr (9). This is also suggested by the results of Frézal et al. (3) who showed that within 24 hr of replacement of 80% of the RBC mass in a patient with α - β -lipoproteinemia, most of the cells were morphologically altered. It is thus possible that reconstitution of the lipid content of red cells is abnormal in the presence of abnormal plasma lipids. Since we have previously shown an abnormal lipid composition of the plasma in the hypercholesteremic, anemic guinea pig (12), an abnormal remodeling of the circulating RBC membrane in the presence of an abnormal plasma lipid milieu could well account for the results presented in this paper. According to this view, the abnormal plasma lipid composition induced by dietary cholesterol produces its effects on RBC kinetics in guinea pigs by inducing abnormal proportions

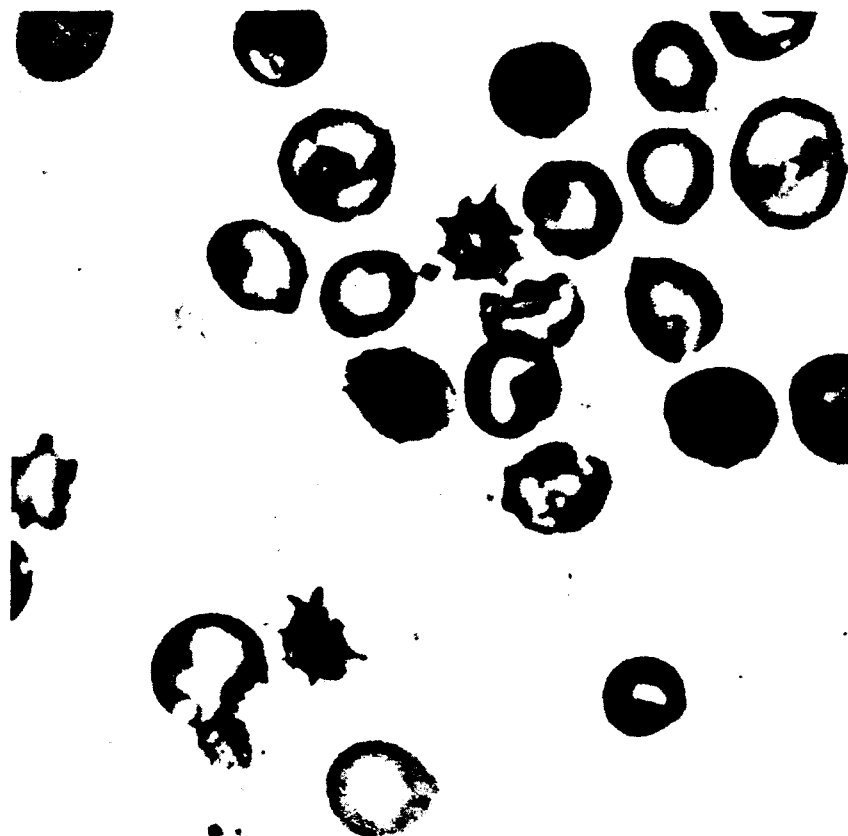


Fig. 5. Morphology of circulating red cells of an anemic, hypercholesteremic guinea pig. Peripheral blood smear. Wright-Gimsa stain. Magnification $\times 1860$. Note paleophilic stippling, a normoblast, and "horny" cells similar to those seen in acanthocytosis.

XBB677-4144

of lipid constituents in the red-cell membrane during the formation of the cell (resulting in an "intracorporeal defect") and during the remodeling of the lipid portions of the cell membrane in the circulation (resulting in "extracorporeal factors").

Present data are insufficient to rule out other contributing factors. The spleens of anemic guinea pigs are greatly enlarged due to erythropoietic proliferation, red-cell congestion, and fatty infiltration (12, 21). Splenectomy has, however, been shown not to alter the hemolytic anemia associated with dietary cholesterol in this species. Hemolysis secondary to lipid microangiopathy or the presence of hemolytic constituents in plasma are other possible causative factors. Such hemolytic agents have been suggested in the hemolysis and hyperlipemia attendant on Zieve's syndrome in man (7) and in chylous lymph. The latter, however, is hemolytic on contact, while the cholesterol-induced anemia develops slowly over a period of 8-12 weeks. Occasional members of our anemic, hypercholesteremic guinea pig population showed red-cell inclusion bodies which could possibly represent hemobartonella. However, neither inclusion bodies nor anemia was noted in six control and two cholesterol-fed

1175241

pre-anemic animals from the same colony within 1 month following splenectomy. Thus, while some parasitic destruction of red blood cells cannot be ruled out, it probably was not significant.

SUMMARY

Dietary hypercholesteremia in guinea pigs leads to a hemolytic anemia. In order to define the erythrokinetics, the survival of circulating red cells in normal and cholesterol-fed anemic guinea pigs was determined. The MST of RBC from normal guinea pigs was found to be 59-64 days. The linearity of survival indicated little random hemolysis. The MST of RBC from anemic guinea pigs was decreased to 5-20 days. The pattern of their survival was consistent with random hemolysis. A marked reduction of MST of normal cells when transfused into an anemic recipient suggested the presence of an extracorporeal, hemolytic factor in the anemic guinea pig. The MST of cells from an anemic animal transfused into a normal recipient remained well below normal indicating an intracorporeal defect of these cells. It is suggested that both the intracorporeal defect and the extracorporeal factor are the result of an abnormal lipid composition of the RBC membrane secondary to abnormal proportions of plasma lipids.

ACKNOWLEDGMENT

This work was supported in part by U. S. Public Health Service grant AM-08480.

REFERENCES

1. Berlin, N. I.; Waldmann, T. A., and Weissman, S. N.; Lifespan of Red Blood Cells; *Physiol. Rev.* 39: 577-616, 1959.
2. Everett, N. B., and Yoffey, J. M.; Life of Guinea Pig Circulating Erythrocyte and Its Relation to Erythrocyte Population of Bone Marrow; *Proc. Soc. Exptl. Biol. Med.* 101: 318-319, 1959.
3. Frézal, J.; Rey, J.; Polonowski, J.; Lévy, G. and Lamy, M.; L'absence Congénitale de β -lipoprotéines: Étude de l'absorption des Graisses Après Exsanguino-Transfusion Mesure de la Demi-Vie des β -lipoprotéines Injectées; *Rev. Franc. Clin. Biol.* 6: 677-683, 1961.
4. Grönroos, P.; The Life-Span of Guinea Pig Red Cells Estimated by the Use of $\text{Na}_2^{51}\text{CrO}_4$; *Austral. J. Science* 23: 195-196, 1960.
5. Hestorff, R.; Ways, P., and Palmer, S.; The Pathophysiology of "Cholesterol Anemia" in Rabbits; *J. Clin. Invest.* 44: 1059, 1965.
6. Ignatowski, A.; Über die Wirkung des tierischen Eiweisses auf die Aorta und die Parenchymatösen Organe des Känninchen; *Virchows Arch. Path. Anat.* 198: 248-270, 1909.
7. Kessel, L.; Acute Transient Hyperlipemia Due to Hepatopancreatic Damage in Chronic Alcoholism (Zieve's Syndrome); *Am. J. Med.* 32: 747-757, 1962.
8. Kögl, F.; de Gier, J.; Mulder, I., and Van Deenen, L.; Metabolism and Function of Phosphatides. Specific Fatty Acid Composition of the Red Blood Cell Membrane; *Biochim. Biophys. Acta* 43: 95-103, 1960.
9. Murphy, J. R.; Erythrocyte Metabolism. 4. Equilibration of Cholesterol- 4^{14}C Between

1175242

- Erythrocytes and Various Treated Sera; *J. Lab. Clin. Med.* 60: 571-578, 1962.
- Okey, R., and Greaves, V. D.; Anemia Caused by Feeding Cholesterol to Guinea Pigs; *J. Biol. Chem.* 129: 111-123, 1939.
- Okey, R.; Cholesterol Injury in the Guinea Pig; *J. Biol. Chem.* 156: 179-190, 1944.
- Ostwald, R., and Shannon, A.; Composition of Tissue Lipids and Anemia of Guinea Pigs in Response to Dietary Cholesterol; *Biochem. J.* 91: 146-154, 1964.
- Ostwald, R.; Darwish, O.; Irwin, D., and Okey, R.; Bone Marrow Composition of Cholesterol-Fed Guinea Pigs; *Proc. Soc. Exptl. Biol. Med.* 123: 220-224, 1966.
- Pinter, G. G., and Bailey, R. E.; Anemia of Rabbits Fed a Cholesterol-Containing Diet; *Am. J. Physiol.* 200: 292-296, 1961.
- Salt, H. B.; Wolff, O. H.; Lloyd, J. K.; Fosbrooke, A. S.; Cameron, A. H., and Hubble, D. V.; On Having No Beta-Lipoprotein. A Syndrome Comprising α -beta-lipoproteinemia, Acanthocytosis and Steatorrhea; *Lancet* 2: 325-329, 1960.
- Silver, M. M.; McMillan, G. C., and Silver, M. D.; Haemolytic Anaemia in Cholesterol-Fed Rabbits; *Brit. J. Haematol.* 10: 271-280, 1964.
- Smith, L. H., and McKinley, T. W., Jr.; Erythrocyte Survival in Guinea Pigs; *Proc. Soc. Exptl. Biol. Med.* 111: 768-771, 1962.
- Stanbury, J. B.; Wyngaarden, J. B., and Fredrickson, D. S.; *The Metabolic Basis of Inherited Disease*, 2nd ed., New York, McGraw-Hill, Inc., 1966, pp. 509-522.
- Ways, P.; Reed, C. F., and Hanahan, D. J.; Red Cell and Plasma Lipids in Acanthocytosis; *J. Clin. Invest.* 42: 1248-1260, 1963.
- Winchell, S. H.; Quantitation of Red Cell and Heme Production and Destruction Using Radioisotope Kinetics, in *Progress in Atomic Medicine*, New York, Gruene and Stratton, 1967.
- Zieve, L.; Jaundice, Hyperlipemia and Hemolytic Anemia: A Heretofore Unrecognized Syndrome Associated with Alcoholic Fatty Liver and Cirrhosis, *Ann. Int. Med.* 48: 471-496, 1958.

1175243

Similarity in Distribution of Skeletal Blood Flow and Erythropoietic Marrow

Donald C. Van Dyke

When studies were first begun on the use of radio-fluoride as an indicator of bone blood flow (1) and radioiron to map the distribution of erythropoietic marrow (2), the striking similarity between the distribution of blood flow and the distribution of marrow in the skeleton became apparent. This was true both in normal man and animals and in a variety of pathological conditions. These results clearly demonstrated a close relationship between bone blood perfusion rate and marrow growth and indicated that marrow proliferates only in those parts of the skeleton most richly supplied with blood, or that the growth of hematopoietic marrow induces a high blood perfusion rate in the surrounding bone.

The relationship between bone and hematopoietic marrow is one of the mysteries of biology. The fact that in fetal life and in disease erythropoiesis and granulopoiesis can occur outside the medullary cavity does not alter the fact that in the normal adult man hematopoietic marrow grows not only near bone, but only when surrounded by bone. In the fetus, erythropoiesis migrates from liver to the skeleton as soon as true calcified bone formation is established.

The fact that pathologically produced ectopic bone formation may be accompanied by the formation of a central cavity filled with hematopoietic marrow (3) emphasizes the mysterious connection between these tissues, but brings us no closer to an understanding of the special factor which a surrounding of bone provides to make the center attractive to primitive marrow precursor cells which migrate constantly through the circulation (4).

If one accepts the fact that there is something special about the medullary cavity for the growth of marrow, there is then the problem of why marrow growth in the adult is restricted to the cavities of certain bones or parts of bones. Why does hematopoietic marrow leave the bones of the extremities during maturation to become concentrated in the central part of

The object of this report is to demonstrate the remarkable correlation between distribution of skeletal blood flow and erythropoietic marrow and to speculate on the importance of skeletal blood perfusion rate as a controlling factor in marrow proliferation.

MATERIALS AND METHODS

THE POSITRON SCINTILLATION CAMERA The scintillation camera is a nonscanning electronic instrument for making pictures of the distribution of gamma-ray and positron-emitting nuclides *in vivo* (6). It contains an 11-1/2 in. diameter by 1/2-in. -thick sodium iodide crystal viewed by a hexagonal array of nineteen 3 in. diameter photomultiplier tubes. Scintillations produced in the crystal by gamma rays are displayed on an image-readout oscilloscope as bright flashes of light that correspond in position with the original scintillations. The flashes are recorded over a period of time, usually on Polaroid film where the 1000 - 10,000 or more dots that appear on the developed film form an image of the radioactive subject.

Pulse height selection is used so that only those scintillations that fall within a narrow range of brightness are reproduced in the image readout oscilloscope. With this system most background dots from stray and scattered gamma rays are eliminated.

Images of positron emitters are produced by detecting in coincidence the gamma-ray pairs that come from positron annihilation. The patient is placed as close to the image detector as possible and "collimation" is achieved by the positron focal detector located below the patient (2, 6). The focal detector has a single $9 \times 1\text{-}1/2$ in. crystal viewed by seven photomultiplier tubes.

The method of preparation of ^{18}F has been described elsewhere (7). The distribution of ^{18}F in the skeleton is determined by taking positron camera pictures 1 hr after intravenous administration of the tracer in the form of sodium fluoride. At this time uptake by the skeleton is maximum, and the blood level has fallen sufficiently so as not to interfere.

Because of its 2 hr half-life, ^{18}F delivers a relatively small radiation dose to the patient. Half of the administered dose is normally excreted via the urine. Assuming an intravenously administered dose of 200 μCi , and urine output at the normal rate of 1500 ml/day, and that the bladder is empty at the time of administration (the condition that results in the highest radiation dose), the integral radiation dose to the bladder is about 0.5-1 rad. The average dose received by the rest of the body, excluding bone, is less than 20 millirads. Areas of bone that concentrate ^{18}F receive a higher dose that is difficult to estimate. However, assuming an extreme case where 1/10 of the administered dose is taken up by 10 g of bone, the radiation dose is still below 1 rad. These estimates are similar to those of Blau et al. (8).

For the animal studies, adult rats, dogs, rabbits, monkeys, and an opossum were given ^{18}F intravenously and 1 hr later pictures were taken with the animal under barbiturate anesthesia.

1175245

The method of preparation of ^{52}Fe has been described in the literature (9). Iron-52 has an 8.2 hr half-life and decays 57% by positron emission and 43% by electron capture to the radioactive daughter (metastable) $^{52}\text{Mn}^m$. The daughter decays 100% by positron emission with a half-life of 21.3 minutes. The scintillation camera detects annihilation radiation from both nuclides, and there is no method of discriminating between them. This is a possible source of ambiguity in the pictures if the $^{52}\text{Mn}^m$ becomes free and able to travel about the body. However, there is no evidence that the $^{52}\text{Mn}^m$ does indeed become free. Manganese ion is removed from blood in the liver, but most patients examined by this method show no radioactivity in the liver. Those with known abnormal retention of iron in the liver have shown the expected uptake. The tentative conclusion has been made that the $^{52}\text{Mn}^m$ stays in the vicinity where it was formed by ^{52}Fe decay, or at least does not concentrate in any specific organ.

The upper limit of radiation dose to the bone marrow of a normal adult has been calculated to be 2.5 R for a 100 μCi dose, if immediate uptake of the ^{52}Fe in 1500 g of marrow is assumed, and if it is assumed that $^{52}\text{Mn}^m$ decays in the marrow. The irradiation is delivered almost entirely by positrons before they are converted to gamma-ray pairs. The average range of the positron is a few millimeters in soft tissue. Therefore the fat associated with marrow is irradiated, and its mass is included in the dose calculations.

A small amount of ^{55}Fe (approximately 5 μCi) is produced when 100 μCi of ^{52}Fe are made by bombardment of natural chromium. The half-life of ^{55}Fe is 2.6 years, but it decays entirely by electron capture and emits only 5.5 keV X rays. This radiation is not detectable by the scintillation camera. The permitted continuous body burden of this isotope is 1 mCi (10), so the few microcuries administered are of no practical consequence.

Pictures are taken about 16 hr after intravenous administration of 50 to 150 μCi of ^{52}Fe , when its uptake in marrow is maximum and its concentration in the blood is low. The field of view of the scintillation camera shows the marrow distribution in an area 20 cm in diameter with each exposure. Ten-minute exposures are taken of the areas where marrow may be found. To provide orientation, the pictures are cut out and glued to a drawing of a typical skeleton. For this purpose, plate 21 of Vesalius' Fabrica is used.

These studies of the similarity in distribution of skeletal blood flow and erythropoietic marrow required that the patient come one afternoon and the following morning. After completion of the ^{18}F bone blood flow study, ^{52}Fe was given and erythropoietic marrow distribution recorded the following morning.

Whenever possible a complete hematological work-up including iron kinetics studies and assay of the red cell-stimulating hormone, erythropoietin (11), were done at the Donner Laboratory clinic.

RESULTS

Development of the positron camera has made it possible to rapidly obtain pictures

of the distribution of radioactive ^{18}F in the living animal or human being. The initial uptake of fluoride occurs by exchange with the two calcium phosphate constituents of bone (12). The distribution of ^{18}F administered intravenously as fluoride ion is uneven in the normal skeleton. Furthermore, it is markedly altered in pathological conditions and accumulates at fracture sites, tumor sites, areas of osteomyelitis, in the lesions of Paget's disease, etc. The initial uptake of fluoride in bone is dependent on the rate of delivery of the isotope to each bone (blood perfusion rate) and the extraction efficiency of that bone. Evidence has been presented indicating that fluoride distribution in the skeleton is determined by differences in blood perfusion rate to the various bones rather than differences in extraction efficiency (1). We feel that ^{18}F distribution is an indicator of blood flow to bone.

Development of the positron camera has also made it possible to record the distribution of erythropoietic marrow in human subjects, using a dose of ^{52}Fe that is within that permitted for diagnostic purposes (2, 13). From such studies it has become apparent that wide variations in the distribution of marrow occur and that expansion and atrophy of the marrow may be classified into several characteristic patterns, but with considerable variation in detail (5).

In the normal adult human being, marrow is concentrated in the spine, pelvis, sternum, ribs, and proximal portion of the extremities. There are also variable amounts in the skull. The changing pattern during maturation has not yet been studied.

When the marrow of the human being is called upon to produce red cells at a rate somewhat in excess of normal, hypertrophy of erythroid marrow occurs at the expense of fat within those areas of the skeleton that contain marrow normally. Under such circumstances the gross distribution of erythroid marrow remains normal, as shown in Fig. 1B.

When the need for hypertrophy is greater than can be accommodated by replacement of fat, or when the usual sites are occupied by other elements, such as tumor or fibrous tissue, marrow expands into the bones of the extremities.

Marrow characteristically expands centrifugally, but there are great variations in detail (5). In some patients the bones of the legs will be more involved than those of the arms and vice versa. Heavy concentrations of marrow may extend to the distal ends of the femur without extension of marrow into the tibia. The tibia may be densely filled, with little or no marrow in the distal femur. The erythropoietic marrow is not always distributed with complete bilateral symmetry even in the absence of any known bone injury or disease. A given bone may be filled quite unevenly; i.e., the distal end of the femur may contain large amounts of marrow with little in the shaft, or the shaft may be filled evenly down to the lower $1/4$ where it stops abruptly. Within an otherwise completely filled femur or humerus there may be local areas devoid of marrow. In one case a completely isolated "hot spot" of erythropoietic marrow was found (11). Even in childhood or in the presence of massive marrow hypertrophy and peripheral extension in the adult, the caudal half of the sacrum rarely contains either erythropoietic or reticuloendothelial marrow (5). The local factors favoring or inhibiting the growth

1175247

of hypertrophied marrow are as obscure as are the factors determining the centripetal distribution of marrow in the normal adult subject.

It is known that the hemopoietic marrow is widely distributed throughout the skeleton in children and becomes centralized as the individual becomes mature (14). What variation there is in the age at which the mature pattern is established has not been determined by this method as no normal children or teen-agers have been studied, but the mature centralized pattern seems to be established by the age of 25 years.

Figure 1 compares the characteristic distribution of ^{18}F (bone blood flow) and ^{52}Fe (erythropoietic marrow) in adult human beings. The patient in Fig. 1A had multiple skeletal metastases from mammary carcinoma which were not associated with a change in ^{18}F uptake, and the patient in Fig. 1B had polycythemia secondary to congenital heart disease, but the distribution of isotope in the two cases was characteristic of the pattern seen in normal subjects. Comparison of the two figures shows that distribution of the two isotopes is identical except that normally the bones adjacent to the knee have a significant fluoride uptake but do not normally harbor hematopoietic marrow. Note the absence of uptake of either fluoride or iron in the caudal half of the sacrum.

Figure 2 compares bone blood flow and marrow distribution in a case of primary erythrocytosis in a 4-year-old girl. Extensive investigation revealed no evidence of cardiac, pulmonary, renal, or central nervous system pathology. Her hemoglobin was 18.5 g and hematocrit was 56%. The total circulating red cell volume was 59 ml/kg (normal children: 25-33 ml/kg). Typical of primary polycythemia, erythropoietin was not detectable in a 72-hr urine sample concentrated by collodion adsorption (11). Note the heavy concentration of both fluoride and iron in the knee and ankle. The bright spot in the pelvis in Fig. 2A is excreted ^{18}F remaining in the bladder.

Figure 3 compares bone blood flow and marrow distribution in the case of a 45-year-old woman with pernicious anemia and early myelofibrosis. Note the heavy uptake of ^{18}F in the distal femora and the similar distribution of erythropoietic bone marrow, ^{52}Fe . The increased uptake of fluoride in the elbow and wrist was not associated with erythropoietic marrow.

Figure 4 compares bone blood flow and marrow distribution in a 19-year-old girl 4 months after a midfemoral fracture. Note the increased uptake of fluoride in the femur distal to the fracture and the similarly distributed increase in erythropoietic marrow. Fluoride-18 is seen in the bladder in Fig. 4A.

Figure 5 shows ^{18}F uptake and ^{52}Fe distribution in a patient with hemolytic anemia of 3 years duration. There was an abnormally high bone blood flow in the knee, ankle, and elbow, Fig. 5A, corresponding to the pattern of peripheral extension of marrow, Fig. 5B.

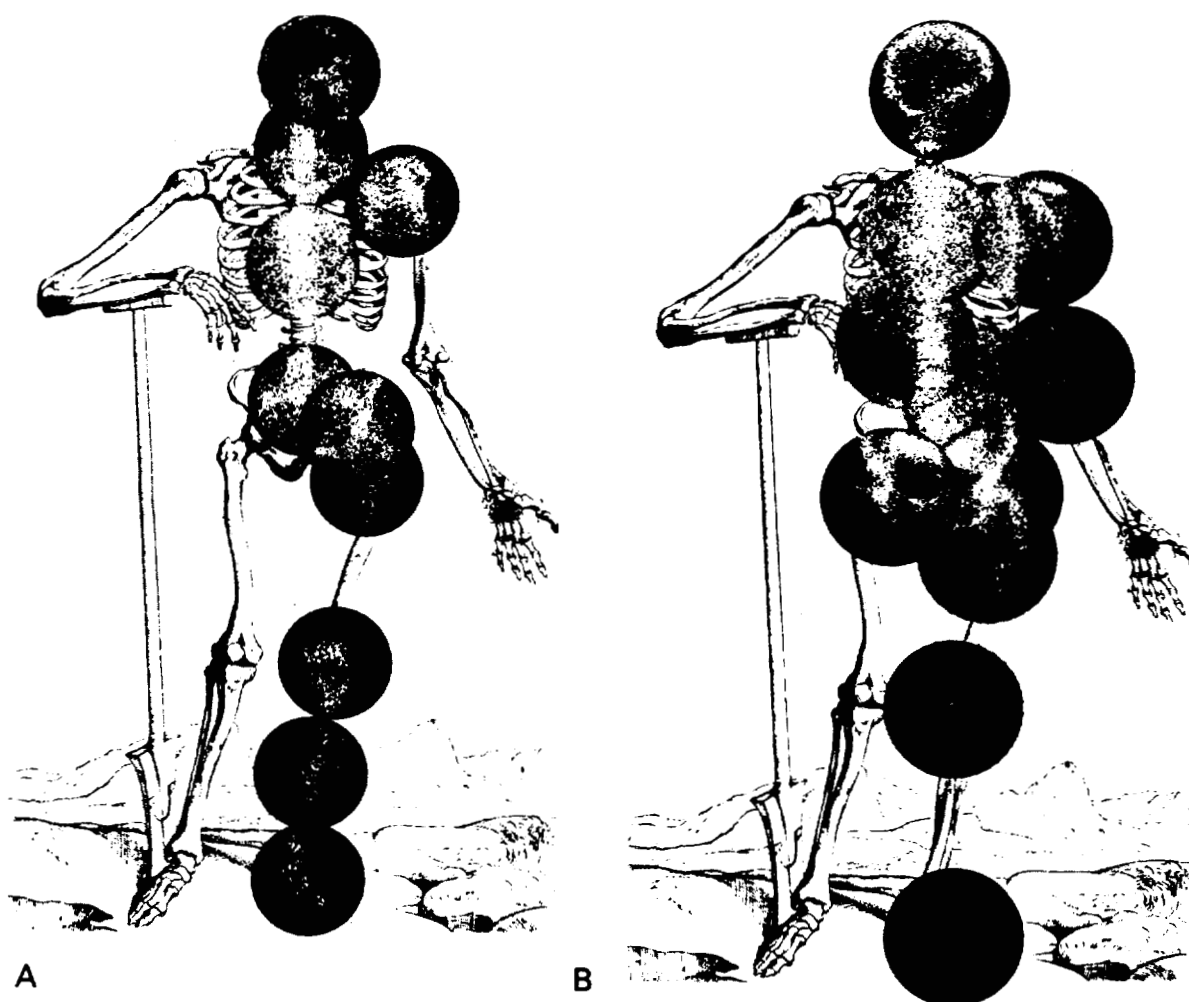


Fig. 1. Characteristic distribution of bone blood flow (A) and erythropoietic marrow (B) in adult human beings.

XBB677-4113 and XBB677-4114

Figure 6 shows abnormal extension of erythropoietic marrow into the extremities of a patient with far-advanced Paget's disease. Figure 6A shows the characteristically high blood flow to the diseased parts of the skeleton, and Fig. 6B shows peripheral distribution of marrow corresponding exactly to the distribution of the disease.

Figure 7 shows another case of far-advanced Paget's disease in which the diseased tibia with its high perfusion rate, Fig. 7A, has been invaded by erythropoietic marrow. Note that portions of the central skeleton which normally contain marrow lose most of their marrow when they become involved in the disease process (right shoulder, right side of pelvis, and two vertebral bodies). This is presumably because of obliteration of the marrow cavity by hypertrophied bone.

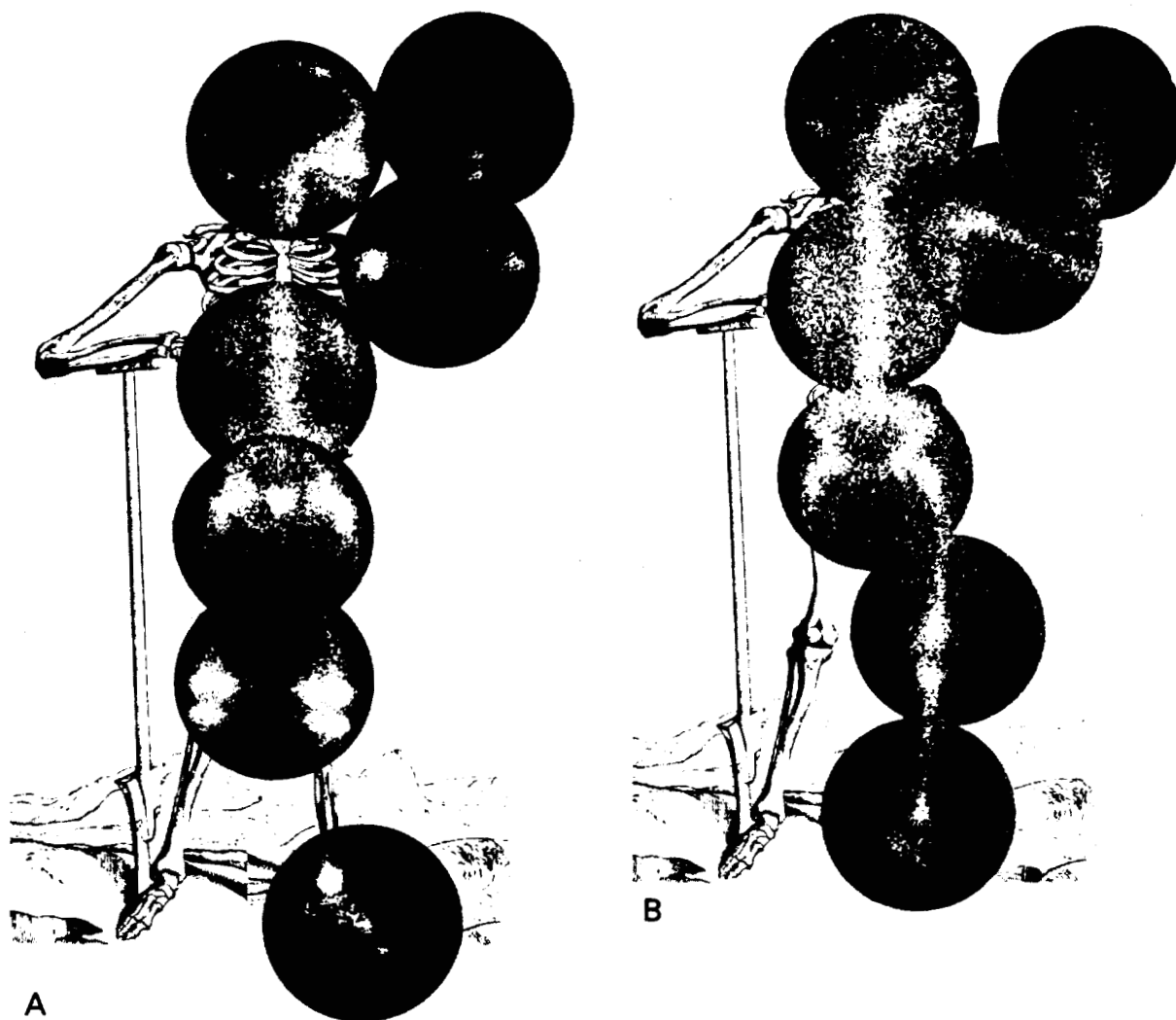


Fig. 2. Comparison of distribution of bone blood flow (A) and erythropoietic marrow (B) in a 4-year-old girl with primary erythrocytosis.

XBB677-4115 and XBB677-4116

Figure 8 compares the distribution of skeletal blood flow with the distribution of erythropoietic marrow in an adult monkey (A), rabbit (B), opossum (C), and dog (D). In each case ^{18}F is to the left and ^{52}Fe is to the right. In the monkey, rabbit, and opossum, the distribution of bone blood flow and marrow is so similar that one cannot easily tell from the pattern whether ^{18}F or ^{52}Fe had been used in the study.

There was divergence of distribution of the two isotopes in the dog, there being active uptake of ^{18}F in the feet (left) without marrow being present (right).

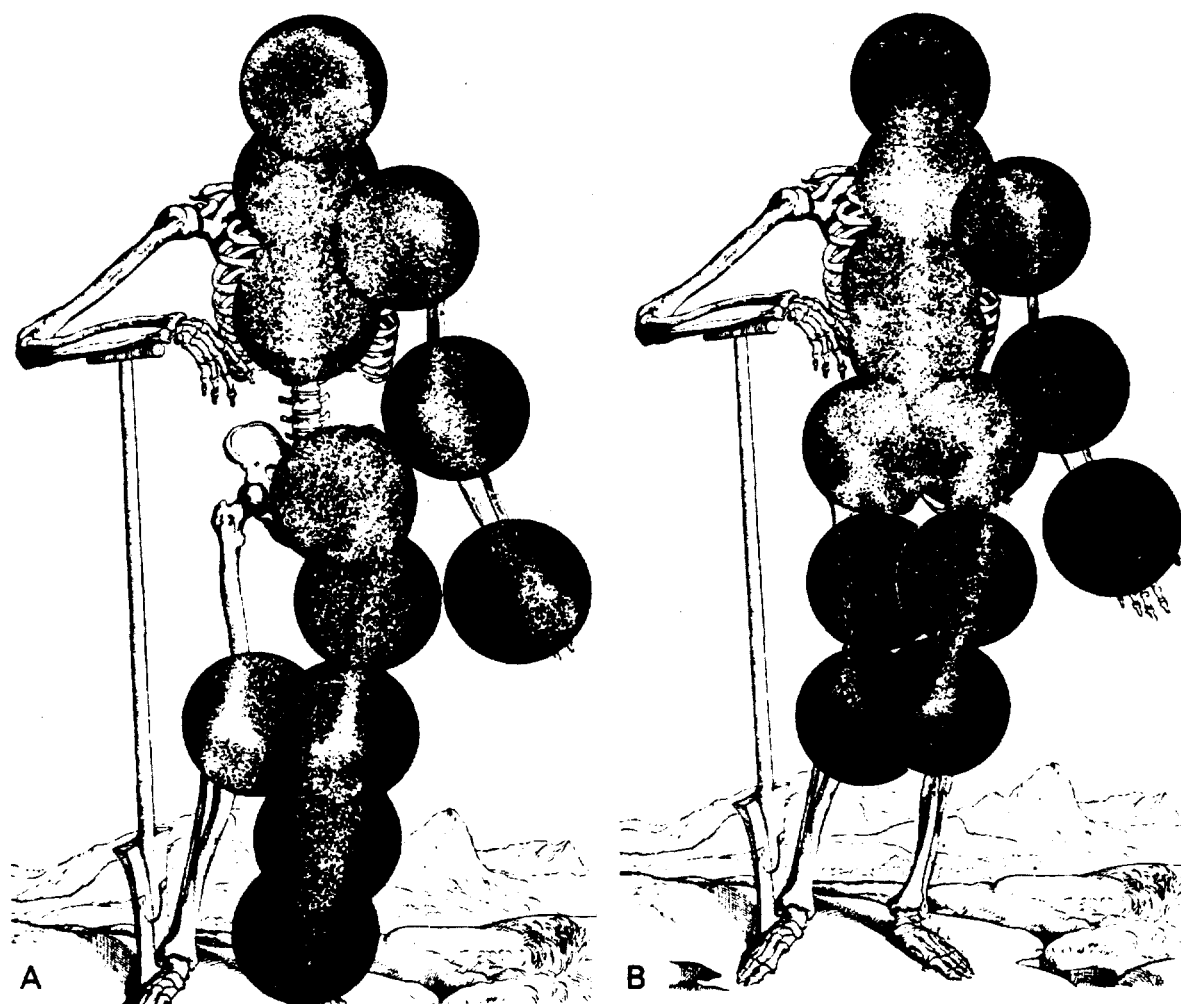


Fig. 3. Comparison of distribution of bone blood flow (A) and erythropoietic marrow (B) in a 45-year-old woman with pernicious anemia and early myelofibrosis.

XBB677-4117 and XBB677-4118

DISCUSSION

No amount of erythropoietic stimulation (bleeding, hypoxia, or cobaltous chloride) will induce hematopoietic marrow to grow in the vertebrae in the end of the adult rat's tail, and yet Huggins and Blocksom (15) have shown that abdominal implantation of the tip of the tail results in repopulation of the vertebral cavities with hematopoietic marrow. Thus abdominal implantation alters the local environment from a completely unsuitable site to an ideal one for marrow growth. The authors attributed this effect to an increase in temperature which they point out is accompanied by an increase in vascularity. They conclude that "there are two ways in which a physiological elevation of temperature may affect the bone marrow, namely a primary effect on tissue metabolism and a secondary vasomotor effect. While both effects are presumably operative, no evidence could be derived from these experiments as to

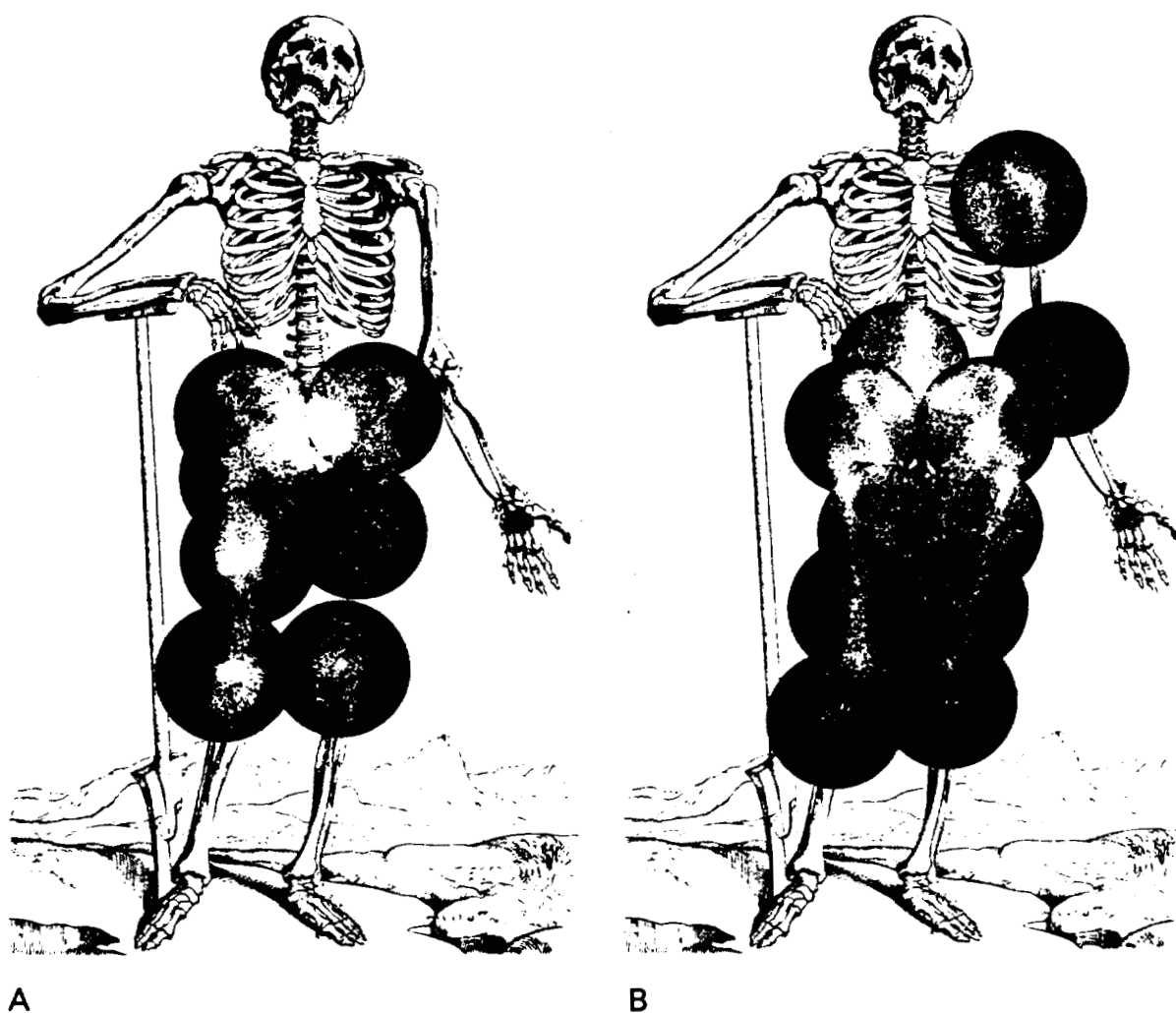


Fig. 4. Comparison of distribution of bone blood flow (A) and erythropoietic marrow (B) in a 19-year-old girl 4 months after a mid-femoral fracture.

XBB677-4119 and XBB677-4120

the mechanism by which an elevation in temperature facilitated hemopoiesis." Efforts to demonstrate directly a temperature gradient explanation for the distribution of marrow in rats, mice, and humans have been unsuccessful (16, 17). Using ^{18}F we have shown that abdominal implantation of the rat's tail is accompanied by a 3-fold increase in bone blood flow in the implanted segment. This suggests that the primary factor in the induction of hemopoiesis in the implanted segment is the increased bone blood flow which occurs secondary to the increased temperature. This, plus the finding in patients of erythropoiesis in the peripheral lesions of Paget's disease (Figs. 6 and 7) and occasionally adjacent to fracture (Fig. 4), conditions well known to be associated with increased bone blood flow, provides evidence that a high bone blood perfusion rate may be an important factor in the growth of marrow. Centralization of the skeletal blood supply during maturation may account for the centripetal migration of the marrow from childhood to adult (Fig. 2). As suggested by Askanazy (18), this apparently

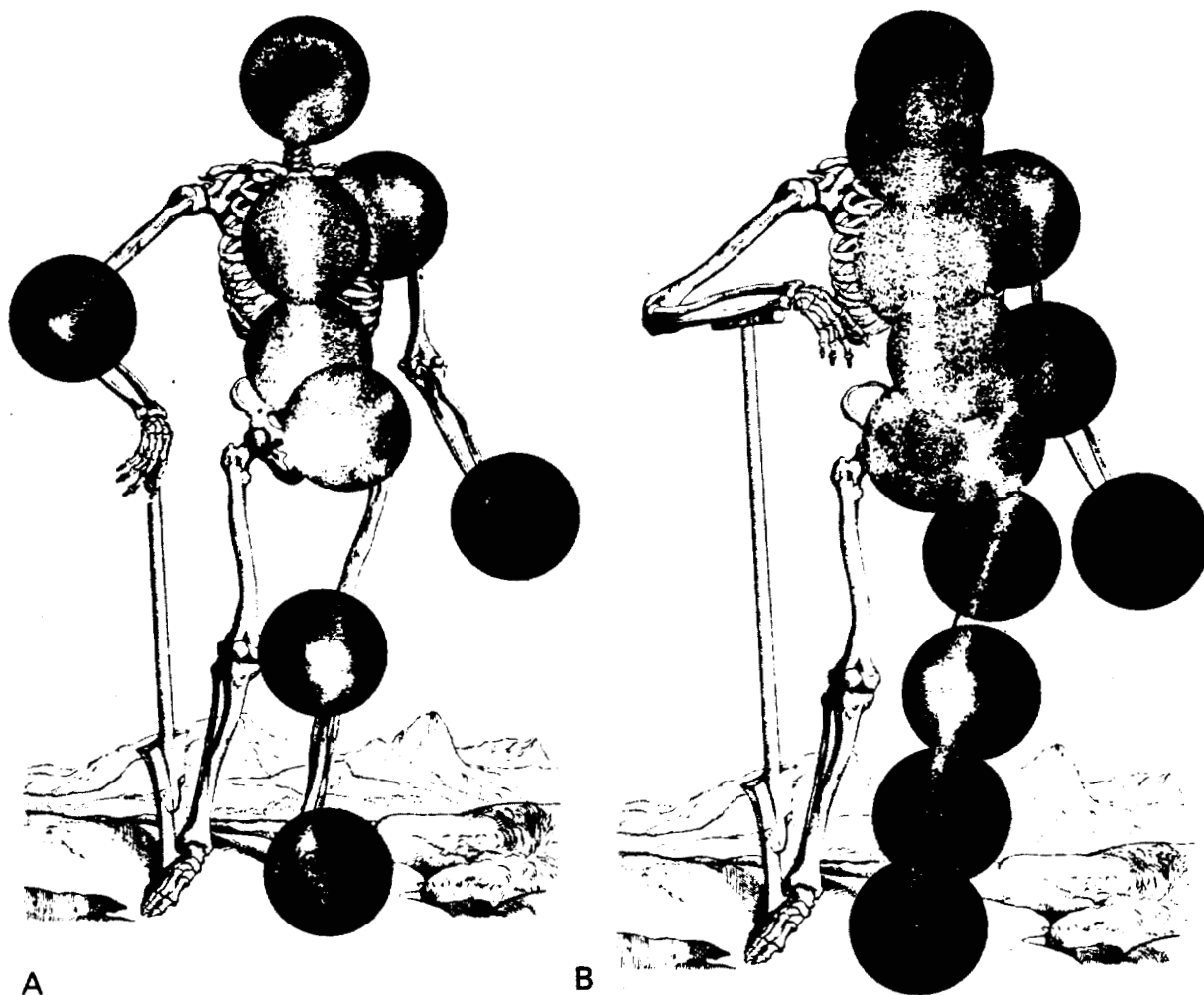


Fig. 5. Comparison of distribution of bone blood flow (A) and erythropoietic marrow (B) in a patient with hemolytic anemia of 3 years duration.

XBB677-4121 and XBB677-4122

normal physiological migration may in fact represent an early form of vascular senescence with subsequent lipomatous involution of the marrow.

In cases of extreme erythropoietic demand resulting in peripheral extension of marrow, the associated increase in bone blood flow, Fig. 5., appears most likely to be due to, rather than the cause of, marrow growth in the area. Cause and effect cannot be determined in such cases, but in the best-controlled experimental situation, the abdominally implanted rat tail, an increase in bone blood flow certainly preceded marrow growth. Also in the occasional case where an increase in marrow activity occurs adjacent to fracture, Fig. 4, it seems reasonable to conclude that the fracture results in hyperemia of the bone and that marrow growth occurs secondarily.

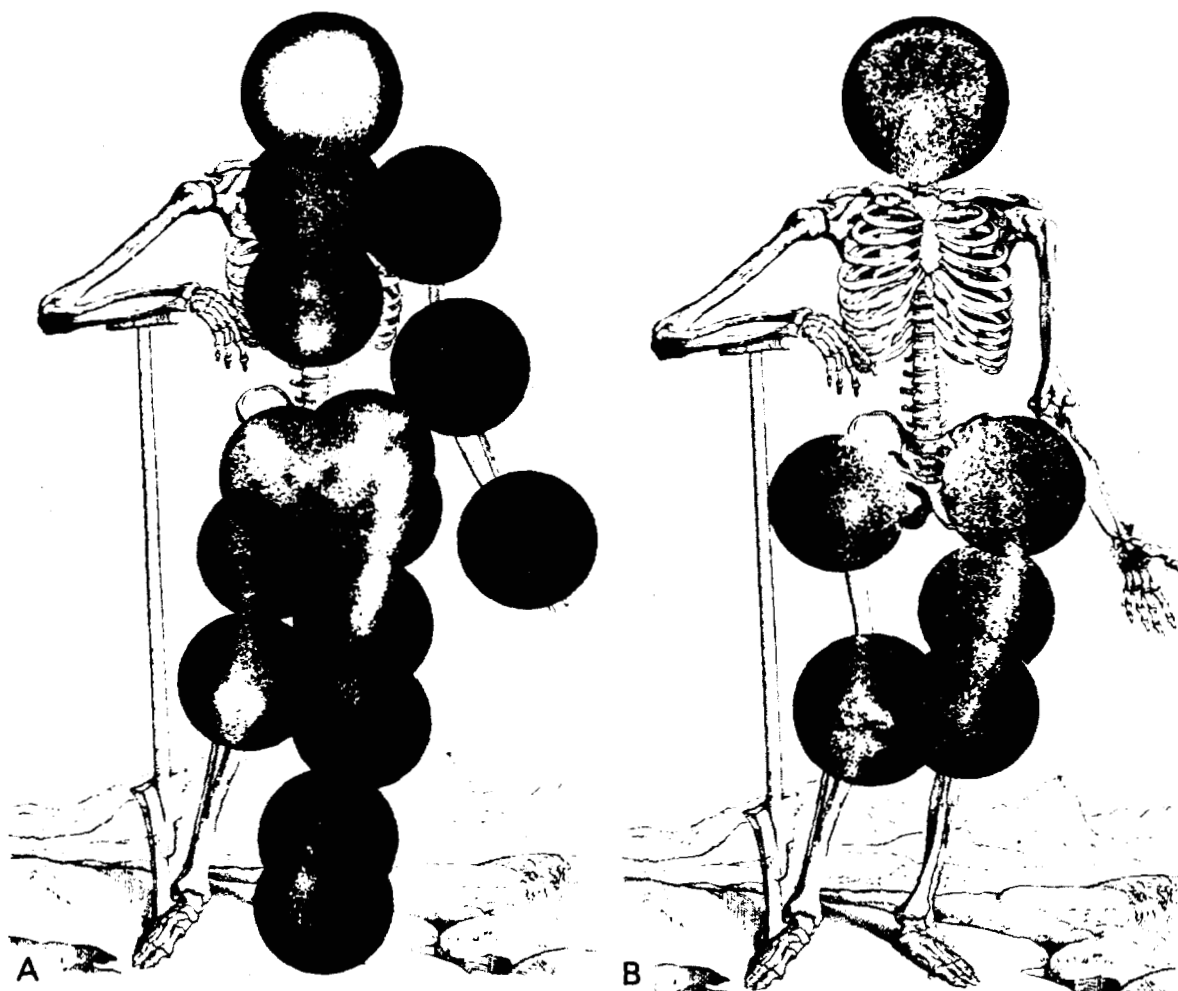


Fig. 6. Positron camera pictures showing similarity in distribution of bone blood flow (A) and erythropoietic marrow (B) in a patient with far-advanced Paget's disease.

XBB677-4123 and XBB677-4124

Of fundamental importance to these considerations is whether the high bone blood perfusion rate associated with active marrow is simply a reflection of active blood flow in the marrow cavity or whether it is the high bone blood flow itself which is important. Until methods are developed for direct measurement of marrow blood flow, one can only speculate. It is well known that stimulated marrow is much more vascular than marrow of low activity (19), and it may well be that because bone and marrow share a common blood supply, the increase is seen in the adjacent bone. On the other hand, it has been shown that a portal system exists between the blood supply of bone and marrow, Fig. 9. Brookes has presented evidence supporting the concept of a centrifugal blood flow in bone cortex (20). However, Branemark (19) states that "capillaries stemming from marrow arterioles enter the Haversian canals to supply endosteal parts of diaphyseal bone. The capillaries then swing back into the marrow to empty into sinusoids or directly into collecting venules." Heřt and Lišková (21) state that

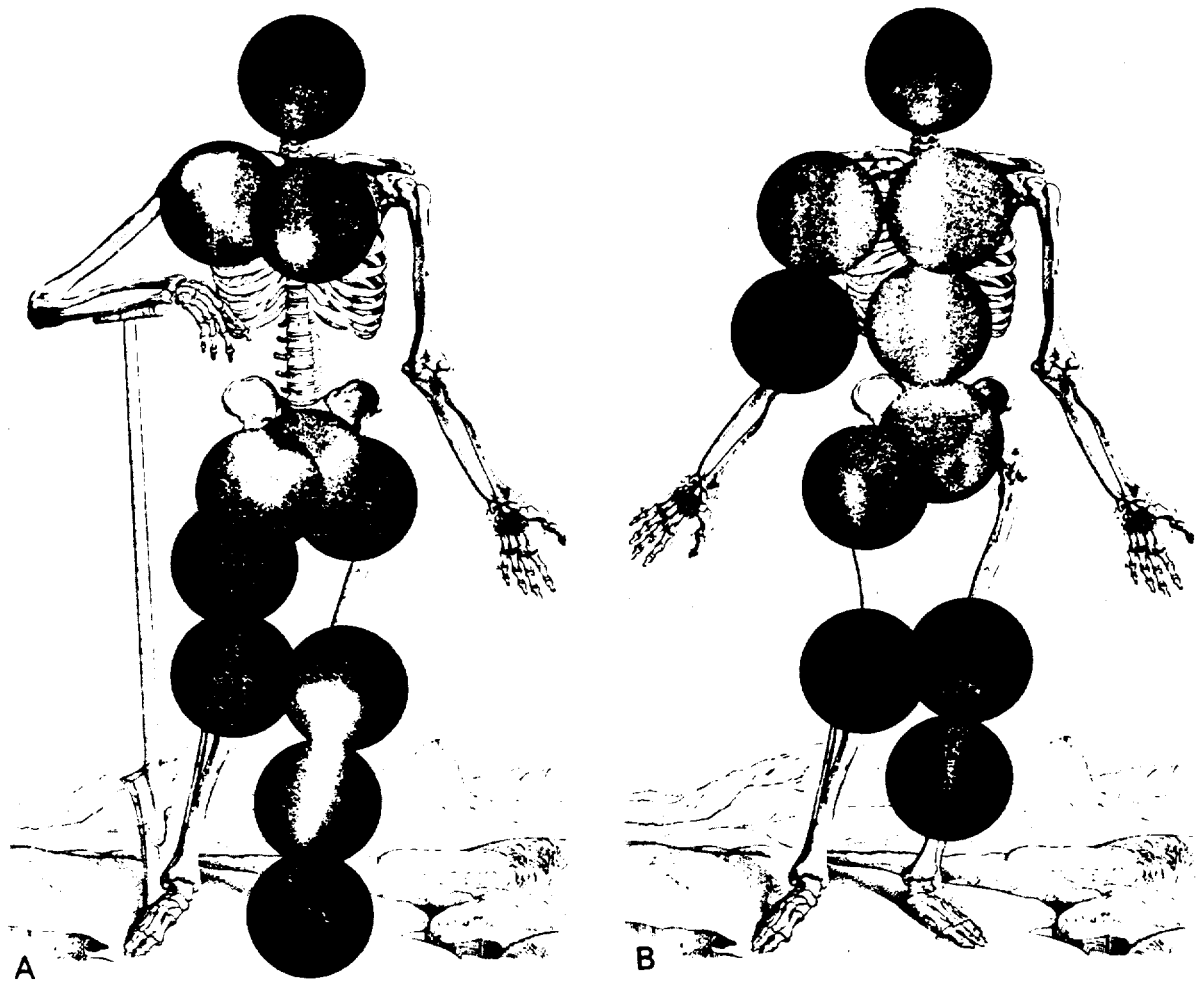


Fig. 7. Positron camera pictures showing distribution of bone blood flow (A) and erythropoietic marrow (B) in a patient with far-advanced Paget's disease.

XBB677-4125 and XBB677-4126

"blood flow through the compact bone has not a one-way, centrifugal direction; the venous blood returns along the correspondent arteries, by preference into the bone marrow." It is attractive to speculate on the possibility that a significant fraction of the flow is from bone to marrow and that this bone-bone marrow portal system may be a key to the fundamental question as to why marrow grows best in bone.

Petrakis (17) concludes: "This constant intimate relationship between bone and marrow suggests that the tissue environment associated with bone may provide essential substances for differentiation and function of hematopoietic stem cells. The mechanism whereby this result arises is not understood. The vascularity of the body tissue may be an important factor which promotes marrow development, as noted by Huggins and Blocksom and Noonan. Hematopoiesis occurring in the portion of the tail in the abdominal cavity might result from the

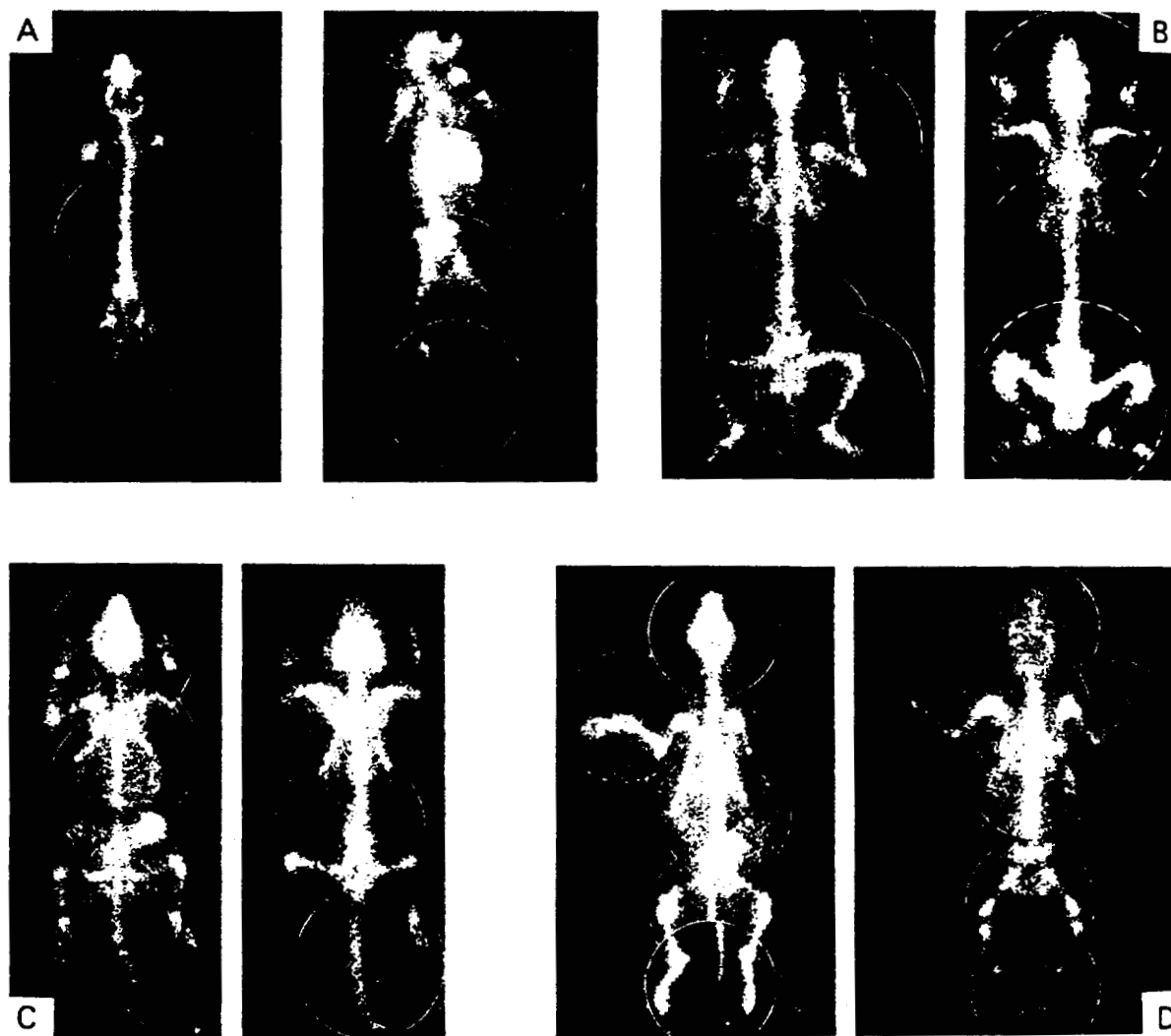


Fig. 8. Comparison of distribution of skeletal blood flow with the distribution of erythropoietic marrow in an adult monkey (A), rabbit (B), opossum (C), and dog (D). In each case ^{18}F is to the left and ^{52}Fe is to the right.

XBB677-4127, 4128, 4129, 4130

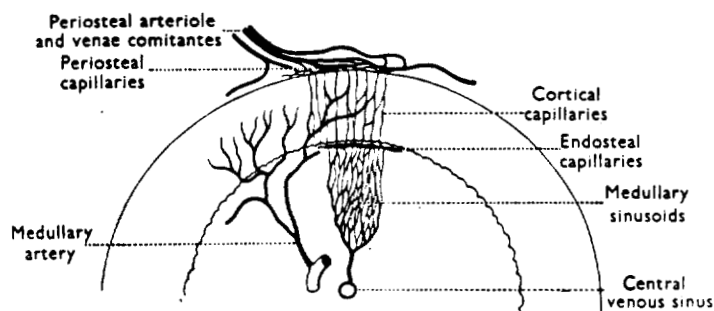


Fig. 9. The blood vascular organization of diaphyseal tubular bone represented diagrammatically in transverse section (from Brookes, ref. 32).

1175256

effects of an increased blood supply to the implanted vertebrae, resulting in the activation of dormant marrow stem cells, colonization of the marrow spaces by circulating stem cells, or both."

Failure of hematopoietic marrow to repopulate an area of the skeleton having received therapeutic doses of irradiation is an example of importance of local environmental factors in marrow proliferation. If all the marrow cells were destroyed, it should require only days or weeks for such a rapidly dividing tissue to repopulate the area from circulating stem cells, and yet it characteristically takes many months before marrow will re-establish itself in the area, typical fatty marrow having taken its place (22). By what mechanism has irradiation rendered the site unsuitable? Bone is there but its special ability to attract active marrow is gone. It is comparable at this stage to the bones of the extremities of the human or the tail of the rat. Whatever special influence bone exerts on marrow would appear to be enhanced by heating and abolished by irradiation. It is reasonable to assume that large doses of irradiation may seriously injure the vascular supply of bone or marrow or both. The literature on the effect of therapeutic irradiation on the blood supply of bone is contradictory. Ewing (23), Gratzek et al. (24), and Hinkel (25) found impairment of bone blood supply following heavy therapeutic irradiation, whereas Bonfiglio (26) and Carlson et al. (27) found no evidence of morphologic change. The ^{18}F method for bone blood flow measurement has not been applied to studies of irradiation effect. The permanent damaging effects of large dose of irradiation on the characteristic and essential sinusoidal microcirculation of the marrow itself have been presented recently by Knospe et al. (28).

It seems worthwhile to consider the possibility that the relationship between bone and marrow is comparable to the relationship between hypothalamus and anterior pituitary, i.e., where stimulating substances produced in the hypothalamus are carried to the pituitary via the hypothalamic-pituitary portal vessels. Hemopoietic-stimulating factors produced or activated in bone may be carried directly to the marrow via the bone-bone marrow portal vessels, or an inhibitor might be removed by passage through bone. It may be that marrow grows best in that blood which has just passed through bone.

Although the tissue of origin of the red cell-stimulating hormone, erythropoietin, has not been conclusively established (29), its long biological survival (30) and predominant effect on erythropoiesis do not implicate it in this system. However, a host factor essential for stem-cell colony formation, as demonstrated by McCulloch et al. (31), would fit the system proposed.

McCulloch et al., studying isologous hemopoietic grafts in the mouse, have shown that the controlled behavior of mammalian hemopoietic tissue depends on interactions between blood-forming cells and their environment. They have shown that at least two genetic loci control functions essential for successful colony formation, and that the site of action of one is intrinsic to colony-forming cells, while the site of action of the other is a host factor extrinsic to colony-forming cells, a factor specific for the progenitors of erythrocytic, myelocytic,

and megakaryocytic cells. The influence of this factor must extend beyond the borders of a cell, and a diffusible substance must be required for transfer of this information.

SUMMARY

Recently developed methods for visualization of the distribution of blood flow to the skeleton and distribution of erythropoietic marrow within the skeleton have demonstrated a remarkable similarity between bone blood flow and marrow distribution. It is postulated that marrow grows best in blood which has just passed through bone. The relationship between bone and marrow may be comparable to the relationship between pituitary and hypothalamus, i.e., that stimulating factor(s) produced in bone are carried directly to the marrow via bone-bone marrow portal vessels.

ACKNOWLEDGMENT

This work was supported in part by the U.S. Atomic Energy Commission and in part by grant #5 ROICA 08370-02 from the National Cancer Institute of the National Institutes of Health.

REFERENCES

1. Van Dyke, D. C.; Anger, H. O.; Yano, Y., and Bozzini, C.; Bone Blood Flow Shown with F^{18} and the Positron Camera; Am. J. Physiol. 209: 65-70, 1965.
2. Anger, H. O., and Van Dyke, D. C.; Human Bone Marrow Distribution Shown in vivo by Iron-52 and the Positron Scintillation Camera; Science 144: 1587-9, 1964.
3. Selye, H.; Lemire, Y., and Bajusz, E.; Induction of Bone Cartilage and Hemopoietic Tissue by Subcutaneously Implanted Tissue Diaphragms; Roux Arch. für Entwicklungsmechanik 151: 572-85, 1960.
4. Goodman, J. W., and Hodgson, G. S.; Evidence for Stem Cells in Peripheral Blood of Mice; Blood 19: 702-14, 1962.
5. Van Dyke, D. C.; Anger, H. O., and Yano, Y.; Progress in Determining Bone Marrow Distribution in vivo; Progress in Atomic Medicine, in press.
6. Anger, H. O.; Van Dyke, D. C.; Gottschalk, A.; Yano, Y., and Schaer, L. R.; The Scintillation Camera in Diagnosis and Research; Nucleonics 23, #1, 57-62, 1965.
7. Wallace-Durbin, P.; The Metabolism of Fluorine in the Rat Using F^{18} as a Tracer; J. Dental Res. 33: 789-800, 1954.
8. Blau, M.; Nagler, W., and Bender, M. S.; Fluorine-18: A New Isotope for Bone Scanning; J. Nucl. Med. 3: 322-4, 1962.
9. Yano, Y., and Anger, H. O.; Production and Chemical Processing of Iron-52 for Medical Use; Intern. J. Appl. Radiation Isotopes 16: 153-6, 1965.
10. Nat. Bur. Std. U. S. Handbook 69: 30, 1959.
11. Van Dyke, D. C.; Nohr, M. L., and Lawrence, J. H.; Erythropoietin in the Urine of Normal and Erythropoietically Abnormal Human Beings; Blood 28: 535-43, 1966.
12. Termine, J. D., and Posner, A. S.; Infrared Analysis of Rat Bone: Age Dependency of Amorphous and Crystalline Mineral Fractions; Science 153 (Sept 23): 1523-25, 1966.
13. Van Dyke, D. C., and Anger, H. O.; Patterns of Marrow Hypertrophy and Atrophy in Man; J. Nucl. Med. 6: 109-120, 1965.

14. Custer, R. P.: *An Atlas of the Blood and Bone Marrow*, Philadelphia, W. B. Saunders Co., 1949.
15. Huggins, C., and Blocksom, B. H., Jr.; Changes in Outlying Bone Marrow Accompanying a Local Increase of Temperature Within Physiological Limits; *J. Exptl. Med.* 64: 253-74, 1936.
16. Petrakis, N. L.; Temperature of Human Bone Marrow; *J. Appl. Physiol.* 4: 549-53, 1952.
17. Petrakis, N. L.; Some Physiological and Developmental Considerations of the Temperature-Gradient Hypothesis of Bone Marrow Distribution; *Am. J. Phys. Anthropol.* 25: #2, 119-30, 1966.
18. Askanazy, M.; in Henke, F., and Lubarsch, O.: *Handbuch der Speziellen Pathologischen Anatomie und Histologie*, Berlin, Julius Springer, 1 & 2, 1927.
19. Branemark, P.; Vital Microscopy of Bone Marrow in Rabbit; *Supp. 38, Scand. J. Clin. and Lab. Invest.* 11: 1-82, 1959.
20. Brookes, M.; The Vascular Architecture of Mammalian Bone Cortex; *J. Anat.* 95: 615, 1961.
21. Heřt, J., and Lišková, M.; Blood Circulation in the Compact Haversian Bone of Long Bones; *Folia Morphologica* 14: 151-159, 1966.
22. Edwards, C. L.; Andrews, G. A.; Sitterson, B. W., and Knisely, R. M.; Clinical Bone Marrow Scanning with Radioisotopes; *Blood* 23: 741-56, 1964.
23. Ewing, J.; Radiation Osteitis; *Acta Radiol.* 6: 399-412, 1926.
24. Gratzek, F. R.; Holmstrom, E. G., and Rigler, L. G.; Post-Irradiation Bone Changes; *Am. J. Roentgenol. Radium Therapy* 53: 62-76, 1945.
25. Hinkel, C. L.; The Effect of Irradiation upon the Composition and Vascularity of Growing Rat Bones; *Am. J. Roentgenol. Radium Therapy* 50: 516-26, 1943.
26. Bonfiglio, M.; The Pathology of Fractures of the Femoral Neck Following Irradiation; *ibid.* 70: 449-59, 1953.
27. Carlson, H. C.; Williams, M. M. D.; Childs, D. S., Jr.; Dockerty, M. B., and Janes, J. M.; Microangiography of Bone in the Study of Radiation Changes; *Radiology* 74: 113-14, 1960.
28. Knospe, W. H.; Blom, J., and Crosby, W. H.; Regeneration of Locally Irradiated Bone Marrow I. Dose Dependent, Long-Term Changes in the Rat, with Particular Emphasis upon Vascular and Stromal Reaction; *Blood* 28: 398-415, 1966.
29. New York Academy of Sciences, Conference on Erythropoietin, 1966.
30. Naets, J. P., and Wittek, M.; Effect of Erythroid Hyperplasia on Utilization of Erythropoietin; *Nature* 206: 726-7, May 15, 1965.
31. McCulloch, E. A.; Till, J. E., and Siminovitch, L.; Host-Cell Interactions in Mice Bearing Isologous Hemopoietic Grafts, in *La Greffe des Cellules Hématopoiétiques Allogéniques*, Centre National de la Recherche Scientifique, Paris, 1965, p. 61.
32. Brookes, M.; The Vascularization of Long Bones in the Human Foetus; *J. Anat.* 92: 261-67, 1958.

Differences in Distribution of Erythropoietic and Reticuloendothelial Marrow in Hematologic Disease

*Donald C. Van Dyke, Carol J. Shkurkin, David C. Price,
Yukio Yano and Hal O. Anger*

In normal animals and man, reticuloendothelial cells are a constant constituent of red bone marrow. The ratio of phagocytic cells to hematopoietic cells is relatively constant, so that the skeletal distributions of myeloid, erythroid, and reticuloendothelial elements in normal animals are the same (1). Since knowledge of the distribution of the active marrow may be needed in investigative work on the marrow (2) and may be helpful in the care of patients whose treatment or primary disease involves the bone marrow (3), tracer methods for visualizing the distribution of active marrow have been developed. The reticuloendothelial elements can be labeled with radiocolloids (4,5), and the erythropoietic elements can be labeled with radioiron (6). Then their distributions can be determined with an isotope scanner or scintillation camera. There is at present no method to effectively label the granulocytic precursors in the bone marrow for clinical scanning.

In normal animals or human beings, similar marrow distribution patterns can be expected by either of the above scanning methods. However, since it is not in the normal subject that such information is most needed, and since the various components of the marrow may be quite differently affected by treatment or disease, the two methods of labeling (phagocytic and hemoglobin synthesis) may give quite different distributions, each providing useful but different information. Since few direct comparisons of the two methods have been made in abnormal subjects (3), the present study was undertaken. All patients on whom a marrow distribution study was indicated were investigated simultaneously with $^{99}\text{Tc}^m$ -sulfur colloid and ^{52}Fe . The results of the comparison are presented here.

MATERIALS AND METHODS

For labeling the erythropoietic portion of the marrow, the best results are obtained with the short-lived (T-1/2, 8 hr) positron-emitting isotope ^{52}Fe . The distribution of activity is recorded with the positron scintillation camera (6) or with the whole-body scanner, Mark II (7). ^{59}Fe may be used in place of ^{52}Fe , but scanners specially designed for high-energy gamma-ray emitters must be used, and the images obtained so far are not as satisfactory.

The reticuloendothelial portion of the marrow can be labeled with any colloid of the proper particle size (4,8). The most satisfactory at present, because of availability, cost,

and low radiation dose to the patient, is the short-lived ($T_{1/2}$, 6 hr) $^{99}\text{Tc}^m$ -sulfur colloid (9). After labeling with this colloid, the marrow, liver, and spleen can be visualized with a conventional radioisotope scanner or with the gamma-ray mode of the scintillation camera.

The scintillation camera, a nonscanning electronic instrument for making pictures of the distribution of gamma-ray and positron-emitting nuclides in vivo, has been described in detail in a previous publication (10).

The Donner Laboratory whole-body scanner, Mark II, has 64 scintillation counters, each with a 1×1 -in. sodium iodide crystal, in a massive lead shield (7). The length of the array of counters is 27 in., wide enough to cover the width of the body. The patient lies on a table that moves at a constant rate over the counters. With a single sweep of the table, a 4-line scan of the subject results. Nine feet above the patient is a 500 mCi source of americium-241 which emits 60 keV gamma rays. By detecting these rays and displaying them, one gets a transmission picture of the body outline of the patient. The final readout is obtained with a Polaroid scope camera. The patient table and the film cassette are mechanically coupled together, so that the photographic film moves up or down in synchrony with the patient table. Flickering points on the cathode-ray tube screen become lines of varying density on the final image. The usual scanning time for either ^{52}Fe or ^{59}Fe is 5-15 min for head-to-toe pictures. For $^{99}\text{Tc}^m$ the scanning time is 0.75-3 min.

In our laboratory the Mark II whole-body scanner and the positron scintillation camera are located in the same area so that a quick whole-body scan can be taken first to be used as a guide in taking the smaller but more detailed positron camera pictures.

The radiation doses to the bone marrow in a 70 kg man for the three isotopes used have been estimated to be as follows: 2.5 rads to bone marrow for a 100 μCi dose of ^{52}Fe (6), 1.0 rad for a 20 μCi dose of ^{59}Fe (11), and 0.09 rad for a 3 mCi dose of $^{99}\text{Tc}^m$ -sulfur colloid (12).

The methods of preparation of ^{52}Fe and $^{99}\text{Tc}^m$ -sulfur colloid have been described in the literature (13, 9).

All patients were evaluated by members of the Donner Laboratory medical staff, and in most cases therapy and long-term followup were managed through the Donner Laboratory outpatient clinic. Complete records were kept of all procedures and therapy performed elsewhere, throughout the entire course of the patient's disease. All patients with polycythemia vera were in the early stages of the disease, classes I and II as defined by Pollycove et al. (14).

METHOD OF MARROW LABELING When using radioiron, pictures of the bone marrow must be taken at the time of maximum marrow uptake, after the iron has cleared the plasma and before it has passed from the marrow to the peripheral blood. For most patients this means 10-24 hr after intravenous administration of ^{52}Fe (15). The patient is injected

1175261

in the afternoon with 100-150 μCi ^{52}Fe as ferric citrate and pictures are taken the following morning. The specific activity of the ^{52}Fe was 0.5 μCi per μg in the earlier studies, subsequently improved to 12 μCi per μg .

When using a colloidal preparation of sulfur labeled with $^{99}\text{Tc}^{\text{m}}$, most of the colloid localizes in the liver, spleen, and hemopoietic marrow within five minutes. Picture-taking can be begun very soon after intravenous administration of the labeled colloid and the study completed during a single visit. In the present studies, 2.5-3.0 mCi of $^{99}\text{Tc}^{\text{m}}$ -sulfur colloid were given.

In each study, scintiphotos of ^{52}Fe distribution are made first with the camera in the positron mode, taking 5-10 min per 9-in. -diameter field. At the completion of the ^{52}Fe picture, the technetium colloid is injected, and 10-15 min later the same areas are photographed with the scintillation camera in gamma mode, using a thin-septum multichannel collimator, an appropriate narrow energy window, and exposures of 1 minute or less.

RESULTS

Direct comparison of the distributions of erythropoietic and reticuloendothelial marrow in patients with diseased marrow demonstrates a range from identical to totally dissimilar. Table 1 summarizes the results and gives an indication of the degrees of correlation between the distributions of the two marrow functions in 25 patients studied to date. Arbitrary estimates of correlation ranging from "no correlation" to "identical" are given in the table to provide an indication of the frequency of marked or minor differences in results using the two techniques. Examples of the different categories are given in the figures.

Figure 1 (#23 in the table) shows identical distribution of hemoglobin synthesis and phagocytic activity in the marrow of a patient with polycythemia associated with renal vascular anomalies and an increased erythropoietin production. Urinary excretion of erythropoietin was 10 times normal and easily measurable concentrations of erythropoietin were found in plasma (16). Except for slight extension down the humerus, the pattern is that found in normal adults.

Figure 2 shows a perfectly normal marrow distribution pattern as judged by $^{99}\text{Tc}^{\text{m}}$ -sulfur colloid in a 20-year-old patient (#1 in the table) with congenital absence of erythropoietic marrow. Iron kinetics and ^{52}Fe positron camera studies showed complete absence of erythropoiesis. A summary of this case has been published elsewhere (3).

Figure 3B shows hypertrophied, peripherally extended marrow as seen with $^{99}\text{Tc}^{\text{m}}$ in a middle-aged man with severe idiopathic hypoplastic anemia (patient #2 in the table). Virtual absence of erythropoietic marrow is demonstrated in the radioiron scintiphotos (Fig. 3A), although a very faint outline of residual peripheral erythropoiesis is seen in the femur and humerus.

Table 1. Correlation of erythropoietic and reticuloendothelial marrow distribution in hematologic disease.

Patient number	Diagnosis	Estimate of correlation
1	Congenital red cell aplasia	No correlation (Fig. 2)
2	Hypoplastic anemia	Markedly different (Fig. 3)
3	Treated Hodgkin's disease	Markedly different (Fig. 4)
4	Treated Hodgkin's disease	Different (Fig. 5)
5	Polycythemia vera	Different
6	Combined irradiation and chemotherapy	Different
7	Myelofibrosis	Different
8	Aplastic anemia	Similar
9	Hypoplastic anemia	Similar
10	Polycythemia vera	Similar
11	Polycythemia vera	Similar
12	Polycythemia vera	Similar
13	Hypoplastic anemia	Similar
14	Pancytopenia	Similar
15	Hypoplastic anemia	Similar
16	Unexplained anemia	Similar
17	Hypoplastic anemia	Identical
18	Polycythemia vera	Identical
19	Chronic myelocytic leukemia	Identical
20	Chronic anemia	Identical
21	Secondary polycythemia	Identical
22	Acute hemolytic anemia	Identical
23	Secondary polycythemia	Identical (Fig. 1)
24	Hypoplastic anemia	Identical
25	Polycythemia vera	Identical

Figures 4 and 5 have been selected to illustrate various degrees of difference in functional distribution. Figure 4A shows the erythropoietic marrow (^{52}Fe) in a patient with long-standing Hodgkin's disease treated with irradiation and chemotherapy (patient #3 in the table). Erythropoietic marrow was widely, but irregularly, distributed throughout the skeleton. The irregularities are attributed to the presence of tumor and previous irradiation therapy. Figure 4B shows the uptake of $^{99}\text{Tc}^{\text{m}}$ -sulfur colloid by the reticuloendothelial cells of the same patient on the same day. Splenic and hepatic uptake of most of the colloid is demonstrated with rather poor uptake by the marrow. Comparison of Figs. 4A and B shows similarities in the distribution in the knees and dissimilarity in the shoulders and elbows. The patchiness apparent in the erythropoietic pattern in the pelvis and right arm and leg was not apparent in the phagocytic pattern.

1175263



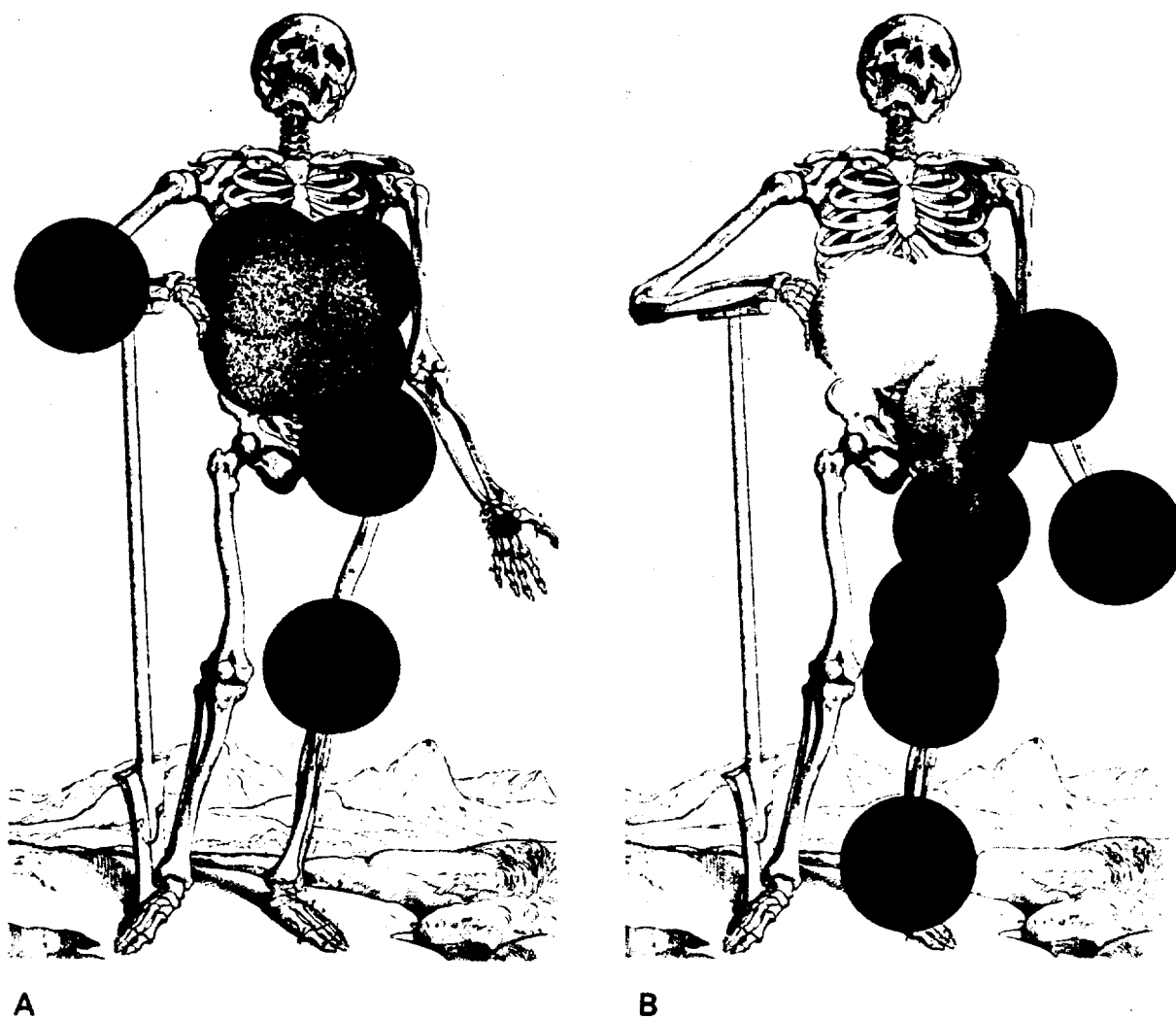


Fig. 2. Distribution of erythropoietic marrow (A) and phagocytic marrow (B) in a patient with congenital absence of erythropoietic marrow. There was no medullary uptake of ^{52}Fe , all the iron being deposited in liver and spleen. Uptake and distribution of colloid in marrow, liver, and spleen was normal (B).

XBB677-4133 and XBB677-4134

the central portion of the skeleton (ribs, spine, pelvis, scapula, and clavicle), with the exception of the caudal half of the sacrum. In the extremities some marrow is always found in the head of the humerus and the area of the lesser trochanter of the femur. There is considerable individual variation in the amount of marrow in the skull, and in the extent to which it extends down the shafts of the humerus and femur. Marrow is usually confined to the proximal $1/4$ of the humerus and femur in the adult, and extension beyond the proximal $1/3$ is considered abnormal.

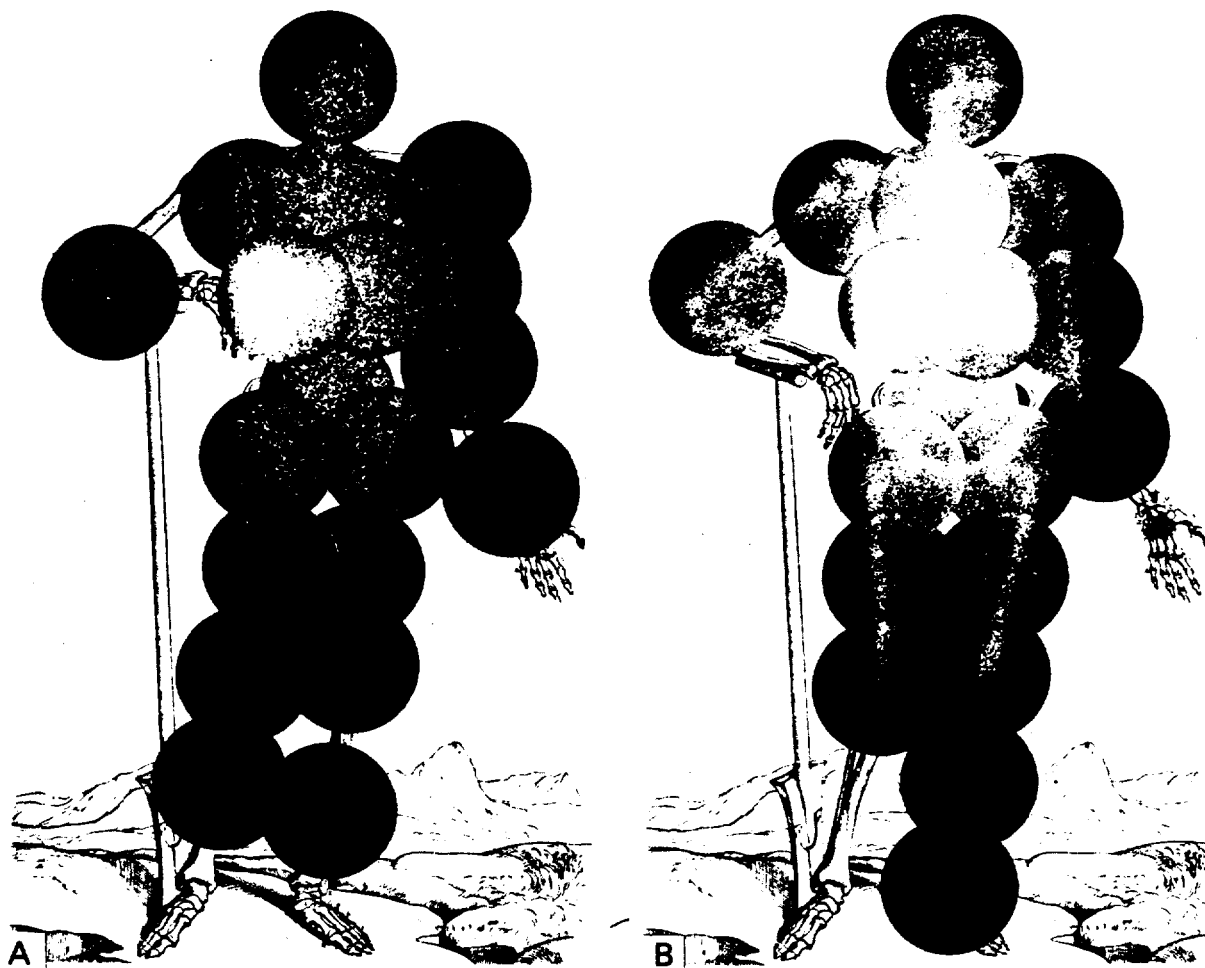


Fig. 3. Distribution of erythropoietic marrow (A) and phagocytic marrow (B) in a patient with idiopathic hypoplastic anemia. Hypertrophied and peripherally extended marrow is seen with the $^{99}\text{Tc}^{\text{m}}$ -sulfur colloid, whereas the erythropoietic marrow is essentially absent except for slight residual activity in the femur and humerus.

XBB677-4135 and XBB677-4136

Marrow characteristically expands peripherally on increased demand for red cells (18), but there are great variations in detail (3). The bones of the legs may be more involved than those of the arms, or vice versa. Heavy concentrations of marrow may extend to the distal ends of the femur without extension of marrow into the tibia. Conversely, the tibia may be densely filled, with little or no marrow in the distal femur. The marrow is not always distributed with complete bilateral symmetry, even in the absence of any known bone injury or disease. A given bone may be filled quite unevenly; e.g., the distal end of the femur may contain large amounts of marrow with little in the shaft, or the shaft may be filled evenly down

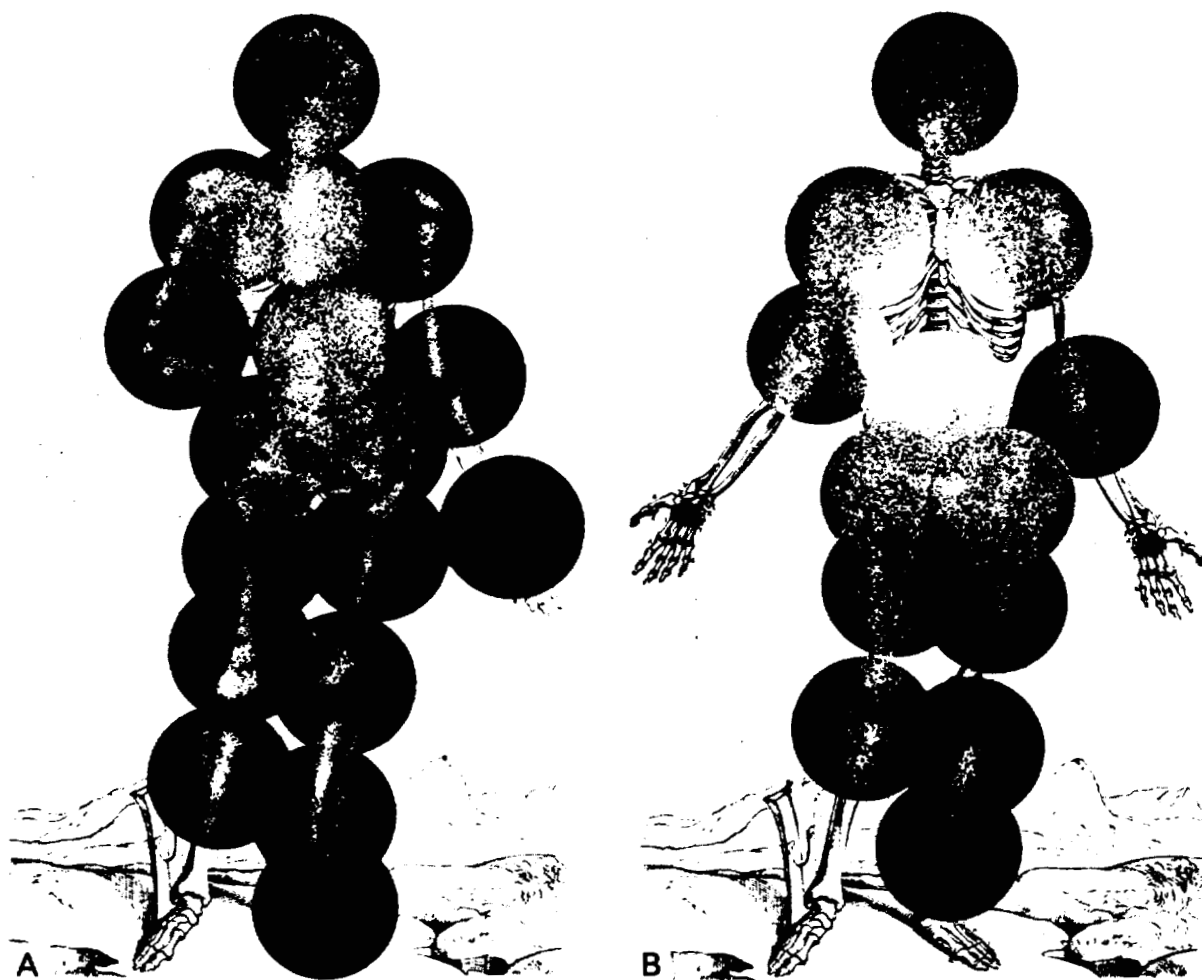


Fig. 4. Distribution of erythropoietic marrow (A) and phagocytic marrow (B) in a patient with Hodgkin's disease treated with irradiation and chemotherapy.

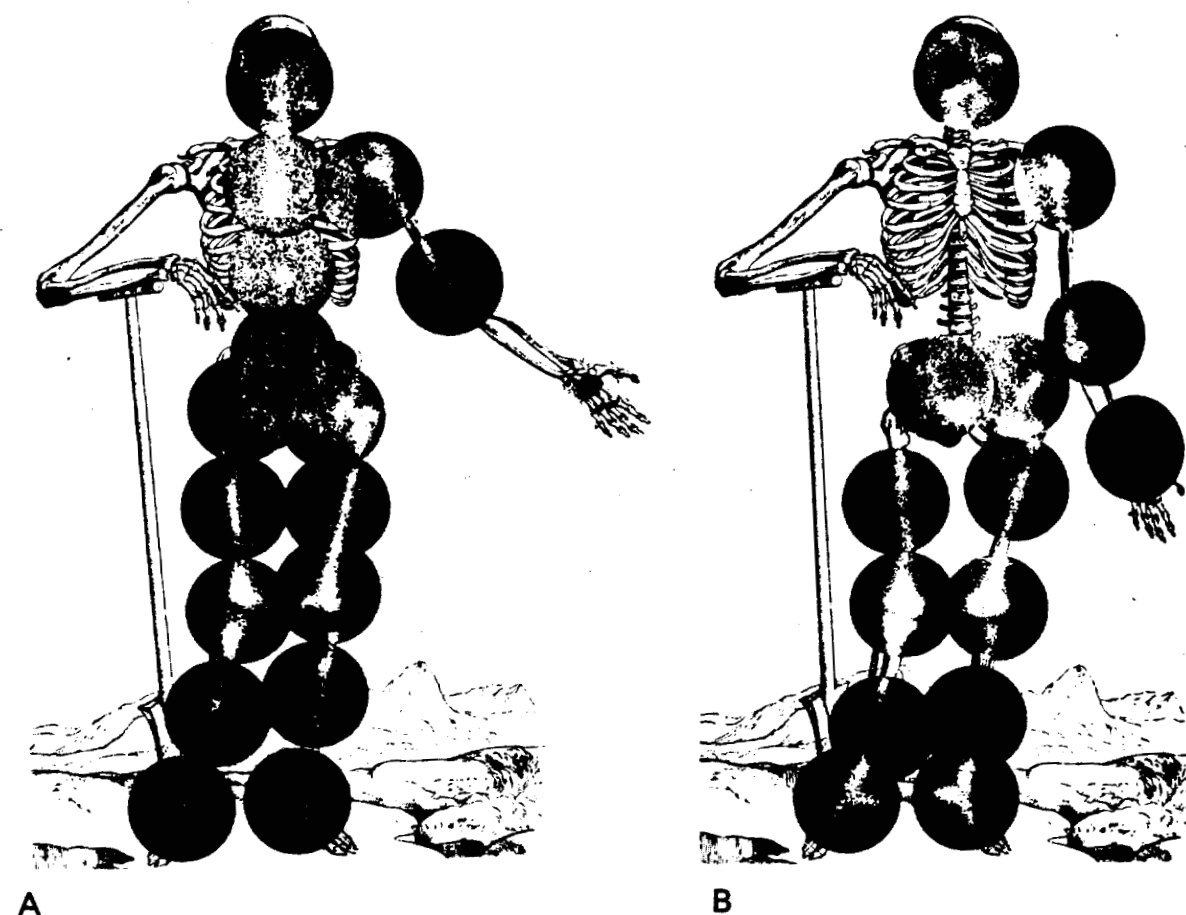
XBB677-4137 and XBB677-4138

to the lower 1/4 where it stops abruptly. Within an otherwise completely filled femur or humerus, there may be local areas devoid of marrow (3).

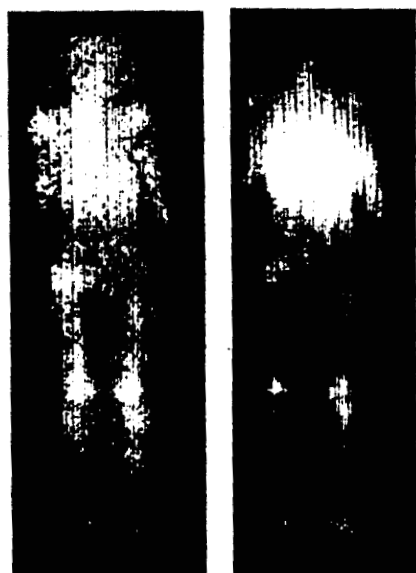
$^{99}\text{Tc}^{\text{m}}$ -sulfur colloid used to label the reticuloendothelial portion of the marrow has the advantage of being inexpensive and readily available. It delivers an extremely low dose of irradiation to the patient, and it has the added advantage that rapid uptake by the reticuloendothelial system makes it possible to complete the study during a single visit.

Major disadvantages of the use of colloid to visualize the marrow are that one does not label the usually clinically important marrow functions by this method, and that 96% of the dose goes to liver and spleen (1, 19), making it impossible to visualize the large fraction

1175267



XBB677-4139 and XBB677-4140



C

D

XBB677-4141 and XBB677-4142

Fig. 5. Positron scintillation camera pictures of distribution of erythropoietic marrow (A) and phagocytic marrow (B) in a patient with Hodgkin's disease treated with irradiation and chemotherapy. Figures 5C and D show Mark II whole-body scanner pictures of ^{52}Fe (C) and ^{99}Tcm -sulfur colloid (D) taken just prior to the more detailed camera study. In Figs. C and D the patient's right is to the right of the photograph.

1175268

of the marrow in the spine behind these organs. Loss of marrow from the spine, even in the presence of peripheral extension, may be an important finding of any individual study (18).

Since granulocytopoiesis and erythropoiesis are almost always accompanied by phagocytic cells, the colloid method is useful in demonstrating marrow extension within the skeleton (4). Phagocytic activity may persist in the presence of partial or complete failure of erythropoiesis, however. Therefore, the colloid method is not suitable for the study of patients with hypoplastic or aplastic anemia.

^{52}Fe , on the other hand, must be produced in a cyclotron and is not widely available. Because of this and its short half-life, it can be used in few locations for scanning of erythropoietic marrow. Invariable correlation of reticuloendothelial and erythropoietic marrow would make the $^{99}\text{Tc}^{\text{m}}$ -sulfur colloid the ideal agent for bone marrow scanning. Unfortunately, the present study demonstrated that these two marrow functions do not always coincide.

SUMMARY AND CONCLUSIONS

Although reticuloendothelial cells are an invariable component of normal marrow, the distribution of phagocytic activity may or may not correspond to the distribution of erythropoietic activity in the presence of disease affecting the marrow. A direct comparison of the distributions of reticuloendothelial marrow (using $^{99}\text{Tc}^{\text{m}}$ -sulfur colloid) and erythropoietic marrow (using ^{52}Fe) in patients receiving treatment for various diseases affecting the bone marrow has been made. In the presence of hematologic disease, the correlation between the distributions of these two marrow functions has varied from identical to totally dissimilar.

Unless one is studying normal subjects, knows a priori that marrow composition is normal, or is specifically studying the reticuloendothelial component of the marrow, one must be cautious in equating marrow distributions obtained with colloidal material to erythropoietic marrow distribution.

ACKNOWLEDGMENTS

The authors are indebted to the following for referral of patients: Dr. Cooney, Palo Alto, California (Fig. 4); Dr. Barkin, Stanford Medical School (Fig. 5); and to Dr. Leonard Schaer, Donner Laboratory, for permission to use Fig. 2.

This work was supported in part by the United States Atomic Energy Commission and in part by grant #5ROICA08370-02 from the National Cancer Institute of the National Institutes of Health.

REFERENCES

1. Greenberg, M. L.; Atkins, H. L., and Schiffer, L. M.; Erythropoietic and Reticuloendothelial Function in Bone Marrow in Dogs; *Science* 152: 526, (April 22) 1966.
2. Van Dyke, D. C.; Anger, H. O., and Pollycove, M.; The Effect of Erythropoietic Stimulation on Marrow Distribution in Man, Rabbit, and Rat as Shown by Fe^{59} and Fe^{52} ; *Blood* 24: 356, 1964.

1175269

3. Van Dyke, D. C.; Anger, H. O., and Yano, Y.; Progress in Determining Bone Marrow Distribution in vivo; in Progress in Atomic Medicine, in press.
4. Edwards, C. L.; Andrews, G. A.; Sitterson, B. W., and Knisely, R. M.; Clinical Bone Marrow Scanning with Radioisotopes; Blood 23: 741, 1964.
5. Knisely, R. M.; Andrews, G. A.; Tanida, R.; Edwards, C. L., and Kyker, G. C.; Delineation of Active Marrow by Whole-Body Scanning with Radioactive Colloids; J. Nucl. Med. 7: 575, 1966.
6. Anger, H. O., and Van Dyke, D. C.; Human Bone Marrow Distribution Shown in vivo by Iron-52 and the Positron Scintillation Camera; Science 144: 1587, (June 26) 1964.
7. Anger, H. O.; Whole-Body Scanner, Mark II; J. Nucl. Med., in press.
8. Miale, A., Jr.; Gagnon, A.; DeCesare, W., and Rath, C.; Scintillation Camera Studies of Bone Marrow in Blood Dyscrasias; J. Nucl. Med. 7: 347, 1966.
9. Harper, P. V.; Lathrop, K. A., and Richards, P.; Tc^{99m} as a Radio-Colloid; J. Nucl. Med. 5: 382, 1964.
10. Anger, H. O.; Van Dyke, D. C.; Gottschalk, A.; Yano, Y., and Schaer, L. R.; The Scintillation Camera in Diagnosis and Research; Nucleonics, 23 #1: 57, 1965.
11. Bothwell, T. H., and Finch, C. A.: Iron Metabolism, Boston, Little, Brown and Co., 1962, p. 39.
12. Smith, E. M.; Internal Dose Calculation for ^{99m}Tc; J. Nucl. Med. 6: 231, 1965.
13. Yano, Y., and Anger, H. O.; Production and Chemical Processing of Iron-52 for Medical Use; Intern. J. Appl. Radiation Isotopes 16: 153, 1965.
14. Pollycove, M.; Winchell, H. S., and Lawrence, J. H.; Classification and Evolution of Patterns of Erythropoiesis in Polycythemia Vera as Studied by Iron Kinetics; Blood 28: 807, 1966.
15. Pollycove, M.; Ferrokinetics: Techniques, in Eisenstoffwechsel: Beitrage zur Forschung und Klinik, Stuttgart, G. T. Verlag, 1959, p. 20.
16. Van Dyke, D. C.; Nohr, M. L., and Lawrence, J. H.; Erythropoietin in the Urine of Normal and Erythropoietically Abnormal Human Beings; Blood 28: 535, 1966.
17. Custer, R. P.: An Atlas of the Blood and Bone Marrow, Philadelphia, W. B. Saunders Co., 1949.
18. Van Dyke, D. C., and Anger, H. O.; Patterns of Marrow Hypertrophy and Atrophy in Man; J. Nucl. Med. 6: 109, 1965.
19. Zilversmit, D. B.; Boyd, G. A., and Brucer, M.; The Effect of Particle Size on Blood Clearance and Tissue Distribution of Radioactive Gold Colloids; J. Lab. Clin. Med. 40: 255, 1952.

First-Pass Hepatic Deposition of Intestinally Absorbed Iron in Patients with Low Plasma Latent Iron-Binding Capacity

*Rashid A. Fawwaz, H. Saul Winchell, Myron Pollycove
and Thornton W. Sargent*

Wheby and Jones demonstrated that rats, whose plasma iron-binding capacity was saturated by an acute intravenous infusion of iron, deposited a large fraction of intestinally absorbed iron in the liver during the first pass of portal venous blood through this organ (1). Subsequently Wheby and Umpiere demonstrated similar results in normal human subjects infused with sufficient iron to acutely saturate their plasma iron-binding capacity (2). Our results in patients with chronic spontaneous low plasma latent iron-binding capacity agree with those obtained by Wheby and Umpiere.

The present results were obtained by using a new triple radioiron-isotope technique (3) which allows for simultaneous measurement of the fraction of orally administered iron absorbed into the body during a 2-week period, the fraction of orally administered iron appearing in the systemic circulation over a 6-hr period, the fraction of orally administered iron absorbed and deposited in the liver during this 6-hr period, and the fraction of iron initially deposited in the liver and then released into the systemic circulation during the subsequent 2 weeks. This technique further allows for visualization of the distribution of iron in the intestinal tract and the remainder of the body while intestinal absorption is occurring.

MATERIALS AND METHODS

Intestinal iron absorption was studied in four normal subjects and six patients with low plasma latent iron-binding capacity: three with hemochromatosis (studied over 3 months after cessation of phlebotomy therapy), two with sideroblastic anemia, and one with prophyria cutanea tarda. The kinetics of intestinal iron absorption was studied by oral administration of 40 μCi of ^{52}Fe and 1 μCi of ^{59}Fe in 4-mg carrier ferrous sulfate, following an 8-hr fast. Concurrent with the administration of the above isotopes, plasma iron turnover was measured by administering intravenously 60 μCi of ^{55}Fe as ferrous ammonium citrate (specific activity 1 μCi per 1 μg) which had been incubated for 1/2 hr with 10 ml of autologous plasma. Plasma samples for radioiron activity were obtained at 15- to 30-min intervals for the initial 6- to 8-hr period. A blood sample for red cell radioiron activity was obtained on the 14th day.

Radioiron absorption from the gastrointestinal tract following its oral administration was calculated by three separate methods:

- 1) The percent of orally administered ^{59}Fe absorbed into the body over a 14-day period was calculated by utilizing the whole-body counter (4).
- 2) The percent of orally administered ^{59}Fe absorbed as calculated by red cell incorporation at the 14th day was determined according to the method of Saylor and Finch (5).
- 3) The rate at which orally administered ^{52}Fe appeared in the systemic circulation over a 6-hr period was calculated using the method of Hallberg and Solvell (6). The total amount of iron absorbed and appearing in the systemic circulation was taken as the integrated rate of absorption over this time interval.

The ^{52}Fe activity was separated from the ^{59}Fe activity by immediate counting of the plasma samples by using a thallium-activated sodium iodide, well-type, scintillation counter, and similarly recounting them after 7 days, at which time the ^{52}Fe ($T_{1/2} = 8.2$ hr) had decayed to a negligible level. The ^{55}Fe plasma and red cell activity was determined by counting the samples in a gas-flow counter under beryllium filters and correcting for activity due to ^{59}Fe (7).

The distribution of orally administered ^{52}Fe in the subject was visualized throughout the study by using the Anger positron camera (3). Semi-quantitative estimates of the ^{52}Fe deposition in the liver were obtained from external coincidence counting rates over the liver, expressed as a fraction of the total external coincidence counting rate of the entire ^{52}Fe bolus.

In one patient (), with a plasma latent iron-binding capacity of 9 μg per 100 ml, the plasma volume determined by using ^{131}I albumin was compared with that determined in two different fashions, using ^{59}Fe . In this patient radionuclides were used to determine plasma volumes by the following methods:

- 1) One μCi of ^{59}Fe as ferrous ammonium citrate, specific activity 10 μCi per 1 μg , and 10 μCi of ^{131}I albumin were simultaneously incubated for 1/2 hr with 250 ml of the patient's blood and reinjected intravenously.
- 2) One μCi of ^{59}Fe as ferrous ammonium citrate, specific activity 10 μCi per 1 μg , and 10 μCi of ^{131}I albumin were simultaneously incubated with 5 ml of normal donor plasma and injected intravenously.

Hemoglobin concentration, serum iron, and plasma latent iron-binding capacity were determined on the initial blood sample of each patient. Serum iron was determined by the method of Peters (8), while the plasma latent iron-binding capacity was determined by the method of Tauxe (9). All patients had plasma volumes determined with ^{131}I albumin.

RESULTS

Figure 1 correlates the location of the ^{52}Fe in the gastrointestinal tract with its rate of absorption into the plasma at various times after its oral administration to a normal subject (). It is seen that there is no detectable radioiron over the liver area.

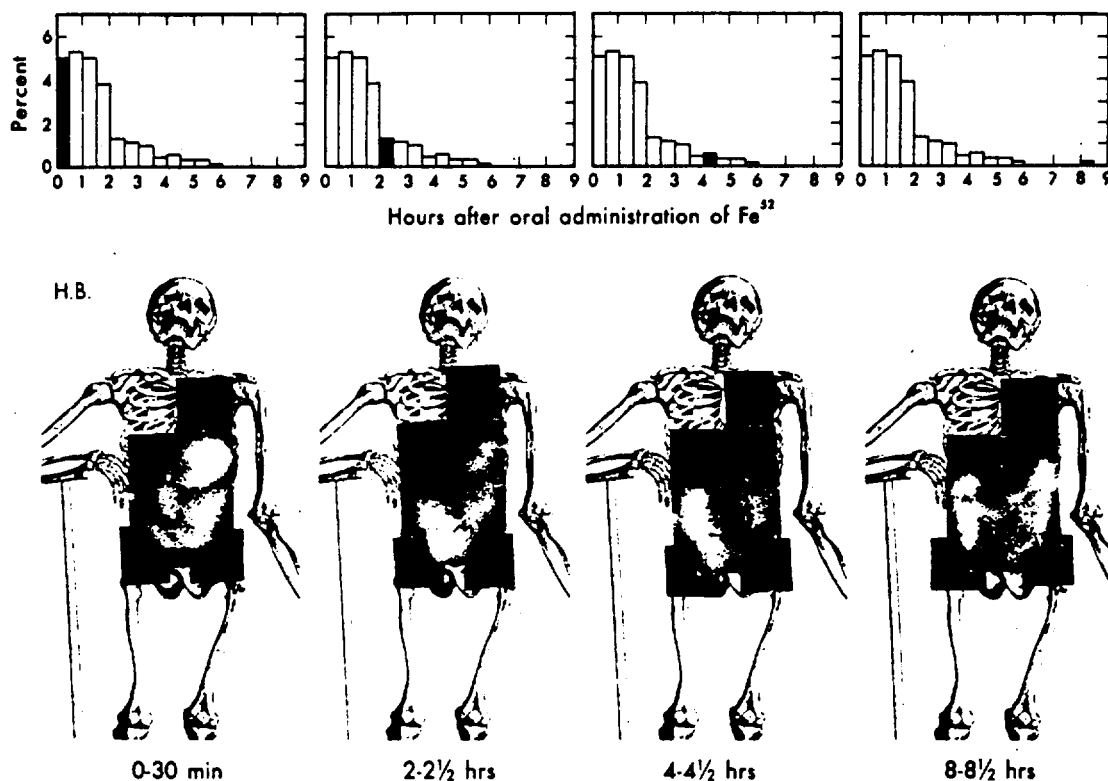












Fig. 1. Correlation of the location of the ^{52}Fe in the gastrointestinal tract with its rate of absorption into the plasma at various times after its oral administration to a normal subject (H.B.). The percent ^{52}Fe absorbed and appearing in the systemic plasma during 1/2-hr intervals is plotted above each photoscan. The shaded areas of the graphs represent the time at which the corresponding photoscan was taken. Note that no radioiron is detectable in the liver area at any time during the study.

MUB-12795 + JHL-6550

Close agreement was obtained in the two normal subjects in whom the iron absorption calculated by using total body retention of ^{59}Fe (whole-body counter) was compared with that calculated using double isotope incorporation into red cells (Table 1). In the four normal subjects, between 40 to 80% of the total radioiron absorbed appeared in the systemic plasma during the first 6 hr of the study. A discrepancy was obtained in the four patients having low plasma latent iron-binding capacity in whom the iron absorption calculated by using total body retention of ^{59}Fe (whole-body counter) was compared to that calculated by using double isotope incorporation into red cells. The iron absorption calculated by double isotope incorporation into red cells was less than 12% of that calculated by total body retention of ^{59}Fe . In the six patients with low plasma latent iron-binding capacity, less than 16% of the total radioiron absorbed appeared in the systemic plasma during the first 6 hr of the study.

Figure 2 correlates the location of the ^{52}Fe in the gastrointestinal tract with its rate of absorption into the systemic plasma at various times after its oral administration to a patient () with hemochromatosis and a low plasma latent iron-binding capacity. This study was performed 10 months after an initial course of 120 phlebotomies. It can be seen that

Table 1. Summary of results of iron-absorption studies obtained on four normal subjects and six patients with low plasma latent iron-binding capacity. Note that in patients with low plasma latent iron-binding capacity there is a discrepancy between the percent radioiron absorbed into the body at 2 weeks (whole-body counter) and the percent radioiron absorbed as calculated by red cell incorporation at the 14th day. In these patients there also is an abnormal discrepancy between the percent radioiron absorbed into the body at 2 weeks and the percent radioiron absorbed and appearing in the systemic plasma during the first 6 hr (and are female, the remaining subjects are male).

Diagnosis	Hemoglobin concentration, g/100 ml	Fasting serum iron, $\mu\text{g}/100\text{ ml}$	Fasting latent iron-binding capacity, $\mu\text{g}/100\text{ ml}$	% ^{59}Fe absorbed into body at 2 weeks (1)	% ^{59}Fe absorbed and incorporated into red cells at 2 weeks (2)	% ^{52}Fe absorbed and appearing in the plasma over 6 hr (3)
Normal						
	14.2	116	295	12.0	Not done	6.1
	12.9	126	227	28.9	26.2	23.6
	13.4	72	216	7.5	8.0	3.1
	14.8	130	308	16.0	Not done	8.2
Hemochromatosis						
	15.0	210	15	73.0	8.2	8.7
	12.9	229	9	29.0	Not done	4.5
	14.4	193	46	56.0	6.2	8.1
Porphyria cutanea tarda						
	14.4	230	13	21.8	1.2	1.5
Sideroblastic anemia						
	11.0	290	20	12.0	Not done	1.1
	10.0	160	66	45.0	5.0	3.9

within 2 hr after the initiation of the study, considerable orally administered ^{52}Fe was deposited in the liver. At 6 hr, 8.2% of the radioiron was absorbed and appeared in the systemic plasma, and an estimated 40% of the ingested ^{52}Fe was deposited in the liver. Thus four-fifths of the radioiron absorbed from the gastrointestinal tract during the first 6 hr was deposited in the liver. Similar results were obtained in the five other patients with low plasma latent iron-binding capacity.

Patient () was studied again 3 months after completion of a second course of 10 phlebotomies. His plasma latent iron-binding capacity at this time was 180 μg per 100 ml. Figure 3 compares the photoscans taken following an oral radioiron dose administered at this time (scan on the right) as compared with the initial study when the plasma latent iron-binding capacity was 15 μg per 100 ml (scan on the left). It can be seen that after 5 hr of radioiron

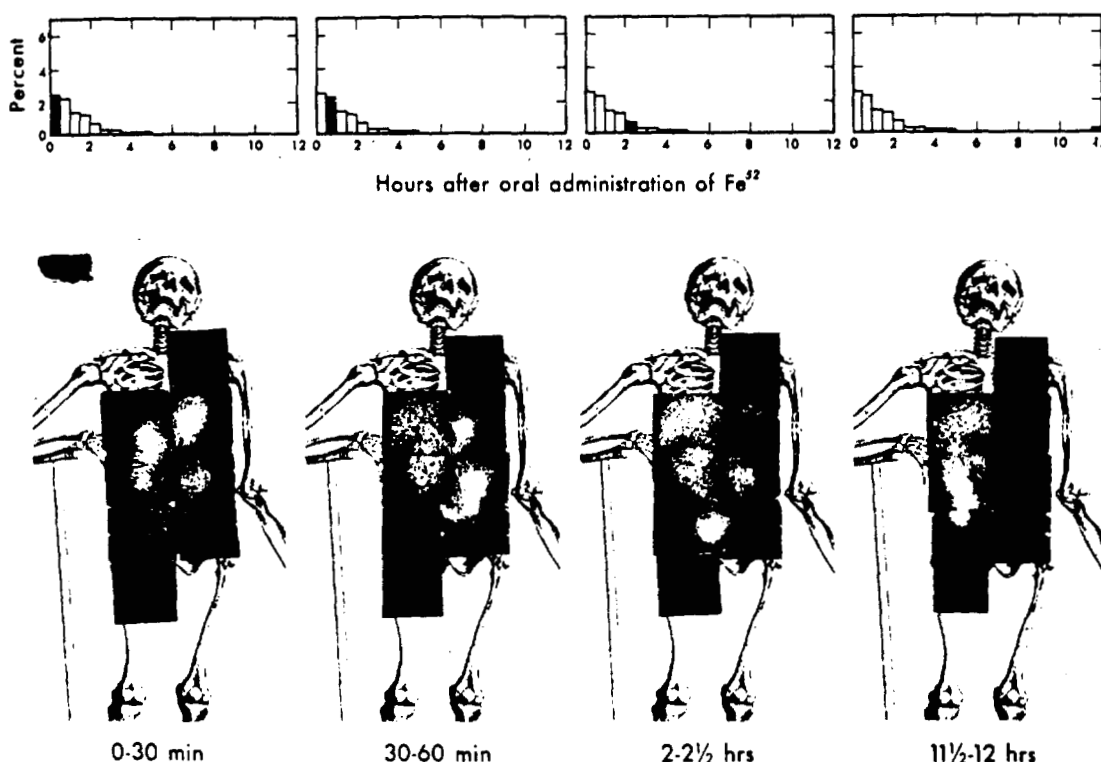


Fig. 2. Correlation of the location of the ^{52}Fe in the gastrointestinal tract with its rate of absorption into the plasma at various times after its oral administration to a patient (████) with hemochromatosis and low plasma latent iron-binding capacity. The percent ^{52}Fe absorbed into the plasma during 1/2-hr intervals is plotted above each photoscan. The shaded areas of the graphs represent the time at which the corresponding photoscan was obtained. Note the early and significant radioiron deposition in the liver.

MUB-12794 + JHL-6551

ingestion a considerable amount was deposited in the liver when the plasma latent iron-binding capacity was low, but none was detectable in the liver when the plasma latent iron-binding capacity was normal.

Figure 4 represents two different plasma radioiron clearance studies performed on patient (████), a hemochromatotic with a plasma latent iron-binding capacity of $9 \mu\text{g}$ per 100 ml. The ordinate is expressed as the percent of the administered dose present in the plasma and is calculated on the assumption that the ^{131}I albumin plasma volume represents the true plasma volume. When the radioiron was incubated with normal donor plasma prior to its intravenous administration, its initial distribution volume was identical to that obtained with ^{131}I albumin. However, a rapid initial phase of plasma radioiron clearance with a resulting spuriously low zero-time extrapolate was obtained when radioiron was previously incubated with 250 ml of autologous blood. In each instance the slope of the plasma radioiron clearance after 15 min was consistent with removal of transferrin-bound radioiron from the plasma.

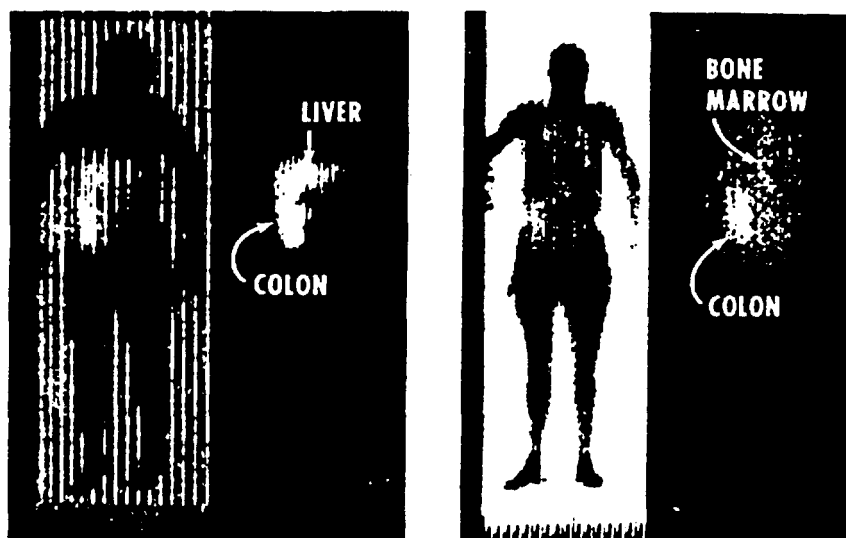


Fig. 3. Total body scans obtained 5 hr after an oral dose of ^{52}Fe , in a patient with hemochromatosis (●). The scan on the left was obtained subsequent to an initial course of phlebotomy at a time when his plasma latent iron-binding capacity was 15 μg percent. The scan on the right was obtained 4 months after a second course of phlebotomy at which time his plasma latent iron-binding capacity was 180 μg percent. In both instances total body absorption of iron (whole-body counter) was 73% of the orally administered 4-mg dose. Note the deposition of radioiron in the liver when the latent iron-binding capacity is low, and its absence from the liver when the latent iron-binding capacity is normal.

JHL-6490

DISCUSSION

Our results in the patients with spontaneous chronic low plasma latent iron-binding capacity were similar to those obtained by Wheby and Umpiere in normal human subjects in whom the plasma transferrin was acutely saturated. As shown in Table 1, in our patients with low plasma latent iron-binding capacity, the fraction of orally administered iron absorbed into the body, calculated by utilizing double isotope incorporation into red cells, was much lower than that calculated by utilizing total body retention of radioiron (whole-body counter). Correspondingly, the fraction of orally administered iron absorbed and appearing in the systemic plasma during the initial 6-hr period was also abnormally low in patients with low plasma latent iron-binding capacity. Clearly, in these patients a large fraction of the iron absorbed from the gastrointestinal tract into the portal vein did not reach the systemic circulation. Photoscans of patients with low plasma latent iron-binding capacity demonstrated that there was significant deposition of iron in the liver within 2 hr of its oral administration

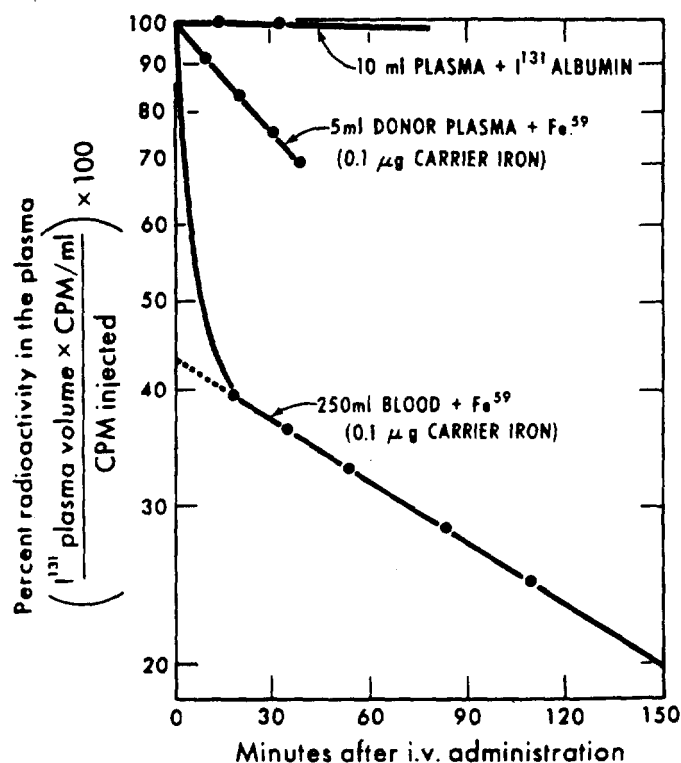


Fig. 4. Clearance of radionuclides from the plasma in patient () with hematochromatosis and a low plasma latent iron-binding capacity ($9 \mu\text{g}$ per 100 ml) following the intravenous administration of (1) 10 ml of the patient's plasma incubated for 1/2 hr with ^{131}I albumin, (2) 5 ml of donor plasma (normal plasma latent iron-binding capacity) incubated for 1/2 hr with ^{59}Fe ferrous ammonium citrate ($0.1 \mu\text{g}$ carrier ferrous ammonium citrate), and (3) 250 ml of the patient's blood incubated for 1/2 hr with ^{59}Fe ferrous ammonium citrate ($0.1 \mu\text{g}$ carrier ferrous ammonium citrate).

XBL672-1205

(Fig. 2). At 6 hr an estimated four-fifths of the total iron absorbed from the gastrointestinal tract is deposited in the liver. Thus, in these patients with spontaneous chronic low plasma latent iron-binding capacity, a major fraction of the iron absorbed from the gastrointestinal tract into the portal vein was deposited in the liver without prior appearance in the systemic circulation. Moreover, such hepatic iron was not released to any considerable extent during the subsequent 2 weeks, as evidenced by the marked discrepancy between calculations of total radioiron absorption at 2 weeks, measured by the whole-body counter, and the iron absorption measured by double isotope incorporation into red cells 2 weeks after the initiation of the study (Table 1).

That this initial rapid radioiron deposition in the liver is related to the transferrin saturation with iron is demonstrated in patient () with hemochromatosis. This patient showed the characteristic hepatic iron deposition within 2 hr after its oral administration at a time when the plasma latent iron-binding capacity was low, but hepatic iron was not detectable when the plasma latent iron-binding capacity was normal (Fig. 3).

To elucidate the mechanism by which intestinally absorbed iron is deposited in the liver in patients with low plasma latent iron-binding capacity, studies were performed on hepatic uptake of intravenously administered radioiron. In patient (), a hemochromatotic with a plasma iron-binding capacity of $9 \mu\text{g}$ per 100 ml, the initial distribution volume of radioiron incubated with normal donor plasma agreed well with the initial distribution volume

1175277

(plasma volume) of ^{131}I albumin (Fig. 4), indicating no initial rapid component of hepatic iron deposition. However, in studies on this patient where radioiron was administered intravenously as ferrous ammonium citrate subsequent to incubation with 250 ml of autologous blood, initial rapid clearance of radioiron from the plasma was noted, and an abnormally high distribution volume was obtained (Fig. 4). In both studies the rate of plasma clearance of radioiron after 15 min was consistent with the slow removal of transferrin-bound radioiron from the plasma (Fig. 4). These results suggest that in this patient with low plasma iron-binding capacity, iron incubated with a large volume of autologous plasma existed in two forms when it reached the liver: a) bound to transferrin in a normal fashion, resulting in a subsequent relatively slow rate of plasma clearance of such iron; and b) either not bound to transferrin or abnormally bound, resulting in a relatively rapid initial plasma clearance of such iron consequent to its rapid deposition in the liver.

As previously postulated by Wheby and Jones (1) and Wheby and Umpiere (2), we may explain our intestinal absorption results in patients with spontaneous chronic low latent iron-binding capacity by postulating that iron absorbed from the gastrointestinal tract is not initially bound to transferrin. When the plasma latent iron-binding capacity is low, much of the intestinally absorbed iron either does not become bound to transferrin or is abnormally bound, and is removed by the liver on the first pass of portal venous blood through this organ.

SUMMARY

In patients with spontaneous chronic low plasma latent iron-binding capacity, a large fraction of the intestinally absorbed iron is deposited in the liver without prior appearance in the systemic plasma. Such hepatic iron is not released to any large extent during the subsequent 2 weeks.

Our results are consistent with the hypothesis that iron absorbed from the intestinal tract is not initially bound to transferrin. When the plasma latent iron-binding capacity is normal, iron binds to transferrin prior to reaching the liver; when the plasma latent iron-binding capacity is low, a portion of the iron reaches the liver either unbound or abnormally bound to transferrin, resulting in its immediate hepatic deposition.

REFERENCES

1. Wheby, M. S., and Jones, L. G.; Role of Transferrin Iron Absorption; *J. Clin. Invest.* 42: 1007-1016, 1963.
2. Wheby, M. S., and Umpiere, G.; Effect of Transferrin Saturation on Iron Absorption in Man; *New Engl. J. Med.* 271: 1391-1395, 1964.
3. Fawwaz, R. A.; Winchell, H. S.; Pollycove, M.; Sargent, T., and Lawrence, J. H.; Intestinal Iron Absorption Studies Using Fe^{52} and Anger Positron Camera; *J. Nucl. Med.* 7: 569-574, 1966.
4. Saito, L.; Sargent, T.; Parker, H. C., and Lawrence, J. H.; Whole-body Iron Loss in Normal Man Measured with Gamma Ray Spectrometer; *J. Nucl. Med.* 5: 571-580, 1964.
5. Saylor, L., and Finch, C. A.; Determination of Iron Absorption Using Two Isotopes of Iron; *Am. J. Physiol.* 172: 372-376, 1953.

6. Hallberg, L., and Solvell, L.; Determination of the Absorption Rate of Iron in Man; Acta Med. Scand. 168, Suppl. 358: 3-17, 1960.
7. Hallberg, L., and Brise, H.; Determination of Fe⁵⁵ and Fe⁵⁹ in Blood; Intern. J. Appl. Radiation Isotopes 9: 100-108, 1960.
8. Peters, T.; Giovanniello, T. J.; Apt, L., and Ross, J. F.; A Simple Method for the Determination of the Serum Iron. II.; J. Lab. Clin. Med. 48: 280-287, 1965.
9. Tauxe, W. N.; A Rapid Radioactive Method for the Determination of the Serum Iron Binding Capacity; Am. J. Clin. Pathol. 35: 403-406, 1961.

Decreased Thymidine Synthesis and Increased ^3H -Thymidine Incorporation into DNA by Human Bone Marrow Cultured with Aminopterin

Serene L. Vimokesant, H. Saul Winchell, Myron Pollycove and Matthew B. Fish

De novo synthesis of thymidine is dependent upon the enzyme dihydrofolic acid reductase, which has been demonstrated to be inhibited by extremely low concentrations of 4-amino analogues of folic acid such as aminopterin, amethopterin, pyrimethamine and 2, 4, 7-triamino-6-phenyl-pteridine (Triamterin) (1). While addition of such 4-amino analogues of folic acid has been shown to inhibit de novo synthesis of thymidine in bacteria and animal tissues (2), apparently their effects on utilization of preformed nucleic acid in DNA synthesis has not been established. The simultaneous effect of aminopterin on thymidine synthesis, as estimated by ^{14}C incorporation into DNA thymidine from L-serine-3- ^{14}C , and the incorporation of thymidine into DNA, as estimated by ^3H -thymidine incorporation, in short-term normal human bone marrow culture is reported in this paper.

MATERIALS AND METHODS

Heparinized bone marrow was obtained by aspiration from the iliac crest of seven normal subjects. Each individual sample was well mixed in order to obtain a homogeneous suspension. Two ml aliquots were taken from each sample and suspended in five incubation tubes containing media and various additives. Previous experiments in dogs indicated that the number of marrow cells present in each aliquot of the same subject was consistent ($\pm\sigma = 2.8\%$). Incubation was done in Gey's balanced salt solution at pH 7.6 (Grand Island Biological Co.) under nitrogen. Five microcuries of L-serine-3- ^{14}C (Nuclear Chicago, 20.4 mCi/mmole) and 20 microcuries of thymidine- CH_3 - ^3H (New England Nuclear, 2.02 Ci/mmole) were added to each incubation tube. The total concentration of added thymidine (10^{-8}M) was shown in preliminary experiments with bone marrow from dogs to be insufficient to influence the rate of de novo thymidine synthesis from L-serine-3- ^{14}C . Aminopterin (Cal Biochem) was added to the first tube at 10^{-4}M concentration. The second tube served as control and received no additives. B_{12} coenzyme (5' deoxyadenosyl cobalamine) (3) was obtained through the courtesy of Dr. H. A. Barker of the Department of Biochemistry, University of California, Berkeley, and was added to the third tube at a final concentration of $1.7\text{ }\mu\text{g/ml}$ ($1.04 \times 10^{-9}\text{M}$). Deoxyuridine, deoxycytidine, deoxyguanosine, deoxyadenosine, and uridine were obtained from Nutritional Biochemical Corporation. The deoxyribosides were added to

the fourth tube at a final concentration of 10^{-8} M each. Uridine was added to the fifth tube at a final concentration of 10^{-8} M. Gey's balanced salt solution was added to each tube to obtain 4 ml final volume. After 3 hr of incubation in a Dubnoff metabolic shaker at 37°C , all tubes were removed and placed in ice. Cells were spun down and washed three times with ice-cold Gey's balanced salt solution. DNA was isolated by using the technique of Kay et al. (4) adapted for small samples. The isolated DNA was then hydrolyzed in formic acid at 175°C for 35 min in a sealed tube free of air (5). One hundred microliter aliquots were taken and spotted on Whatman paper #1 and thymine was separated by paper chromatography in an isopropyl: hydrochloric acid: water solvent system (6). The thymine spot was located under UV light and was eluted from the paper with 0.01 N HCl. Aliquots were taken and counted in a Nuclear Chicago liquid scintillation counter for ^{14}C and ^3H . Total thymine was estimated in a Beckman DU spectrophotometer by using UV absorption at 264 m μ . The fraction of thymidine synthesized by utilizing ^{14}C from L-serine-3- ^{14}C added to the culture was calculated by dividing the μCi of ^{14}C per mole of DNA thymidine by the specific activity of the L-serine-3- ^{14}C added to the culture. The fraction of thymidine incorporated into DNA was calculated by dividing the μCi of ^3H per mole of DNA thymidine by the specific activity of ^3H -thymidine added to the culture. Results were expressed as 10^{-4} moles of thymidine synthesized from L-serine-3- ^{14}C added to the culture, or thymidine added to the culture, which were incorporated into DNA per mole DNA thymidine.

RESULTS

Table 1 gives the fraction of DNA thymidine synthesized from L-serine-3- ^{14}C added to the bone marrow cultures from seven normal subjects. It is seen that aminopterin exerts a profound inhibitory effect on such *de novo* synthesis of thymidine. On the other hand, in the presence of aminopterin there is a simultaneous significant ($P < 0.005$, Table 2) and consistent ($r = 0.945$) increase in the incorporation into DNA of the ^3H -thymidine added to the culture. At the concentration used, no effect was observed of added B_{12} coenzyme, deoxyribosides, or uridine on such thymidine synthesis on the incorporation of ^3H -thymidine into DNA. The total DNA thymine isolated from each of the cultures derived from a given subject were found to be comparable. The fraction of thymidine added to the culture which was incorporated into DNA was calculated and found to be less than 0.05.

DISCUSSION

Since 70% of "1 C" fragments is normally derived from the number 3 carbon atom of L-serine (7), one may estimate *de novo* synthesis of thymidine from ^{14}C labeling of DNA thymidine following incubation with L-serine-3- ^{14}C . Thus, diminution in ^{14}C concentration in DNA thymidine in the experiments described utilizing aminopterin may be interpreted as additional evidence for suppression of thymidine synthesis in the presence of aminopterin.

The presence of increased incorporation of ^3H -thymidine into DNA while *de novo* synthesis of thymidine is diminished secondary to inhibition of tetrahydrofolic acid (THF) formation by aminopterin can be explained by postulating either: 1) increased utilization for DNA synthesis of nucleic acids present prior to inhibition of THF synthesis, or 2) diminution of either intracellular or extracellular thymidine pool size, resulting in increased specific

EFFECT OF AMINOPTERIN ON DNA SYNTHESIS IN BONE MARROW CULTURE

Table 1. Effect of aminopterin on the synthesis of ^{14}C thymidine from L-serine-3- ^{14}C .

Subjects	Aminopterin (10^{-4}M)	Control	B ₁₂ coenz. ($1.04 \times 10^{-9}\text{M}$)	d-ribosides (10^{-8}M)	Uridine (10^{-8}M)
	1.0	6.1	5.6	5.2	--
	0.0	9.2	7.0	7.4	--
	1.5	5.7	7.2	6.9	--
	0.8	5.7	5.3	4.8	4.7
	1.0	4.4	2.8	3.9	2.5
	3.1	7.1	7.5	8.3	--
	0.0	4.4	4.6	4.6	5.1
Mean \pm S. E.	1.1 ± 0.4	6.1 ± 0.6	5.7 ± 0.6	5.8 ± 0.6	4.1 ± 0.8

Table 1 summarizes results of the synthesis of ^{14}C thymidine from L-serine-3- ^{14}C added to the cultures of normal human bone marrow. Each column represents values obtained from short-term tissue culture containing the additive heading each column. The values presented are expressed as the fraction $\times 10^{-4}$ of DNA thymidine which was synthesized during the time of incubation, utilizing the L-serine-3- ^{14}C added to the culture.

Table 2. Effect of aminopterin on the incorporation of ^3H -thymidine into DNA.

Subjects	Aminopterin (10^{-4}M)	Control	B ₁₂ coenz. ($1.04 \times 10^{-9}\text{M}$)	d-ribosides (10^{-8}M)	Uridine (10^{-8}M)
	27.2	18.4	18.6	22.5	--
	35.5	26.8	15.7	23.7	--
	14.9	8.8	11.1	9.6	--
	28.4	19.9	16.4	18.3	14.4
	27.0	18.7	14.4	17.2	18.6
	55.4	36.3	38.7	39.7	--
	16.5	18.5	17.8	21.5	18.2
Mean \pm S. E.	29.3 ± 5.1	21.0 ± 3.2	19.0 ± 3.4	21.8 ± 3.4	17.1 ± 1.3

Table 2 summarizes results of ^3H -thymidine incorporation into DNA in cultured normal human bone marrow. Each column represents values obtained from short-term tissue culture containing the additive heading each column. The values presented are expressed as the fraction $\times 10^{-4}$ of DNA thymidine which was incorporated during the time of incubation, from thymidine added to the culture.

activity of ^3H -thymidine involved in DNA synthesis. This latter possibility appears improbable since the size of the intracellular thymidine pool in normal bone marrow cells at any instant is normally quite small (8) in relation to the total thymidine added to the culture, so that its diminution subsequent to decreased synthesis of thymidine would not be expected to significantly alter the specific activity of the ^3H -thymidine pool. While a diminution in the pool size of the extracellular thymidine pool could result from diminished catabolism of DNA, such a process does not appear to be a function of aminopterin. Moreover, the total quantity of thymidine incorporated into DNA from the ^3H -thymidine pool represented a small fraction of this pool (0.05).

The lack of effect of addition of deoxyribosides, uridine, or excess B_{12} coenzyme on either the *de novo* synthesis of thymidine or the incorporation of thymidine into DNA indicates that such syntheses are independent of increases in pool sizes of these materials under these experimental conditions. These results further suggest that the increase in ^3H -thymidine incorporation into DNA with the use of aminopterin was not related to increase in DNA polymerase activity induced by moderate increase in deoxyribosides concentration (9).

SUMMARY

When incubated with normal human bone marrow cells in the presence of L-serine- $3\text{-}^{14}\text{C}$ and ^3H -thymidine, aminopterin decreases synthesis of ^{14}C -thymidine to 16%, while incorporation of ^3H -thymidine into DNA is increased to 140%, of control values. These results are interpreted as evidence for increased utilization of preformed nucleic acids in DNA synthesis in the presence of aminopterin.

REFERENCES AND NOTES

1. Hamfelt, A., and Wilmanns, W.; Clin. Chim. Acta 12: 144, 1965.
2. Bertino, J. R.; Booth, A.; Bieber, A. L.; Cashmore, A., and Sartorelli, A. C.; J. Biol. Chem. 239: 479, 1964.
3. Barker, H. A.; Smyth, R. D.; Weissbach, H.; Toohey, J. I.; Ladd, J. N., and Volcani, B. E.; J. Biol. Chem. 235: 480, 1960.
4. Kay, E. R. M.; Simmons, N. S., and Dounce, A. L.; J. Am. Chem. Soc. 74: 1724, 1952.
5. Jordan, D. O.: The Chemistry of Nucleic Acids, London, Butterworth and Co., Ltd., 1960, p. 80.
6. Wyatt, G. R.; Biochem. J. 48: 584, 1951.
7. Spinsor, D. B.: A Symposium on Amino Acid Metabolism, edited by W. D. McElroy and H. B. Glass, Baltimore, Johns Hopkins Press, 1955, p. 608.
8. Feinendegen, L. E.; Bond, V. P., and Hughes, W. L.; Proc. Soc. Exptl. Biol. Med. 122: 448, 1966.
9. Hiatt, H. H., and Bojorski, T. B.; Cold Spring Harbor Symposium Quant. Biol. 26: 357, 1961.

Serene L. Vimokesant is a Fellow of the International Atomic Energy Agency sponsored by the National Academy of Sciences, National Research Council, Washington, D. C. Present address: Faculty of Medical Science, University of Medical Sciences, Bangkok, Thailand.

1175283

A Summary of Some Studies on Erythropoiesis Using Anti-Erythropoietin Immune Serum

*John C. Schooley, Joseph F. Garcia, Linda N. Cantor
and Virginia W. Havens*

Several years ago Schooley and Garcia (1) demonstrated that serum obtained from some rabbits immunized with human urinary erythropoietin could neutralize the biological effects of erythropoietin. Lange and co-workers (2) confirmed this observation and produced immune serum after immunization with sheep plasma erythropoietin. The present paper summarizes various studies from this laboratory on the preparation and properties of the anti-erythropoietin serum and some examples of the usefulness of this immune serum in investigations of the physiology of erythropoiesis.

PREPARATION OF THE IMMUNE SERUM Young male New Zealand rabbits of about 5 to 6 lb have been immunized with concentrates of human urine containing erythropoietin (ESF) by various schedules (3). Immune sera having the highest titers have generally been obtained after immunization with alum-precipitated human urinary ESF, but this method of immunization requires rather large amounts of ESF. We have utilized the following immunization schedule with fair success. Multiple subcutaneous injections at weekly intervals were made of about 2 ml of a 1:1 mixture of complete Freund's adjuvant and 10 mg of human urinary ESF in saline (about 200 cobalt units). Some rabbits have detectable anti-erythropoietin (anti-ESF) titers after 3 or 4 weeks, i.e., after the injection of 30 mg or 600 cobalt units of ESF. The time of harvesting serum from immunized rabbits, regardless of the schedule of immunization used, is critical. We have previously noted (3) that rabbits having high anti-ESF titers were anemic and it was demonstrated that the immune serum could neutralize rabbit ESF (4). However, if the rabbit becomes too severely anemic as a result of neutralization of its own ESF, a marked increase in ESF production is triggered which is more than sufficient to combine with the antibody produced as a result of the immunization. Some rabbits have been observed to alternate between periods of detectable antibody production and periods of excessive production of endogenous ESF. Therefore, it is important to follow the hematocrit and reticulocyte levels of immunized rabbits and harvest the immune serum when these parameters just begin to become depressed.

It is important to realize that some sera containing anti-ESF as tested in polycythemic mice are toxic if injected in the larger amounts necessary for experiments with non-polycythemic mice. Such toxicity often disappears if the sera are stored frozen for several months.

of practical significance is the observation that many rabbits will produce very low-titer anti-ESF that is impossible to use in most experiments. In such cases isolation and subsequent concentration of the γ -globulin yields a more potent antibody preparation.

Garcia and Schooley (4) previously demonstrated that the biological activity of erythropoietins found in serum or plasma of mice, rats, sheep, humans, and rabbits can be neutralized by anti-ESF obtained from rabbits immunized with human urinary ESF. Other investigators have shown that the erythropoietic activity of renal cyst fluid (5, 6) as well as cerebellar hemangioblastoma cyst fluid (5) is neutralized by anti-ESF. It is evident that the erythropoietins obtained from these different sources are similar. Of interest is the fact that in the immunized rabbit the cyclic relationship between anti-ESF and ESF levels was evident during the early stages of immunization but not after prolonged immunization. Serum obtained from this rabbit after prolonged immunization, when the rabbit was not anemic, was able to neutralize human and sheep ESF but not rabbit ESF (7). This suggests that although the erythropoietins of different animals are similar, they are not necessarily identical.

The fact that in most rabbits a severe anemia results as a consequence of immunization with human urinary ESF suggests that an auto-immune state has been experimentally produced. Similar auto-immune inhibitions of erythropoiesis undoubtedly occur clinically. Boyer and Lowenstein have quite recently (8) presented evidence for an inhibitor of erythropoiesis in patients with erythroblastopenia which exhibits a biological behavior similar to that of anti-sera against ESF.

PROPERTIES OF THE IMMUNE SERUM Injection of anti-ESF into polycythemic mice at the same time as injection of exogenous ESF completely prevents an erythropoietic response. Injection of anti-ESF into polycythemic mice 1 or 2 days after the initiation of a wave of erythropoiesis by injection of ESF has little or no effect on the magnitude of the erythropoietic response (3). The magnitude of the erythropoietic response depends upon the dose of ESF injected and the time of anti-ESF injection (3). Injections of anti-sera against ceruloplasmin, transferrin, orosomucoid, α_1 -acid glycoproteins, human urinary proteins, bovine serum albumin, bovine growth hormone, hog renin, and sheep interstitial-cell-stimulating hormone do not inhibit the erythropoietic response of polycythemic mice to injections of ESF. The neutralizing ability of anti-ESF sera was not affected by absorption with kidney, spleen, or liver of normal, polycythemic, cobalt- nor phenylhydrazine-injected mice, nor with normal mouse serum nor human urinary proteins. The addition to anti-ESF of ESF previously inactivated by acid hydrolysis only slightly decreased the subsequent ability of the anti-ESF to compete with biologically active ESF. Biologically active ESF is the only one of all the proteins that have thus far been used which blocks the neutralizing ability of anti-ESF (3).

The neutralizing ability of the immune serum is associated with the γ -globulins (3). Electrophoresis in agar and immunodiffusion studies of the purified γ -globulin using goat anti-rabbit γ -globulin have recently confirmed the purity of the isolated γ -globulin. Studies of the properties of the immune serum prepared by ultracentrifugation in sucrose gradients indicate that the neutralizing ability of the immune serum is associated with the 19S γ -globulins.

Further evidence of the importance of γ -globulin in the neutralization reaction was obtained in the following experiment. The amount of goat anti-rabbit γ -globulin (goat ARGG) required for maximum precipitation of the γ -globulin in one anti-ESF preparation was determined. The amount of that anti-ESF required to neutralize a given amount of ESF was determined by bioassay, since no precipitate results from the reaction between ESF and anti-ESF. Equal aliquots of ESF, anti-ESF or normal rabbit serum, and goat ARGG were mixed in different sequences. In the first sample, ESF and anti-ESF were mixed, incubated overnight, and then goat ARGG was added; in the second sample, anti-ESF was replaced by normal rabbit serum. In the third sample, the goat ARGG was added to the anti-ESF, incubated overnight, and then the ESF was added. The precipitates formed after the goat ARGG additions were removed by centrifugation and the erythropoietic activity of the supernatant was determined, after suitable dilutions, in hypertransfused polycythemic mice by procedures previously described (3). The results, as shown in Table 1, indicate that if the γ -globulin of the immune serum is removed by precipitation with goat ARGG prior to the addition of ESF, no neutralization of the ESF occurs. Since ESF is neutralized if the goat ARGG is added after the mixing of anti-ESF and ESF, the neutralization reaction must have occurred prior to the addition of the goat ARGG. This shows that although the evidence for neutralization requires an *in vivo* biological assay system the actual combination between ESF and anti-ESF can occur *in vitro*. These experiments all support the view that the neutralization of ESF by anti-ESF is the result of an antigen-antibody reaction.

Table 1.

Sample		Percent ^{59}Fe uptake (72 hr) in RBC of polycythemic mice
1	(ESF + anti-ESF) + goat ARGG	$0.25 \pm 0.08^*$
2	(ESF + normal rabbit serum) + goat ARGG	5.25 ± 0.62
3	(Anti-ESF + goat ARGG) + ESF	7.61 ± 0.96
4	Normal rabbit serum	0.13 ± 0.01

* Standard error of the mean.

The availability of this immune serum provides a potent tool for investigating many problems of the regulation of erythropoiesis and stem cell kinetics. In the second portion of this paper we will briefly describe various published and unpublished experiments of Schooley, Cantor and Havens using anti-ESF.

ERYTHROPOIESIS IN NORMAL ADULT MICE We have emphasized previously that injections of adequate amounts of anti-ESF into normal mice can essentially abolish erythropoiesis, although granulocytopoiesis and megakaryocytopoiesis are little affected (9). In Fig. 1 a section of the spleen of an anti-ESF injected mouse (B) is compared with a section of the spleen of a mouse injected with normal rabbit serum (A). Sections of the bone marrow from



Fig. 1. A comparison of sections of spleens of normal mice (A) injected with normal rabbit serum and (B) injected with anti-erythropoietin.

XBB677-4106

1175287

the same mice are shown in Fig. 2. The mice were injected subcutaneously with 0.25 ml of either of the two sera daily for 4 days and killed on the 5th day. It is obvious that nucleated erythroid cells have been virtually eliminated in the anti-ESF injected mice (B of Figs. 1 and 2). This observation seems to us to be the best evidence currently available that ESF is necessary for the normal regulation of erythropoiesis even though its presence cannot be demonstrated in the blood of normal mice by current assay procedures.

ERYTHROPOIESIS IN TESTOSTERONE INJECTED POLYCYTHEMIC MICE The injection of testosterone into the polycythemic mouse is followed by a wave of erythropoietic activity observable several days later than that caused by injection of ESF (10). It has been further demonstrated by several groups of investigators (11-14) that plasma taken from several animal species after injections of testosterone stimulates erythropoiesis in the polycythemic mouse. This stimulation has been generally assumed to be due to the presence of ESF in the plasma taken from the testosterone-injected animals; however, as Fried and Gurney (13) have stated, it is equally possible that a metabolic product of testosterone is responsible for the stimulation. Schooley (15) has recently shown that the injection of anti-ESF completely abolishes the erythropoietic response observed in the polycythemic mouse after testosterone injections. These results support the view that the erythropoietic stimulation resulting from testosterone injection is mediated by the production of ESF.

ERYTHROPOIESIS IN WW^V MUTANT MICE Russell and co-workers (16) have studied extensively the W-series mutant mouse which suffers from a severe inherited macrocytic anemia which is well established at birth. The fact that transplants of hemopoietic tissue from normal *ww* mice can restore erythropoiesis in WW^V mice indicates that the genetic defect in the WW^V mouse occurs in the hematopoietic cells themselves (16). McCulloch et al. (17) presented evidence that the genetic defect occurs in spleen colony-forming cells; other evidence suggests that the colony-forming cell corresponds to the hematopoietic stem cell (18).

Keighley et al. (19) found that WW^V mice failed to respond with increased erythropoietic activity to injections of exogenous ESF although they did respond erythropoietically when exposed to simulated altitude. It was therefore of interest to study the role of ESF in the regulation of erythropoiesis in WW^V mice by using anti-ESF.

Male mice of the WW^V and normal *ww* genotype, 4 to 5 months of age, obtained from the Roscoe B. Jackson Memorial Laboratory, Bar Harbor, Maine, were injected intraperitoneally with 0.25 ml of anti-ESF or normal rabbit serum daily for 4 consecutive days. On the 5th day, 0.5 μ Ci of ^{59}Fe as iron citrate (specific activity approximately 10 μ Ci/mg) was injected intravenously, and 24 hr later blood was taken by cardiac puncture. A measured amount of blood was washed with saline and the ^{59}Fe uptake determined. The ^{59}Fe uptake is given as the percent ^{59}Fe in the calculated blood volume; the blood volume was assumed to be 5.5% of the body weight, according to the data of Keighley et al. (19). Hematocrits were measured and smears of the bone marrow made. The percentage of reticulocytes in the peripheral blood and the percentage of erythroid cells present in the marrow were determined.

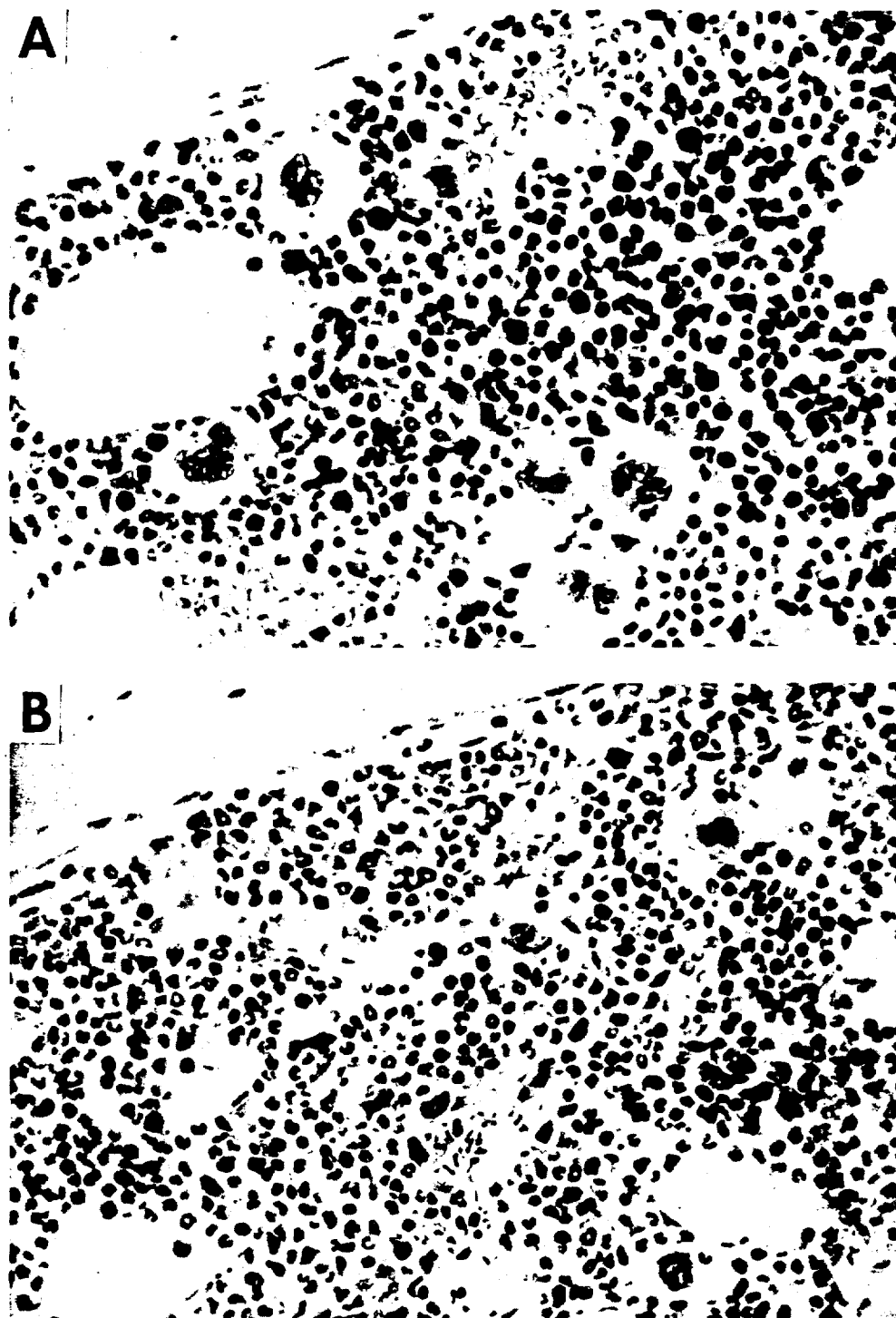


Fig. 2. A comparison of sections of bone marrow of normal mice (A) injected with normal rabbit serum and (B) injected with anti-erythropoietin.

XBB677-4107

1175289

The results are shown in Table 2. A marked decrease in the hematocrits of the WW^V mice injected with anti-ESF was observed, as well as a decrease in percentage of erythroid cells in the bone marrow, number of reticulocytes in the peripheral blood, and ^{59}Fe uptake in the peripheral blood. We conclude that erythropoiesis in the WW^V mouse, as in the normal mouse, is regulated by ESF. Keighley has also demonstrated some inhibition of erythropoiesis after injections of anti-ESF (20).

Table 2. Effect of anti-erythropoietin on erythropoiesis in WW^V and ww mice.

	WW^V		ww	
	NRS	Anti-ESF	NRS	Anti-ESF
Weight (g)	$35.3 \pm 1.29^*$	34.8 ± 0.88	33.6 ± 0.37	33.7 ± 0.77
Hematocrit (%)	37.1 ± 0.40	31.1 ± 0.94	44.4 ± 0.72	40.4 ± 0.63
24-hr ^{59}Fe uptake (%)	37.7 ± 1.74	0.63 ± 0.21	40.0 ± 1.58	0.38 ± 0.06
Erythroid cells in marrow (%)	12.2 ± 0.82	<0.4	12.5 ± 0.84	<0.4
Reticulocytes in blood (%)	4.12 ± 0.31	<0.00	2.54 ± 0.11	<0.00

* Standard error of the mean.

In a similar experiment, spleens from WW^V mice injected for 4 consecutive days with anti-ESF or normal rabbit serum were removed, pooled by sex, and a single cell suspension was prepared in medium 858. The spleen suspension was diluted with the medium to 20×10^6 cells/ml, and 0.5 ml (10^7 cells) was injected into heavily irradiated host ww , Ww , or W^Vw mice of the same sex as the donor. The number of macroscopically visible colonies on the spleen was determined 10 days after irradiation and transplantation. The total colony-forming cells from WW^V mice injected with normal rabbit serum was 1.36 ± 0.31 per 10^7 cells in 44 recipient mice and from WW^V mice injected with anti-ESF was 2.13 ± 0.37 per 10^7 cells in 47 recipients. The total number of colony formers in the spleens of these mice is less than 1% of that observed in non-mutant mice. Thus, in agreement with McCulloch et al. (17), we found very few colony formers in the spleens of the WW^V mice. Interestingly, the suppression of erythropoiesis for this period of time in these WW^V mice did not change significantly the number of colony-formers per spleen.

ERYTHROPOIESIS IN NORMAL MICE EXPOSED TO SIMULATED ALTITUDE

During acclimatization to altitude a marked increase in the red cell volume occurs and increased levels of ESF are found in the blood soon after exposure to altitude. The effect of anti-ESF on the erythropoietic response of female C_3H mice, 5 to 6 weeks of age, exposed to a simulated altitude was investigated. Two groups of six mice each were placed in an altitude chamber at a simulated altitude of 18,000 feet for 5 days. The altitude chamber was returned daily to normal atmospheric pressure for approximately 15 minutes and one of the groups of mice was injected intraperitoneally with 0.25 ml of anti-ESF each day for 5 days.

Another group of mice, not exposed to altitude, was used as a control. On the 4th day of exposure to altitude ^{59}Fe was injected intravenously and 24 hr later blood was obtained by cardiac puncture. A measured amount of blood was washed with saline and the ^{59}Fe uptake determined. The ^{59}Fe uptake is given as the percent ^{59}Fe in the blood volume; the blood volume was assumed to be 5.5% of the body weight. Hematocrits were measured and the percentage of reticulocytes in the blood was determined. The spleens of the mice from each group were pooled and a single cell suspension was prepared by using a modified Eagle's medium without calcium. The total number of nucleated cells per spleen was determined and the suspension was injected, after suitable dilution, into heavily irradiated isologous mice. Smears of the injected spleen cell suspension were examined for the presence of erythroid cells. The total number of spleen colonies was determined 10 days after transplantation; the total number of colony-forming cells per spleen was then calculated. The results are shown in Table 3.

Table 3. Effect of anti-erythropoietin on erythropoiesis and on the content of colony-forming cells in the spleens of hypoxic mice.

	Control-non hypoxic	Hypoxic for 5 days	
		Non-injected	Anti-ESF injected
Weight (g)	$20.3 \pm 0.31^*$	18.5 ± 0.41	16.9 ± 0.69
Hematocrit (%)	40.5 ± 0.43	51.2 ± 0.99	39.4 ± 0.71
24-hr ^{59}Fe uptake (%)	22.5 ± 0.94	43.8 ± 0.57	4.97 ± 1.12
Reticulocytes (%)	4.56 ± 0.87	17.2 ± 1.00	1.24 ± 0.33
Cells/spleen	182×10^6	313×10^6	144×10^6
CFU/spleen	5366 ± 300	3100 ± 393	1111 ± 100
% Decrease		42	79

*Standard error of the mean.

It is evident both on the basis of ^{59}Fe uptake and the reticulocyte levels that a marked stimulation of erythropoiesis occurred in mice following exposure to simulated altitude as compared to the non-hypoxic mice. This erythropoietic stimulation did not occur in hypoxic mice injected with anti-ESF. In fact, the erythropoietic response in these animals was almost 75% lower than in the normal non-hypoxic animals, but it was not decreased to the extent that one would observe in non-hypoxic mice injected with the same amount of anti-ESF. Presumably this is due to the fact that the amount of anti-ESF injected was not sufficient to neutralize all of the ESF produced as a result of the hypoxic exposure.

The changes in the total number of colony-forming cells in the spleens of hypoxic mice and hypoxic mice injected with anti-ESF compared to the spleens of normal mice is of

1175291

particular interest because of the current concepts of the interrelationship between colony-forming cells and erythropoietin-sensitive cells. Bruce and McCulloch (21) observed a progressive decrease in the total number of colony-forming cells in the spleens of mice exposed to hypoxia, but no decrease in the colony-forming cells in the marrow. They interpreted their results as indicating that ESF did not act directly on the colony-forming cell. Schooley (22) observed that the overall doubling time of colony-forming cells after transplantation into heavily irradiated polycythemic mice was not altered by the injection of exogenous ESF. In addition, it was found that the daily injection of ESF into polycythemic hosts did not decrease the total number of spleen colonies observable on the host spleen 10 days after transplantation from the levels found in the non-ESF injected control mice.

The changes in the total number of cells and colony-formers in the spleens of polycythemic host mice following heavy irradiation and transplantation with 2×10^6 bone marrow cells was compared in ESF and non-ESF injected mice (23). This inoculum of bone marrow contained 420 colony-formers. In both groups, 4 days after transplantation there were 250 colony-formers detected in the spleen and by the 6th day there were 1000. However, during this same time interval there was an increase of about 30×10^6 nucleated cells in the spleens of the mice given erythropoietin, whereas there was only a slight increase in the number of nucleated cells in the spleens of the mice receiving no ESF. Differential counts of the nucleated cells in the ESF-injected mice indicated that at least 25×10^6 erythroid cells were produced in the spleens in this 2-day interval. What was the source of these erythroid cells? Assuming a generation time of 8 hr, it would be impossible to produce the numbers of nucleated erythroid cells found in the spleen, even if all the colony-formers in the mouse, not only in the spleen but in the rest of the body, were stimulated to differentiate into erythroid cells. It is obvious that if all the colony-formers were stimulated to differentiate, the replication of colony-formers themselves should either be abolished or markedly inhibited, yet the growth curve indicates a significant increase in colony-formers in the spleen during this time of increased production of nucleated erythroid cells. These observations suggest that the nucleated erythroid cells produced during this 2-day interval are not the result of the action of ESF directly on colony-forming cells, but the result of the action of ESF on much larger numbers of erythropoietin-sensitive cells present either in the bone marrow at the time of transplantation and/or produced from colony-forming cells during the first 4 days after transplantation. This possibility, that many of the colony-forming cells which initially settle in the spleen after transplantation become ESF-sensitive cells, may explain both the initial decrease and the lag observed before the transplanted colony-forming cells enter an exponential stage of growth. Therefore it is concluded, in agreement with Bruce and McCulloch (21), that ESF does not act directly upon the colony-forming cell, but upon some ESF-sensitive progeny of the colony-forming cell. The presence of this pool of cells sensitive to differentiative agents could explain the observation that colony-forming cells, or stem cells, can maintain themselves even when differentiative pressures are markedly increased.

If the above interpretations are valid, numerous questions arise regarding the properties of the progeny of colony-forming cells that are capable of responding to differentiative agents such as ESF. What regulates the movement of colony-forming cells into ESF-sensitive cells? What is the size of the ESF-sensitive pool of cells? Are all of the ESF-sensitive cells actually able to respond to ESF at any one time? Are ESF-sensitive cells continuously derived from colony-forming cells in the absence of ESF? If so, what is the fate of these cells? Does the pool of ESF-sensitive cells increase exclusively by the movement of colony-forming cells into ESF-sensitive cells or are ESF-sensitive cells capable of a limited proliferative capacity? Do ESF-sensitive cells simply die if not triggered within some limited time period to differentiate? Is the radiation sensitivity of ESF-sensitive cells different from that of colony-forming cells? Are ESF-sensitive cells pluripotent, i. e., can they also upon appropriate stimulation differentiate into granulocytic, megakaryocytic, or perhaps even lymphoid cells? Can ESF-sensitive cells after transplantation into heavily irradiated hosts settle in the spleen, proliferate, and give rise to macroscopic spleen colonies? The answers to these questions are of considerable importance in interpreting experiments on the colony-forming cell. Some experimental data is available which allows reasonable speculation about at least some of these questions.

Utilizing the technique of injecting ESF into polycythemic mice and limiting the time of action by subsequent neutralization with anti-ESF, Schooley (24) has presented evidence suggesting that the ESF-sensitive cell is able to respond to ESF only at some limited period of its individual life cycle.

The fact that mice kept polycythemic for 1 month do not have an increased response to ESF compared to the response observed when the same dose of ESF is injected into mice kept polycythemic for one week suggests that large numbers of ESF-sensitive cells do not accumulate in the absence of erythropoietic stimulation (unpublished observations). We have observed that the total number of colony-formers in the spleens of polycythemic mice is consistently higher than in non-polycythemic mice, which suggests that the movement of colony-formers into ESF-sensitive cells is decreased in polycythemic mice where ESF stimulation is minimal, and therefore there are increased numbers of colony-forming cells.

After 5 days of exposure to hypoxic conditions the total number of colony-formers in the spleens of mice injected with anti-ESF decreased by about 80% of normal as compared to about a 40% decrease in the control hypoxic mice (see Table 3). This suggests that in the hypoxic mouse the colony-forming population is stimulated to replace the ESF-sensitive cells which have matured in response to increased ESF production, and the colony-forming cell pool is therefore depleted. An even greater decrease in the colony-forming population occurs when the ESF in hypoxic mice is neutralized by anti-ESF, indicating that it is not the presence of increased levels of ESF which regulates the movement of colony-forming cells into ESF-sensitive cells, but that either hypoxia or some agent other than ESF produced as a result of the hypoxic condition is responsible for the regulation. It seems unlikely that the size of the ESF-sensitive cell pool itself is involved in this regulation since a considerable increase in the

size of the pool should occur in the hypoxic mice injected with anti-ESF, unless the cells' life cycle is very short.

There is some evidence which suggests that the ESF-sensitive cell is itself capable of division. The number of endogenous spleen colonies in a group of heavily irradiated mice was 3 to 4 times greater than normal if the mice were exposed to hypoxia after irradiation. The number in the normal mice was 1.23 ± 0.39 as compared to the hypoxic value of 4.67 ± 1.20 . Since the total number of colony-forming cells which can be extracted from the spleens of hypoxic mice is decreased from normal, as shown in Table 3, it is rather surprising to find that in hypoxic mice the number of observable endogenous spleen colonies is increased over control non-hypoxic mice. These data suggest that some ESF-sensitive cells survive the irradiation and proliferate sufficiently to give rise to a detectable spleen colony. Bruce and McCulloch (17) found that the number of endogenous colonies in mice irradiated after a 10-day exposure to hypoxia was significantly less than that found in non-hypoxic controls. We suggest that in their experiments the available pool of ESF-sensitive cells is extremely low at the time of irradiation because of the previous hypoxic exposure, and therefore very few ESF-sensitive cells are present to produce colonies. The colonies that are observed are presumably derived from colony-forming cells.

On the basis of mature cell types in any given colony, numerous investigators have classified colonies as exclusively one cell type or as mixtures of granulocytic, erythroid, or megakaryocytic cells. We find after the transplantation of normal bone marrow cells that about 60% of the colonies can be classified as exclusively erythroid. It is our impression, however, that following the transplantation of regenerating hematopoietic tissue almost all of the colonies are mixed. We have studied the cellular composition of spleen colonies in heavily irradiated polycythemic mice on the 10th day after transplantation of bone marrow when ESF has been injected on either the 8th or 9th day, and have observed that foci of as many as 20,000 erythroid cells are found within obvious granulocytic colonies as well as in areas beneath the splenic capsule where no other mature hematopoietic cells are present. The possibility that ESF-sensitive cells themselves have a proliferative capacity sufficient to form distinct colonies may explain the observed cellular compositions.

The failure of some accumulations of cells within the spleen to become granulocytic or megakaryocytic in the absence of ESF (23) and the observations that other accumulations of cells within granulocytic colonies can become erythroid in the presence of ESF (23), suggests that the ESF-sensitive cell is only capable of stimulation into the erythroid series; i.e., it is not a pluripotential cell. This view would propose that the colony-forming cell is a pluripotential cell which gives rise to progeny which are unipotential. If this interpretation is correct, the speculations concerning the behavior of ESF-sensitive cells would apply equally to cells capable of differentiation into the granulocytic and megakaryocytic series.

To summarize, we feel, on the basis of the evidence presented above, that it is probable that not all of the colonies observed on the surface of the spleen are derived directly from colony-forming cells, but some colonies are derived from cells which are sensitive to

1175294

differentiative agents and have a limited proliferative capacity adequate to give a detectable colony. Thus, a rigorous definition of a colony derived from a colony-forming cell should perhaps include the requirements: (1) the colony is mixed and/or (2) retransplantation of the colony gives rise to mixed colonies.

ERYTHROPOIESIS IN MICE AFTER 200R IRRADIATION Temporal changes in the precursor cell populations which give rise to spleen colonies and which respond to ESF were measured in polycythemic mice before and at various times after 200R whole-body ^{60}Co irradiation (22). The results are shown in Fig. 3. Immediately after irradiation, the responsiveness of the mice to the intravenous injection of 1 cobalt unit of ESF was depressed to about 75% of normal; by the 5th day after irradiation the response approached normal and during the 9th to 12th day the response was slightly above normal. These data of ESF sensitivity essentially agree with the data of Alexanian et al. (25), Gurney et al. (26) and Gurney (27). The total number of spleen colony formers in the spleen and femurs was depressed to about 20-30% of normal; this depression continued for at least 13 days after irradiation. The number of colony-formers in the spleen by the 15th day after irradiation increased to about 4 times the normal level; the marrow colony formers by the 20th day increased to but did not rise above the normal level. Till (28) has reported that the recovery of colony-forming cells in the marrow after 155 rads follows a pattern similar to that shown above, and he has also indicated that following 400 rads, the colony-formers in the spleen recover much more rapidly than we have shown after 200R. Therefore, the increased responsiveness of these irradiated mice to ESF occurs at a time when the number of colony-formers in the spleen and bone marrow is far below normal and no greater than that observed immediately after irradiation, when the response to ESF is very low. Blackett et al. (29) have also observed that the recovery of erythropoiesis in rats irradiated with 200R occurs before the recovery of the repopulating ability of the marrow. This repopulating ability is presumably a measure of the number of stem cells (or by definition, colony-forming cells) in the recovering bone marrow. Other data (22), using the mitotic poison, vinblastine, according to the technique of Becker (30), show that a large proportion of the colony-forming cells are actively dividing soon after exposure to 200R. Since the number of colony-formers does not increase at this time, it seems probable that the colony-forming cells immediately move into a population of cells sensitive to ESF or other differentiative agents.

If 1 cobalt unit of ESF is injected into a polycythemic mouse and 6 hr later enough antibody against ESF is injected in the mouse to neutralize all the ESF which has not acted, a small but measurable erythropoietic response occurs. During the 9th to 12th days after 200-R irradiation, if ESF acts in the polycythemic mouse for only 6 hr, an erythropoietic response of about 4 times that observed in the non-irradiated polycythemic mouse occurs, as shown in Fig. 4. These results suggest that 4 times the number of ESF-sensitive cells exist in the irradiated polycythemic mouse at this time than in a non-irradiated polycythemic mouse. It is unlikely that these ESF-sensitive cells could have been produced by division of the available colony-forming cells or ESF-sensitive cells in 6 hr.

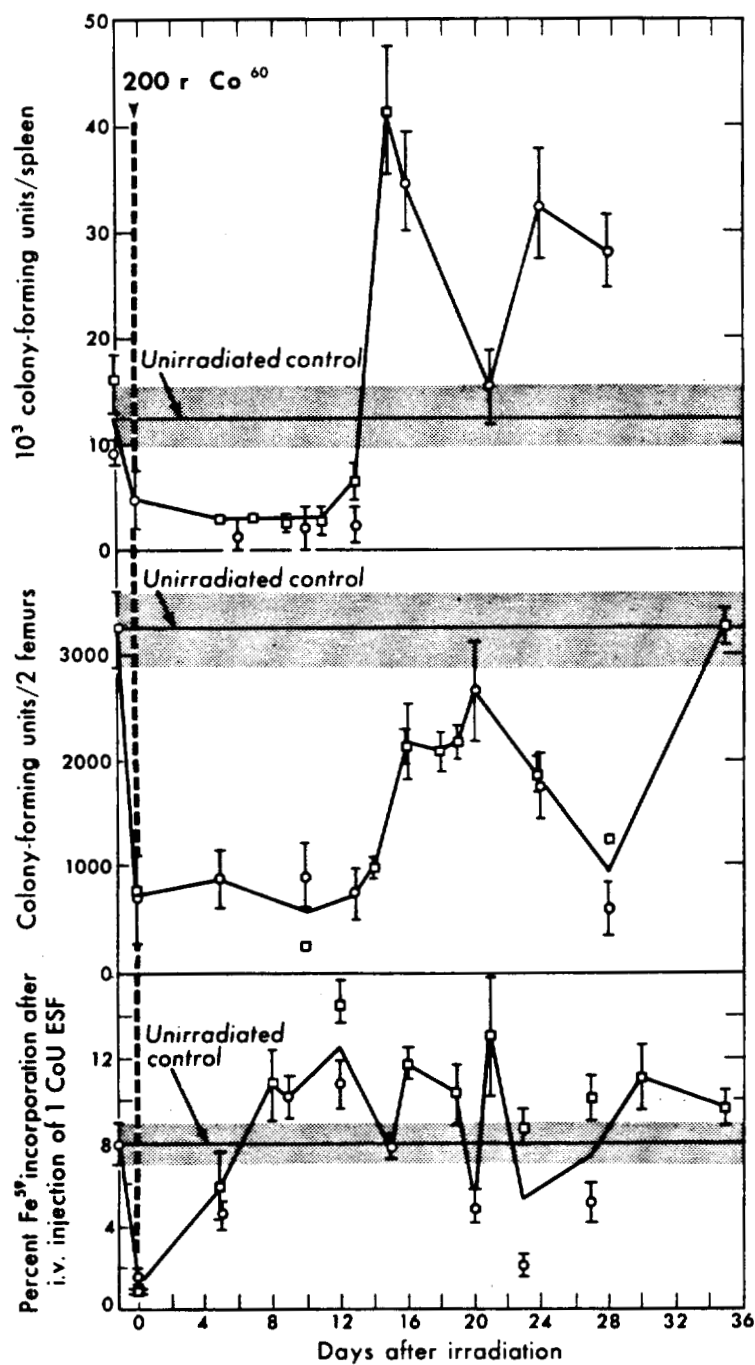


Fig. 3. A comparison as a function of time of erythropoietin sensitivity and colony-forming cells in the bone marrow and spleens of polycythemic mice irradiated with 200-R whole-body ⁶⁰Co gamma rays. Standard errors of the mean are shown.

MUB-8542

1175296

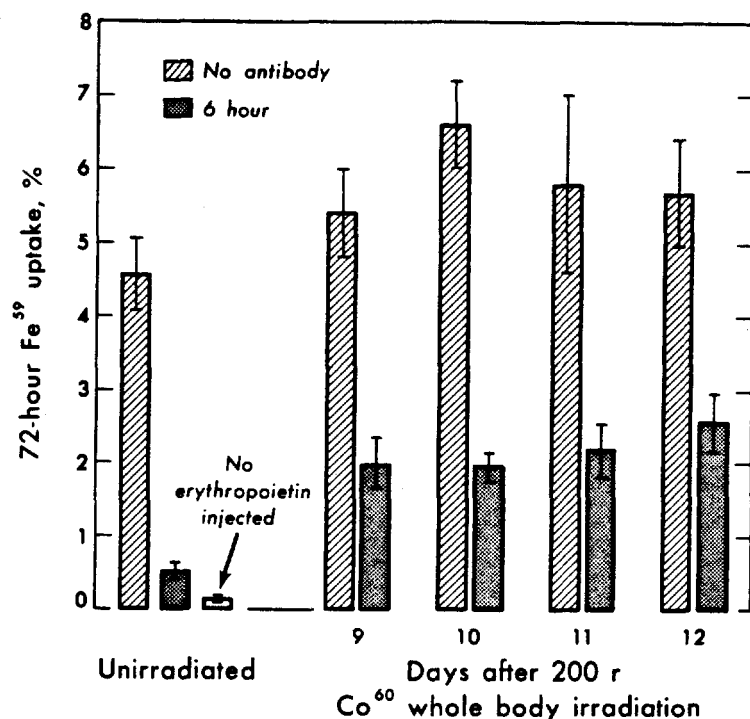


Fig. 4. Effect of limiting the time of action of 1 cobalt unit of erythropoietin to 6 hr on the responsiveness of irradiated and unirradiated polycythemic mice.

MUB-8867

ERYTHROPOIESIS IN THE NEWBORN RAT Jacobson et al. observed several years ago (31) that transfusion of a pregnant mouse resulted in suppression of erythropoiesis in the mother but not in the fetuses. Schooley and Giger (unpublished observations) confirmed Jacobson's observations and, in addition, found that after injection of anti-ESF into pregnant mice, erythropoiesis was significantly suppressed in the mother and in some but not all of the fetuses.

The effect of anti-ESF on the erythropoiesis of newborn rats was investigated. Several litters of rats were used; half of each litter received injections of 0.1 ml of anti-ESF each morning and evening for 6 days. On the 5th day after birth, 0.5 μ Ci ⁵⁹Fe was injected intraperitoneally and 24 hr later blood was taken by cardiac puncture. The ⁵⁹Fe uptakes were determined and the results expressed as the percentage of the injected ⁵⁹Fe in the blood volume; the blood volume was assumed to be 7% of the body weight, according to the data of Garcia (32). Hematocrits were measured, smears of the femoral marrow were made, and the spleen and liver fixed in Bouin's fixative for histological examination. The results are shown in Table 4. It is evident that a marked suppression of erythropoiesis on the basis of ⁵⁹Fe uptake occurred. Nucleated erythroid cells were rarely observed in the spleen and bone marrow, and the erythropoietic foci present in the livers of the control mice were absent in the anti-ESF injected mice. Very few reticulocytes with well developed reticulum were observed in the anti-ESF injected animals.

Table 4. Effect of anti-erythropoietin on erythropoiesis in newborn rats.

	Control-uninjected	Anti-ESF-injected
No. of rats	14	18
Weight (g)	11.0 ± 0.25 *	10.6 ± 0.19
Hematocrit (%)	30.2 ± 0.48	17.2 ± 0.48
24-hr ⁵⁹ Fe uptake (%)	51.0 ± 2.64	3.77 ± 0.47

*Standard error of the mean.

The erythropoietic activity of 1 ml of plasma obtained from 5-day old rats was assayed in the polycythemic mouse. The percent ⁵⁹Fe uptake in the assay mice was 0.54 ± 0.05, compared to 0.11 ± 0.01 when adult rat serum was injected. This difference is highly significant ($P < 0.001$), indicating that detectable amounts of ESF occur in the newborn rat.

Lucarelli et al. (33) have recently demonstrated that erythropoiesis is little affected by nephrectomy in newborn rats. They concluded that erythropoiesis in the newborn rat is controlled independently of a renally produced ESF. Our experiments with newborn rats indicate that ESF does control erythropoiesis at this age, but they provide no information about the organ producing the hormone. The inhibition of biological activity of ESF in both newborn and adult animals by anti-ESF does not necessarily indicate that the entire ESF molecule is identical at the two ages but suggests that identical sites are involved in the neutralization reaction.

SUMMARY

In the first section of this paper we have discussed current information on the preparation and properties of anti-erythropoietin immune serum and presented new evidence indicating that the neutralization of erythropoietin by the immune serum depends on the presence of γ -globulin. The available evidence supports the concept that the neutralization of the biological activity of erythropoietin by the immune serum is the result of an antigen-antibody reaction.

In the remainder of this paper we have illustrated the usefulness of anti-erythropoietin in various studies on the regulation of erythropoiesis. We have shown that erythropoiesis in normal adult mice, in WW^V mutant mice, in normal mice exposed to hypoxia, and in newborn rats is either completely abolished or markedly inhibited by the injection of anti-ESF.

The behavior of colony-forming cells in hypoxic mice injected with anti-erythropoietin, in polycythemic mice irradiated with 200R, and in heavily irradiated mice given a bone marrow transplant supports the concept that erythropoietin does not act directly upon the colony-forming cell but upon a population of erythropoietin-sensitive cells derived from the

colony-forming cell population. Some speculations regarding the characteristics and behavior of the erythropoietin-sensitive cell have been presented.

ACKNOWLEDGMENTS

We wish to thank Mrs. Caroline N. Schooley for taking the photomicrographs.

This work was supported in part by the U. S. Atomic Energy Commission and in part by Cancer Research Funds of the University of California.

REFERENCES AND NOTES

1. Schooley, J. C., and Garcia, J. F.; Immunochemical Studies of Human Urinary Erythropoietin; in *Proc. Soc. Exptl. Biol. Med.* 109: 325-328, 1962.
2. Lange, R. D.; Gardner, E., Jr.; Wright, C. -S., and Gallagher, N. I.; Neutralization of the Biological Activity of Erythropoietin by Immune Sera; in *Brit. J. Haematol.* 10: 69-74, 1964.
3. Schooley, J. C., and Garcia, J. F.; Some Properties of Serum Obtained from Rabbits Immunized with Human Urinary Erythropoietin; in *Blood* 25: 204-217, 1965.
4. Garcia, J. F., and Schooley, J. C.; Immunological Neutralization of Various Erythropoietins; in *Proc. Soc. Exptl. Biol. Med.* 112: 712-714, 1963.
5. Rosse, W. F., and Waldmann, T. A.; A Comparison of Some Physical and Chemical Properties of Erythropoiesis-Stimulating Factors from Different Sources; *Blood* 24: 739-749, 1964.
6. Van Dyke, D.; personal communication.
7. Garcia, J. F.; in preparation.
8. Jepson, J. H., and Lowenstein, L.; Inhibition of Erythropoiesis by a Factor Present in the Plasma of Patients with Erythroblastopenia; in *Blood* 27: 425-434, 1966.
9. Schooley, J. C., and Garcia, J. F.; Immunologic Studies on the Mechanism of Action of Erythropoietin; in *Proc. Soc. Exptl. Biol. Med.* 110: 636-641, 1962.
10. Fried, W.; DeGowin, R., and Gurney, C. W.; Erythropoietic Effect of Testosterone in the Polycythemic Mouse; in *Proc. Soc. Exptl. Biol. Med.* 117: 839-842, 1964.
11. Fried, W., and Gurney, C. W.; Use of Mild Plethora to Demonstrate an Erythropoietic Effect from Small Amounts of Androgens; in *Proc. Soc. Exptl. Biol. Med.* 120: 519-521, 1965.
12. Janda, W. E.; Fried, W., and Gurney, C. W.; Combined Effect of Cobalt and Testosterone on Erythropoiesis; in *Proc. Soc. Exptl. Biol. Med.* 120: 443-446, 1965.
13. Fried, W., and Gurney, C. W.; Erythropoietic Effect of Plasma from Mice Receiving Testosterone; in *Nature* 206: 1160-1161, 1965.
14. Mirand, E. A.; Gordon, A. S., and Wenig, J.; Mechanism of Testosterone Action in Erythropoiesis; in *Nature* 206: 270-272, 1965.
15. Schooley, J. C.; Inhibition of Erythropoietic Stimulation by Testosterone in Polycythemic Mice Receiving Anti-Erythropoietin, in *Proc. Soc. Exptl. Biol. Med.* 122: 402-403, 1966.
16. Russell, E. S.; Problems and Potentialities in the Study of Genic Action in the Mouse; in *Methodology in Mammalian Genetics*, edited by W. J. Burdette, San Francisco, Holden-Day, Inc., 1963, pp. 217-232.

17. McCulloch, E. A.; Siminovitch, L., and Till, J. E.; Spleen Colony Formation in Anemic Mice of Genotype WW^V ; in *Science* 144: 844-846, 1964.
18. McCulloch, E. A.; Till, J. E., and Siminovitch, L.; Host-Cell Interactions in Mice Bearing Isologous Hemopoietic Grafts; in *La Greffe des Cellules Hématopoïétiques Allogéniques*, edited by G. Mathé, J. -L. Amiel, and L. Schwarzenburg, Paris, Éditions du Centre National de la Recherche Scientifique, 1965, pp. 61-71.
19. Keighley, G.; Russell, E. S., and Lowy, P. H.; Response of Normal and Genetically Anaemic Mice to Erythropoietic Stimuli; in *Brit. J. Haematol.* 8: 429-441, 1962.
20. Keighley, G.; personal communication.
21. Bruce, W. R., and McCulloch, E. A.; The Effect of Erythropoietic Stimulation on the Hemopoietic Colony-Forming Cells of Mice; in *Blood* 23: 216-232, 1964.
22. Schooley, J. C.; Cantor, L. N., and Havens, V. W.; Relationship Between Growth of Colony-Forming Cells and Erythropoietin-Sensitive Cells in Mice Irradiated with 200R of ^{60}Co Gamma Rays; in *Exptl. Haematol.* 9: 55-56, 1966 (abstract).
23. Schooley, J. C.; The Effect of Erythropoietin on the Growth and Development of Spleen Colony-Forming Cells; in *J. Cellular Physiol.* 68: 249-262, 1966.
24. Schooley, J. C.; Responsiveness of Hematopoietic Tissue to Erythropoietin in Relation to the Time of Administration and Duration of Action of the Hormone; in *Blood* 25: 795-808, 1965.
25. Alexanian, R.; Porteous, D. D., and Lajtha, L. G.; Stem-Cell Kinetics After Irradiation; *Intern. J. Radiation Biol.* 7: 87-94, 1963.
26. Gurney, C. W.; Lajtha, L. G., and Oliver, R.; A Method for Investigation of Stem-Cell Kinetics; *Brit. J. Haematol.* 8: 461-466, 1962.
27. Gurney, C. W.; Effect of Radiation on the Mouse Stem Cell Compartment *in vivo*; in *Perspectives Biol. Med.* 6: 233-245, 1963.
28. Till, J. E.; Quantitative Aspects of Radiation Lethality at the Cellular Level; in *Am. J. Roentgenol., Radium Therapy Nucl. Med.* 90: 917-927, 1963.
29. Blackett, N. M.; Roylance, P. J., and Adams, K.; Studies of the Capacity of Bone-Marrow Cells to Restore Erythropoiesis in Heavily Irradiated Rats; in *Brit. J. Haematol.* 10: 453-467, 1964.
30. Becker, A. J.; A Radiobiological Study of Murine Hemopoietic Stem Cells; Thesis, University of Toronto, Ontario, Canada, 1964.
31. Jacobson, L. O.; Marks, E. K., and Gaston, E. O.; Studies on Erythropoiesis XII: The Effect of Transfusion-Induced Polycythemia in the Mother on the Fetus; in *Blood* 14: 644-653, 1959.
32. Garcia, J. F.; Changes in Blood, Plasma and Red Cell Volume in the Male Rat, as a Function of Age; in *Am. J. Physiol.* 190: 19-24, 1957.
33. Lucarelli, G.; Howard, D., and Stohlman, F., Jr.; Regulation of Erythropoiesis XV. Neonatal Erythropoiesis and the Effect of Nephrectomy; in *J. Clin. Invest.* 43: 2195-2203, 1964.

This paper was presented at the New York Academy of Sciences Conference on Erythropoietin, New York, June 1966.

Erythropoietin Therapy in the Renoprival Patient

Donald C. Van Dyke, Myron Pollycove and John H. Lawrence

On the basis of considerable evidence indicating that the kidney may be the major site of production of erythropoietin, Jacobson (1) originally and many others (2-4) subsequently have proposed that inability to produce adequate amounts of erythropoietin may be a contributory factor in the anemia which accompanies severe renal disease or the renoprival state. It is known that the anemia associated with chronic renal disease and marked azotemia is hemolytic as well as aregenerative (5-8), a form of uncompensated hemolytic anemia. Inability to compensate adequately may be the result of 1) an inability to increase erythropoietin production, which may involve absence of the renal erythropoietic factor (9), or 2) a decreased responsiveness of the marrow to erythropoietin.

If the anemia which accompanies renal disease could be treated by erythropoietin administration, the considerable cost, the risk of hepatitis, the risk of additional injury to the kidney from transfusion reactions would be eliminated. Erslev (10) found that the erythropoietic tissue of uremic rabbits failed to respond in a normal manner to the administration of serum containing erythropoietic factor. Naets (11), using dogs, and Reissmann (12), using rats, have shown that although erythropoietin will stimulate erythropoiesis in the nephrectomized animal, the response obtained is considerably less than that obtained in normal controls. Reissmann has shown that a similar decrease in response occurs in rats made uremic by mercury poisoning. However, Fisher (13) concluded that nephrectomy did not alter the response of rats to sheep erythropoietin.

Having determined the dose of human urinary erythropoietin needed to stimulate erythropoiesis in normal human volunteers (14), it was decided to investigate the effect of such a dose in a patient with moderate anemia secondary to chronic glomerulonephritis.

MATERIALS AND METHODS

The patient was a 65-year-old white, male printer with chronic glomerulonephritis in the terminal stage and rheumatic heart disease. He had scarlet fever as a child and persistent albuminuria from the time of first discovery at age 18 years. He was asymptomatic until age 42 when he developed ankle edema, malaise, and weakness. Subsequently he developed increased ankle edema, dyspnea on exertion, greater fatigue, and intermittent nausea. Examination at the time of this study revealed pallor, cardiomegaly and complete heart block with a grade-3 pansystolic murmur maximal at the lower left sternal border and apex and

3+ bilateral pretibial and ankle edema. Laboratory examination showed 3+ albuminuria with a few hyaline and granular casts and microscopic hematuria. The hemoglobin was 8 g/100 ml with an hematocrit of 23%. Serum chemistries were as follows: sodium, 139 mg/l; potassium, 5.0 mg/l; chloride, 105 mg/l; NPN, 106 mg%; and creatinine, 8.0 mg%. The blood pressure was 170/70 and the body weight was 170 lb. The diagnosis was 1) chronic glomerulonephritis, 2) secondary uremia and anemia, and 3) rheumatic heart disease.

Treatment consisted of low protein and low sodium diet, digitalis, and occasional transfusions. He had not been transfused for 3 months prior to start of this study.

The erythropoietin was obtained from the urine of a patient with complete red cell aplasia (15) who had developed thrombocytopenia by the time the erythropoietin for these studies was collected. The erythropoietin concentrate was prepared by adsorption on collo-dion, precipitation in ether-alcohol, and alcohol fractionation, as previously described (16). The potency of the preparation was determined by using the starved rat ^{59}Fe red cell incorporation assay of Fried et al. (17).

Hematocrit, hemoglobin concentration, reticulocyte, platelet, leucocyte, and differential counts were determined daily before, during, and following erythropoietin administration. A complete *in vivo* iron kinetics study and blood volume determination were done before and after erythropoietin administration.

Human urinary erythropoietin with an activity of 51 IRP* units/mg was given as a single subcutaneous injection (82 mg in 1 ml) daily for 3 days.

RESULTS

The patient was given the equivalent of 4180 IRP units (body weight: 77 kg) or 54 units per kilogram daily for 3 days. The concentrated but impure human urinary erythropoietin preparation used caused considerable local and systemic reaction in this patient. Tenderness, redness, and swelling occurred at the injection site within a few hours and persisted for 36 hr. The local reaction was accompanied by mild fever and malaise which were maximum 8 hr after injection.

Daily hematocrit, hemoglobin concentration, reticulocyte, platelet, leucocyte, and differential counts done for 10 days prior to erythropoietin administration showed no change. During and for 16 days following erythropoietin administration there was no change in hematocrit, hemoglobin concentration, reticulocyte, or platelet count. There was a transient rise in total leucocyte count occurring during and for 2 days following erythropoietin administration. Differential counts showed the increase in total leucocyte count to be entirely due to an increase in granulocytes.

* International Reference Preparation, obtained from Medical Research Council of Great Britain.

A complete ferrokinetic study completed just prior to erythropoietin administration showed a high normal rate of hemoglobin synthesis (1.6 g/l blood/day; normal range: 1.0-1.6), with a moderate reduction in red cell survival (49 days; normal range: 102-132) (18). Although the absolute rate of hemoglobin synthesis was normal, it was markedly subnormal relative to the usual compensatory increase ($> 7\times$) in rate of hemoglobin synthesis occurring normally in response to a chronic anemia of 8 g Hb/100 ml (7). These findings were similar to one of the cases reported by Nathan et al. (19). A second ferrokinetic study started 4 days after the last erythropoietin injection showed no significant change from the pre-treatment study (Hb synthesis: 1.7 g/l blood/day; RBC survival: 41 days).

DISCUSSION

In a previous study (14) using normal human volunteers, it was concluded that "the minimum dose necessary to produce reticulocytosis in a normal human being is approximately 20 (IRP) units/kg/day for a period of several days. The dose necessary to produce an unquestionable increase in total circulating red cell volume is estimated to be approximately 50 units/kg/day for 7-14 days."

The uremic patient in this study received 54 IRP units/kg/day for 3 days without evidence of increased red cell production as judged by percent reticulocytes or by repeated ferrokinetic studies. This one patient with anemia associated with chronic renal disease and uremia appears to have been less responsive to erythropoietin than a normal human being. This result is in agreement with the results of Erslev (10), Naets (11), and Reissmann et al. (12), who found that the nephrectomized animal's response to erythropoietin was considerably less than that obtained in the normal controls. Reissmann et al. (12) state that erythropoietin injections increased reticulocytes and iron incorporation significantly in the renoprival animals, but a comparison with the effect of erythropoietin injection in the ureter-ligated or control group shows the limited extent of this response. They also showed that the daily injection of 8 times the dose of extract which produced a significant response in non-uremic controls was required to produce a response in the uremic animals.

The study of this one patient would seem to indicate that, as in the nephrectomized rabbit, dog, or rat, the defect in red cell production in man which accompanies uremia secondary to chronic renal disease (glomerulonephritis) is at least to some extent the result of a decreased responsiveness to erythropoietin. Inability to increase erythropoietin production sufficiently to compensate for the shortened red cell survival may also be a factor. If one accepts the evidence that the uremic subject is less responsive to erythropoietin and at the same time makes a normal number of red cells (the anemia being associated with a reduced red cell survival), one must assume that erythropoietin production has been increased in order to maintain the normal production rate. If one assumes that the uremic subject, like the uremic rat, requires 8 times the dose of erythropoietin to obtain a normal response, then one may assume that the subject was producing erythropoietin at 8 times the normal rate in order

beings (20), an 8-fold increase would be 0.025 unit/ml, which is still well below detectable levels by presently available assay methods [0.05 unit (24)].

In spite of the apparent diminished sensitivity to erythropoietin, evidence that the patient had partially compensated by increasing his erythropoietin titer in response to the anemia was shown by the high-normal daily hemoglobin synthesis and by the persistent slight reticulocytosis (2.2%).

Although other possibilities are not eliminated, the anemia in a case such as the one presented could be explained predominantly on the basis of diminished responsiveness to erythropoietin. It has been shown that the rate of erythropoietin production is a function of the degree of anemia (15), so that a given degree of anemia serves as the stimulus for a given increase in erythropoietin production. Chronic hemolysis producing an anemia of 8 g Hb/100 ml would thus stimulate an 8- to 12-fold increase of erythropoiesis (7). In the presence of a decreased responsiveness to erythropoietin, the normal increase in erythropoietin titer is insufficient to produce increased erythropoiesis, and a new steady state (anemic) develops.

It is predicted that successful treatment of the anemia which accompanies renal disease in man may require a dose in the range of 200 units per kg/day, or 14,000 units per day. The only currently feasible approach to determining the therapeutic possibilities of erythropoietin is the infusion of highly active urine or plasma. The highest activity found so far in unmodified urine has been 14 units/ml (15). If the above estimate of 14,000 units per day is realistic, this would mean the intravenous infusion of 1000 ml of unmodified urine daily for a test period of 10 days, which would be a heavy load of excretory products. If water-loading diuresis could be induced in the donor without reducing erythropoietin concentration in the urine, and if the urine could be pre-dialyzed, administration of 14,000 units per day might be feasible.

Limited therapeutic trials may be possible by using human urinary erythropoietin extracted from the urine of patients severely anemic from hookworm infestation (22). The only currently organized serious collection program yields approximately 500,000 units of crude hormone per year. If the entire collection were allocated to the study of anephric man, the first requirement would be to purify the material sufficiently to be tolerated by the patients. If adequate purification could be achieved with a 30% recovery of activity (150,000 units), there would be enough hormone to treat only one patient for 10 days.

The human erythropoietin collection center in Argentina occasionally encounters patients whose erythropoietin is as high as 14 units/ml of unmodified urine. The plasma concentration is usually higher than that of urine and may be 5, 10, or 20 times higher. Presumably some of the hookworm-infested donors may have plasma concentrations in the neighborhood of 150 units/ml. The daily requirement for therapeutic trial in the renoprival patient has been estimated to be 14,000 units, which could mean as little as 100 ml of plasma per day. For the study of non-uremic patients, the requirements would be 1/10 of the above: 10 ml of

1175304

plasma per day or 50 ml for a 5-day test period. The difficulty in obtaining large amounts of plasma from severely anemic patients is obvious.

If the dose estimates given above are correct, the only practical approach to therapeutic trials at present is to use sterilized, dialyzed, but otherwise unmodified (undenatured) active urine. Efforts should be made to collect the most active urine possible, to collect it into pyrogen-free bottles in as clean a way as possible, and to investigate methods of dialysis which will remove as much material as possible, leaving erythropoietin behind, and which do not involve denaturation of the residual proteins. In other words, to provide a highly active, sterile, non-toxic urinary extract of liter amounts of urine which can be tolerated intravenously by the renoprival patient.

It is not known whether the non-dialyzable portion of normal human urine would contain the symptom-producing toxins which are so detrimental to the renoprival patient. If not, the administration of non-dialyzable normal urinary products in amounts sufficient to test the responsiveness of such patients' marrow might be done with impunity.

If further investigation demonstrates that the renoprival patient is equally as sensitive to erythropoietin as normal animals and man, the problem of erythropoietin therapy becomes easier by an order of magnitude: 100 ml of active urine a day would be needed and the erythropoietin collection agency could provide material for testing in 10 patients. The answer to dose requirements will depend on further testing which should be based realistically on the more pessimistic estimates.

SUMMARY

It has been proposed that inability to produce adequate amounts of erythropoietin may be a contributory factor in the uncompensated hemolytic anemia which accompanies severe renal disease or the renoprival state. However, several investigators have shown that although erythropoietin will stimulate erythropoiesis in nephrectomized animals, the response is approximately 1/10 that obtained in normal controls. Such results suggest that the inability of the uremic to compensate for the shortened red cell survival may result primarily from a decreased responsiveness of the marrow to erythropoietin, rather than an inability to increase erythropoietin production.

Administration of erythropoietin to a patient with moderate anemia secondary to chronic glomerulonephritis produced no evidence of erythropoietic stimulation as judged by reticulocyte count or iron kinetic studies done before and after treatment. The dose of erythropoietin (54 IRP units/kg/day for 3 days) was thought from previous studies to be more than adequate to produce a significant reticulocytosis in normal human subjects.

It is suggested that the uremic patient, like nephrectomized rats and dogs, may require on the order of 10 times the normal amount of erythropoietin. It is predicted that successful treatment of the anemia which accompanies severe uremia in man may require a dose of erythropoietin in the range of 200 IRP units/kg/day. Until much more abundant sources

1175305

and more efficient methods of concentration of erythropoietin become available, administration of highly active urine unmodified except for thorough dialysis and sterilization by passage through a bacterial filter, or highly active plasma, seems to be the only currently available method for further therapeutic trials in the renoprival patient.

ACKNOWLEDGMENTS

This work was supported in part by the United States Atomic Energy Commission and in part by Grant #5ROICA08370-02 from the National Cancer Institute of the National Institutes of Health.

REFERENCES

1. Jacobson, L. O.; Goldwasser, E.; Fried, W., and Plzak, L. F.; *Trans. Assoc. Am. Physicians* 19: 305, 1957.
2. Naets, J. P., and Heuse, A. F.; *J. Lab. Clin. Med.* 60: 365, 1962.
3. Gallagher, N. I.; McCarthy, J. M., and Lange, R. D.; *Ann. Internal Med.* 52: 1201, 1960.
4. Penington, D. G., *Lancet*, 301, Feb. 11, 1961.
5. Loge, J. P.; Lange, R. D., and Moore, C. V.; *J. Clin. Invest.* 29: 830, 1950.
6. Joske, R. A.; McAlister, J. M., and Panker, R. A.; *Clin. Sci.* 15: 511, 1966.
7. Pollycove, M.; *Seminars in Hematology* 3: 235, 1966.
8. Eschbach, J. W., Jr.; Funk, O.; Adamson, J.; Kuhn, I.; Scribner, B. H., and Finch, C. A.; *New Eng. J. Med.* 276: 653, 1967.
9. Contrera, J. F., and Gordon, A. S.; *Science* 152: 653, 1966.
10. Erslev, A. J.; *AMA Arch. Internal Med.* 101: 407, 1958.
11. Naets, J. P.; *J. Clin. Invest.* 39: 102, 1960.
12. Reissmann, K. R.; Nomura, T.; Gunn, R., and Brosius, F.; *Blood* 16: 1411, 1960.
13. Fisher, J. W.; Sanzari, N. P.; Birdwell, B. J., and Crook, J. J.; in *Erythropoiesis*, New York, Grune & Stratton, 1962, p. 78.
14. Van Dyke, D. C.; Lawrence, J. H.; Pollycove, M., and Lowy, P.; *Hormones and the Kidney*, Scotland, Aberdeen University Press, Ltd., 1962.
15. Van Dyke, D. C.; Layrisse, M.; Lawrence, J. H.; Garcia, J. F., and Pollycove, M.; *Blood* 18: 187, 1961.
16. Van Dyke, D. C.; *Haemopoiesis*, London, J. & A. Churchill, Ltd., 1960.
17. Fried, W.; Plzak, L. F.; Jacobson, L. O., and Goldwasser, E.; *Proc. Soc. Exptl. Biol. Med.* 94: 237, 1957.
18. Pollycove, M., and Mortimer, R. J.; *J. Clin. Invest.* 40: 753, 1961.
19. Nathan, D. G.; Schupak, E.; Stohlman, F., Jr., and Merrill, J. P.; *J. Clin. Invest.* 43: 2158, 1964.
20. Van Dyke, D. C., and Pollycove, M.; in *Erythropoiesis*, New York, Grune & Stratton, 1962.
21. DeGowin, R. L.; Hofstra, D., and Gurney, C. W.; *Proc. Soc. Exptl. Biol. Med.* 110: 48, 1962.
22. Gutnisky, A.; Nohr, M. L.; Malgor, L., and Van Dyke, D.; *N. Y. Acad. Sci. Symp.* on Erythropoietin, in press.

1175306

Pulsed High Intensity X Rays:

Inactivation of Human Cells Cultured *in vitro* and Limitations on Usefulness in Radiotherapy

Paul W. Todd, H. Saul Winchell, Jose M. Feola and Gary E. Jones

The suggestion that neoplastic cells are frequently more hypoxic than their normal counterparts (1), in conjunction with the observation that hypoxic cells are partially protected from effects of ionizing radiation (2), has stimulated efforts to seek radiation the action of which is independent of the presence of oxygen. Some decrease in the "oxygen effect" with the use of high intensity electron beams has been observed in chemical systems (6) and in bacteria (3) and with high intensity proton beams in water (7). Decreased incidence of chromosome breakage at high radiation dose rates has also been reported (5).

If the reduced oxygen effect noted in these early experiments with high intensity radiations are to be applicable in clinical radiotherapy, such effects must be present within the appropriate dose range for human treatment. In addition, therapeutic applicability requires the use of radiation with adequate penetration. The recent availability of linear accelerators for the production of high energy, high intensity photons suggested experiments to determine the dose dependency of radiation-induced inhibition of colony formation by cultured human cells under aerated and anoxic conditions. Our experimental results define the limitations of such high intensity radiation in human radiotherapy.

MATERIALS AND METHODS

Human kidney cells, line T1 originally obtained from Barendsen (1), used in these experiments were serially propagated in Eagle's "Minimum Essential Medium" (4) and 10% fetal bovine serum. We irradiated 6- to 8-hr single-cell cultures growing in 35 mm plastic petri dishes on day-old "feeder layers" of 5×10^4 irradiated (4000 rads) cells per 35 mm dish.

We used 10 MVp X rays generated from a Physics International (2700 Merced St., San Leandro, Calif.) pulsed electron accelerator in the dose rate range of 10^{12} to 10^{13} rads/min. Each total dose was delivered in a single pulse of 3×10^{-8} sec duration. For comparison we used ^{60}Co gamma rays at a dose rate of 150 ± 10 rads/min. For both radiations, the dose delivered to each group of exposed cultures was determined by LiF thermoluminescence—a method found to be dose-rate-independent in the range used. Dosimetry capsules and cultures were simultaneously exposed to each dose. Both radiations were filtered by 1 in. of polyethylene.

The petri dishes containing the cells to be irradiated were mounted in a Mylar-film-faced aluminum exposure wheel (8). Medium was removed from the petri dishes just prior to irradiation, and the dishes were exposed vertically so that they were perpendicular to the incident radiation beams. In those experiments in which oxygen was removed, high-purity nitrogen was passed over the cultures for 20 min prior to exposure. Subsequent to exposure, medium was replaced, and the cultures were incubated at 37°C and fed with fresh medium every 5 days until visible colonies developed (≈ 2 weeks). Surviving fractions were determined on the basis of colony counts in exposed and control cultures.

RESULTS

Survival curves for cells exposed to pulsed X rays and ^{60}Co gamma rays under aerated conditions are presented in Fig. 1. Vertical error bars represent the standard errors of mean survival propagated from the relative errors of the mean colony counts on control and irradiated plates. Horizontal error bars represent standard deviations of doses determined by the multiple (9 or more) LiF dosimeters used in measuring the dose at each individual dose point. The dose rate in rads/sec at each dose of pulsed X rays was different and was equivalent to the dose at that point divided by 3×10^{-8} sec. The highest dose rate represented in this graph is approximately 3×10^{11} rads/sec. The two curves of Fig. 1 do not differ significantly, considering the experimental conditions.

The survival curve for cells exposed to pulsed X rays while in a nitrogen atmosphere is presented in Fig. 2 and compared with that obtained under aerated conditions. The results suggest that fully anoxic conditions were not achieved in the experiment, since the ratio of doses in nitrogen to those in air required for equivalent survival is less than that anticipated under complete anoxia (8). However, it can be concluded that the effect of oxygen at atmospheric pressure did not disappear at these radiation intensities.

DISCUSSION

Shalek and Bonner (7), using hydrogen peroxide formation in pure water as their end-point at total proton doses in excess of 10^7 rads, found that the difference between yields in air-saturated water and helium-saturated water disappeared at dose rates greater than 10^8 rads/sec. These published observations suggest that all ionization produced at intensities greater than 10^8 rads/sec is equally effective in eliminating the oxygen effect. If the mechanism whereby high intensity reduces the oxygen effect is the "use-up" of available intracellular oxygen at a rate greater than the diffusion of available oxygen into the irradiated volume, then the minimum dose rate (10^8 rads/sec, obtained by Shalek and Bonner) is a measure of the rate of oxygen diffusion into the irradiated volume.

Dewey and Boag (3), using dose rates in excess of 10^8 rads/sec (actually about 10^{10} rads/sec) found that doses greater than 13,000 rads were adequate for eliminating the effect of 1% oxygen in nitrogen in irradiated cultures of the bacterium *Serratia marcescens*. If we take the value of 13,000 rads as representing the minimum dose required for "use-up" of intracellular oxygen at this partial pressure (about 7.6 mm Hg), then one would anticipate a

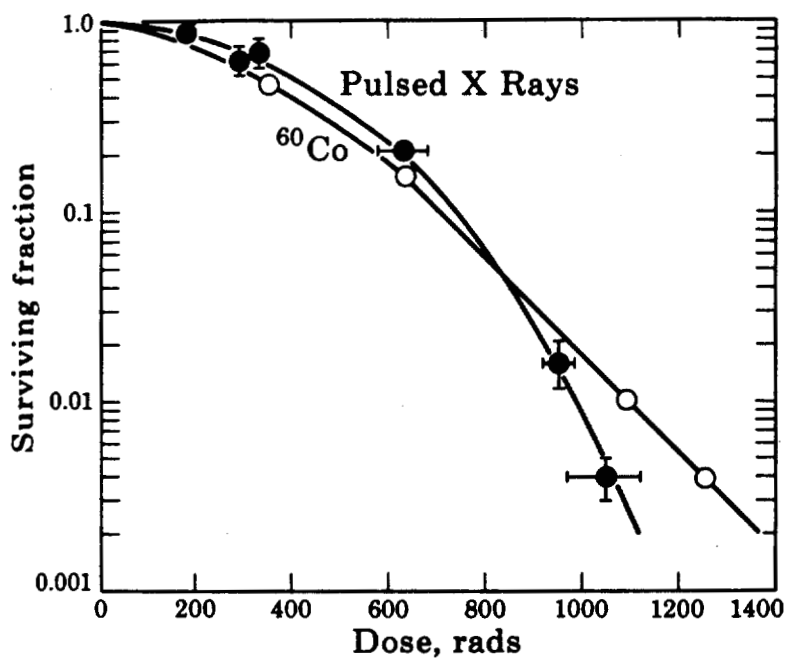


Fig. 1. Survival curves for cultured human kidney cells exposed to ^{60}Co gamma rays at 150 ± 10 rads/min (open circles) and pulsed 10 MVp X rays with the total dose being delivered in 3×10^{-8} sec (solid circles), both under aerated conditions.
XBL672-571

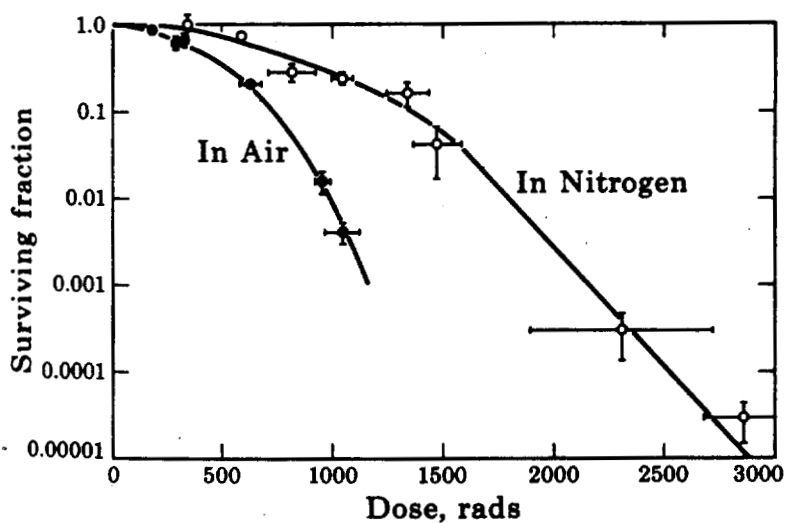


Fig. 2. Survival curves for cultured human kidney cells exposed to pulsed 10 MVp X rays. The "In Air" curve differs in that purified nitrogen was passed over the cells for 15 min prior to irradiation.
XBL672-572

1175309

required dose of 260,000 rads ($20 \times 13,000$) to "use up" intracellular oxygen at atmospheric pressure (about 152 mm Hg).

It is therefore not surprising that the experiments we describe in this work did not demonstrate a reduced oxygen effect under aerated conditions at dose rates of 10^{11} to 10^{12} rads/sec and in the dose range of 200 to 1050 rads.

On the basis of the quantitative considerations just presented, an estimation may be made of the required partial pressure of oxygen in tissue to allow complete oxygen "use-up" by therapeutically usable radiation doses. If we assume 2000 rads to be the largest single acceptable therapeutic dose, then a high-intensity radiation pulse (delivered at more than 10^{11} rads/sec) of this magnitude would require that the oxygen partial pressure in the irradiated tissue be less than 1.1 mm Hg to insure "use-up" of the residual oxygen with resultant elimination of the oxygen effect. Therefore, in order to utilize in radiotherapy the diminished oxygen effect seen in high-intensity radiation experiments, it would be necessary to reduce the partial pressure of oxygen in the target-area tissue to about 1.1 mm Hg for the duration of the radiation pulse. Such a procedure is limited by considerations of the human physiological effects of temporary extreme hypoxia.

SUMMARY AND CONCLUSIONS

Pulse 10 MVp X rays administered at dose rates of 10^{11} to 10^{12} rads/sec and in the total dose range of 200 to 1050 rads/pulse did not differ significantly from ^{60}Co gamma rays in their ability to inactivate aerated cultured human cells.

It is estimated that a total dose of 260,000 rads delivered at dose rates greater than 10^8 rads/sec is necessary to eliminate the oxygen effect in aerated cells. Assuming that a total single dose of 2000 rads is the maximum acceptable in therapeutic procedures, it is estimated that at dose rates greater than 10^8 rads/sec the partial pressure of oxygen in tissue would have to be reduced to less than about 1.1 mm Hg prior to irradiation to eliminate the oxygen effect.

ACKNOWLEDGMENTS

We are greatly indebted to Mrs. C. L. Boerke and Mrs. W. M. Jackson for unstinting laboratory assistance and to Mr. B. Bernstein and the staff of Physics International, San Leandro, California, for performing the irradiations and dosimetry and for their generous sharing of their facilities and equipment.

This research was jointly supported by the U. S. Atomic Energy Commission and the National Aeronautics and Space Administration.

REFERENCES

1. Barendsen, G. W.; Beusker, T. L. J.; Vergroesen, A. J., and Budke, L.; Effects of Different Ionizing Radiations on Human Cells in Tissue Culture. II. Biological Experiments; Radiation Res. 13: 841-849, 1960.

1175310

- ... Dewey, D. L.; Effect of Oxygen and Nitric Oxide on the Radiosensitivity of Human Cells in Tissue Culture; *Nature* 186: 780-782, 1960.
- ... Dewey, D. L., and Boag, J. W.; Modification of the Oxygen Effect When Bacteria are Given Large Pulses of Radiation; *Nature* 183: 1450-1451, 1959.
- 4. Eagle, H.; Amino Acid Metabolism in Mammalian Cell Cultures; *Science* 130: 432-437, 1954.
- ... Kirby-Smith, J. S., and Dolphin, G. W.; Chromosome Breakage at High Radiation Dose Rates; *Nature* 182: 270-271, 1958.
- ... Rotblat, J., and Sutton, H. C.; The Effects of High Dose Rate of Ionizing Radiations on Solutions of Iron and Cerium Salts; *Proc. Roy. Soc. (London) A*, 255, 490-508, 1960.
- ... Shalek, R. J., and Bonner, T. W.; Formation of Hydrogen Peroxide in Water by 1-MeV Protons; *Nature* 172: 259-260, 1953.
- ... Todd, P. W.; Reversible and Irreversible Effects of Densely Ionizing Radiations Upon the Reproductive Capacity of Cultured Human Cells; in *Medical College of Virginia Quarterly* 1(4), 2-14, 1966.

Sensitivity of *Micrococcus radiodurans* to Densely Ionizing Radiations

David L. Dewey and Robert H. Haynes

INTRODUCTION

The non-sporulating tetracoccus *Micrococcus radiodurans* is the most radioresistant organism known to exist: a million rads of X or γ radiation are required to reduce its viability by 50% (1-3). It is similarly resistant to ultraviolet (UV) radiation, though its thermal resistance is not unusually high (2, 3). Several hypotheses have been put forward to account for the high X-ray and UV resistance of this bacterium, but there is still no general agreement as to whether a single or several different mechanisms might be involved (3-6). Its high resistance to ionizing radiation has been attributed both to the presence of a high intracellular concentration of radical trapping materials (5) and to the existence of an unusually efficient enzymic repair system which serves to eliminate radiation-induced structural defects from the cell's DNA (3, 6). Its high UV resistance is most easily explained in terms of the well-known DNA repair system which excises UV-induced pyrimidine dimers and replaces the damaged nucleotide segments through the process of repair replication (4).

The X-ray dose-survival curve under normal oxygenated conditions, for *M. radiodurans* is sigmoidal in shape. It is characterized by a large initial shoulder that extends to a dose of about 500 krad with no detectable loss of viability; survival is reduced to the 50% level at a dose of 1 Mrad and the final exponential portion of the curve has associated with it an LD₉₀ of about 200 krad. Any possible changes in the characteristics of this dose-survival curve with increasing linear energy transfer (LET) of the radiation could not be predicted from pre-existing data. A transition from a sigmoidal to a near-exponential survival curve with increasing LET has been observed in many types of cells, including *Aspergillus* spores (7), *Artemia* eggs (8), and mammalian cells in culture (9, 10). In contrast, the survival curves for diploid yeast remain sigmoid even at the highest values of LET available (11). In the experiments to be reported here we present further evidence in support of the view that the radioresistance of *M. radiodurans* may, in large part, be attributed to its possession of an unusually efficient repair system. Furthermore, essentially no reduction in the extent of the survival curve shoulder was found for high-LET radiations; this suggests that *M. radiodurans*, like diploid yeast, is able to repair high-LET radiation damage.

MATERIALS AND METHODS

The radiation source used in these experiments was the Berkeley Heavy Ion Linear Accelerator (Hilac). The beams used were fully stripped nuclei of helium, lithium, boron, carbon, oxygen, and neon and partially stripped argon nuclei. Particles were accelerated

1175312

approximately 10 MeV per nucleon, so that the proportion of energy dissipated as δ rays was constant for all particles. After passing through the end window foil, the energy at the material surface was calculated to vary between 8.0 and 9.9 MeV per nucleon, depending on the type of particle.

Various subcultures of M. radiodurans were obtained from C. J. Dean of the Chester Beatty Research Institute, and B. E. B. Moseley of Cambridge University. The cells were grown overnight on a nutrient agar slope at 37°C and were then harvested by washing into phosphate buffer at pH 7.0. The suspensions were agitated with a vortex mixer to break up any clumps that might be present. The resulting suspensions consisted of particles of 4 cells (tetrads) each. The tetrads are not further dispersed by this procedure. The resulting suspensions contained approximately 10^8 tetrads per ml. Using a micrometer syringe, 20 μ l samples were placed at the center of gelatine-agar laminated discs which were 13 mm in diameter and 1.5 mm thick; the bottom layer consisted of a 2% agar gel and the top layer a 1% gelatine gel. The cell suspensions were spread evenly over the upper gelatine surface with the aid of a fine glass spreader. About 30 minutes was required for the suspending solution to diffuse into the discs, leaving the cells on the gelatine surface. The discs were transported to the Hilac in sterile petri dishes resting on crushed ice. The bacteria were kept cold at all times except during the actual period of irradiation. During irradiation the discs were supported in a closed chamber in front of the Hilac exit window. The chamber was flushed with oxygen before and during irradiation.

After irradiation the discs were dropped into test tubes containing 10 ml of phosphate buffer at 37°C to dissolve the gelatine and return the cells to a uniform suspension of tetrads. The cells were re-chilled and plated by using appropriate dilutions on nutrient agar, and also on nutrient agar containing 20 μ g/ml of acridine orange. All the dilution and plating procedures were carried out in dim light to avoid possible photodynamic effects on the plates containing acridine orange. The plates were incubated at 37°C in the dark for 2 days before counting colonies.

RESULTS

The effect of irradiation at high LET on the colony-forming ability of M. radiodurans is shown in Figs. 1 and 2. The main effect on survival curve shape of increasing the LET from 100 to 1000 MeV-cm²/g (helium to boron) is to increase the apparent limiting slope of the curves; the extent of the shoulder is not significantly altered. The maximum sensitivity was obtained with boron. As the LET of the radiation was increased beyond 1000 MeV-cm²/g, there was both a reduction in the limiting slope and an increase in the extent of the shoulder. These changes in shoulder and slope with increasing LET are shown in Fig. 3. The limiting slope was taken to be that of a line linking the best fit by eye through the points lying in the final "exponential" portion of the curves. The shoulder was measured in terms of the dose associated with the back extrapolation of the apparent limiting slope on the abscissa.

The bacteria from each dilution tube were plated both on nutrient agar and on nutrient agar containing 20 μ g/ml of acridine orange. There was no effect of acridine orange on the

1175313

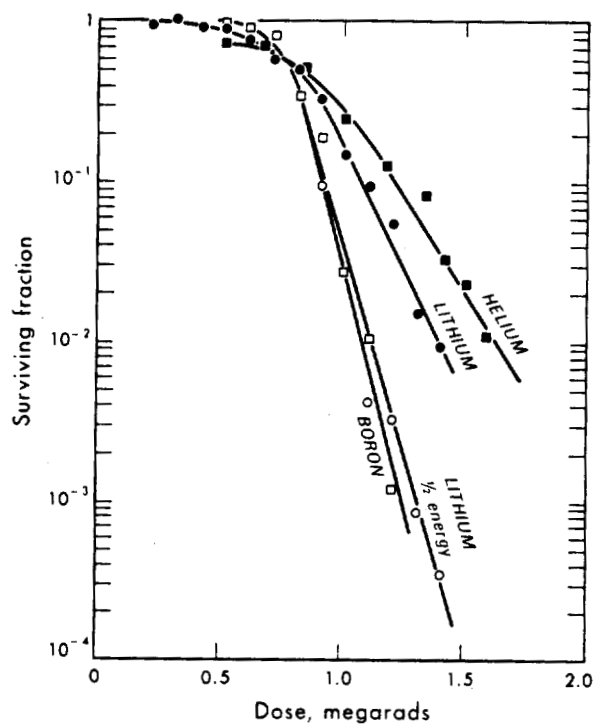


Figure 1.

DBL 677-1689

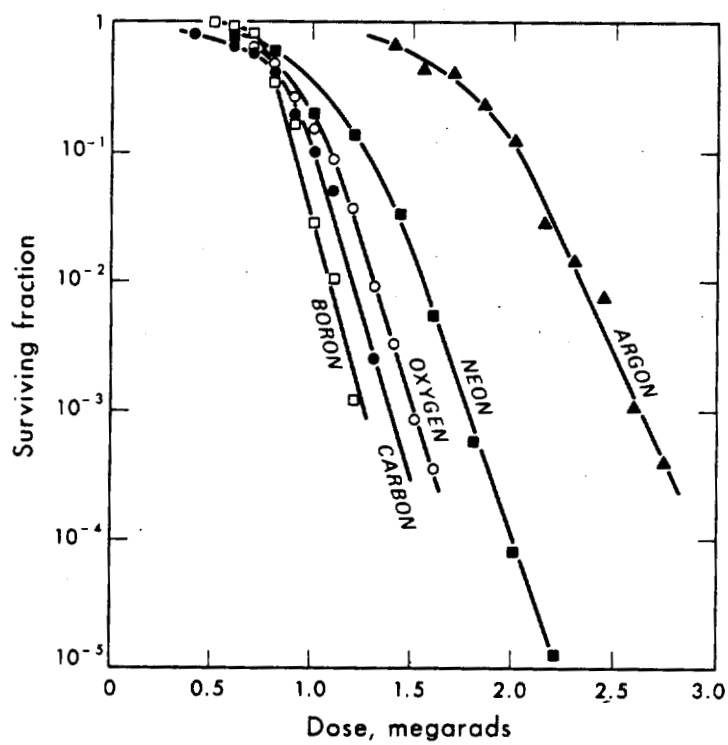


Figure 2.

1175314

unirradiated control cells, nor on those samples which had received only small doses of radiation. The design of the Hilac target chamber allowed for ten samples plus controls at one loading. After preliminary experiments had shown virtually no killing at low doses, these low-dose points were omitted from the later experiments whose results are plotted in Fig. 4. The effect of including acridine orange in the plates is shown in Fig. 4. There is quite clearly a decrease in the extent of the shoulder without any change in the apparent limiting slope. Unfortunately, no inferences can be drawn from the relative amounts of shoulder reduction by acridine orange for the various heavy-ion irradiations shown in this figure, because the salt concentration in the plates was not the same in each case and this parameter is known to affect the uptake of acridine orange by the cells.

DISCUSSION

The effect of acridine orange on the shoulder of the survival curves in Fig. 4 further supports the view that the radioresistance of M. radiodurans arises at least in part from its ability to repair radiation damage to its own DNA. This inference is made plausible on the basis of the following facts: first, acridine orange is a basic dye that binds to nucleic acids and is known to inhibit the excision of UV-induced photoproducts from bacterial DNA (12); second, acridine dyes inhibit other reactivation and recovery processes in irradiated bacteriophages (13), anthrax spores (13), E. coli (14) and diploid yeast (15). Thus, it is reasonable to conclude that the reduced shoulder of the survival curves obtained from the acridine plates is due to partial inhibition of repair in M. radiodurans (16, 17).

If one allows that the resistance of M. radiodurans arises from its ability to repair radiation damage with an unusually high efficiency, then the inability of high-LET radiations to reduce the survival curve shoulders (Figs. 1-3) suggests that this repair system(s) resembles more the liquid-holding recovery process in diploid yeast than the reactivation mechanism of E. coli B/r. This conclusion is based on the fact that in E. coli the differential sensitivity between B/r and the repair-deficient mutant B_{s-1} decreases with increasing LET (17, 18)—thus indicating that high-LET radiation damage cannot be repaired in B/r—whereas in diploid yeast neither the survival curve shoulder nor the magnitude of liquid-holding recovery is reduced at high LET (19). Unfortunately, the biochemical basis of liquid-holding recovery in yeast is unknown and so this analogy cannot at present be pursued any further.

One further general point can be made on the basis of the various inactivation studies of M. radiodurans that have been reported here and by other workers. This concerns the relative efficiency of repair of ionizing and UV radiation damage in E. coli B/r and M. radiodurans. In the latter case the very broad shoulder observed for all ionizing radiations as well as for UV suggests that its repair processes deal with both classes of damage with essentially 100% efficiency even at relatively high radiation doses. On the other hand, only UV damage is repaired with 100% efficiency—and this only at very low doses—in E. coli B/r. However, it may still be necessary to invoke a number of different repair systems with differing properties in order to account for the unusually high apparent limiting slope of the M. radiodurans radiation survival curve.

1175315

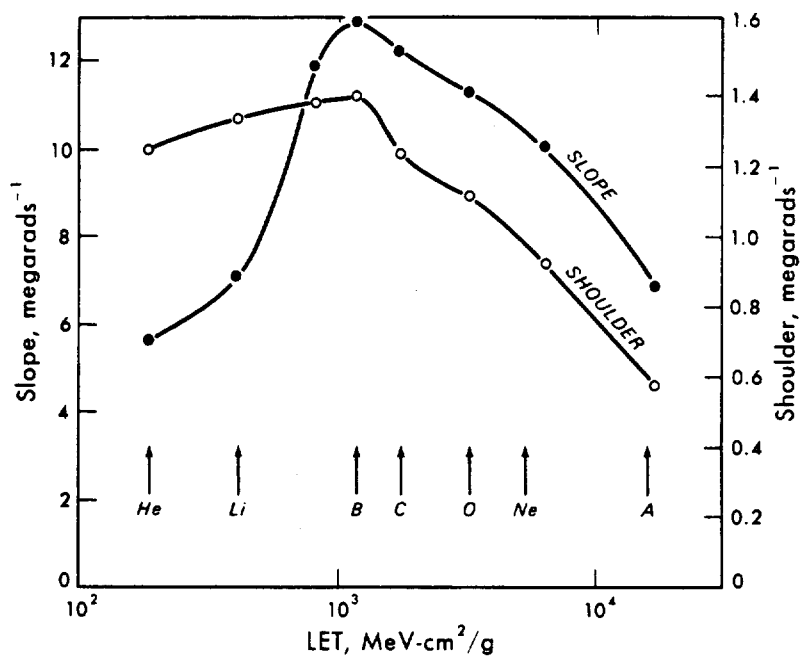
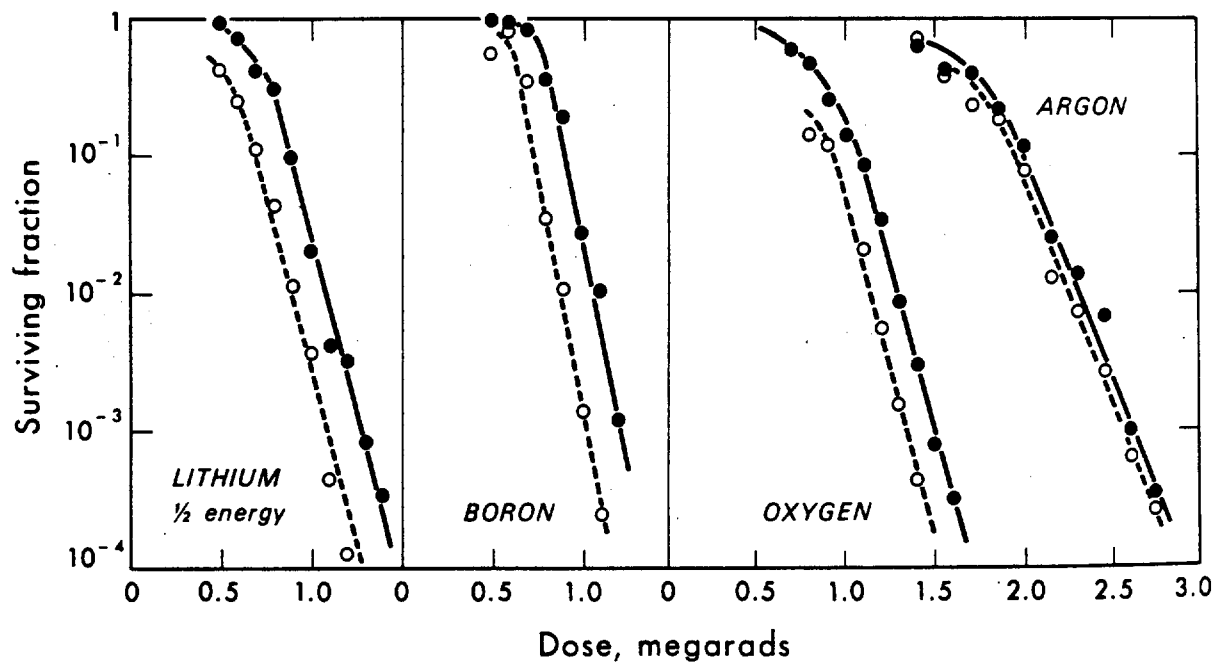


Figure 3.

DBL 677-1691



DBL 677-1692

Figure 4.

1175316

SUMMARY

(1) The radiation dose-survival curves for M. radiodurans were measured for a number of 10 MeV/amu heavy-ion beams produced by the Berkeley Hilac. All the curves, even for the highest LET available, were found to have a broad shoulder approximately 1 Mrad long.

(2) For values of LET up to about 1000 MeV-cm²/g (i.e., the helium, lithium, and boron beams), the apparent limiting slope of the curves increases by about a factor of 3, but there is little change in the magnitude of the shoulder over this range of LET.

(3) For values of LET greater than 1000 MeV-cm²/g (i.e. the carbon, oxygen, neon, and argon beams), the shoulder increases and the slope decreases, indicating a general decrease in the relative biological efficiency over this range of LET.

(4) Addition of acridine orange to the plates used to assay survival serves to increase the apparent sensitivity of the cells for all values of LET used. This may be taken as further evidence that the resistance of M. radiodurans is due to its possession of a very efficient DNA repair mechanism, and further, that even the damage produced by high-LET radiations can be repaired in this organism.

ACKNOWLEDGMENTS

This research was jointly supported by the U. S. Atomic Energy Commission and the National Aeronautics and Space Administration.

REFERENCES AND NOTE

1. Anderson, A. W.; Nordan, H. C.; Cain, R. F.; Parrish, G., and Duggan, D.; Food Technol. 10: 575-577, 1956.
2. Duggan, D. E.; Anderson, A. W.; Elliker, P. R., and Cain, R. F.; Food Res. 24: 376-382, 1959.
3. Moseley, B. E. B., and Laser, H.; Proc. Roy. Soc. (London) B 162: 210-222, 1965.
4. Setlow, J. K.; Photochem. Photobiol. 3: 405-414, 1964.
5. Bruce, A. D., and Malchman, W. M.; Radiation Res. 24: 473-481, 1965.
6. Lett, J. T.; Feldschreiber, P.; Little, J. G.; Steele, K., and Dean, C. J.; Proc. Roy. Soc. (London) B 167: 184-201, 1967.
7. Zirkle, R. E.; Marchbank, D. F., and Kuck, K. D.; J. Cellular Comp. Physiol. 39, Suppl. 1: 75-85, 1952.
8. Easter, S. S., and Hutchinson, F.; Radiation Res. 15: 333-340, 1961.
9. Todd, P. W.; Ph.D. thesis, University of California, Lawrence Radiation Laboratory Report UCRL-11614, 1965.
10. Barendsen, G. W., and Walter, H. M. D.; Radiation Res. 21: 314-329, 1964.
11. Mortimer, R. K.; Brustad, T., and Cormack, D. V.; Radiation Res. 26: 465-482, 1965.
12. Setlow, R. B.; J. Cellular Comp. Physiol. 64, Suppl. 1: 51-68, 1964.
13. Alper, T.; Nature 200: 539, 1963.

1175317

14. Haynes, R. H.; unpublished observations, 1963.
15. Patrick, M. H., and Haynes, R. H.; Radiation Res. 23: 564-579, 1964.
16. Haynes, R. H.; Photochem Photobiol. 3: 429-450, 1964.
17. Haynes, R. H.; Radiation Res., Suppl. 6: 1-29, 1966.
18. Inch, W. R., and Haynes, R. H.; Radiation Res. 27: 545, 1966.
19. Lyman, J. T., and Haynes, R. H.; Radiation Res., Suppl. 7, 1967, in press.

David L. Dewey's present address is British Empire Cancer Campaign, Research Unit in Radiobiology, Mount Vernon Hospital, Northwood, Middlesex, England.

Effect of Negative Pions on the Proliferative Capacity of Ascites Tumor Cells (Lymphoma) Grown *in vivo*

Jose M. Feola, Chaim Richman, Mudundi R. Raju,
Stanley B. Curtis and John H. Lawrence

We have attempted to determine the relative biological effectiveness (RBE) of negative pions in the Bragg-peak region as compared to the plateau region and to gamma rays. We irradiated LAF₁ mice, bearing 5-day-old lymphoma ascites tumors, in the peak and plateau regions of a 90-MeV pion beam for 40 hr in temperature-controlled holders. The animals were then sacrificed; lymphoma cells were withdrawn and titrated into adult female LAF₁ mice. The proliferative capacity of the irradiated tumor cells was evaluated after 8 weeks by observing the percentage of animals developing ascites tumors. Surviving fractions were then calculated from LD₅₀'s of control and irradiated animals. Radiation doses in the plateau region were measured with LiF dosimeters calibrated against ⁶⁰Co γ rays. We calculated peak doses from those at the plateau, using a measured average peak-to-plateau ionization ratio of 1.5. Doses in the plateau region ranged from 145 to 250 rads; doses in the peak region ranged from 220 to 380 rads. The survival curve for cells irradiated in the peak region gave a D₀ of 65 ± 15 rads. The plateau points were not reliable. A replicate experiment was performed using ⁶⁰Co γ rays, yielding a survival-curve D₀ of 350 ± 50 rads. If the γ-ray D₀ is taken as a baseline, an RBE of 5.4 ± 1.8 is obtained for negative pions in the peak region, based on the ratio of peak-region D₀ to ⁶⁰Co D₀.

INTRODUCTION

It has been suggested (1-5) that negative pions (π⁻ mesons) might have applications in radiotherapy if a beam of sufficient intensity could be made available. Negative pions have the unusual property of being captured by atomic nuclei when they come to rest in matter. In tissue, pion capture by the light elements (carbon, nitrogen, and oxygen) results in nuclear disintegration and a yield of short-range but highly ionizing charged particles, mostly α particles and protons. This additional energy enhances the high ionization density produced by the Bragg peak at the end of a charged particle's range. Furthermore, by choosing pion energy properly, we can stop pions at a preselected distance within the volume to be treated. In the following discussion, the initial low-ionizing portion of the pion's path will be called the "plateau" region and the increased ionization at the end of the pion's range will be called the "peak" region.

Studies of the therapeutic possibilities of negative pions have been carried out in this Laboratory (3, 4). The results indicate that further investigations, of increased refinement, should be made. The proliferative capacity of murine lymphoma cells grown and irradiated in vivo and in vitro has been investigated in this Laboratory for a number of years with X rays, α particles, and various heavy ions, under various conditions of oxygenation (6, 7). The study of this system has progressed to a stage where an attempt can be made to estimate quantitatively the effects of pions in tissue despite the low dose rates now available. Initial work in this Laboratory (8, 9), on the lymphoma cell system in mice, demonstrated a peak-to-plateau difference in the cytological effects produced by negative-pion beams. These experiments were later extended (10) by using a plant-cell system. Vicia faba roots were exposed to a negative-pion beam, and significant peak-to-plateau differences were found for growth rate of the roots after irradiation, for anaphase abnormalities, and for cells containing micronuclei. These results, coupled with improved dosimetry (11), stimulated the experiments reported here.

MATERIALS AND METHODS

Four types of experiments were performed: A) Pion effects in vivo with environmental control; B) ^{60}Co replication of Experiment A; C) Pion effects in vivo without environmental control; and D) Acute X-ray irradiation in vivo.

Experiment A: Pion effects in vivo with environmental control.

Full descriptions of the apparatus associated with the 184-inch synchrocyclotron, and methods of using it to produce the 90 MeV pion beam, have already been reported (3, 4, 5). The beam-transport system consists of a small quadrupole focusing magnet, a beam-bending magnet, and a large quadrupole focusing magnet that delivers the beam from the cyclotron tank to the meson cave. In these experiments, the final focusing magnet was made part of a second shielding wall placed in the cave to protect the counting equipment from ambient neutrons. The complete experimental setup is shown in Fig. 1.

Two wooden boxes with Lucite ends provided environmental control, one for the mice to be irradiated in the beam, and the other for control mice. The temperature of the air circulating through the boxes was continuously recorded, and kept at $21.5 \pm 0.5^\circ\text{C}$ by a thermostat with heater and blowers.

The mice were placed in Lucite holders, each built to hold 8 mice. The dimensions of the holders were $54 \times 98 \times 106$ mm; the mice were placed in cylindrical holes 24 mm in diameter and 75 mm long, with small lateral holes for ventilation. One group of 8 mice was placed in the plateau region of the negative-pion beam, one group in the peak region, and one group was used as a control. The mice were of the LAF₁ strain, 15 weeks old, from Jackson Laboratory, Bar Harbor, Maine. They were fed wet food during irradiation and had four equally spaced 1-hr rest periods for drying, eating and drinking at will. Figure 2 is a photograph of the arrangement inside the temperature-controlled irradiation box. The negative-pion beam entered from the right and passed first through the gas ionization-chamber monitor (96% argon + 4% CO₂), then through 3 in. of Lucite absorber and holder to the "plateau" mice.

1175320

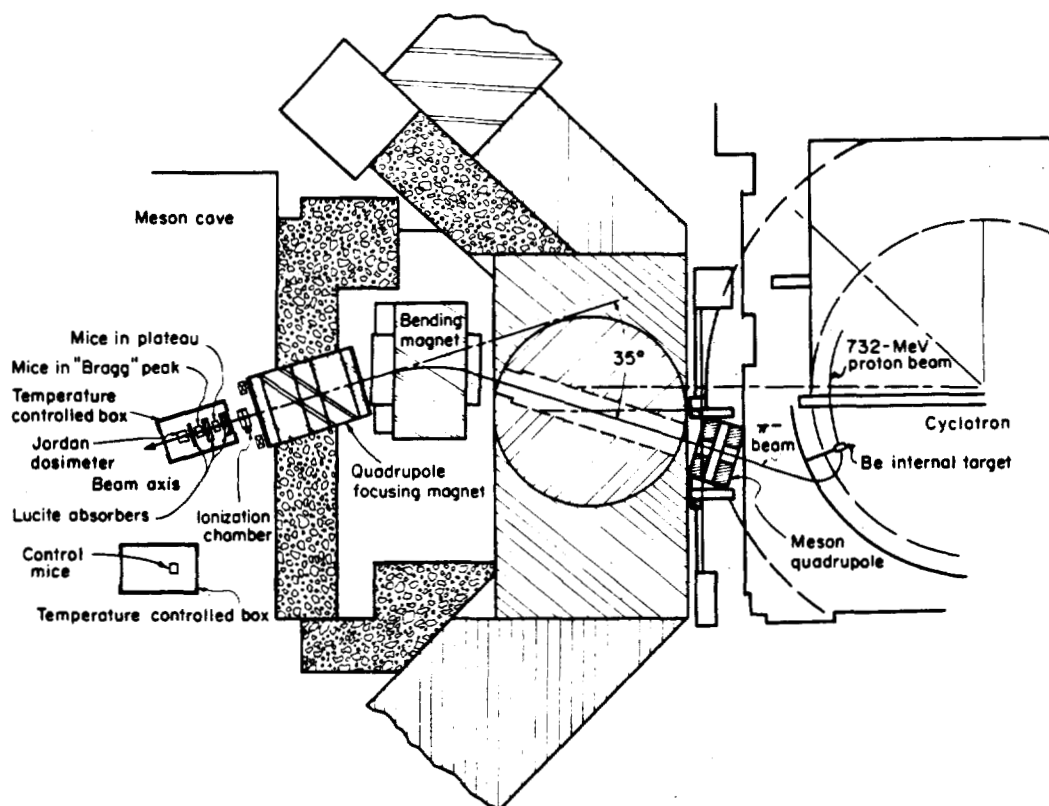


Fig. 1. Schematic view of apparatus for production and focusing of the π^- beam. The position of the ionization chamber, Jordan dosimeter, and mice holders can be seen in the meson cave.
MUB-7905

After passing through 4 more inches of Lucite, the beam entered the "peak" holder. This thickness was determined with a lithium-drifted silicon detector (12). The Jordan dosimeter was placed behind 1/2 in. of Lucite adjacent to the last holder and served as a second monitor and dose-rate meter. This monitor was frequently checked from the control room via closed-circuit television. The holder with the control mice is also shown in Fig. 2. In the actual experiment, this holder was in a separate, temperature-controlled box away from the beam.

Five days before beginning irradiation, all the mice were injected intraperitoneally with L#2 lymphoma cells, whose tumor-forming ability has not changed in the last three years.

The total irradiation time, excluding the 1-hr rest periods, was 40 hr. At the end of the irradiation, the animals were sacrificed and peritoneal ascites fluid with lymphoma cells was withdrawn. In this part of the study, five plateau-region mice and five peak-region mice were used. The cells were counted and injected intraperitoneally at various dilutions into 710 healthy adult female LAF₁ recipient mice. Cells from four control mice were pooled from two groups of two animals each, and handled in the same way as the experimental mice. The remaining experimental mice were used for cytological studies (13). The recipient mice

1175321

were divided into groups of ten animals each, and each member of a group received an identical injection. Each group, however, received a different concentration of cells. We evaluated the cells' proliferative capacity at the end of 8 weeks by noting the percentage of animals developing ascitic tumors in each group. The LD_{50} (the number of cells necessary to produce tumors in 50% of the animals) and 95%-confidence intervals were calculated by the method of Litchfield and Wilcoxon (14). Finally, surviving fractions were calculated by forming the ratio of LD_{50} of the control mice to that of each of the irradiated mice.

Radiation doses were measured with LiF dosimeters (^{60}Co calibration), distributed in front and in back of the mouse holder in the plateau region. Since the LET of the pions in the plateau region is less than $1 \text{ keV}/\mu\text{m}$, LiF dosimetry was applicable. The situation in the peak region was more complicated (11, 12). Here the pion beam was a mixture of high- and low-LET radiations. Peak-region doses were calculated from those in the plateau region, using an average peak-to-plateau ionization ratio of 1.5. This ratio was estimated from measurements made through the peak and plateau regions with a silicon detector. Some uncertainties in the measurement still exist and are being investigated, but we believe that ionization in the peak region is adequately measured by the silicon detector. The total doses in the plateau region ranged from 145 to 250 rads, and the doses in the peak region ranged from 220 to 380 rads.

Experiment B: ^{60}Co replication of Experiment A.

Since it is difficult to perform a parallel experiment with X rays because of the long irradiation times required, an experiment was done by using ^{60}Co gamma rays. Two dose rates were used: 5 and 12.5 rad/hr. The animals, all bearing 5-day-old tumors at the beginning of the experiment, were kept in the holders for the same length of time as in the pion experiment to keep the stress the same. The irradiation times varied with the dose used. Four animals were used as controls, and two were irradiated at each of the following doses: 100, 150, 200, 300, 400, and 500 rads. The irradiated lymphoma cells were injected into 410 female LAF_1 mice at various dilutions, and the surviving fractions were determined as already described.

Experiment C: Pion effects in vivo without environmental control.

This experiment, preliminary to Experiment A and without environmental control, was designed to detect the effect of hypoxia (15) on the surviving fraction of cells irradiated in vivo in the plateau and peak regions. Four mice were exposed in each pion-beam region; two had 3-day-old tumors (supposedly well-oxygenated), and two had 7-day-old tumors (supposedly more hypoxic). The irradiated cells were injected into 510 LAF_1 female mice at various dilutions as described above.

Experiment D: Acute X-ray irradiation in vivo.

In order to compare the effect of acute X-ray irradiation with "chronic" ^{60}Co irradiation, animals bearing 7-day-old tumors were irradiated with 220 kV X rays [half value layer (HVL) = 1.4 mm Cu] at a dose rate of 150 rads/min. Doses of 100, 250, 400, 500, and 750

1175322

rads were given, and the procedure described above was followed; 350 female LAF₁ mice were injected at various dilutions.

RESULTS

Experiments A and B.

The resulting surviving fractions in the peak and plateau regions and in the low-dose-rate ⁶⁰Co experimental are given in Fig. 3. Inconsistent data from the plateau-region irradiation prevented a reliable determination of dose dependence of the surviving fraction in this region. The peak region and ⁶⁰Co data yielded sufficiently consistent results so that estimations of D₀ could be made. (D₀ is called the mean lethal dose and it is the dose in rads required to reduce the proportion of surviving cells from 1 to 0.37 in the exponential region of survival curves). The computed D₀ values are:

$$D_0(\text{peak}) = 65 \pm 15 \text{ rads}; \quad D_0(^{60}\text{Co}) = 350 \pm 50 \text{ rads}.$$

The RBE for the π^- mesons at peak based on these values is:

$$\text{RBE} = \frac{D_0(^{60}\text{Co})}{D_0(\text{Pk})} = 5.4 \pm 1.8.$$

Experiment C.

Unpublished data obtained in this laboratory indicate that the lack of environmental control in this experiment would make quantitative evaluations somewhat unreliable. It was found that there was no significant difference between results from 3-day-old ("normal") and 7-day-old (relatively hypoxic) tumors. On the other hand, a significant difference between the surviving fractions obtained from pion irradiation in the peak and plateau regions encouraged the design of the environmentally controlled Experiment A.

Experiment D.

The value obtained for D₀ in acute X-ray irradiation in vivo is 280 ± 50 rads. Comparison of this value with acute X-ray in vitro values of 105 ± 15 rads for the hyperoxic case and 375 ± 45 rads for the anoxic case, recently measured in this laboratory (16), indicates the in vivo 7-day-old tumor cells are considerably less well-oxygenated than the hyperoxic in vitro cells. In fact, the in vivo D₀ lies closer to the in vitro anoxic D₀ than the average of the hyperoxic and anoxic values (240 rads). These results are consistent with the observation that tumors, especially well-advanced ones, contain poorly oxygenated cells.

DISCUSSION

The study of the action of negative pions on mammalian cells grown in vivo is difficult to carry out due to the low dose-rates available at present. In the pion plateau region the average dose-rate of 5 rads/hr in this experiment requires long irradiation times to cause measurable biological damage. For long irradiation episodes the animals must be confined and therefore are under stress. During irradiation the cell population undergoes many poorly understood dynamic processes and a certain amount of recovery and repair. Technical problems in keeping a biological system anoxic for the required time make pion-beam study of the oxygen effect extremely difficult.

1175323

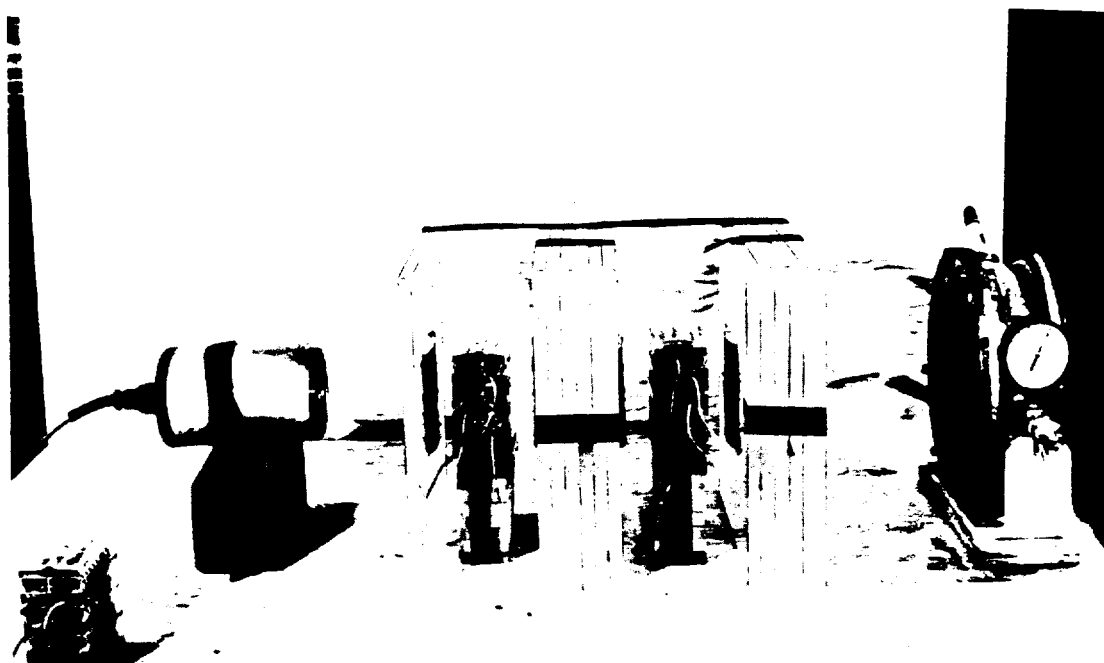


Fig. 2. Photograph showing the arrangement inside the temperature-controlled irradiation box. JHL-6417A

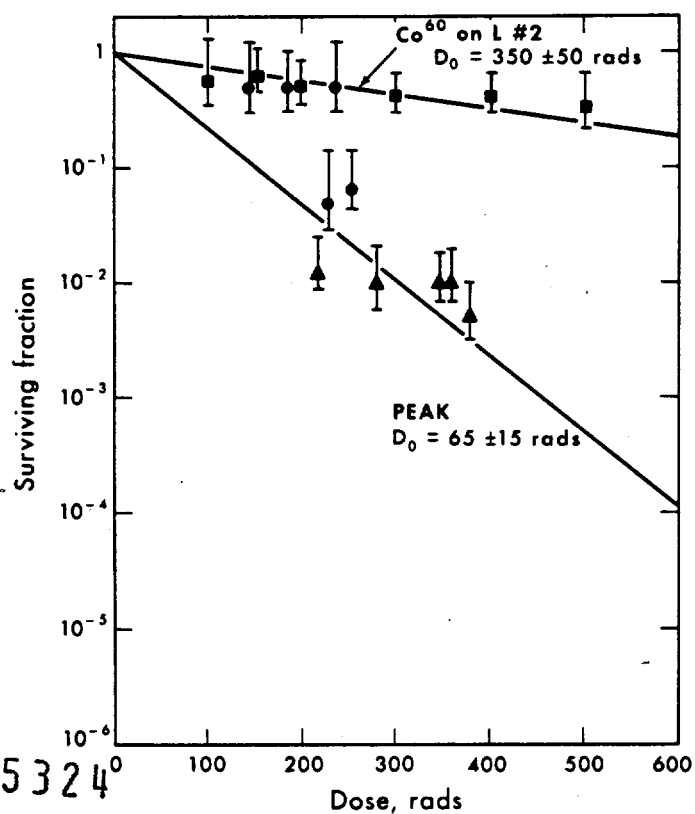


Fig. 3. Survival curves of lymphoma cells irradiated *in vivo* with a beam of negative pions and with ^{60}Co γ rays under similar conditions. Circles show plateau points.

XBL672-778

Despite the uncertainties arising from these uncontrollable factors, the results give a clear indication that the peak region of the pion beam is more effective than the plateau region in inhibiting the proliferative capacity of these lymphoma cells. In addition, peak-region irradiation inhibits the proliferative capacity significantly more than low-dose-rate ^{60}Co γ rays do. The ratio of D_0 's from the ^{60}Co data and from the pion peak-region data gives an RBE of 5.4 ± 1.8 in the peak region relative to γ rays. The size of the error here indicates that considerable uncertainty exists in the determination of the D_0 's, as is seen in Fig. 3. If an RBE of 0.8 is assumed for γ rays relative to X rays, as has been reported (17, 18, 19), the RBE becomes 4.3 ± 1.8 relative to X rays.

In evaluating this type of radiation for cancer therapy, we note that the RBE measured at such low dose-rates need not equal the RBE at the necessarily higher therapeutic dose-rates. The damage caused by the low-LET ^{60}Co γ rays will probably be considerably more repairable than the damage caused by the high-LET components of the pion beam in the peak region. Recovery from γ irradiation during a low-dose-rate experiment would manifest itself by increasing the γ -ray D_0 . This would increase the RBE over that expected in higher-dose-rate experiments when there is less time for repair. Thus, the D_0 ratio, which is RBE, would decrease.

Although the results in the plateau region are inconclusive because of the inconsistency of the data, the average LET in this region is expected to be between 0.2 and 0.3 keV/ μm and so should be no more effective than X or γ rays in causing biological damage. An experiment must be performed to substantiate this, however. Loughman has indicated this may be true for certain nonlethal radiation effects (13).

In conclusion, we have shown that the peak region of a pion beam is considerably more effective than an equivalent dose of γ rays in inhibiting the proliferative capacity of lymphoma cells *in vivo*. This result implies that there is a biologically significant component of high-LET radiation in the peak region of a pion beam, as predicted by calculation (2, 20). This in turn implies that the oxygen-enhancement ratio will be low, making the peak-region radiation of a pion beam more effective than conventional radiation in killing the anoxic cells found in tumors (21). More experimentation is indicated before the evaluation of this new type of radiation is decisive, but it appears at present that negative pions have interesting possibilities in tumor radiotherapy.

ACKNOWLEDGMENTS

It is a pleasure to express our appreciation to Drs. C. A. Tobias and Robert L. Thornton for their interest and assistance in this work. We wish to thank the 184-inch-cyclotron crew, under the supervision of Mr. James Vale, for their invaluable assistance and for making these experiments possible.

Miss Alice Beckmann and Miss Henriette Cozza gave expert assistance in the tumor-cell assays.

Finally, we wish to thank Mr. W. D. Loughman for his many helpful suggestions.

This work was done under the auspices of the U. S. Atomic Energy Commission, American Cancer Society, and Office of Naval Research.

REFERENCES AND NOTE

1. Fowler, P. H., and Perkins, D. H.; The Possibility of Therapeutic Applications of Beams of Negative π -Mesons; *Nature* 189: 524-528, 1961.
2. Fowler, P. H.; 1964 Rutherford Memorial Lecture: π -Mesons Versus Cancer?; *Proc. Phys. Soc. (London)* 85: 1051-1066, 1965.
3. Richman, C.; Aceto, Henry, Jr.; Raju, M. R., and Schwartz, B.; The Radiotherapeutic Possibilities of Negative Pions; *Am. J. Roentgenol., Radium Therapy Nuc. Med.* 96: 777-790, 1966.
4. Aceto, Henry, Jr.; A Feasibility Study of the Therapeutic Possibilities of π -Mesons, Ph.D. thesis, Lawrence Radiation Laboratory Report UCRL-11482, July 1964.
5. Richman, C.; Aceto, H., Jr.; Raju, M. R.; Schwartz, B., and Weissbluth, M.; On the Dosimetry of Negative Pions with a View Toward Their Trial in Cancer Therapy; Semiannual Report, Donner Laboratory, Lawrence Radiation Laboratory Report UCRL-11387, 1964, pp. 114-126.
6. Schmidlin, Y.; Lawrence, J. H.; Sillesen, K.; Welch, G., and Lyman, J.; Effect of Heavy Particles on the Proliferative Capacity of Ascites Tumor Cells (Lymphoma) Grown *in vivo*; Semiannual Report, Donner Laboratory, Lawrence Radiation Laboratory Report UCRL-11833, 1964, pp. 80-94.
7. Sillesen, K.; Lawrence, J. H., and Lyman, J. T.; Heavy-Particle Ionization (He, Li, B, Ne) and the Proliferative Capacity of Neoplastic Cells "in vivo"; *Acta Isotopica* 3: 107-126, 1963.
8. Loughman, W. D., et al.; Differential Cytologic Effects of Negative Pion Beams in Plateau and "Star" Regions; Lawrence Radiation Laboratory Report UCRL-16246, 1965, pp. 100-102.
9. Loughman, W. D.; Winchell, H. S.; Raju, M. R., and Lawrence, J. H.; A Significant Difference in Mammalian Cell Polyploidy Induction Between Plateau and "Star" Regions of a Negative Pion Beam; Semiannual Report, Donner Laboratory, Lawrence Radiation Laboratory Report UCRL-16898, 1966, pp. 11-13.
10. Richman, S. P., et al.; Studies of *Vicia faba* Root Meristems Irradiated with a Pion Beam; Lawrence Radiation Laboratory Report UCRL-16643, 1965, pp. 15-22.
11. Raju, M. R.; Aceto, Henry, Jr., and Richman, C.; Pion Studies with Silicon Detectors; *Nucl. Inst. Methods* 37: 152-158, 1965.
12. Raju, M. R.; Lampo, E. J.; Curtis, S. B.; Sperinde, J. M., and Richman, C.; Lithium-Drifted Silicon Detector Used as a Pulse Dosimeter; Lawrence Radiation Laboratory Report UCRL-16924, 1966, to be published.
13. Loughman, W. D., et al.; to be submitted to *Radiation Res.*
14. Litchfield, J. T., and Wilcoxon, F.; A Simplified Method of Evaluating Dose-Effect Experiments; *J. Pharmacol. Exptl. Therap.* 96: 99-113, 1949.

15. Feola, J. M.; Richman, C.; Raju, M. R., and Lawrence, J. H.; Effect of Negative Pions on the Proliferative Capacity of Ascites Tumor Cells (Lymphoma L#2) Grown in vivo; Radiation Res. 27: 542, 1966.
16. Feola, J. M.; Lawrence, J. H., and Welch, G. P.; The Measurement of the Effects of X-rays and Alpha Particles on the Proliferative Capacity of Lymphoma Ascites Tumor Cells in vivo, unpublished.
17. Storer, J. B.; Harris, P. S.; Furchner, J. E., and Langham, W. H.; The Relative Biological Effectiveness of Various Ionizing Radiations in Mammalian Systems; Radiation Res. 6: 188-288, 1957.
18. Sinclair, W. K.; Gunter, S. E., and Cole, A.; The Relative Biological Effectiveness of 200-kVp X-rays, Co⁶⁰ γ-rays and 22-MeVp X-rays Determined from the Dose-Survival Curve of Saccharomyces cerevisiae; Radiation Res. 10: 418-432, 1959.
19. Hall, E. J.; The Relative Biological Efficiency of X-rays Generated at 220 kVp and Gamma Radiation from a Cobalt-60 Therapy Unit; Brit. J. Radiol. 34: 313-317, 1961.
20. Curtis, S. B.; Raju, M. R., and Richman, C.; Calculation of the Physical Characteristics of Negative Pion Beams—Energy Loss Distribution and Bragg Curves; to be submitted to Radiation Res.
21. Fowler, J. F.; Radiation Biology as Applied to Radiotherapy; in Current Topics in Radiation Research, Vol. II, edited by M. Ebert and H. Howard, Amsterdam, North-Holland Pub. Co., 1966, pp. 305-364.

Chaim Richman's present address is Graduate Research Center of the Southwest, Dallas, Texas.

The Role of Capillaries in the Pathogenesis of Delayed Radionecrosis of Brain

Larry W. McDonald and Thomas L. Hayes

Necrosis appearing in tissue of the central nervous system months or even years after local exposure of the tissue to ionizing radiation is a limiting factor in radiation therapy when either the brain or spinal cord must be included in the radiation field (1-3). Many authors have stressed the importance of blood vessels in the pathogenesis of late radionecrosis of brain and spinal cord because of the marked sclerosis of small arteries that one sees about areas of delayed radionecrosis (4, 5). Some have attributed the lesion partly to vascular effects, but much more to differential effects on various cellular elements in the area of injury (6). Others have studied the lesion during its early development and, using nucleosides labeled with tritium, have noted increased labeling of glial cells and increased numbers of glial cells immediately preceding the appearance of the necrosis (7).

Since sclerosis of blood vessels is usually not observed with the light microscope prior to the appearance of distinct necrosis, it has often been considered secondary to the general tissue breakdown and not a primary cause of the necrosis. When it occurs, necrosis involves most cellular components, and for this reason failure of the vascular supply would explain the lesion. Because the structures of the capillary wall are at the limits of resolution of the light microscope, alterations in these vessels produced by radiation and preceding or accompanying radionecrosis have not been given attention. The present study was undertaken to determine if alterations in the capillary could be found with the electron microscope to precede or occur concomitantly with the tissue necrosis.

MATERIALS AND METHODS

Twenty-two male New Zealand White rabbits were used in the study. The ages of the animals at the time of irradiation and post-irradiation intervals to the time of sacrifice are given in Tables 1, 2, 3, 4, and 5. In order to insure well-localized radiation, the cyclotron-produced particle beams were used throughout (8-11). The sensory cortex was irradiated by using radiographs of the head to position the beam (Fig. 1). When the proton beam was used, the beam was directed dorsoventrally; the range of this beam was 1.3 to 1.6 cm. When the alpha-particle beam was used, it was directed transversely through the same area of cerebral cortex. The range of this beam is more than 20 cm, so that it passed through the head and out the other side. All doses were given as single exposures with dose rates of 500 to 1000 rads/min for the alpha particles and 10,000 to 30,000 rads/min for the protons. Most

Table 1. Results with proton irradiation using doses greater than 20 krad and an aperture of 1/8 inch.

Rabbit No.	Area tissue studied	Dose, krad	Energy, MeV	Age at irradi., days	Days aft. irradi. at sacrifice	Microscopic findings*					
						Light microscopy			Electron microscopy		
						Hemor- rhage	Gli-osis	Demye- lina- tion	Capil. basal lamina thick.†	Incr. fibrils in foot processes	Endo- thel. swell. Capil. stasis
1	Irrad.† Control	26.6 0	37.5 —	54 —	33 —	NE 0	NE 0	NE 0	110/4 85/4	+++ 0	+++ 0
2	Irrad. Control	20.6 0	42.0 —	56 —	67 —	0 0	+++ +	++ 0	NE NE	NE NE	NE NE
3	Irrad. Control	25.0 0	37.5 —	86 —	69 —	0 0	++ 0	++ 0	NE 67/6	NE 0	NE +
4	Irrad. Control	26.3 0	37.5 —	84 —	69 —	++ 0	+++ 0	++ 0	185/5 66/5	+++ 0	++ 0

*NE, not examined.

†Expressed as average thickness in millimicrons per number of measurements on different capillaries.

‡Electron microscopic section taken from edge of necrosis.

1175329

Table 2. Results with proton and alpha-particle irradiation, using doses between 6.7 and 7.7 krad and large-block recovery method for preparation of tissues.

Microscopic findings														
Rabbit No.*	Area tissue studied	Dose, krad	Energy, Mev	Aperture diam., in.	Age at irradi., days	Days aft. irradi. at sacrifice	Light microscopy				Electron microscopy †			
							Gross les.	Hemor- rhage	Gli- osis	Demye- lina- tion	Capil. basal lamina thick.f	Incr. fibrils in foot processes	Endo- thel. swell.	Capil. stasis
5	Irrad.	7.0	910	3/8	75	57	—	—	—	—	—	—	—	—
	Near les.						+	+	++	++	200/5	++	+	+
	Free of les. Control	0	—	—	—	—	0	0	0	0	100/3 85/14	+	+	0
6	Irrad.	7.0	910	3/8	75	61	—	—	—	—	—	—	—	—
	Near les.						+	+	++	++	267/3	++	+++	++
	Free of les. Control	0	—	—	—	—	0	0	0	0	116/6 86/3	++	++	0
7	Irrad.	7.0	910	3/8	75	61	—	—	—	—	—	—	—	—
	Near les.						+	++	++	++	166/3	+++	++	+
	Free of les. Control	0	—	—	—	—	0	0	0	0	90/2 96/3	+	0	0
8	Irrad.	6.8	38	1/4	64	88	+	0	+	+	166/3	NE	++	+
	Control	0	—	—	—	—	0	0	0	0	90/2	0	0	0
9	Irrad.	7.6	40	1/4	59	225	0	0	0	0	NE	NE	NE	NE
	Control	0	—	—	—	—	0	0	0	0	NE	NE	NE	NE

* Brain tissue of Rabbits 5, 6, and 7 was irradiated with alpha-particle radiation; that of Rabbits 8 and 9, with proton radiation.

† NE, not examined.

‡ Expressed as average thickness in millimicrons per number of measurements on different capillaries.

1175330

Table 3. Results with proton irradiation using doses between 6.0 and 6.5 krad and an aperture of 1/4 inch.

Rabbit No.	Area tissue studied	Dose, krad	Energy, MeV	Age at irradi., days	Days aft. irradi. at sacrifice	Microscopic findings*						
						Light microscopy			Electron microscopy			
						Gross les.	Hemor-rhage	Gliosis	Demyelination	Capil. basal lamina thick†	Incr. fibrils in foot processes	Endo-thel. swell. Capil. stasis
10	Irrad. Control	6.4 0	42 —	56 —	24 —	0 0	0 0	0 0	0 0	175/2 NE	++ NE	+ NE
11	Irrad. Control	6.2 0	42 —	56 —	28 —	0 0	0 0	0 0	0 0	91/7 NE	0 NE	0 NE
12†	Irrad. Control	6.0 0	37.5 —	84 —	33 —	0 0	++ 0	++ 0	++ 0	76/3 85/4	++ 0	+++ 0
13§	Irrad. Control	6.2 0	42 —	56 —	67 —	0 0	0 0	+++ +	++ 0	90/7 NE	++ NE	++ NE
14	Irrad. Control	6.1 0	37.5 —	84 —	69 —	0 0	NE 0	NE 0	NE 0	97/7 66/5	++ 0	+ 0
15**	Irrad. Control	6.3 0	37.5 —	86 —	69 —	0 0	NE 0	NE 0	NE 0	70/3 67/6	++ 0	++ +

* NE, not examined.

† Expressed as average thickness in millimicrons per number of measurements on different capillaries.

‡ Same animal as Rabbit 1, but opposite side of brain.

§ Same animal as Rabbit 2, but opposite side of brain.

|| Same animal as Rabbit 4, but opposite side of brain.

** Same animal as Rabbit 3, but opposite side of brain.

1175331

Table 4. Results with alpha-particle irradiation using a dose of 5.5 krad and 910 MeV.

Rabbit No.	Area tissue studied	Age at irradiation, days	Days aft. irradiation, sacrifice	Gross lesions	Microscopic findings			Electron microscopy *		
					Light microscopy		Capil. basal lamina thick.	Incr. fibrils in foot processes	Endothel. swell.	Capil. stasis
					Hemorrhage	Gliosis				
16	Irrad. Control	1/4	75	0	0	0	47/9 52/4	0	0	0
17	Irrad. Control	1/4	75	0	++	+++ [†]	150/6 93/3	++	0	0
18	Irrad. Control	1/4	75	0	0	+	66/3 55/4	++	0	0
19	Irrad. Control	1/4	75	0	0	0	51/4 65/4	++	0	0
20	Irrad. Control	3/8	63	0	0	0	200/1 66/3	+++	+	0
21	Irrad. Control	3/8	63	0	+	0	40/3 NE	+	NE	NE
22	Irrad. Control	1/4	75	0	++ [§]	+++	48/4 50/3	++	0	0
23	Irrad. Control	3/8	63	0	+	0	75/6 65/5	+	+	0

* NE, not examined.

[†] Expressed as average thickness in millimicrons per number of measurements on different capillaries.[‡] Microscopic area of necrosis 0.5 mm in diameter in white matter.[§] Areas of frank tissue necrosis.

1175332

Table 5. Results with proton irradiation using doses between 2.4 and 5.49 krad.

Microscopic findings														
Rabbit No.	Area tissue studied	Dose, krad	Energy, MeV	Aperture diam., in.	Age at irradi., days	Days aft. irradi. at sacrifice	Gross les.	Light microscopy			Electron microscopy *			
								Hemor-rhage	Gliosis	Demyelination	Capil. basal lamina thick†	Incr. fibrils in foot processes	Endothel. swell.	Capil. stasis
24	Irrad. Control	5.4 0	47.5 —	1/4 —	56 —	12 —	0 0	0 0	0 0	95.8 80/4	++ +	+	+	0 —
25†	Irrad. Control	5.3 0	40 —	1/4 —	57 —	225 —	+	0 0	++ 0	+	416/3 62/2	++ +	+	0 0
26	Irrad. Control	2.5 0	37.5 —	1/8 —	86 —	196 —	+	++ 0	++ 0	+	NE NE	NE NE	NE NE	NE NE

*NE, not examined.

†Expressed as average thickness in millimicrons per number of measurements on different capillaries.

‡The large-block recovery method was used in preparing tissue from Rabbit 25 for examination.

1175333

animals were injected intravenously with 1 ml of 10% trypan blue solution the day preceding sacrifice to help identify the irradiated area. All animals were perfused through the ascending aorta with 5% glutaraldehyde in 0.1 M phosphate buffer while under pentobarbital anesthesia. Some animals were premedicated with chlorpromazine. A perfusion pressure of 100 mm of water was used. Heparin solution (0.5 cc of a 1:1000 dilution) and 0.5 cc of 2% NaNO_2 solution were injected into the left ventricle immediately prior to inserting the cannula into the ascending aorta to start the perfusion. The blood was flushed from the vascular bed with about 150 ml of Palay's (12) balanced salt solution at room temperature until the flow from the incised right atrium began to clear. Then the glutaraldehyde at 4°C was started and ran at a rate of 800 ml in 45 min.

After completion of the perfusion the brain was cut transversely through the irradiated area, half of the irradiated area being taken for light microscopy and the other half being used for electron microscopy. All tissue for light microscopy was stained with hematoxylin and eosin and luxol fast blue. In addition, many tissue sections were stained with cresyl violet, phosphotungstic acid hematoxylin (PTAH), periodic acid-Schiff (PAS), or Holmes' silver stain for nerve fibers. Tissue for electron microscopy was handled in two ways. In all animals except Rabbits 5, 6, 7, 8, 9, and 25 (Tables 2 and 5), tissue from the presumed irradiated area and control tissue from at least 1 cm anterior to the irradiated area was minced in Palade's fixative at 4°C. Fixation was then continued in Palade's fixative for 1 hr. Then the tissue was dehydrated in graded alcohols and embedded in Araldite according to the procedure of Glauret (13) or in Epon 812 using the procedure of Luft (14). Sections were cut on a Sorvall MT-2 ultramicrotome using glass knives and stained on the grids with uranyl acetate and Reynold's (15) lead citrate solution. Specimens were examined and photographed using a Hitachi HU-11 electron microscope. Basal lamina thickness measurements were made from one outermost border to the other.

In order to examine specifically areas of early necrosis measuring less than a few hundred microns in diameter, a large-block embedding and recovery procedure was developed so that the local areas of radionecrosis could first be found with the light microscope and then taken for examination in the electron microscope. We have also used this procedure successfully to isolate microscopic areas of skin and bone marrow for electron microscopy. The procedure was used for Rabbits 5, 6, 7, 8, and 9, as indicated in Table 2, and for Rabbit 25, as indicated in Table 5. This technique consists of taking a block of tissue from the presumed irradiated area after completion of the glutaraldehyde perfusion as described above. This block of tissue, 4 mm in thickness and generally consisting of the entire cross section of one cerebral hemisphere, is placed in a 40% solution of OsO_4 in carbon tetrachloride of 4°C for 1 hr, following which dehydration and embedding in Epon 812 are done according to the following schedule:

1. 70%, 80%, and 95% ethanol, 30 min each.
2. 100% ethanol, three changes, 1 hr in each.
3. Propylene oxide, three changes, 1 hr in each.
4. Epon 812, 2 hr in partial vacuum or overnight.

1175334

5. Epon 812, 12 hr in partial vacuum.
6. Epon 812, 24 hr in partial vacuum.
7. Embed in Epon 812 with 0.015 parts of DMP-30 added.

The tissues in the embedding molds are kept at room temperature and atmospheric pressure for 24 hr, following which they are transferred to a 55-60°C oven until polymerization is complete (about 72 hr). All Epon mixtures, made according to Luft (14), are used with an A to B ratio of 1 to 1. The vacuum used is adjusted to a predetermined gauge reading such that bubbles will not quite appear in the plastic. After completion of the polymerization, sections are cut at 4 μ by using a heavy sledge microtome, the Jung Model K microtome, and a No. K-2 knife. These sections may be collected dry with a brush or with a brush dipped in 70% alcohol and mounted on slides by floating on an absolute alcohol bath. After taking the sections to xylene, cover slips are applied with Permount. The sections can be examined unstained or they may be stained with a stock Giemsa solution for 30 min. After examining the mounted sections and finding the desired area for electron microscopy, the slide is matched to the cut tissue-block face under the dissecting microscope and the desired area is removed from the block in a 0.5 mm cube with a pointed Bard-Parker (No. 11) scalpel blade. This small 0.5 mm block is then placed in 1 part propylene oxide and 1 part of Epon 812. After 30 min it is transferred to pure Epon with 1.5% DMP-30 in the capsules. After polymerization for 48 hr at 60°C the ultrathin sections are cut and stained with uranyl acetate and Reynold's lead citrate (15), and examined in the electron microscope as above.

Since the initiation of this work, Grimley (16) has independently developed a similar technique. He, however, does not use tissue blocks as thick as those that can be examined by the method described here. This is because the 40% OsO_4 employed in our method has double the penetration of a 1% aqueous solution, and thus allows the use of thicker blocks. Grimley (16) also re-embeds the tissue from the light-microscopy section for ultrathin sectioning for electron microscopy. We have tried this since the appearance of his paper, but find some difficulty with fracturing of the tissue when it is removed from the section for electron microscopy as he described. In the technique developed by De Bruijn and McGee-Russell (17), which has similarities to both our technique and that of Grimley (16), one cuts out the selected area from the large block for ultrathin sectioning by using a small trephine or one grinds down the block face around the selected area with a dental burr.

In order to confirm capillary changes in areas adjacent to necrotic tissue, we have used the scanning electron microscope (18). We have developed a technique for examining standard-size light-microscopy sections with this instrument. The details of this technique are reported elsewhere (19). Secondary electrons were used to build up the scanning microscope image.

To evaluate capillary alterations further, focal necrosis was produced in the right cerebrum of one rabbit by injecting a 2% suspension of glass beads 14-40 μ in diameter into the right internal carotid artery. Two weeks following the injection, the animal was sacrificed

and examined by conventional light microscopy with the stains already described. In addition, large blocks were embedded in Epon 812, and areas adjacent to necrotic foci were taken for transmission electron microscopy, using the large-block recovery method.

RESULTS

Microscopic changes are recorded in Tables 1, 2, 3, 4, and 5. In the proton-irradiated brains, the area at the end of the beam path (Bragg peak) was not studied because the effective radiation dose [as compared to conventional X ray (9)] is higher there than indicated in the tables. With doses greater than 20 krad (Table 1), a radiation-induced hole in the sensory cortex is usually seen (Fig. 1). This lesion has a "punched-out" appearance and on light microscopy it is found to have a narrow band of reactive astrocytes along its edges. At lower radiation doses producing delayed radionecrosis (Table 2), the typical lesion as seen in the light microscope consists of a central area of gitter cells, or occasionally a spongy neuropil with a few recognizable cells will remain. Sclerosed blood vessels are often recognizable in and about these areas. Perivascular hemorrhages are sometimes observed, usually separate from any area of distinct necrosis. White matter tends to be more involved than does gray matter. Demyelination is seen about areas of necrosis and perivascular hemorrhage. About the edges of areas of frank necrosis, gliosis is often intense. In those instances in which frank necrosis has not yet occurred, there may be some increase in the glial cells and fibrils, but this is not usually marked. Where there is no frank necrosis and gliosis, there is no vessel sclerosis. Accumulations of amyloid-like material are only occasionally found.

Electron-microscopic examination of areas within the radiation field, but not showing necrosis by gross examination, shows swelling of the endothelial cells and thickening of capillary basal lamina; e.g., 110 m μ versus 90 m μ [the term "basal lamina," as proposed by Fawcett (20), is used rather than "basement membrane," which has a less restricted meaning in light microscopy]. An increase in glial fibrils, both in astrocytic foot processes and at sites removed from the capillary wall, is also seen. In addition, there are increased numbers of irregularly shaped and irregularly staining inclusions and vacuoles in the astrocytic foot processes.

In material taken directly for osmification from the glutaraldehyde-perfused brain, one is never sure that the tissue being examined in the electron microscope is not in or adjacent to an area of necrosis, and the changes observed in capillaries might therefore be secondary to the necrosis rather than related to the development of necrosis. In tissue from Rabbits 5, 6, and 7, in the study of which the large-block recovery method was used (Table 2), however, it is possible to exclude any nearby necrosis by preliminary light microscopy [Fig. 2(a)] over the entire 1-cm-square section. In those tissues in which the large-block recovery method was used, three areas were taken for electron microscopy. These areas were: tissue adjacent to areas showing early radionecrosis [Fig. 2(b)]; the tissue in the beam path but showing no relationship to areas of radiation necrosis by light microscopy [Fig. 3(a)]; and the control tissue out of the beam path taken from the boundary between the gray and white matter [Fig. 3(b)]. Areas adjacent to early radiation necrosis were characterized by capillary basal lamina thickening (Fig. 4), excrescences of the basal lamina and morphologic changes in the



Fig. 1. Brain (Rabbit 3) with radiation-induced hole in sensory cortex of right lobe of cerebrum. Dose was 25 krads, using 0.3-cm-diameter, 37.5 MeV proton beam; animal was sacrificed 69 days following irradiation.

XBB677-4108

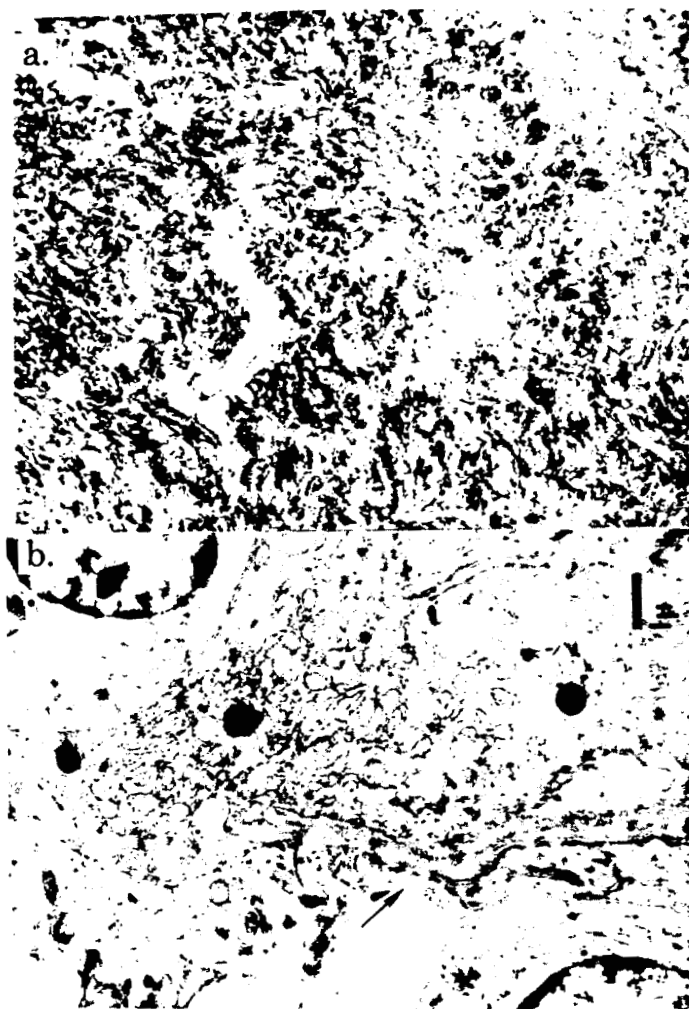


Fig. 2 (a). Brain tissue, 8- μ -thick section (Rabbit 6). Material obtained by large-block recovery method. Small areas of necrotic tissue at right of center, with ghost outlines of tissue components remaining. Giemsa stain. $\times 170$.

(b). Areas of increased electron density where glial fibrils meet plasma membrane (arrow) cross field adjacent to thickened capillary basal lamina.

XBB677-4109

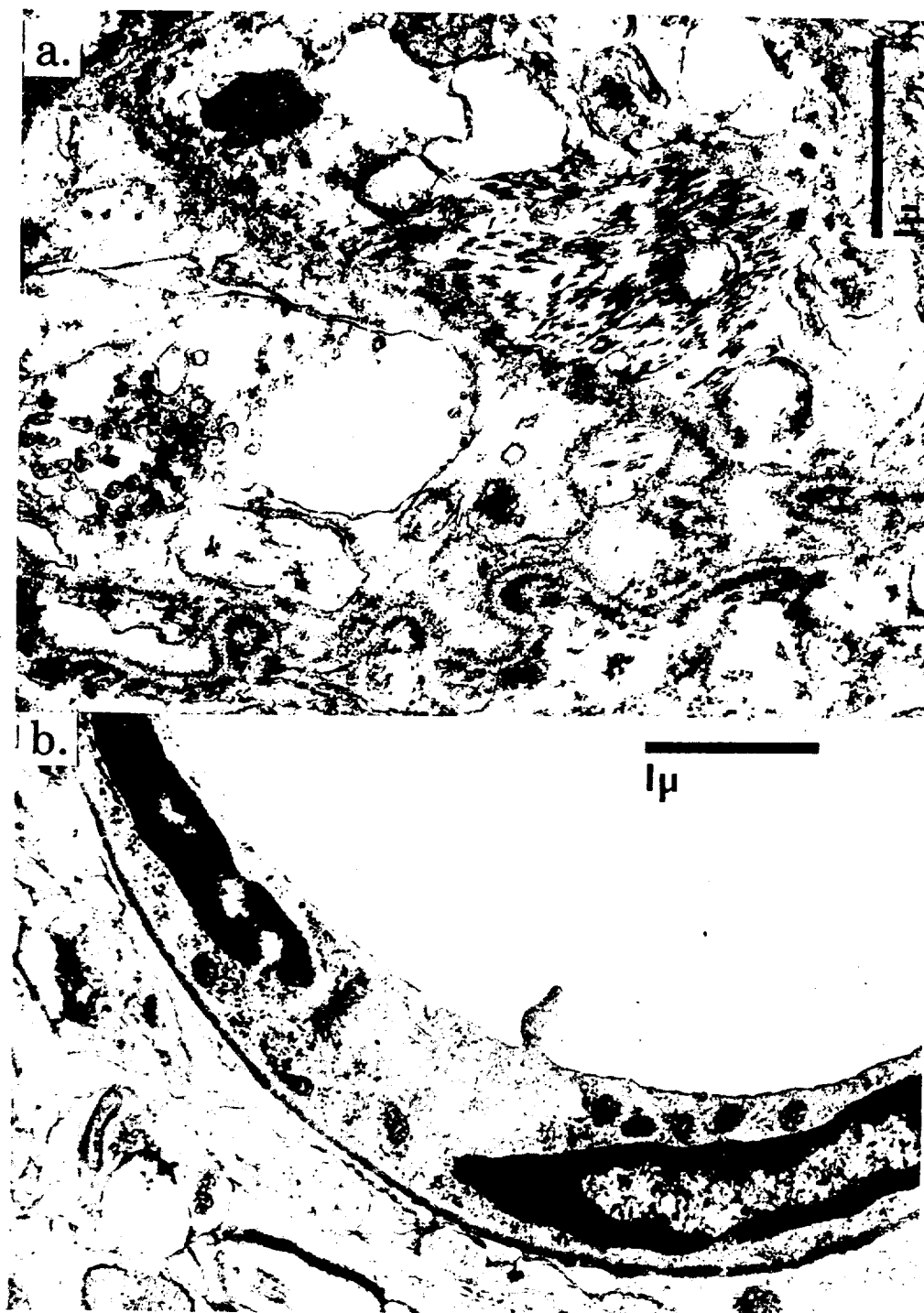


Fig. 3(a). Tissue from same block [Fig. 2(a)], within beam path but removed from radionecrosis, shows splitting of capillary basal lamina, edema of pericyte and endothelial-cell cytoplasm, and increased numbers of various inclusions.

(b). Capillary outside radiation field [same tissue block as Fig. 2(a)].

XBB677-4110

1175338

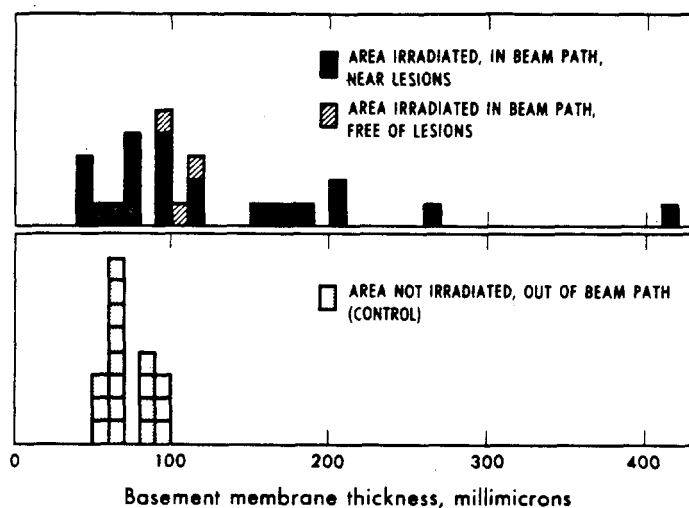


Fig. 4. Distribution of basal lamina thickness (averages from Tables 1-5) of control and irradiated areas of brains of 22 animals. Blocks with narrow diagonals indicate area irradiated in beam path, near lesions (in Tables, "irradiated"—without mention of relationship to lesions). Blocks with wide diagonals, area irradiated in beam path, free of lesions; determined by large-block recovery method. Blocks with stippling, control (not irradiated, out of beam path) and from left cerebrum of glass-bead injected animal. Average basal lamina thickness, 100 m μ .

MUB 12512

cytoplasm of endothelial cells and pericytes [Fig. 2(b)]. These changes consisted of an increase in multivesicular bodies and in number and size of vacuoles, a decrease in endoplasmic reticulum and ribosomes, and loss of general staining of the background cytoplasm. The extracellular space appeared to be increased, and glial processes adjacent to the capillary basal lamina had increased number of dark inclusions and electron-dense banding of the plasma membrane adjacent to the basal lamina.

Tissue in the beam path, but showing no relationship to areas of necrosis, also showed capillary basal lamina thickening but to a lesser degree (Fig. 4). The morphologic changes in endothelial cells and pericytes described above were also found in this tissue but were not generally as advanced as in the case of tissue adjacent to necrotic areas. In Fig. 3(a), however, the changes are shown to be quite advanced, with marked vacuolation of the endothelial cell cytoplasm at the left of the field. There is irregular splitting of the basal lamina running diagonally across the field, and many irregular inclusions are present in the pericyte cytoplasm in the upper right of the field.

Scanning electron microscopy produced stereoscopic information about the structure of capillaries of hemorrhagic [Fig. 5(a)] and control [Fig. 5(b)] areas of the brain. The depth of the section (4 μ) can be seen, and the inside of the capillary wall, the more rigid basal lamina at the crest of the wall, red blood cells, and the surrounding neuropil are all shown in three-dimensional aspect. The basal lamina appears much thinner in the control region [Fig. 5(b)] than in the hemorrhagic area [Fig. 5(a)], supporting the results of the measurement done by standard two-dimensional electron microscopy (Fig. 4).

The necrotic areas produced by the injection of the 14-40 μ glass beads were found more often in white matter than in gray matter. Irregular inclusions, vacuoles, and apparently degenerating mitochondria are present in the astrocyte cytoplasm, and prominent electron-dense "beading" is apparent where glial fibrils meet the cytoplasmic membrane



Fig. 5(a). Scanning-beam electron micrograph, using secondary electron mode. Tissue is from area of perivascular hemorrhage (Rabbit 7). Red cells appear in three-dimensional aspect within blood vessel at top. Prominent basal lamina stands out at edge of vessel (arrow). Part of capillary is present across lumen (double arrow), where glass supporting section is seen as dark background. $\times 5000$; 45° specimen tilt.

(b). Scanning electron micrograph taken outside beam path shows capillary wall cut longitudinally (Rabbit 7). Inside wall of capillary at bottom, neuropil at top. $\times 5000$; 45° specimen tilt.

XBB677-4111

1175340

adjacent to the basal lamina. The basal lamina itself is often split or broken although the endothelial cytoplasm may appear normal near necrotic areas produced by glass-bead injection.

DISCUSSION

From the results presented, there is no doubt that thickening of capillary basal lamina occurs following particle radiation of the rabbit brain. Similar findings have been reported by Cervós-Navarro (21) using ^{60}Co gamma radiation. Even before the large-block recovery method was developed, it was thought that this thickening of the basal lamina precedes or occurs independent of necrosis. By using the large-block recovery method, it was found that capillaries distant from areas of necrotic tissue but in the beam path show basal lamina thickening but less than that seen near areas of necrotic tissue; basal lamina splitting and apparently autolytic changes in the cytoplasm of all cellular components adjacent to the capillary are seen in these irradiated areas not related to necrotic tissue. Similar capillary changes have been described in chronic turpentine abscesses in muscle (22).

Capillary alterations appear to precede general tissue necrosis. The fact that there are fewer capillaries in white matter (23) would explain necrosis occurring selectively here where the failure of one capillary makes up a higher percentage of the total capillary supply than where more capillaries are present, as in gray matter.

In the scanning electron micrographs there is increased prominence of the basal lamina in the irradiated area with perivascular hemorrhage [Figs. 5(a) and (b)]. The prominence of the basal lamina is due both to its thickness and its height above the adjacent section surface. It appears that the basal lamina has more rigidity than other tissue components that are retracted down to form a lower level of the sectioned surface. In nonirradiated areas, the entire capillary basal lamina and endothelium is thinner than in the irradiated area. With the scanning electron microscope, one has a stereoscopic image of surfaces with the additional advantage of continuous magnification from less than $\times 50$ (for surveying 1-sq.-cm tissue sections) to an effective magnification of more than $\times 5000$ (with a resolution of better than $0.1\ \mu$). With newer instruments of this type becoming available, resolution should be better than $200\ \text{\AA}$.

Following glass-bead injection, the necrotic foci involve white matter more than gray matter. Astrogliosis is present but generally less marked than in the radiation-induced lesions. Also, sclerosis of vessels in the lesion is not a feature as in the case of the radiation-induced lesion. The electron micrographs show some splitting of basal lamina of capillaries, but the basal lamina is less thickened and without surface irregularities. Interestingly, one sees beads of increased electron density where glial fibrils (microtubules) come in contact with plasma membrane adjacent to the basal lamina. The plasma membrane is indistinct in these areas. Similar changes are seen in the plasma membrane in irradiated brains [Figs. 2(b) and 6]. One is tempted to conjecture that these changes in glial fibrils are related to alterations in the transfer of metabolites by the glial cells. With aldehyde fixation such microtubules as glial fibrils are being shown to interconnect many of the membrane systems of the cell. Sandborn (24) has demonstrated connections between microtubules and other membrane structures, such as mitochondria, endoplasmic reticulum, and plasma membrane.



Fig. 6. Electron-dense banding (Rabbit 5) where glial fibrils meet plasma membrane (arrows). Capillary lumen at lower right. 7.0 krads near lesion. $\times 31,000$.

XBB677-4112

He believes these microtubules may serve a transport function within the cell, as well as providing mechanical support function within the cell or as a means of mechanical motion as has been the usual interpretation.

Using a fourfold chi-square test with the Yates small-number correction, the thickening of the capillary basal lamina is significant to $p < 0.01$. There is considerable overlap of measurements of both irradiated and control areas, but more important is the lack of any control measurements greater than $100 \text{ m}\mu$ (Fig. 4). Our experience with localization of cyclotron beams makes us confident that the control tissue lay outside of the beam path and did not receive more than 1% of the radiation dose. However, without any gross or microscopic lesions in the beam path, there is always the possibility that the "irradiated" tissue taken for electron microscopy was not in the beam path. Thus it is to be expected that some "irradiated" capillary basal lamina measurements would fall in the control range because, in fact, the tissue was not irradiated. The control areas, however, were never irradiated and never have capillary basal lamina thicknesses in the radiated range (greater than $100 \text{ m}\mu$).

While the present study strongly supports the hypothesis that capillary alterations are the primary cause of radionecrosis, certain observations suggesting primary effects on glial cells should be noted. Studies of Zeman (7) showed disturbances of nucleic acid metabolism of glial cells preceding delayed radionecrosis, and the morphologic observations of Bailly (6) demonstrated differential radiosensitivity of cells in chronic lesions. Alteration in capillary structure, as shown in the present paper, appears to be sufficient to interfere both with passage of blood through the lumens and with maintenance of permeability of the capillary wall. Changes in nucleic acid metabolism and in morphology of the glial cells could occur secondarily to capillary failure and subsequent tissue injury (25). The primary effects of central nervous system irradiation leading to delayed necrosis appear to be associated with the capillary bed.

1175342

SUMMARY

Increase in capillary basal lamina thickness is regularly seen from 1 to 3 months following proton or alpha-particle irradiation of the rabbit brain. This thickening is present in areas adjacent to radionecrotic tissue.

Radiation changes that appear in areas not related to necrotic tissue include endothelial- and perivascular-cell edema. The number and size of cytoplasmic vacuoles and inclusions is increased. Splitting of capillary basal lamina is present, but thickening of basal lamina is not so marked as in areas adjacent to necrotic tissue.

The scanning electron microscope and a large-block recovery method for transmission electron microscopy were used to show that the capillary changes are limited to the irradiated area and that capillary basal lamina thickening is found primarily in areas adjacent to necrotic tissue.

ACKNOWLEDGMENTS

The authors wish to thank Dr. R. F. W. Pease, Department of Electrical Engineering, for his help and advice in using the scanning electron microscope. The construction of the microscope was largely supported by the United States Air Force Avionics Laboratory and by the University of California Electronics Research Laboratory.

Thanks are also due Mrs. Frances Taylor for technical help in preparing ultrathin sections; Mr. Michael P. Donovan and Mrs. Winifred M. Palmer for their help in preparing the large sections of the epoxy-embedded tissue, using the Jung microtome; and to the crews of the 88-inch cyclotron and the 184-inch cyclotron used in the irradiation of the animals.

REFERENCES

1. Lindgren, M.; On Tolerance of Brain Tissue and Sensitivity of Brain Tumors to Irradiation; *Acta Radiol.* 170 (Supp.): 1-73, 1958.
2. Boellaard, J. W., and Jacoby, W.; Roentgenspättschäden des Gehirns; *Acta Neurochir.* (Wien) 10: 533-566, 1962.
3. Dynes, J. B., and Smedal, M. I.; Radiation Myelitis; *Amer. J. Roentgenol., Radium Therapy Nucl. Med.* 83: 78-87, 1960.
4. Scholz, W.; Über die Empfindlichkeit des Gehirns für Röntgen- und Radium-strahlen; *Klin. Wochschr.* 14: 189-193, 1935.
5. Russell, D. S.; Wilson, C. W., and Tansley, K.; Experimental Radio-necrosis of the Brain in Rabbits; *J. Neurol. Neurosurg. Psychiat.* 12: 187-195, 1949.
6. Bailey, O. T.; Woodard, J. S., and Putnam, T. J.; Tissue Reactions of the Human Frontal White Matter to Gamma Radiation; in *Response of Nervous System to Ionizing Radiation*, edited by T. J. Haley and R. S. Snider, Boston, Little, 1964, pp. 3-18.
7. Zeman, W.; Disturbances of Nucleic Acid Metabolism Preceding Delayed Radio-necrosis of Nervous Tissue; *Proc. Natl. Acad. Sci. U. S.* 50: 626-630, 1963.
8. Lawrence, J. H.; Tobias, C. A.; Born, J. L.; Wang, C. C., and Linfoot, J. H.; Heavy-Particle Irradiation in Neoplastic and Neurologic Disease; *J. Neurosurg.* 19: 717-722, 1962.

1175343

9. Tobias, C. A.; Anger, H. O., and Lawrence, J. H.; Radiological Use of High Energy Deuterons and Alpha Particles; *Amer. J. Roentgenol., Radium Therapy Nucl. Med.* 67: 1-27, 1952.
10. Larsson, B.; Leksell, L., and Rexed, B.; The Use of High Energy Protons for Cerebral Surgery in Man; *Acta Chir. Scand.* 125: 1-7, 1963.
11. Birge, A. C.; Anger, H. O., and Tobias, C. A.; Heavy Charged-Particle Beams; in *Radiation Dosimetry*, edited by G. J. Hine and G. L. Brownell, New York, Academic Press, 1965, pp. 623-665.
12. Palay, S. L.; McGee-Russell, S. M.; Gordon, S., Jr., and Grillo, M. A.; Fixation of Neural Tissues for Electron Microscopy by Perfusion with Solutions of Osmium Tetroxide; *J. Cell Biol.* 12: 385-410, 1962.
13. Glauert, A. M., and Glauert, R. H.; Araldite as an Embedding Medium for Electron Microscopy; *J. Biophys. Biochem. Cytol.* 4: 191-194, 1958.
14. Luft, J. H.; Improvements in Epoxy Resin Embedding Methods; *J. Biophys. Biochem. Cytol.* 9: 409-414, 1961.
15. Reynolds, E. S.; The Use of Lead Citrate at High pH as an Electron-Opaque Stain in Electron Microscopy; *J. Cell. Biol.* 17: 208-212, 1963.
16. Grimley, P. M.; Selection for Electron Microscopy of Specific Areas in Large Epoxy Tissue Sections; *Stain Technol.* 40: 259-263, 1965.
17. De Bruijn, W. C., and McGee-Russell, S. M.; Bridging a Gap in Pathology and Histology; *J. Roy Microscop. Soc.* 85: 77-90, 1966.
18. Oatley, C. W.; Nixon, W. C., and Pease, R. F. W.; Scanning Electron Microscopy; *Advan. Electron. Electron Phys.* 21: 181-247, 1965.
19. McDonald, L. W.; Pease, R. F. W., and Hayes, T. L.; Scanning Electron Microscopy of Sectioned Tissue; *Lab. Invest.* 14: 13-18, 1967.
20. Fawcett, D. W.; *The Cell, Its Organelles and Inclusions: An Atlas of Fine Structure*, Philadelphia, Saunders, 1966, p. 353.
21. Cervós-Navarro, J.; Elektronenmikroskopische Befunde an den Capillaren des Kaninchengehirns nach der Einwirkung ionisierender Strahlen; *Arch. Psychiat. Nervenkr.* 205: 204-222, 1964.
22. Fuchs, U.; Die Ultrastruktur der Blutcapillaren bei einer chronischen Entzündung; *Frankfurter Z. Pathol.* 74: 544-554, 1965.
23. Cobb, S.; The Cerebrospinal Blood Vessels, in *Cytology and Cellular Pathology of the Nervous System*, Vol. 2, edited by W. Penfield, New York, Hafner, 1965, pp. 577-610.
24. Sandborn, E.; Szeberenyi, A.; Messier, P. E., and Bois, P.; A New Membrane Model Derived from a Study of Filaments, Microtubules and Membranes; *Rev. Can. Biol.* 24: 243-276, 1965.
25. Königsmark, B. W., and Sidman, R. L.; Origin of Brain Macrophages in the Mouse; *J. Neuropathol. Exp. Neurol.* 22: 643-676, 1963.

STAFF PUBLICATIONS

- Anger, H. O.: Sensitivity Resolution and Linearity of the Scintillation Camera, IEEE Trans. Nucl. Sci. NS-13, no. 3: 380-392, June 1966.
- Anger, H. O.: Survey of Radioisotope Cameras, ISA Trans. 5: 311-334, 1966.
- Brownson, R. H., and McDonald, L. W.: Selective, Acute Destruction of Granule-Cell Precursors in the Dentate Gyrus by Proton Irradiation. Light and Electron Microscopic Study, Am. J. Pathol. 50: 927-942, 1967.
- Durbin, P. W.; Williams, M. H.; Jeung, N., and Arnold, J. S.: Development of Spontaneous Mammary Tumors over the Life-Span of the Female Charles River (Sprague-Dawley) Rat: the Influence of Ovariectomy, Thyroidectomy, and Adrenalectomy-Ovariectomy, Cancer Res. 26: 400-411.
- Fawwaz, R. A.; Winchell, H. S.; Pollycove, M.; Sargent, T.; Anger, H. O., and Lawrence, J. H.: Intestinal Iron Absorption Studies Using Iron-52 and Anger Positron Camera, J. Nucl. Med. 7: 569-574, 1966.
- Fish, V. J.; Winchell, H. S., and Lawrence, J. H.: Thymic and Splenic Irradiation in Treatment of Acute Lymphatic Leukemia, Am. J. Roentgenol. Radium Therapy Nucl. Med. 97: 989-990, 1966.
- Freeman, N. K.; Lampo, E., and Windsor, A. A.: Semi-automatic Analysis of Serum Triglycerides and Cholesteryl Esters by Infrared Absorption, J. Am. Oil Chemists' Soc. 44, no. 2: 1-4, 1967.
- Freifelder, D.: Acridine Orange- and Methylene Blue-Sensitized Induction of Escherichia coli, Virology 30: 567-568, 1966.
- Freifelder, D.: DNA Strand Breakage by X Irradiation, Radiation Res. 29: 329-338, 1966.
- Freifelder, D.: Inactivation of Phage α by Single-Strand Breakage, Virology 30: 328-332, 1966.
- Freifelder, D.: Lethal Changes in Bacteriophage DNA Produced by X Rays, Radiation Res. Suppl. 6: 80-96, 1966.
- Freifelder, D., and Uretz, R. B.: Mechanism of Photoinactivation of Coliphage T7 Sensitized by Acridine Orange, Virology 30: 97-103, 1966.
- Fujii, T.; Ikenaga, M., and Lyman, J. T.: Radiation Effects of Arabidopsis thaliana - II. Killing and Mutagenic Efficiencies of Heavy Ionizing Particles, Radiation Botany 6: 297-306, 1966.
- Gaffey, C. T.: Blockage of Pupillodilation with Cyclotron-Accelerated Alpha Particles, Acta Radiol. 5: 105-117, 1966.
- Garcia, J. F., and Geschwind, I. I.: Increase in Plasma Growth Hormone Level in the Monkey Following the Administration of Sheep Hypothalamic Extracts, Nature 211: 372-374, 1966.
- Gilmore, R. A., and Mortimer, R. K.: Super-suppressor Mutations in Saccharomyces cerevisiae, J. Mol. Biol. 20: 307-311, 1966.

- Grundy, R. D., and Sargent, T. W.: Whole-Body Counting Studies Using Cesium-132, J. Nucl. Med. 7: 676-686, 1966.
- Hanawalt, P. C., and Haynes, R. H.: The Repair of DNA, Sc. Am. 216, no. 2: 37-43, Feb. 1967.
- Hatch, F. T.; Freeman, N. K.; Jensen, L. C.; Stevens, G. T., and Lindgren, F. T.: Ultracentrifugal Isolation of Serum Chylomicron-Containing Fractions with Quantitation by Infrared Spectrometry and NCH Elemental Analysis, Lipids 2: 183-191, 1967.
- Hayes, T. L.; Pease, R. F. W., and McDonald, L. W.: Applications of the Scanning Electron Microscope to Biologic Investigations, Lab. Invest. 15: 1320-1326, 1966.
- Hayes, T. L.; Pease, R. F. W.; McDonald, L. W., and Camp, A. S.: A Device for Multi-Dimensional Electron Microscopy, Clin. Res. 15: 116, 1967.
- Haynes, R. H.: The Interpretation of Microbial Inactivation and Recovery Phenomena, Radiation Res. Suppl. 6: 1-29, 1966.
- Hildreth, P. E., and Lucchesi, J. C.: Fertilization in *Drosophila*. III. A Reevaluation of the Role of Polyspermy in Development of the Mutant Deep Orange, Develop. Biol. 15: 536-552, 1967.
- Hildreth, P. C.: Lack of Mutagenic Influence of Temperature Shock on Presyngamic Sperm Nuclei, Mutation Res. 4: 213-218, 1967.
- Jensen, L. C.; Ewing, A. M.; Wills, R. D., and Lindgren, F. T.: The Use of the Computer in Serum Lipid and Lipoprotein Analysis, J. Am. Oil Chemists' Soc. 44, no. 1: 5-10, 1967.
- King, J. L.: Continuously Distributed Factors Affecting Fitness, Genetics 55: 483-492, 1967.
- Landaw, S. A., and Winchell, H. S.: Endogenous Production of Carbon-14 Labeled Carbon Monoxide: an *in vivo* Technique for the Study of Heme Catabolism, J. Nuc. Med. 7: 696-707, 1966.
- La Roche, G.; Johnson, C. L., and Woodall, A. N.: Iodine Metabolism in Young Chinook Salmon (*Oncorhynchus tshawytscha*, Walbaum). I. Thyroidal Impairment with the Use of I-131, Gen. Comp. Endocrinol. 67: 512-524, 1966.
- La Roche, G., and Johnson, C. L.: Simulated Altitude and Iodine Metabolism in Rats: I. Acute Effects on Serum and Thyroid Components, Aerospace Med. 38: 499-506, 1967.
- La Roche, G.; Woodall, A. N.; Johnson, C. L., and Halver, J. E.: Thyroid Function in the Rainbow Trout (*Salmo gairdnerii* Rich.) II. Effects of Thyroidectomy on the Development of Young Fish, Gen. Comp. Endocrinol. 6: 249-266, 1966.
- Lawrence, J. H., and Tobias, C. A.: Heavy Particles in Therapy, in Modern Trends in Radiotherapy, edited by T. J. Deeley and C. A. P. Wood, London, Butterworths, 1967, pp. 260-276.
- Lindgren, F. T.; Freeman, N. K.; Ewing, A. M., and Jensen, L. C.: Serum Lipoprotein Distribution, Flotation Rates and Protein Analysis, J. Am. Oil Chemists' Soc. 43, no. 5: 281-285, 1966.
- McDonald, L. W., and Hayes, T. L.: The Role of Capillaries in the Pathogenesis of Delayed Radionecrosis of Brain, Am. J. Pathol. 50: 745-764, 1967.
- McDonald, L. W.; Pease, R. F. W., and Hayes, T. L.: Scanning Electron Microscopy of Sectioned Tissue, Lab. Invest. 16: 532-538, 1967.
- Mortimer, R. K., and Hawthorne, D. C.: Yeast Genetics, Ann. Rev. Microbiol. 20: 151-168, 1966.

1175346

- Paulus, J. -M.: Multiple Differentiation in Megakaryocytes and Platelets, *Blood* 29: 407-416, 1967.
- Pease, R. F. W.; Hayes, T. L.; Camp, A. S., and Amer, N. M.: Electron Microscopy of Living Insects, *Science* 154: 1185-1186, 1966.
- Pease, R. F. W., and Hayes, T. L.: Some Biological Applications of the Scanning Electron Microscope, in *International Congress for Electron Microscopy*, 6th Kyoto, 1966, Electron Microscopy, Tokyo, Maruzen Company, Ltd., 1966, Vol. 2, pp. 19-20.
- Pollycove, M.; Winchell, H. S., and Lawrence, J. H.: Classification and Evolution of Patterns of Erythropoiesis in Polycythemia Vera as Studied by Iron Kinetics, *Blood* 28: 807-829, 1966.
- Pollycove, M.: Iron Metabolism and Kinetics, *Seminars Hematol.* 3: 235-298, 1966.
- Powell, M. R., and Anger, H. O.: Blood Flow Visualization with the Scintillation Camera, *J. Nucl. Med.* 7: 729-732, 1966.
- Raju, M. R.; Lampo, E. J.; Curtis, S. B.; Sperinde, J. M., and Richman, C.: Lithium-Drifted Silicon Detector Used as a Pulse Dosimeter, *IEEE Trans. Nucl. Sci.* NS-14, no. 1: 559-562, 1967.
- Raju, M. R.: The Use of the Miniature Silicon Diode as a Radiation Dose Meter, *Phys. Med. Biol.* 11: 371-376, 1966.
- Rescigno, A., and Richardson, I. W.: The Struggle for Life. I. Two Species, *Bull. Math. Biophys.* 29: 377-388, 1967.
- Resnick, M. A., and Mortimer, R. K.: Unsaturated Fatty Acid Mutants of Saccharomyces cerevisiae, *J. Bacteriol.* 92: 597-600, 1966.
- Rosenberg, L. L.; La Roche, G., and Ehlert, J. M.: Evidence for Heterogeneous Turnover of Iodine in Rat Thyroid Glands, *Endocrinology* 79: 927-934, 1966.
- Rubin, M. M., and Katchalsky, A.: Mathematics of Band Centrifugation: Concentration-Independent Sedimentation and Diffusion in Shallow Density Gradients, *Biopolymers* 4: 579-593, 1966.
- Sargent, T. W.; Linfoot, J. A., and Isaac, E. L.: Whole-Body Counting of ^{47}Ca and ^{85}Sr in the Study of Bone Diseases, *Clin. Uses of Whole-Body Counting* (Proceedings of a Panel, Vienna, 28 June-2 July, 1965), 1966, p. 187.
- Schaer, L. R.: Supraorbital Fibrous Dysplasia Demonstrated by Fluorine-18 and the Scintillation (Positron) Camera, *Radiology* 86: 506-508, 1966.
- Schooley, J. C.: The Effect of Erythropoietin on the Growth and Development of Spleen Colony-Forming Cells, *J. Cellular Physiol.* 68: 249-262, 1966.
- Schooley, J. C.: Inhibition of Erythropoietic Stimulation by Testosterone in Polycythemic Mice Receiving Anti-erythropoietin, *Proc. Soc. Exptl. Biol. Med.* 122: 402-403, 1966.
- Schooley, J. C., and Shrewsbury, M. M.: The Thymus and the Recirculating Lymphocyte Pool, in *The Symposium held at Bristol, April 1966, The Lymphocyte in Immunology and Haemopoiesis*, London, Edward Arnold Publishers, Ltd., 1967, pp. 366-376.
- Sherwood, N. M.; Welch, G. P., and Timiras, P. S.: Changes in Electroconvulsive Thresholds and Patterns in Rats After X-Ray and High-Energy Proton Irradiation, *Radiation Res.* 30: 374-390, 1967.
- Siegel, E., and Tobias, C. A.: Actions of Thyroid Hormones on Cultured Human Cells, *Nature* 212: 1318-1321, 1966.

- Siegel, E., and Tobias, C. A.: End-Organ Effects of Thyroid Hormones: Subcellular Interactions in Cultured Cells, *Science* 153: 763-765, 1966.
- Siri, W. E.; Van Dyke, D. C.; Winchell, H. S.; Pollycove, M.; Parker, H. G., and Cleveland, A. S.: Early Erythropoietin, Blood, and Physiological Responses to Severe Hypoxia in Man, *J. Appl. Physiol.* 21: 73-80, 1966.
- Stern, C., and Tokunaga, C.: Nonautonomy in Differentiation of Pattern-Determining Genes in *Drosophila*. I. The Sex Comb of Eyeless-Dominant, *Proc. Natl. Acad. Sci. U. S.* 57: 658-664, 1967.
- Strisower, E. H.: The Combined Use of CPIB and Thyroxine in Treatment of Hyperlipoproteinemias, *Circulation* 33: 291-296, 1966.
- Tobias, C. A., and Todd, P. W.: Heavy Charged Particles in Cancer Therapy; in U. S. Nat. Cancer Inst. Monograph 24, Radiobiology and Radiotherapy, National Cancer Institute, Bethesda, Maryland 1-21, 1967.
- Todd, P. W.; Boerke, C. L., and Armer, R. A.: A Rapid Colony-Selection Method for Cultured Mammalian Cells, *Mutation Res.* 3: 540-542, 1966.
- Todd, P. W.: Reversible and Irreversible Effects of Densely Ionizing Radiations upon the Reproductive Capacity of Cultured Human Cells, *Med. Coll. Virginia Quart.* 1, no. 4: 2-14, Winter 1965.
- Van Dyke, D. C.; Nohr, M. L., and Lawrence, J. H.: Erythropoietin in the Urine of Normal and Erythropoietically Abnormal Human Beings, *Blood* 28: 535-543, 1966.
- Winchell, H. S.; Pollycove, M.; Loughman, W. D.; Richards, V.; Kim, L., and Lawrence, J. H.: Homotransplantation Studies in Dogs Following Selective Radioisotopic Lymphatic Ablation, *J. Nucl. Med.* 7: 416-432, 1966.
- Winchell, H. S., and Lawrence, J. H.: Polycythemia Vera, Method of, in *Current Therapy*, edited by E. F. Conn, Philadelphia and London, W. B. Saunders, 1966, pp. 245-247.

AUTHOR INDEX

Anger, H. O.	86
Camp, A. S.	1
Cantor, L. N.	110
Curtis, S. B.	145
Dewey, D. L.	138
Fawwaz, R. A.	97
Feola, J. M.	133, 145
Fish, M. B.	106
Garcia, J. F.	110
Havens, V. W.	110
Hayes, T. L.	1, 8, 154
Haynes, R. H.	138
Jones, G. E.	133
Landaw, S. A.	43
Lawrence, J. H.	127, 145
McDonald, L. W.	8, 154
Mel, H. C.	16
Nichols, A. V.	16
Ostwald, R.	58
Pease, R. F. W.	1, 8
Pollycove, M.	97, 106, 127
Price, D. C.	86
Raju, M. R.	145
Richman, C.	145
Sargent, T. W.	97
Schooley, J. C.	110
Shkurkin, C. J.	86
Tippetts, R. D.	16
Todd, P. W.	133
Van Dyke, D. C.	70, 86, 127
Vimokesant, S. L.	106
Winchell, H. S.	58, 97, 106, 133
Yamanaka, W. K.	58
Yano, Y.	86

PERSONNEL

Senior Staff

John H. Lawrence, Director
Hal O. Anger
Max W. Biggs
James L. Born
Ernest L. Dobson
Norman K. Freeman
Joseph F. Garcia
Thomas L. Hayes
Robert H. Haynes
Hardin B. Jones
Thomas H. Jukes

Frank T. Lindgren
Howard C. Mel
Robert K. Mortimer
Alexander V. Nichols
Howard G. Parker
Donald J. Rosenthal
John C. Schooley
William E. Siri
Cornelius A. Tobias
Donald C. Van Dyke
Harry Saul Winchell

Medical Investigator Staff

Max W. Biggs
James L. Born
Richard A. Carlson
Claude Y. Cheung
William G. Donald, Jr.
Stephen A. Landau
John H. Lawrence
John A. Linfoot
Edward Manougian

Larry W. McDonald
Howard G. Parker
David C. Price
James Price
Donald J. Rosenthal
Henry H. Stauffer
Donald C. Van Dyke
Harry Saul Winchell

Research Staff

Henry Aceto
Lawrence Adams
Nabil Amer
Brenda Buckhold
H. John Burki
Gerald Connell
Stanley B. Curtis
Patricia Durbin-Heavey
Rashid A. Fawwaz
Jose M. Feola
Cornelius T. Gaffey
Robert M. Glaeser
Thomas E. Gunter
Jerry Howard
Lin Jensen
Lola S. Kelly
Jack L. King

Walter J. Lossow
William D. Loughman
David D. Love
John T. Lyman
James McRae
Myron Pollycove
Douglas W. Pounds
Mudundi R. Raju
Thornton W. Sargent
Richard L. Schoenbrun
Carol J. Shkurkin
John V. Slater
Edward H. Strisower
Chiyoko Tokunaga
Graeme P. Welch
Margaret R. White
Yukio Yano

Postdoctoral Fellows

Michael G. Chen
John C. Cummings
Arnfinn J. Engeset
Gertrude M. Forte
David M. Israelstam
W. Barrie G. Jones

Pierre Jullien
Howard D. Maccabee
Tran Manh Ngo
Louis L. Shane
Martin D. Shetlar
Burton H. Slanger

Technical Staff

Gerald L. Adamson
Hilda M. Alexander
Cathryne C. Allan
Margaret K. Baskin
Alice Beckmann
Adrienne Berkowitz
Patricia J. Blanche
Catharine D. Boerke
Carol S. Bohlen
John F. Bohn
Jonathan Bokelman
Deortra Brooks
Gerald L. Brooks
Barbara A. Bushnell
Dorothy A. Carpenter
Emanuela N. Catena
Elaine L. Coggiola
Mary J. Cornell
Henriette C. Cozza
Susan J. Daniels
Theodora M. Davis
Rosalee Demostene
Michael P. Donovan
Robert E. Doyle
Susan M. Walker
Doris L. Dunn
Ora B. Ellington
Nancy C. Finley
Carolee R. Finney
Myrtle L. Foster
Roscoe Frazier
Charlie M. Fuller
Patricia A. Garbutt
Queen E. Cipson
Michael H. Green
Troy R. Guthridge
Virginia C. Havens
Judith M. Hayes
Willie M. Jackson
Karen Jarratt
Nylan M. Jeung

Kay M. Johnson
Katherine A. Kelly
Natalia Kusubov
Ruth S. Lerner
Virginia C. Lew
Phoebe J. Lindsay
Cynthia Lippincott
Jennie M. London
Jean R. Luce
Josephine A. Lundberg
Justine J. Lynch
Patricia C. Mason
Johnnie A. Maxion
Lafayette McIntosh, Jr.
Tommy J. McKey
Velma B. McNeal
Victor J. Montoya
William D. Nance
Mary L. Nohr
Virginia I. Obie
Anne K. Poley
Rosanne B. Raley
Ralph L. Reynolds
Willie H. Sanders
Carol A. Schweighardt
Thea B. Scott
Barbara A. Shipley
Patricia P. Smith
Virginia M. Spamer
Robert W. Springsteen
Gary R. Stevens
Sandra K. Stoddard
Velta Suna
Frances B. Taylor
Charles Thompson, Jr.
Cole Ulrichs
Elnora Walker
Marilyn A. Williams
Robert D. Wills
Elaine H. Yokoyama
Philip E. Yost

Graduate Students

Raymond Baker
Steven A. Beckwitt
Jeremy N. Bruenn
Elizabeth J. Clark
Robert A. Everson
David E. Garfin
Michael M. Graham
Martin Haas
William J. Horsley
Gordon R. Kepner

Gustave H. Langner, Jr.
Lawrence R. Lawlor
David H. Lin
Max S. Lin
Roderick D. Macgregor, Jr.
Udipi Madhvanath
Abdel M. Mamoon
Ja Rue Manning
Bambino I. Martins
Peter C. Nosler

Graduate Students (cont.)

Paul H. Olague
James B. Pawley
Esther B. Perry
David A. Pistenma
Robert G. Plantz
Donald L. Puppione
Theodore Regimbal
Michael A. Resnick
Ubaldo S. RodarteYramon
Guy Roy

Werner T. Schlapfer
Bernard Schwartz
Paul T. Shafer
Sylvia Spengler
Tom S. Tenforde
Russell Weitzel
Junarden Williams
Myonggeun Yoon
David A. Zelman

Engineering and Technical Support Staff

Robert C. Aker
Elbert L. Benjamine
Delbert H. Coleman
Robert D. Creedy
Dewey D. Dean
Dorothy E. Denney
John A. Despotakis
Edward F. Dowling
James H. Edwards
John P. Flambard
John R. Gurule
Marian P. Hart

Edward A. Heilstad
David A. Hoopes
Victor P. Jensen
Edward J. Lampo
Van L. Miller
Eilis H. Myers
Karen A. Peterson
Marjory H. Simpson
John M. Sweeney
Frank T. Upham
Alfred A. Windsor

Administrative and Office Staff

Igor R. Blake
George Baird Whaley

Betty M. Allen
Sandra L. Bazyouros
Mary M. Bryan
Janice C. DeMoor
Marian F. Edelen
Fern V. Forsberg
Mary C. Harmon

Dorothy B. Hedquist
Donna E. Kennedy
June M. Lattin
Barbara J. Mattox
Shirley C. Peterson
Beverly A. Rovner
Charlotte A. Scott
Ruth T. Showalter
Dorothy S. Sprague
Grace H. Walpole